A genome wide screening approach for investigating the interplay between host defence and parainfluenza viruses

Chloe Jones

A thesis submitted for the degree of PhD
at the
University of St Andrews

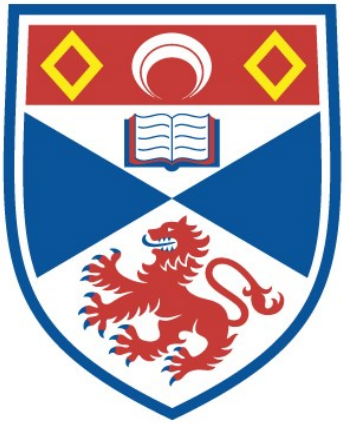

2023

Identifier to use to cite or link to this thesis:
DOI: https://doi.org/10.17630/sta/651

Abstract

Viruses are obligate intracellular pathogens, so virus-host interactions are crucial to their infectivity. A successful infection is a trade-off between the virus's utilisation of host dependency factors that permit virus replication, and its ability to overcome the host innate immune response. Broadening our understanding of what permits or restricts replication may provide us with novel targets for antiviral therapies.

Human parainfluenza virus type 3 (hPIV3) is a leading cause of pneumonia and hospitalisation of children under 5 years worldwide. Using a genome wide CRISPR knockout screen, targeting approximately 18,000 individual genes, we identified host factors that facilitate hPIV3 replication, including solute carrier family 35 member A1 (SLC35A1), a sialic acid transporter, alongside antiviral factors. Infection of independent gene knockout cell lines validated a role of three genes important for the antiviral response: Merlin (NF2), Hydroxysteroid 17-Beta Dehydrogenase 12 (HSD1712), and Zinc Finger CCCH-Type Containing, Antiviral 1 (also known as zinc finger antiviral protein, ZAP). Using flow cytometry and RT-qPCR, we showed that IFN-treated knockout cells were permissive to hPIV3 infection when compared to control cells. We also showed, by RT-qPCR, that all three hits regulated IFN induction. Importantly, NF2 also regulated IFN signalling; a novel phenotype not previously described. Using plaque assays, we demonstrated that all three hits restricted the replication of other paramyxo- and pneumoviruses, revealing their broad antiviral activity.

However, the IFN response is a vast response with significant redundancy and where several interferon stimulated genes (ISGs), that individually have low activity, culminate to restrict infection. Current screening methods rely on strong phenotypes, leading to low power in elucidating antiviral restriction factors. To overcome this, we carried out proof-of-principle studies, using an established ISG15-deficient cell line and model Paramyxovirus, PIV5, to enhance signal-to-noise and expand the quantitative working window required for the discovery of low acting ISGs. Building on this, future work will provide a broad overview of the host antiviral response that could inform the development of new therapeutics.

Candidate's declaration

I, Chloe Jones, do hereby certify that this thesis, submitted for the degree of PhD, which is approximately 53,000 words in length, has been written by me, and that it is the record of work carried out by me, or principally by myself in collaboration with others as acknowledged, and that it has not been submitted in any previous application for any degree. I confirm that any appendices included in my thesis contain only material permitted by the 'Assessment of Postgraduate Research Students' policy.

I was admitted as a research student at the University of St Andrews in September 2019.

I received funding from an organisation or institution and have acknowledged the funder(s) in the full text of my thesis.

Date 26 October 2023 Signature of candidate

Supervisor's declaration

I hereby certify that the candidate has fulfilled the conditions of the Resolution and Regulations appropriate for the degree of PhD in the University of St Andrews and that the candidate is qualified to submit this thesis in application for that degree. I confirm that any appendices included in the thesis contain only material permitted by the 'Assessment of Postgraduate Research Students' policy.

Date 30 October 2023 Signature of supervisor

Permission for publication

In submitting this thesis to the University of St Andrews we understand that we are giving permission for it to be made available for use in accordance with the regulations of the University Library for the time being in force, subject to any copyright vested in the work not being affected thereby. We also understand, unless exempt by an award of an embargo as requested below, that the title and the abstract will be published, and that a copy of the work may be made and supplied to any bona fide library or research worker, that this thesis will be electronically accessible for personal or research use and that the library has the right to migrate this thesis into new electronic forms as required to ensure continued access to the thesis.

I, Chloe Jones, confirm that my thesis does not contain any third-party material that requires copyright clearance.

The following is an agreed request by candidate and supervisor regarding the publication of this thesis:

Printed copy

Embargo on all of print copy for a period of 1 year on the following ground(s):

- Publication could preclude future publication

Supporting statement for printed embargo request

Thesis results are currently being prepared for publication, with future publications pending. Without an embargo, provenance could be at risk.

Electronic copy

Embargo on all of electronic copy for a period of 1 year on the following ground(s):

- Publication would preclude future publication

Supporting statement for electronic embargo request

Thesis results are currently being prepared for publication, with future publications pending. Without an embargo, provenance could be at risk.

Title and Abstract

- I agree to the title and abstract being published.

Date 26 October 2023 Signature of candidate

Date 30 October 2023 Signature of supervisor

Underpinning Research Data or Digital Outputs

Candidate's declaration

I, Chloe Jones, understand that by declaring that I have original research data or digital outputs, I should make every effort in meeting the University's and research funders' requirements on the deposit and sharing of research data or research digital outputs.

Date 26 October 2023 Signature of candidate

Permission for publication of underpinning research data or digital outputs

We understand that for any original research data or digital outputs which are deposited, we are giving permission for them to be made available for use in accordance with the requirements of the University and research funders, for the time being in force.

We also understand that the title and the description will be published, and that the underpinning research data or digital outputs will be electronically accessible for use in accordance with the license specified at the point of deposit, unless exempt by award of an embargo as requested below.

The following is an agreed request by candidate and supervisor regarding the publication of underpinning research data or digital outputs:

Embargo on all of electronic files for a period of 1 year on the following ground(s):

- Publication would preclude future publication

Supporting statement for embargo request

Research in the thesis is currently being prepared for publication, with future publications pending. Without an embargo, provenance could be at risk.

Date 26 October 2023 Signature of candidate

Date 30 October 2023 Signature of supervisor

General acknowledgements

I would first like to thank my supervisor, Dr David Hughes, for taking a chance on me and giving me the opportunity to work within his lab. Thank you for the advice, support, and encouragement, both scientifically and personally throughout what has been an ‘unprecedented time’ to complete a PhD during. I would also like to thank the rest of the Hughes lab, both past and present: Dr Andri Vasou, Mr Andrew Seaton, Miss Lynsey Murray, and Dr Elisabeth Wignall-Fleming (plus undergraduate and masters students that have passed through). You have all been a massive part of this journey, who I have been able to count on for help, advice, and laughs, never resulting in a dull moment.

This PhD would not have been possible without the support of collaborators and colleagues both in St. Andrews and further afield. Firstly, Professor Richard Randall and Mr Dan Young for their invaluable nuggets of wisdom and guidance. Also, a number of people from the Roslin Institute, Edinburgh: Dr Spring Tan, Professor Paul Digard, Dr Finn Grey, Dr Elly Gaunt, and Dr Anna Raper. Without the help of the named, this project would not have been completed and I am indebted to you all. I would like to especially thank Spring Tan who supported me extensively, going above and beyond what was asked - thank you! I would also like to thank everyone that has passed through the WRL or BMS. I have thoroughly enjoyed working with you all; you have made moving buildings and dealing with a pandemic a lot more bearable in this bubble we call home.

Finally, I would like to thank all the people who have supported me personally on this journey. My friends - you have been a source of light relief, a sounding board when times have been tough, and the best people to celebrate with when they’re going right. Mum, Dad, Em (and the pets) - you have been my biggest cheerleaders since before this PhD journey ever began. Thank you for all your love, listening ear (even if you don’t know what I’m talking about), and endless support keeping me positive! Chris - you have put up with every one of my frustrations and been there when I thought I would never finish. But, you have picked me up, cheered me on, and even learnt what an ISG is. Thank you for supporting me and staying by my side!

Funding

This work was supported by the University of St Andrews [School of Biology Studentship]; and TENOVUS Scotland [grant number T20/63].

Research Data/Digital Outputs access statement

Some of the data are already available in the main text of the thesis, but the rest of the data will be made available upon research outputs’ publication.

Table of Contents

Table of Contents 7

List of Figures 12

List of Tables 16

Abbreviations 18

Viruses *18*

Units *19*

Genes and proteins of interest *20*

Other *21*

Chapter 1: Introduction 24

1.1 Introduction *25*

1.2 Antiviral Defence and the IFN Response *25*

1.2.1 Classes of IFN and their properties 26

1.2.2 IFN induction by RNA viruses 27

1.2.2.1 RLRs 28

1.2.2.2 TLRs 29

1.2.3 Type I IFN signalling 30

1.2.4 Interferon Stimulated Gene effectors and their functions 31

1.2.5 Regulation of the type I IFN response 33

1.3 The use of genome wide screening for the identification of antiviral factors *35*

1.3.1 Different approaches to genome wide screening design 35

1.3.2 Alternative screening approaches and their advantages and disadvantages 36

1.3.3 The application and advances of CRISPR/Cas9 screening 38

1.3.4 Identification of antiviral factors using CRISPR/Cas9 genome wide screening 40

1.3.5 Limitations to CRISPR/Cas9 genome wide screening and future directions 42

1.4 The Reliance of Viruses on Host Genes *44*

1.4.1 Identification of viral host dependency factors using CRISPR/Cas9 genome wide screening 45

1.5 Paramyxoviruses and Pneumoviruses *46*

1.5.1 The pathological significance of Paramyxoviruses and Pneumoviruses 46

1.5.2 Taxonomy, phylogeny, and classification of Paramyxoviruses and Pneumoviruses 49

1.5.3 Paramyxovirus virion structure and the infectious cycle 50

1.5.4 Paramyxovirus genome structure, transcription, and replication 53

1.5.4.1 Paramyxovirus genome structure 53

1.5.4.2 Paramyxovirus transcription 54
1.5.4.3 Paramyxovirus replication 56
1.5.5 IFN antagonism by Paramyxoviruses 57
1.5.6 Antiviral restriction factors of Paramyxoviruses 58
1.6 Research Objectives *60*
Chapter 2: Materials 61
2.1 Prokaryotic Cell Culture *62*
2.2 Mammalian Cell Culture *62*
2.3 Viruses *66*
2.4 Plasmids *67*
2.5 Oligonucleotides *70*
2.6 Enzymes *75*
2.7 Standards *76*
2.8 Buffers and Solutions *76*
2.9 Chemicals *77*
2.10 Kits *77*
2.11 Antibodies *78*
2.12 Instruments and Equipment *80*
2.13 Computer Programmes *80*
Chapter 3: Methods 81
3.1 Cell culture *82*
3.1.1 Cell maintenance 82
3.1.2 Single cell cloning 82
3.1.3 Mycoplasma testing of cell cultures 82
3.1.4 Cryopreserving and resuscitation of cells 83
3.1.5 Lentiviral transductions of A549 cell lines 83
3.2 Microbiological methods *84*
3.2.1 Preparation of competent E. coli 84
3.2.2 Storage of E. coli 84
3.3 Molecular biology techniques *85*
3.3.1 Transformation of E. coli by heat shock 85
3.3.2 Transformation of electrocompetent cells with DNA library 85
3.3.3 Small scale plasmid isolation from E. coli 85

3.3.4 Large scale plasmid isolation from E. coli 86
3.3.5 Cloning 86
3.3.6 Restriction digest of cloning vectors 86
3.3.7 Agarose gel electrophoresis 87
3.3.8 Gel and PCR clean-up 87

3.4 Quantitative PCR *87*
3.4.1 Isolation of cellular RNA 87
3.4.2 cDNA synthesis 88
3.4.3 RT-qPCR 88

3.5 Lentiviral vectors *88*
3.5.1 Transfection of 293T cells for lentivirus production by calcium phosphate precipitation 88
3.5.2 Titration of lentivirus using flow cytometry 88
3.5.3 Titration of lentivirus using colony forming units 89

3.6 Virological techniques *89*
3.6.1 Preparation of virus stocks 89
3.6.2 Plaque assay 89
3.6.3 Titration of virus stocks 90
3.6.4 Measuring plaque size 90

3.7 Protein biochemistry *90*
3.7.1 Western blot 90

3.8 Imaging *91*
3.8.1 EVOS microscopy 91

3.9 Flow cytometry and cell sorting *91*
3.9.1 Flow cytometry (fluorescent reporter virus) 91
3.9.2 Flow cytometry (antibody staining) 92
3.9.3 Analysis with FlowJo software 92
3.9.4 Fluorescence activated cell sorting 92

3.10 Genome wide CRISPR/Cas9 knockout screening *93*
3.10.1 Production of screening library lentivirus 93
3.10.2 Transduction of cell with library lentivirus 93
3.10.3 Infection of cells with hPIV3-GFP 93
3.10.4 Harvesting cells for FACS 93
3.10.5 Fluorescence activated cell sorting 94
3.10.6 Isolation of gDNA 94
3.10.7 Preparation of gDNA for NGS 94
3.10.8 Analysis of NGS data (MaGeCK) 96
3.10.9 Analysis of NGS data (Panther Gene Ontology analysis) 96
3.10.10 Analysis of NGS data (DAVID pathway analysis) 97

Chapter 4: Optimisation of a genome wide CRISPR/Cas9 screening platform for the identification of hPIV3 host dependency factors 98

4.1 Introduction *99*

4.2 Overview of assay workflow *99*

4.3 Generation of resources for genome-wide screening *102*

4.4 Optimisation of experimental conditions for genome-wide screening *108*

4.5 Identification of hPIV3-GFP(JS) host dependency factors using genome-wide screening *116*

4.6 Validation of hPIV3-GFP(JS) host dependency factors identified through screening *121*

4.7 Summary *123*

Chapter 5: A genome wide CRISPR/Cas9 screening platform for the identification of hPIV3 antiviral restriction factors 124

5.1 Introduction *125*

5.2 Optimisation of experimental conditions for genome-wide screening *125*

5.3 Identification of hPIV3-GFP(JS) antiviral factors using genome-wide screening *129*

5.4 Development of CRISPR-Cas9 genome-wide screening to improve identification antiviral factors *136*

5.5 Summary *145*

Chapter 6: Characterisation of Paramyxovirus antiviral restriction factors 147

6.1 Introduction *148*

6.2 Characterisation of AF hits as restriction factors of hPIV3-GFP(JS) *148*

6.2.1 Functional characterisation of antiviral restriction factor deficient cell lines 148

6.2.2 Low MOI validation of hPIV3-GFP(JS) antiviral restriction factors 150

6.3 Moesin-Ezrin-Radixin Like (MERLIN) Tumour Suppressor (NF2) *151*

6.3.1 PIV3 NP expression following infection of NF2 deficient cells 151

6.3.2 Virus resistance in NF2 deficient cells following IFN-α pre-treatment 152

6.3.3 Induction and regulation of type I IFN induction in NF2 deficient cells 153

6.3.4 Induction and regulation of type I IFN signalling in NF2 deficient cells 156

6.3.5 Regulation of IRF3 IFN induction by NF2 158

6.4 Hydroxysteroid 17-Beta Dehydrogenase 12 (HSD17B12) *159*

6.4.1 PIV3 NP expression following infection of HSD17B12 deficient cells 159

6.4.2 Virus resistance in HSD17B12 deficient cells following IFN-α pre-treatment 160

6.4.3 Induction and regulation of type I IFN induction in HSD17B12 deficient cells 161

6.4.4 Induction and regulation of type I IFN signalling in HSD17B12 deficient cells 164

6.5 Zinc Finger CCCH-Type Containing, Antiviral 1 (ZAP) *166*
6.5.1 PIV3 NP expression following infection of ZAP deficient cells 166
6.5.2 Virus resistance in ZAP deficient cells following IFN-α pre-treatment 167
6.5.3 Induction and regulation of type I IFN induction in ZAP deficient cells 168
6.5.4 Induction and regulation of type I IFN signalling in ZAP deficient cells 171
6.5.5 CpG dinucleotide analysis of PIV3 173
6.6 Effect of hPIV3(JS) antiviral restriction factors on other Paramyxo- and Pneumoviruses *175*
6.7 Summary *180*
Chapter 7: Discussion 182
7.1 Introduction *183*
7.2 Analysis of hPIV3(JS) host dependency factors *183*
7.2.1 Glycosylation and virus entry 184
7.2.2 Limitations in validating host dependency factors 186
7.3 NF2 *187*
7.3.1 NF2 and the Hippo-YAP pathway 187
7.3.2 A novel role of NF2 in IFN signalling 188
7.4 HSD17B12 *189*
7.4.1 HSD17B12 and lipid droplets 190
7.4.2 The interaction between lipid droplets and ISGs 191
7.4.3 Other implications of HSD17B12 deficiency 192
7.5 ZAP *195*
7.5.1 ZAPS 195
7.5.2 ZAPL 196
7.5.3 The relationship between ZAP function and RNA dinucleotide content 198
7.6 Exploiting the role of ISG15 as a negative regulator of the IFN response *202*
7.7 Conclusion *203*
References 205
Appendix 226

List of Figures

Figure 1.2.1.1: Classes of IFN and their receptors. 27

Figure 1.2.2.1.1: RLR-dependent activation of the IFN induction pathway by RNA viruses. 29

Figure 1.2.3.1: Type I IFN activation of the IFN signalling pathway. 31

Figure 1.2.4.1: Antiviral factors target every stage of the virus life cycle. 32

Figure 1.2.5.1: Regulatory role of ISG15 in IFN signalling. 34

Figure 1.3.5.1: Schematic representation of the quantitative working window for identification of ISGs. 43

Figure 1.5.1.1: Causes of pneumonia cases by pathogen from multi-site etiological study. 48

Figure 1.5.3.1: Model Paramyxovirus virion particle. 50

Figure 1.5.2.1: Phylogenetic tree showing the relationship between Paramyxoviridae and Pneumoviridae. 51

Figure 1.5.4.1.1: Genome structure of Paramyxoviruses across different families. 54

Figure 1.5.4.2.1: Schematic diagram representing Paramyxovirus genome transcription. 55

Figure 1.5.4.3.1: Schematic diagram representing Paramyxovirus genome replication. 57

Figure 4.2.1: Workflow outlining the process of genome-wide CRISPR-Cas9 knockout screening. 101

Figure 4.2.2: Flow chart demonstrating the decision process in refining hits identified during screening for further validation. 102

Figure 4.3.1: Generation of sgRNA lentivirus library for genome-wide screening. 105

Figure 4.3.2: sgRNA coverage in library transduced cells. 106

Figure 4.3.3: Generation of hPIV3-GFP(JS) virus stock. 107

Figure 4.4.1: Optimisation of sorting and infection conditions for genome-wide screening. 110

Figure 4.4.2: Sorting strategy effectively isolates hPIV3-GFP(JS) positive cells. 111

Figure 4.4.3: Gating allows separation of GFP low, medium, and high fractions. 112

Figure 4.4.5: Formaldehyde inactivation of hPIV3-GFP(JS). 115

Figure 4.5.1: Identification of genes within hPIV3-GFP(JS) negative population. 118

Figure 4.5.2: Gene ontology analysis of genes identified within the hPIV3-GFP(JS) negative population. 119

Figure 4.6.1: Validation of hPIV3-GFP(JS) host dependency factors. 123

Figure 5.2.1: Optimisation of infection conditions for identification of antiviral restriction factors. 127

Figure 5.2.2: Sorting and treatment strategy effectively allows isolation of antiviral factor knockout cells. 129

Figure 5.3.1: Identification of genes and processes within hPIV3-GFP(JS) high population within A549-Cas9 cells. 131

Figure 5.3.2: Gene ontology analysis of genes identified within the hPIV3-GFP(JS) high population. 132

Figure 5.3.3: Validation of hPIV3-GFP(JS) antiviral restriction factors. 136

Figure 5.4.1: Functional characterisation of IFIT1-/- clonal cell lines. 137

Figure 5.4.2: ISG15-/- results in enhanced IFN-dependent virus restriction. 141

Figure 5.4.3: Multiple restriction factors are required to inhibit PIV5 replication. 143

Figure 5.4.4: ISG15-/- cells enable identification of antiviral factors that restrict viruses more resistant to IFN. 145

Figure 6.2.1.1: Functional characterisation of antiviral factor deficient cell lines. 149

Figure 6.2.2.1: Antiviral restriction factors are able to restrict virus replication at low multiplicity of infection. 151

Figure 6.3.1.1: hPIV3(JS) NP expression is increased in NF2 deficient cells over time. 152

Figure 6.3.2.1: Permissiveness of A549-Cas9.NF2$^{-/-}$ cells to hPIV3(JS) infection reduces with longer IFN-α pre-treatment. 153

Figure 6.3.3.1: NF2 is not IRF3 inducible but instead, regulates IFN induction. 155

Figure 6.3.4.1: NF2 is not IFN inducible but instead, regulates IFN signalling. 158

Figure 6.3.5.1: Increased IRF3 turnover in NF2 knockout cells following induction of IFN induction. 159

Figure 6.4.1.1: hPIV3(JS) NP expression is increased in HSD17B12 deficient cells over time. 160

Figure 6.4.2.1: Permissiveness of A549-Cas9.HSD17B12$^{-/-}$ cells to hPIV3(JS) infection does not change with longer IFN-α pre-treatment. 161

Figure 6.4.3.1: HSD17B12 is not IRF3 inducible but instead, regulates IFN induction. 163

Figure 6.4.4.1: HSD17B12 is not IFN inducible but instead, regulates IFN signalling. 166

Figure 6.5.1.1: hPIV3(JS) NP expression is increased in ZAP deficient cells over time. 167

Figure 6.5.2.1: Permissiveness of A549-Cas9.ZAP$^{-/-}$ cells to hPIV3(JS) infection does not change with longer IFN-α pre-treatment. 168

Figure 6.5.3.1: ZAP is IRF3 inducible and regulates IFN induction. 170

Figure 6.5.4.1: ZAP does not play a fundamental role during IFN signalling. 173

Figure 6.5.5.1: Analysis of dinucleotide O:E ratios within PIV3 genomes. 174

Figure 6.6.1: NF2, HSD17B12, and ZAP are able to restrict other Paramyxo- and Pneumoviruses additional to hPIV3(JS). 179

Figure 7.2.1.1: Host dependency hits within the glycosylation pathway. 185

Figure 7.3.1: Mechanisms of NF2 in regulating the IFN response. 189

Figure 7.4.1: Role of HSD17B12 is regulating IFN induction. 194

Figure 7.5.1: Schematic of ZAP isoform gene structures. 195

Figure 7.5.2: Mechanism of action of two ZAP isoforms. 198

Figure 7.5.3.1: CpG dinucleotide content across viruses. 200

Figure 7.5.3.2: Mechanism of ZAP evasion by dinucleotide suppression. 201

Appendix 1: Code for the analysis of NGS screening data and generation of volcano plots 227

Appendix 2: Additional data from biological repeats of PIV3 NP time course in NF2, HSD17B12 and ZAP deficient cells. 231

Appendix 3: Additional data from biological repeats investigating IFN-β mRNA expression following DI treatment using RT-qPCR. 232

Appendix 4: Additional data from biological repeats investigating ISG15 mRNA expression following DI treatment using RT-qPCR. 233

Appendix 5: Additional data from biological repeats investigating MxA mRNA expression following IFN treatment using RT-qPCR. 234

Appendix 6: Additional data from biological repeats investigating ISG15 mRNA expression following IFN treatment using RT-qPCR. 235

Appendix 7: Additional data from biological repeats investigating HERC5 mRNA expression following IFN treatment using RT-qPCR. 236

List of Tables

Table 1.5.2.1: Taxonomic summary of the Paramyxovirus and Pneumovirus families. 52

Table 2.1.1: E. coli strains used within thesis. 62

Table 2.1.2: Reagents for E. coli work. 62

Table 2.2.1: Naïve mammalian cell lines used. 62

Table 2.2.2 Mammalian cell lines generated. 62

Table 2.2.3: Mammalian cell culture media, additives, and supplements. 65

Table 2.2.4: Solutions, chemicals, and other reagents used in mammalian cell culture. 65

Table 2.3.1: List of viruses. 66

Table 2.4.1: Table of external plasmids used. 67

Table 2.4.2: Table of generated plasmids used. 68

Table 2. 5.1: Details of RT-qPCR primers used. 70

Table 2.5.2: Details of PCR primers for Mycoplasma testing. 70

Table 2.5.3: Details of sequencing primers used. 70

Table 2.5.4: sgRNA oligonucleotides for gene knockout. 71

Table 2.5.5: Primers used for next generation sequencing of screening gDNA. 74

Table 2.6.1: Restriction enzymes used within thesis. 75

Table 2.6.2: Modifying enzymes used in thesis. 75

Table 2.7.1: List of standards used in thesis. 76

Table 2.8.1: Buffers and Solutions used in thesis. 76

Table 2.9.1: Chemicals not previously mentioned. 77

Table 2.10.1: Commercial kits used in thesis. 77

Table 2.11.1: Details of primary antibodies used. 78

Table 2.11.2: Details of secondary antibodies used. 79

Table 2.12.1: Key instruments and laboratory equipment used within thesis. 80

Table 2.13.1: Details of software and databases used within thesis. 80

Table 3.1.3.1: Reaction set-up for amplification of mycoplasma DNA 83

Table 3.1.3.2: Thermocycler conditions for amplification of mycoplasma DNA. 83

Table 3.10.7.1: Reaction set-up for amplification of isolated gDNA during first round PCR. 95

Table 3.10.7.2: Thermocycler conditions for amplification of isolated gDNA during first round PCR. 95

Table 3.10.7.3: Reaction set-up for barcoding of gDNA fractions during second round PCR. 96

Table 3.10.7.4: Thermocycler conditions for barcoding of gDNA fractions during second round PCR. 96

Table 4.5.1: PANTHER gene ontology analysis of hPIV3-GFP(JS) host dependency factors. 120

Table 5.3.1: PANTHER gene ontology analysis of validated hPIV3-GFP(JS) antiviral factors. 134

Table 6.6.1: Summary of data from figure 6.6.1. 179

Table 6.6.2: MaGeCK rankings of NF2, HSD17B12 and ZAP in genome wide CRISPR/Cas9 screens within the literature. 180

Table 7.2.1: MaGeCK rankings of eight host dependency factor hits selected for validation. 184

Abbreviations

Viruses

AAV	Adeno-associated virus
ASPV	Atlantic salmon paramyxovirus
bPIV3	Bovine parainfluenza virus type 3
BUNV	Bunyamwera virus
BVDV	Bovine viral diarrhoea virus
CDV	Canine distemper virus
CMV	Cytomegalovirus
CPI	Canine parainfluenza virus
DENV	Dengue virus
EBOV	Ebola virus
FDLV	Fer-de-lance virus
HBV	Hepatitis B virus
HCMV	Human cytomegalovirus
HCV	Hepatitis C virus
HeV	Hendra virus
HIV	Human immunodeficiency virus
HMPV	Human metapneumovirus
hPIV2	Human parainfluenza virus type 2
hPIV3	Human parainfluenza virus type 3
HPV	Human papillomavirus
HSV	Herpes simplex virus
IAV	Influenza A virus
JEV	Japanese encephalitis virus
KSHV	Kaposi's sarcoma-associated virus
LCMV	Lymphocytic Choriomeningitis Virus
MeV	Measles virus
MuV	Mumps virus
NDV	Newcastle disease virus
NiV	Nipah virus
PIV	Parainfluenza virus
PIV5	Parainfluenza virus 5
PPRV	Peste des petits ruminants virus
RPV	Rinderpest virus
RSV	Respiratory syncytial virus
RVFV	Rift valley fever virus
SARS-CoV-2	Severe acute respiratory syndrome coronavirus 2
SeV	Sendai virus

SINV	Sindbis virus
SV5	Simian virus 5
VACV	Vaccinia virus
VSV	Vesicular stomatitis virus
WNV	West Nile virus
YFV	Yellow fever virus
ZIKV	Zika virus

Units

%	Percentage
% [v/v]	% (volume per volume)
% [w/v]	% (weight per volume)
°C	Degrees Celsius
a.u	Arbitrary units
CFU	Colony forming units
Ct	Cycle threshold
d.p.i	Days post infection
h	Hour
h.p.i	Hours post infection
kDa	Kilo Dalton
MFI	Mean fluorescence intensity
mg	Milligram
min	Minute
mL	Millitre
mM	Millimolar
MOI	Multiplicity of infection
MW	Molecular weight
nm	Nanometres
nt	Nucleotide
O:E	Observed to expected ratio
PFU	Plaque forming units
rpm	Revolutions per minute
RT	Room temperature
s	Second
SD	Standard deviation
wt	Wild type
x g	Times gravity
µg	Microgram
µl	Microlitre

µM	Micromolar

Genes and proteins of interest

CARD	Caspase activation and recruiting domain
DAXX	Death domain-associated protein
DHX9	DExH-Box Helicase 9
EGFR	Epidermal growth factor receptor
EIF4EBP3	Eukaryotic translation initiation factor 4E-binding protein 3
ELF1	E74-Like Factor 1
GNPTAB	N-Acetylglucosamine-1-Phosphate Transferase Subunits Alpha and Beta
HERC5	HECT And RLD Domain Containing E3 Ubiquitin Protein Ligase 5
HMOX1	Heme oxygenase-1
HSD17B12	17-beta hydroxysteroid dehydrogenase-12
IFIT	Interferon-induced protein with tetratricopeptide repeats
IFITM	Interferon-induced transmembrane protein
IFNAR	Interferon alpha/ beta receptor
IFNGR	Interferon gamma receptor
IFNLR	Interferon lambda receptor
IKK	IκB kinase
IKKε	Inhibitor of nuclear factor kappa-B kinase ε
IMP3	U3 Small Nucleolar Ribonucleoprotein 3
IRAK	Interleukin-1 receptor associated kinase
IRF3	Interferon regulatory factor 3
IRGM	Immunity-related GTPase family M protein
ISG15	Interferon stimulated gene 15
ISGF3	Interferon stimulated gene factor 3
ISRE	Interferon sensitive response element
KHNYN	KH And NYN domain containing protein
LATS1/2	Large Tumour Suppressor Kinase 1/2
MAVS	Mitochondrial antiviral signalling protein
MDA5	Melanoma differentiation associated gene 5
MST1/2	Macrophage Stimulating 1/2
MxA	Human myxovirus resistance protein 1
NEMO	NF-κB essential modulator
NF2	Moesin-Ezrin-Radixin Like (MERLIN) Tumour Suppressor
OAS	2'-5'-oligoadenylate synthetase
OST	Oligosaccharyltransferase
P2RY14	P2Y purinoceptor 14
PKR	Protein kinase R

PPA2	Pyrophosphatase 2
PTAR1	Protein Prenyltransferase Alpha Subunit Repeat Containing 1
RAD51	RAD51 Recombinase
RIG-I	Retinoic acid inducible gene I
SKP2	S-phase kinase-associated protein 2
SLC35A1	Solute carrier family 35 member A1
SMU1	DNA Replication Regulator And Spliceosomal Factor
SPRY	SP1A kinase of Dictyostelium and rabbit Ryanodine receptor
STING	(cGAS)-stimulator of interferon genes
STT3A	Oligosaccharyltransferase Complex Catalytic Subunit A
TAZ	Phospholipid-lysophospholipid transacylase
TDRD7	Tudor Domain Containing 7
TEAD	Transcriptional enhanced associate domain
TRAF	tumour necrosis factor receptor associated factor
TRIM25	Tripartite motif-containing protein 25
UFC1	Ubiquitin-Fold Modifier Conjugating Enzyme 1
USP18	Ubiquitin specific peptidase 18
YAP	Yes-associated protein 1
ZAP	Zinc finger CCCH-type containing, antiviral 1
ZAPL	ZAP long isoform
ZAPS	ZAP short isoform

Other

A549	Adenocarcinoma human alveolar basal epithelial cells
ADP	Adenosine diphosphate
ANOVA	Analysis of variance
BAGEL	Bayesian analysis of gene essentiality
BFP	Blue fluorescent protein
CDC	Centres for disease control and prevention
CMP	Cytidine monophosphate
CO_2	Carbon dioxide
CRISPR	Clustered regularly interspaced short palindromic repeats
DAVID	Database for annotation, visualization and integrated discovery
DI	Defective interfering particles
DMEM	Dulbecco's modified eagle medium
DMSO	Dimethyl sulfoxide
DNA	Deoxyribonucleic acid
dNTP	Deoxynucleotide triphosphate
dsRNA	Double stranded ribonucleic acid

ECL	Enhanced chemiluminescence
EDTA	Ethylenediaminetetraacetic acid
F	Fusion protein
FACS	Fluorescence activated cell sorting
FBS	Foetal bovine serum
FCS	Foetal calf serum
FDA	US food and drug administration
FDR	False discovery rate
FFPE	Formalin-Fixed Paraffin-Embedded
FSC	Forward scatter
GAF	Gamma-activated factor
GAS	Gamma interferon activation site
GE	Gene end
GeCKO	Genome-scale CRISPR-Cas9 knockout screens
GFP	Green fluorescent protein
GS	Gene start
HDF	Host dependency factor
HEK	Human embryonic kidney
HEPES	4-(2-hydroxyethyl)-1-piperazineethanesulfonic acid
HRP	Horseradish peroxidase
IFN	Interferon
IRF	Interferon regulatory factor
ISG	Interferon stimulated gene
JAK	Janus kinase
L	Large protein
LD	Lipid droplet
Le	Leader
LRTI	Lower respiratory tract infection
LTR	Long terminal repeat
M	Molar
M	Matrix protein
MaGeCK	Model-based Analysis of Genome-wide CRISPR-Cas9 Knockout
MOPS	3-(N-morpholino) propane sulfonic acid
mRNA	Messenger ribonucleic acid
MRPS	Multidrug resistance proteins
N	Nucleocapsid protein
NCBI	National centre for biotechnology information
NGS	Next generation sequencing
NHEJ	Non-homologous end joining
NIH	National institutes of health

ns	Non-significant
NS1/2	non-structural protein 1/2
ORF	Open reading frame
P	Polymerase-associated protein
PAMP	Pathogen associated molecular pattern
PARP	Poly (ADP-ribose) polymerases
PBS	Phosphate buffered saline
PCR	Polymerase chain reaction
PERCH	Pneumonia Etiology research for child health
PGE_2	Prostaglandin E2
PNK	Polynucleotide kinase
ppp-RNA	5’ triphosphate single stranded RNA
PRR	Pathogen recognition receptor
PVDF	Polyvinylidene difluoride
RBP	RNA binding protein
RLR	RIG-I like receptor
RNA	Ribonucleic acid
RRA	Robust rank aggregation
Rux	Ruxolitinib
SDS	Sodium dodecyl sulphate
SDS-PAGE	Sodium dodecyl sulphate–polyacrylamide gel electrophoresis
sgRNA	Single guide RNA
SH	Small hydrophobic protein
shRNA	Short hairpin ribonucleic acid
siRNA	Small interfering ribonucleic acid
SSC	Side scatter
ssRNA	Single stranded ribonucleic acid
STAT	Signal transducer and activator of transcription
TBE	Tris-borate-EDTA
TIR	Toll/Interleukin-1 receptor
TLR	Toll like receptor
TNF	Tumour necrosis factor
Tr	Trailer
TYK	Tyrosine kinase
UDP	Uridine diphosphate
UMP	Uridine monophosphate
UTR	Untranslated region
VLCFA	Very long chain fatty acids
vRdRP	RNA-dependent RNA polymerase

Chapter 1: Introduction

1.1 Introduction

As obligate intracellular pathogens, viruses rely on host machinery to complete their replicative cycle; virus-host interactions are therefore crucial to the infectivity of the virus and its ability to cause disease (Robinson et al., 2018). Whilst there are host dependency factors present in cells that permit the replication of viruses, there are also antiviral factors that restrict the pathogen's ability to replicate (Schoggins and Rice, 2011).

Historically, investigating virus-host interactions has been limited to investigating single to a few genes at a time, often in a manner that is hypothesis driven and requires prior knowledge of the system. Advances in molecular tools, have allowed the development of high throughput screening platforms, allowing for the identification of many genes in a single experiment. This therefore lends itself to the study of pathways which have broad signalling systems, such as the IFN response, with many genes that work in concert. Imperatively, it is the development of next generation sequencing (NGS) that has driven the field of genome wide screening forward (Schneeberger, 2014). The method relies on the ability to characterise genes resulting in a desired phenotype, and so the ability to identify and characterise output genes via sequence-based analysis reliably is key. Additionally, improvements in genome editing tools have improved the specific targeting of genes allowing more robust interpretation of resulting phenotypic change and increased reliability in the systems used (Moresco, Li and Beutler, 2013; Shalem, Sanjana and Zhang, 2015).

The most well-known of the genome wide screening techniques, and that utilised in this thesis, is genome wide CRISPR/Cas9 knockout screening. This technique employs clustered regularly interspaced short palindromic repeats (CRISPR) Cas9 genome editing, first described to target, and cleave the human genome in 2013 to introduce loss-of-function mutations, alongside the Cas9 enzyme (Cong et al., 2013; Jinek et al., 2013; Mali et al., 2013). In loss-of-function genetic engineering, the Cas9 enzyme is programmed with a single guide RNA (sgRNA) complementary to the gene of interest. Upon binding of the complex to a complementary sequence, site specific DNA cleavage occurs resulting in a double strand break. Genome engineering exploits this function of the enzyme to cause frameshift mutations resulting in disruption of gene function. These frameshift mutations are as a result of insertions and deletions caused by the error-prone mechanism of non-homologous end joining, used to repair the double strand break induced by the CRISPR/Cas9 complex in the absence of a homologous sequence (Jiang and Doudna, 2017; Khan et al., 2018). As such, this technology can be utilised in a multiplexed manner, via sgRNA libraries, to investigate complex biological systems, including virus-host interactions which will be further discussed (Shalem, Sanjana and Zhang, 2015).

1.2 Antiviral Defence and the IFN Response

The innate immune response is one of the bodies first lines of defence against incoming pathogens, including viruses, prior to the activation of the adaptive immune response. A component of the innate immune response, the interferon (IFN) response has a well-established role in responding to viral infection, with the cytokines first being named for their ability to 'interfere' with virus infection (Isaacs

and Lindenmann, 1987). This is an evolutionary conserved response which is rapid and non-specific; it is critical to the rate at which infection spreads through slowing viral replication prior to the activation of the adaptive immune response (Schneider, Chevillotte and Rice, 2014; Fensterl, Chattopadhyay and Sen, 2015). IFNs themselves are important immunomodulatory cytokines which further regulate the magnitude of this host response. As well as leading to antiviral defence within the cell, they also play other roles in both limiting host tissue damage (Lee and Ashkar, 2018) and promoting it, dependent of the subtype of IFN expressed (Major et al., 2020).

The IFN response is comprised of the IFN induction pathway, whereby incoming pathogens are recognised leading to the production of IFNs, and the IFN signalling pathway, leading to the expression of hundreds of interferon stimulated genes (ISGs). These genes can be powerful antiviral restriction factors, important pathway regulatory factors, or both (Schoggins et al., 2011).

1.2.1 Classes of IFN and their properties

Cytokines within the IFN family have been further subdivided based on the receptor type they bind to; type I IFN and the IFN alpha receptor (IFNAR), type II IFN and the IFN gamma receptor (IFNGR), and type III IFN and the IFN lambda receptor (IFNLR) (Regulation of type i interferon responses; Levy, Marié and Durbin, 2011; Lee and Ashkar, 2018) (figure 1.2.1.1).

Type I IFN consists of 13-16 subtypes, a number debated in the literature, including one IFN-β and multiple IFN-α, all of which maintain similar structural homology (Platanias, 2005; Walter, 2020). There is no cell type specificity for type I IFN production with the route of viral infection and tissue tropism of the virus determining the site. For example, mucosal infections may result in expression of type I IFN from epithelial cells or alveolar macrophages, organ infection may result in production from fibroblasts and systemic infection may result in type I IFN being secreted from monocytes or plasmacytoid dendritic cells (pDCs) (Swiecki and Colonna, 2011). It is known that the bone marrow derived pDCs secrete a large amount of type I IFN and as such, play an important role in the control of viral infections (Cella et al., 1999). Type III IFN, also known as IFN-λ, is able to establish an antiviral state in both the infected cell and surrounding, non-infected cells similar to type I IFNs. The difference to type I IFN lies in the tissue distribution, with type III IFN predominantly acting at epithelial surfaces (Ye, Schnepf and Staeheli, 2019). Conversely, type II IFN consists of IFN-γ which has no structural homology to type I or type III IFN (Platanias, 2005). As well as playing an important role in the innate immune response, it also has a well-known role in the cell-mediated adaptive immune response through immunostimulatory and immunomodulatory functions (Lee and Ashkar, 2018). Unlike type I IFN which has broad cellular sources, type II IFN is primarily secreted by immune cells including CD4+ T helper 1 (Th1) cells, natural killer (NK) cells, and CD8+ cytotoxic T cells. It also plays a key role in adaptive immunity through signalling for immune cell differentiation and activation, and the induction of major histocompatibility complex class II molecule expression (Ivashkiv, 2018).

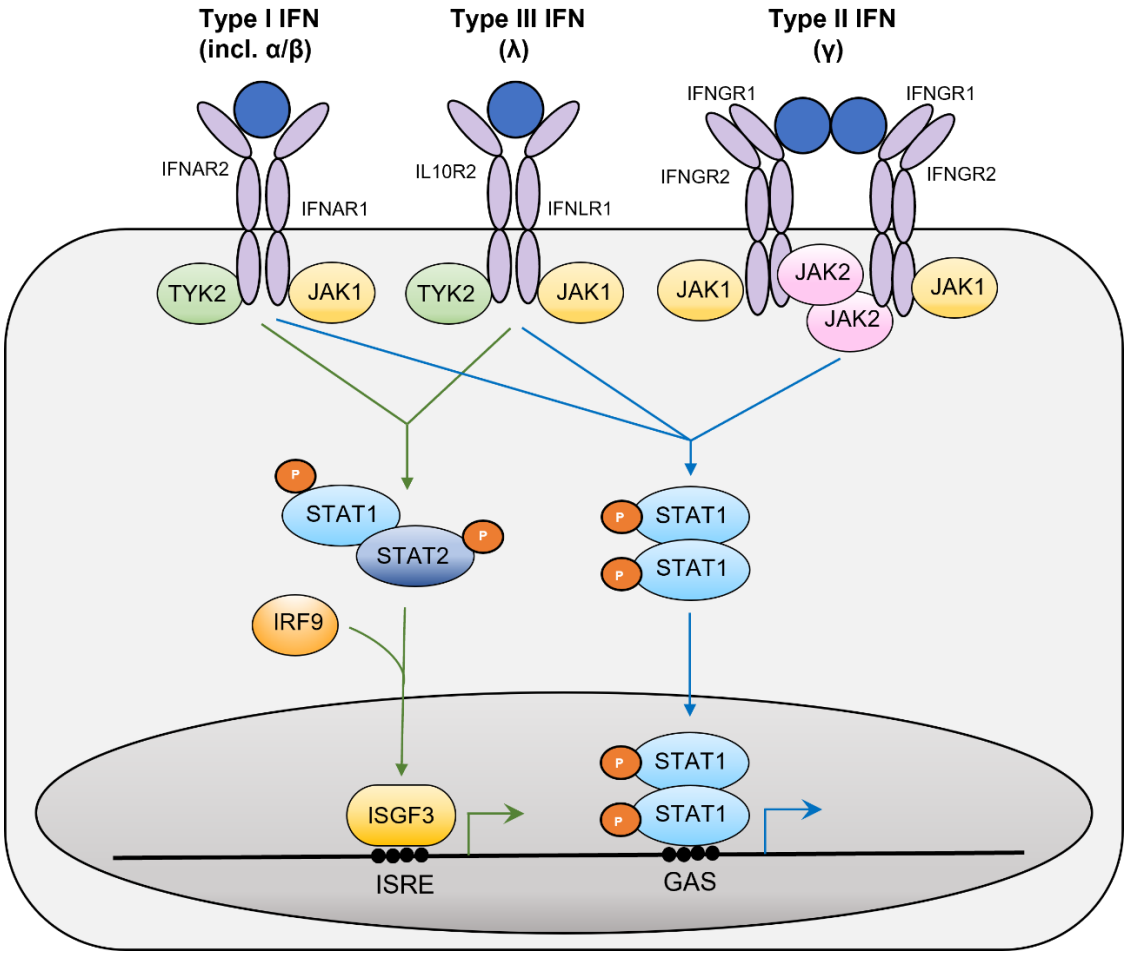

Figure 1.2.1.1: Classes of IFN and their receptors. Type I, II and III IFN (blue circles) bind to IFN alpha, gamma and lambda receptors (purple) respectively to activate downstream JAK/STAT signalling cascades. This either results in STAT1 dimerization, resulting in expression of genes from a GAS element (blue arrows) or the formation of ISGF3 resulting in expression of genes from the ISRE (green arrows).

Whilst there are differences between type I/ III and type II IFN in their respective receptors and signalling cascades the main differentiator is the resulting response with IFN γ (type II) playing an important role within adaptive immunity and IFN α/β/ λ (type I/III) having important implications in innate with the canonical role of type-I IFN being well described in both its mechanism and role in antiviral immunity. For this reason, IFN-α/β will be discussed going forward, being subsequently referred to as the 'IFN response'.

1.2.2 IFN induction by RNA viruses

The IFN induction pathway is activated by the recognition of pathogen-associated molecular patterns (PAMPs) by cellular pattern recognition receptors (PRRs). PRRs present in the cell are able to

determine self from non-self and in the case of viral infection, the PAMP recognised is predominantly viral nucleic acid. This establishes a signalling cascade leading to the production of IFN (McNab et al., 2015). Upon infection with an RNA virus, two predominant PRR types are activated; RIG-I like receptors (RLR), which are cytoplasmic sensors, and the membrane-bound toll-like receptors (TLR) (Nan, Nan and Zhang, 2014; Rehwinkel and Gack, 2020). As such, the pathways of these two receptor types will be subsequently focussed on.

1.2.2.1 RLRs

RLRs recognise virus-derived nucleic acid and include both retinoic acid-inducible gene I (RIG-I) and melanoma differentiation-associated protein 5 (MDA5) which recognise 5' triphosphate ssRNA (ppp-RNA) and long dsRNA, respectively (figure 1.2.2.1.1) (Yoneyama et al., 2004; Pichlmair et al., 2006; Ludwig et al., 2010; Rehwinkel and Gack, 2020). Upon binding of either RIG-I or MDA5 to their respective PAMPS, a conformational change in the proteins exposes a conserved caspase activation and recruitment domains (CARD). This results in a CARD-CARD domain interaction with the adaptor mitochondrial antiviral-signalling protein (MAVS) which subsequently associates with TNF Receptor Associated Factor 3 (TRAF3). Upon association of MAVS and TRAF3, TANK-binding kinase 1 (TBK1) and inhibitor of nuclear factor kappa-B kinase ε (IKKε) are recruited to directly phosphorylate Interferon regulatory factor 3 (IRF3) (Fitzgerald et al., 2003; Kawai et al., 2005). Post-phosphorylation, IRF3 is able to dimerise and translocate to the nucleus where it binds to the IFN-β promoter leading to the expression of type-I IFN and a small number of IRF3 inducible ISGs (Lin et al., 1998; Ashley et al., 2019; Duncan et al., 2023).

Alternatively, the IκB kinase (IKK), comprising of IKKα, IKKβ and IKKγ subunits (also known as NF-κB essential modulator (NEMO)), can be activated following the association of MAVS and TRAF proteins. This recruits NEMO to the MAVS complex and results in the phosphorylation of IκB. Whilst Nuclear factor kappa-light-chain-enhancer of activated B cells (NF-κB) is normally held in the cytosol by members of the IκB family, this phosphorylation event results in the ubiquitination of IκB allowing NF-κB to translocate to the nucleus, bind to κB DNA binding sites and activate downstream gene transcription (Pfeffer, 2011; Liu et al., 2017).

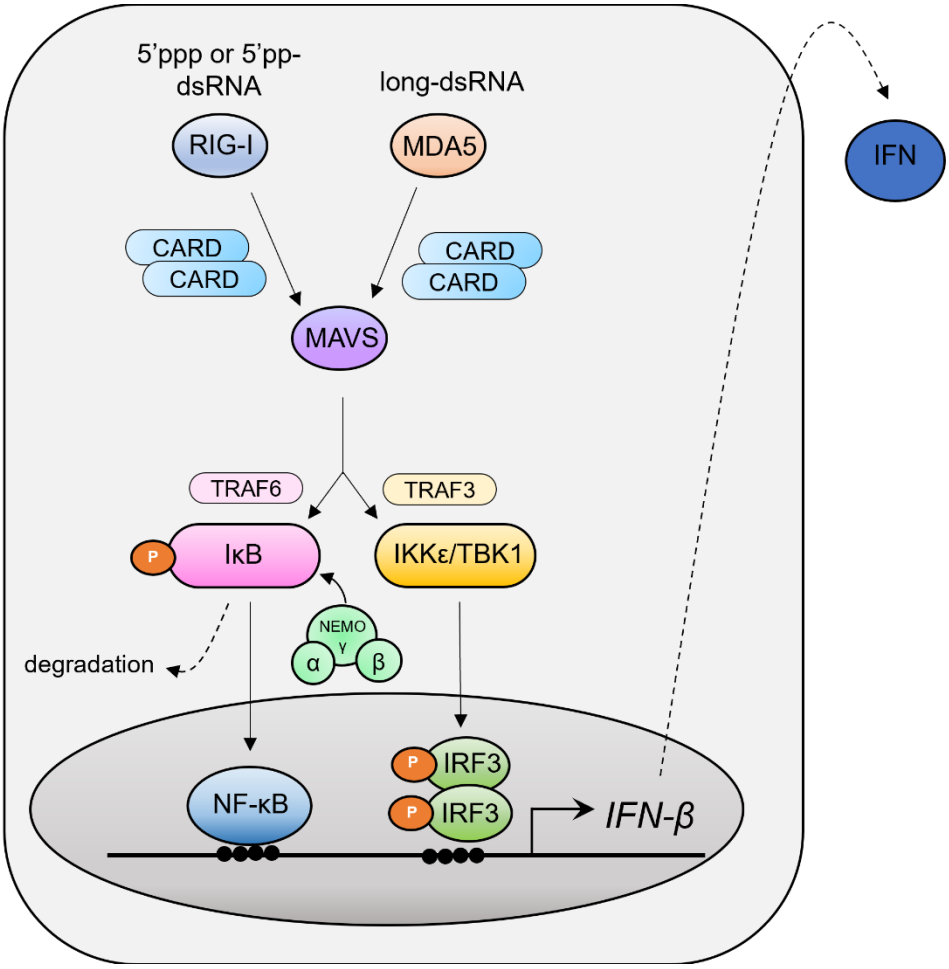

Figure 1.2.2.1.1: RLR-dependent activation of the IFN induction pathway by RNA viruses. 5' triphosphate ssRNA and long dsRNA are recognised in the cytoplasm by RIG-I and MDA-5 respectively. This causes a signalling cascade resulting in the phosphorylation and translocation of either IRF3 or NF-κB to the nucleus resulting in the transcription of IFN-β.

1.2.2.2 TLRs

TLR-7 and TLR-8, two phylogenetically and structurally related toll-like receptors located in endosomal compartments, recognise viral ssRNA through either direct infection, autophagocytic uptake of viral material from cytoplasm or phagocytic uptake of other infected cells or vial particles (Nishiya et al., 2005).

The interaction of TLR-7 or TLR-8 with ssRNA results in the recruitment of MyD88 to the receptor leading to the subsequent activation of NF-κB and IFN regulatory factor 7 (IRF7) alongside other transcription factors. The association of MyD88 to the receptor results in recruitment of interleukin-1 receptor associated kinase (IRAK-)1 and IRAK4 which are subsequently phosphorylated and dissociate from the receptor. For NF-κB activation, this dissociation results in the association of TRAF6 enabling the activation of TAK1, a protein kinase. TAK1 subsequently triggers the activation of the NF-κB transcription factor via the canonical IKK complex (NEMO) as previously described to result in the

expression of proinflammatory cytokines and chemokines (Zhou et al., 2013; Yu et al., 2020). Alternatively, TRAF3 can also be recruited into the IRAK1/ IRAK4/ TRAF6 complex to activate IRF7. IRF7 can then translocate to the nucleus, bind to ISRE elements resulting in the production of IFN-α (Oganesyan et al., 2005).

TLR-7 and TLR-8 receptors have been shown to exhibit sequence specificity that allows them to distinguish self from non-self. They have been suggested to accomplish this via recognising the location of the RNA and through identifying the level of nucleoside modification. Host RNA should contain many nucleoside modifications and non-self RNA, such as viral RNA, few (Karikó et al., 2005). Additionally, whilst the two receptor types are phylogenetically similar and are able to result in the same pathways being activated, cell type tropism and resulting gene transcription is more specific. TLR-7 receptors are primarily found in pDCs and B cells whilst TLR-8 receptors in myeloid DCs and monocytes. As such, they primarily induce IFN-α and related cytokines and proinflammatory cytokines and chemokines respectively (Gorden et al., 2005; Bender et al., 2020).

1.2.3 Type I IFN signalling

Following secretion of IFN from virally infected cells, IFN bind to the Interferon-α/β receptors (IFNAR) on neighbouring cells initiating IFN signalling and the canonical signalling cascade dependent on the Janus kinase (JAK)–signal transducer and activator of transcription (STAT) pathway (Fensterl, Chattopadhyay and Sen, 2015). This subsequently puts the cell into an antiviral state and hinders the replication of newly incoming virus particles to the cell (figure 1.2.3.1).

The IFNAR receptor is comprised of two subunits, IFNAR1 and IFNAR2, which are constitutively associated with tyrosine kinase 2 (TYK2) and Janus kinase 1 (JAK1) respectively. Upon binding of IFN to the receptor, a ligand-dependent rearrangement and dimerization of the subunits occurs resulting in the auto-phosphorylation of JAK1 and subsequent cross-phosphorylation of TYK2. Upon phosphorylation of the associated JAK proteins, signal transduction and activator of transcription proteins, STAT1 and STAT2, are tyrosine-phosphorylated resulting in dimerization. The dimer assembles with interferon regulatory factor 9 (IRF9) to form a tri-molecular complex named Interferon Stimulated Gene Factor 3 (ISGF3). It had previously been assumed that the formation of this complex occurred in the cytoplasm however, more recent studies have suggested that ISGF3 assembly occurs directly on the DNA (Platanitis et al., 2019). Here, ISGF3 binds the IFN stimulated response element (ISRE), directly activating the expression of hundreds of IFN stimulated genes (ISGs) (Schneider, Chevillotte and Rice, 2014; Hu et al., 2021).

As previously mentioned, type I IFN can also signal via STAT1 homodimers, independent of IRF9. Upon phosphorylation of the STAT1 homodimers, they are able to translocate to the nucleus and directly bind to IFN-γ-activated sites (GAS) elements within ISG promoters resulting in the expression of pro-inflammatory genes (Platanias, 2005). This pathway of signalling is also that used by type II IFN whereby binding of IFN-γ to the IFNGR receptor results in the phosphorylation of two JAK molecules and the dimerization of two STAT1 molecules. These are able to directly translocate to the nucleus and

bind to GAS elements, rather than the binding of ISGF3 to ISRE elements, for the expression of ISGs. (Platanias, 2005).

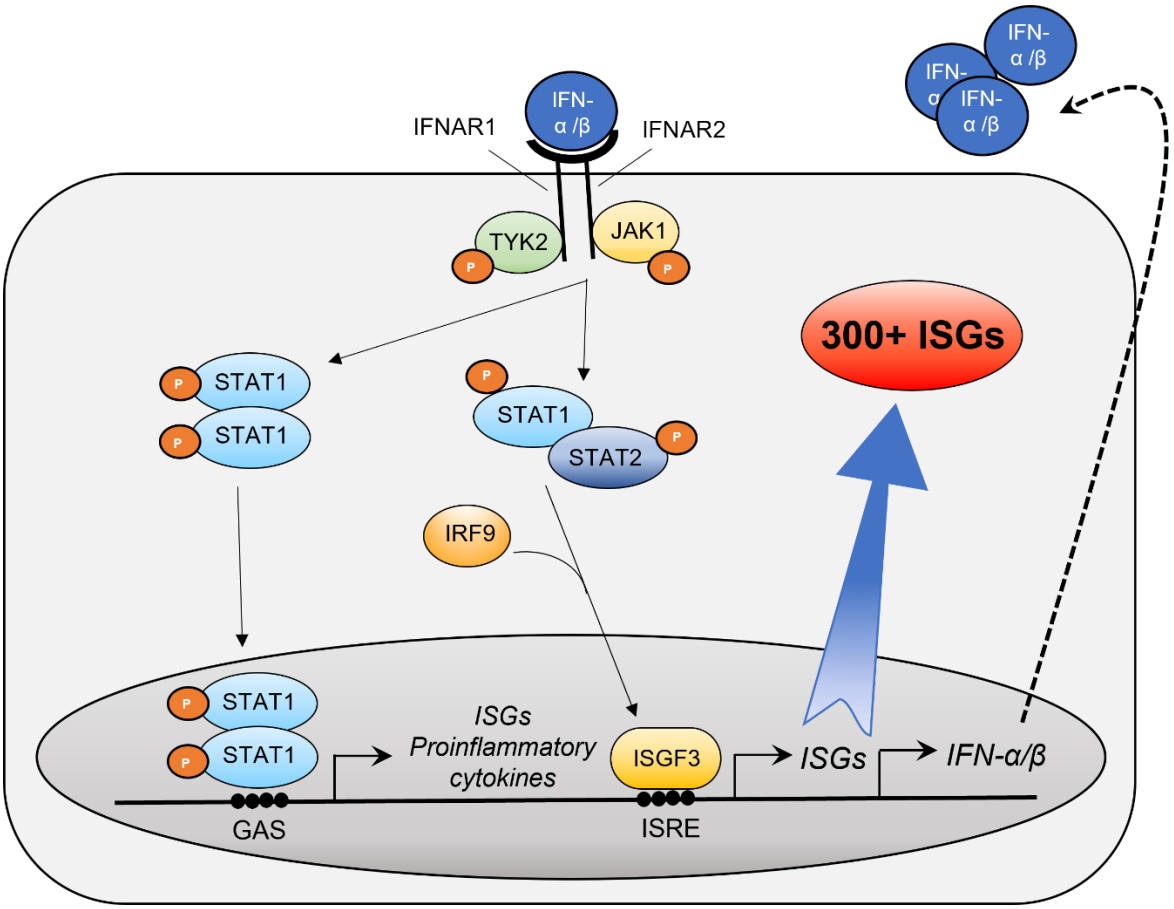

Figure 1.2.3.1: Type I IFN activation of the IFN signalling pathway. Following the binding of IFN-α/β to the IFNAR receptor, the JAK/STAT pathway is activated. This results in the phosphorylation of STAT1 and STAT2, which upon binding of IRF9, forms ISGF3. ISGF3 binds to ISRE-containing promoters in the nucleus and results in the expression of hundreds of ISGs, some of which cause a positive feedback loop for the production of more IFN-α/β. Alternatively, binding of IFN-α/β to the IFNAR receptor can result in the phosphorylation of STAT1 homodimers which can translocate to the nucleus, bind to GAS elements and result in the expression of pro-inflammatory cytokines.

1.2.4 Interferon Stimulated Gene effectors and their functions

The resulting expressed antiviral ISGs have diverse roles that target every stage of the virus life cycle (figure 1.2.4.1) (Schoggins et al., 2011). Many ISGs have broad antiviral activity, and as such can also target host cellular processes, whilst others are very specific to the viruses they target. For example, dsRNA-dependent protein kinase R (PKR) induces the shutdown of general protein translation upon activation and phosphorylation of eukaryotic translation initiation factor 2A (eIF2A), and the 2′,5′-oligoadenylate synthetase (OAS)-RNase L pathway degrades ssRNAs, including mRNAs of cellular

origin as well as viral origin (Balachandran et al., 2000; Silverman, 2007). Others, such as IFN-induced protein with tetratricopeptide repeats (IFIT) and IFN-induced transmembrane (IFITM) proteins inhibit viruses by binding specific virus components, as will be further discussed. However, many viruses remain insensitive to these direct antivirals (Schoggins et al., 2011). Whilst the fundamental role of the IFN response within host defence is known, and the role and function of many ISGs have been elucidated, this is a vast response, with many unknowns remaining. For many viruses which of the 300+ ISGs produced during this response limits infection is unknown and the function(s) of many ISGs remain unexplored. It is therefore imperative that we further understand this response if we are to better determine whether a viral infection is successful or not.

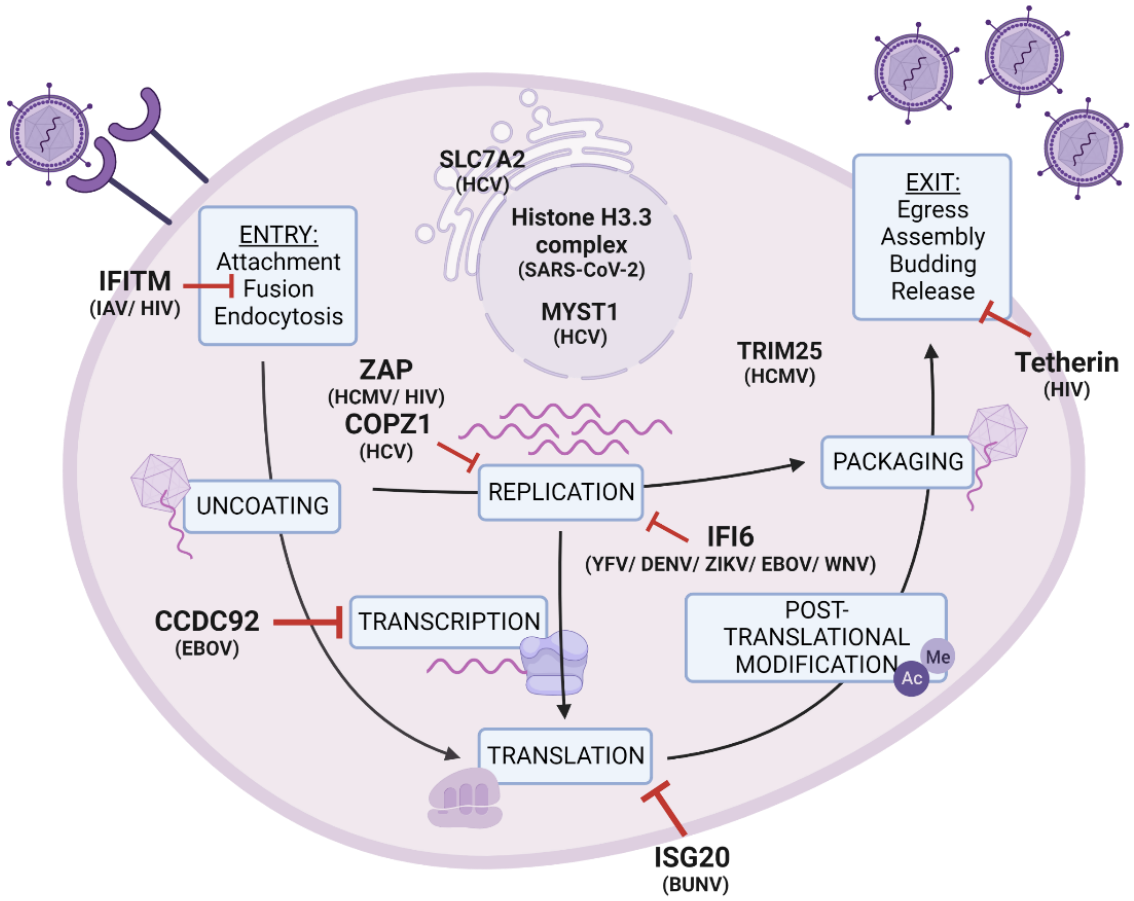

Figure 1.2.4.1: Antiviral factors target every stage of the virus life cycle. Overview of viral lifecycle with example antiviral factors for select stages (Fusco et al., 2013; Li et al., 2013; Feng et al., 2018; OhAinle et al., 2018; Richardson et al., 2018; Kuroda et al., 2020; Lin et al., 2020; Wei et al., 2020). Colours correspond to the screen design that identified them. HCV; Hepatitis C Virus, SARS-CoV-2; Severe Acute Respiratory Syndrome Coronavirus 2, IAV; Influenza A Virus, HIV; Human Immunodeficiency Virus, HCMV; Human Cytomegalovirus, EBOV; Ebola Virus, YFV; Yellow Fever Virus, DENV; Dengue Virus, ZIKV; Zika Virus, WNV; West Nile Virus, BUNV; Bunyavirus.

Notwithstanding ISGs whose role is regulating the IFN response such as ISG15 and USP18 (discussed later), there is redundancy within the direct antiviral role of the IFN response as only a small number of

proteins are expected to contribute to the antiviral response against any one virus. It is often the case that ISGs have a small to moderate antiviral effect when expressed in isolation and instead, multiple ISGs often come together to work in concert providing a synergistic effect (Hubel et al., 2019; Jones et al., 2021). For example, previous work has shown that mice defective in a broad-ranging ISG, such as PKR or OAS, are still able to produce an antiviral response indicating several factors are likely at play (Zhou et al., 1999). Which antiviral factors are responsible for restriction of which virus is mostly unknown, this makes the antiviral defence system difficult to study and finding the associated restriction factor for a virus could be likened to finding a needle in a haystack. Many techniques have been applied to try and tackle this biological question including CRISPR/Cas9 genome wide screening, ISG expression libraries and siRNA screening which will be further discussed (Jones et al., 2021). These genome wide approaches are also well placed to investigate which aspects of this broad response result in a virus-specific antiviral phenotype, and which play the aforementioned critical regulatory role.

1.2.5 Regulation of the type I IFN response

Whilst the IFN response is a key component against responding to extracellular pathogens, it needs to be tightly regulated. Previously, it has been described that IFN expression must fall within a 'Goldilocks Zone' with too little IFN expression resulting in increased susceptibility to infection and too much IFN expression leading to type-I interferonopathy and autoinflammatory disease. As such, the IFN response must be tightly regulated to remain 'just right' to maintain this balance and produced the desired antiviral effect (Taft and Bogunovic, 2018).

Such effects have been seen in patients deficient in *ISG15*, a key regulator of the IFN response. Patients with loss-of functions in ISG15 have been shown to have hallmarks of autoinflammatory disease but no experience of severe infectious disease (Zhang et al., 2015b); now known to be due the enhanced type-I IFN response in ISG15 deficient cells (Speer et al., 2016a; Holthaus et al., 2020)

Intracellular free ISG15 is known to have a regulatory function within innate immunity through the stabilisation of USP18 (Zhang et al., 2015b), a known negative regulator of the IFN response. In the presence of ISG15, USP18 stability is promoted as ubiquitination mediated by SKP2, another negative regulator of the response that causes proteasomal degradation of USP18, is prevented (Vuillier et al., 2019; Kang, Kim and Jeon, 2022). This allows USP18 to be recruited to IFNAR2 by STAT2 and inhibit ternary complex formation, therefore inhibiting subsequent signalling. However, in the absence of ISG15, the mRNA levels of USP18 are higher and the protein levels downregulated. This is due to the more rapid proteolysis of USP18 by SKP2 (Tokarz et al., 2004). Additionally, it has been shown that as well as preventing SKP2-mediated degradation of USP18, ISG15 also facilitates USP18's inhibitory function in an interaction yet characterised (figure 1.2.5.1) (Vasou et al., 2021). This example exemplifies the importance in further identifying novel genes involved in innate immunity and elucidating their mechanisms of action. ISG15 is an ISG expressed as a result of IRF3 and IFN-dependent signalling. Whilst it plays a role as a direct antiviral it also plays a key role in the regulation of the IFN response alongside many others. Despite many viruses encoding countermeasures to these antiviral

factors, our understanding of them is pivotal to understanding their weaknesses and aids our understanding of how infection can be controlled as it is harder for a virus to evolve countermeasures to a regulatory factor than a direct antiviral.

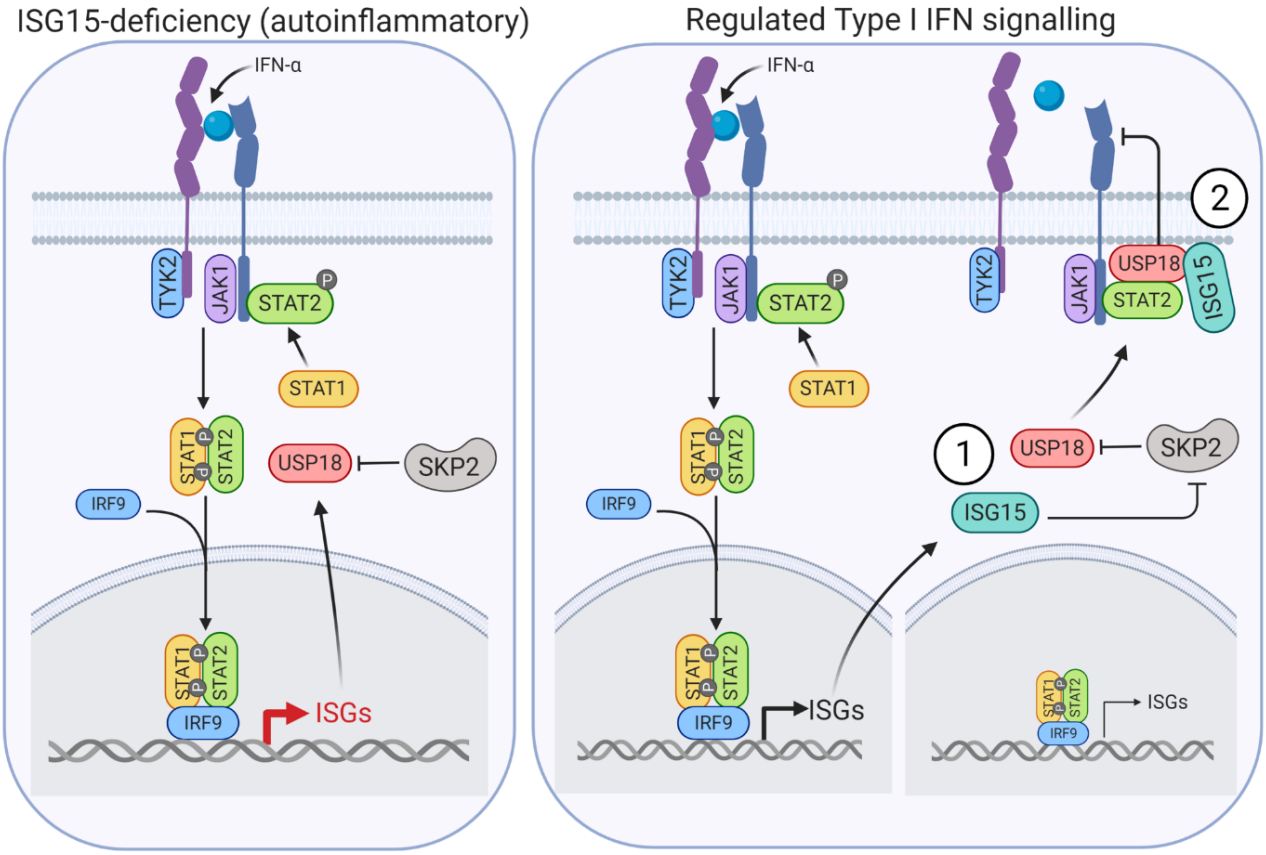

Figure 1.2.5.1: Regulatory role of ISG15 in IFN signalling. In regulated type I IFN signalling, ISG15 stabilises USP18 by preventing SKP2 mediated proteasomal degradation to prevent binding of USP18 to STAT2 at the IFNAR2 receptor. Alternatively, ISG15 can bind to USP18 through non-covalent interactions to facilitate the inhibitory activity of USP18. In cells deficient in ISG15, these interactions do not occur and USP18 is not degraded by SKP2, resulting in the overexpression of ISGs from ISRE-containing promoters (Vasou et al., 2021).

Conversely, primary immunodeficiency is also the result of genetic mutations that result in the patient being unable to clear infections (McCusker and Warrington, 2011). For example, patients were identified to have a homozygous mutation within *STAT2* leading to incorrect splicing subsequently rendering them susceptible to measles infection following routine immunisation (Hambleton et al., 2013). Interestingly, whilst potentially lethal, if *STAT2*-deficient individuals survive childhood, they remain relatively healthy indicating that other routes of ISG expression can take over from ISGF3 signalling to defend against many viral infections (Hambleton et al., 2013). As highlighted by these patients, there is a large amount of redundancy within the IFN response with many genes performing the same role. As such this makes studying this response difficult as phenotypes can be easily overcome. As such,

improvements must be made for the identification of antiviral factors if we are to fully understand the response as will be further discussed.

1.3 The use of genome wide screening for the identification of antiviral factors

As previously described, genome wide screening is a powerful tool to elucidate host genes important in the regulation of viral infection, both those that enable and hinder virus replication. To date, genome wide genetic screening has been utilised widely to identify host dependency factors required for successful virus replication in the cell. However, in comparison, these screens have been underutilised to investigate antiviral factors that hinder virus replication.

Genome wide genetic screening is well placed to identify antiviral restriction factors, including novel genes, and exclude genes not involved in the antiviral response due to the high-throughput nature of the techniques and the size of gene libraries available (Jones et al., 2021). This not only allows the identification of known and novel genes but aids the identification of the aforementioned redundant genes in the response, as will be further discussed (Schoggins et al., 2011). The identification of many genes following subsequent analysis of screening also enables the identification of whole pathways involved in the response; something not possible in single gene studies.

1.3.1 Different approaches to genome wide screening design

High-throughput screening works in a phenotype-to-genotype direction, known as forward screening; identifying a desired phenotype and attributing the genes resulting in the change rather than manipulating genes of interest then observing the resulting phenotype (Moresco, Li and Beutler, 2013; Shalem, Sanjana and Zhang, 2015). As such, the approach allows the identification of genes that would be unlikely to be identified through hypothesis-based reverse genetic screening approaches whereby prior knowledge often informs the experimental design.

Such phenotype-to-genotype screening can be further divided into arrayed or pooled screening with the latter subdivided further into either negative or positive screening (Shalem, Sanjana and Zhang, 2015). Arrayed screening involves genetic perturbators being arranged in multi-well plates where each well contains a single perturbation, whilst pooled screening utilises a library of genetic perturbators in a single environment; each having their advantages and disadvantages. Where only small culture volumes are available or a number of phenotypes are to be investigated, an arrayed format is preferred as individual wells can be treated with varying factors and be monitored with a plate reader output. However, this makes arrayed screening expensive and labour intensive unlike pooled screening which allows for the quantification of constructs within a population (Shalem, Sanjana and Zhang, 2015). With both screening methods, three readout techniques are primarily used: multi-well plate reader (Echeverri and Perrimon, 2006; Ramadan et al., 2007), microscopy (Conrad and Gerlich, 2010), and flow cytometry (Micklem et al., 2014; Misra and Green, 2017).

As mentioned, pooled screens can be further subdivided into positive and negative screens with the difference referring to how genes of interest are identified. Negative screens undergo two rounds of NGS of the sample population, both prior to and at the end of applying a selection pressure, therefore allowing identification of depleted sgRNAs. This makes it well placed to identify genes critical to cell proliferation and survival, termed essential genes. Conversely, positive screens require only a single round of NGS following application of the selection pressure or in the case of virus-host interactions, following infection. This allows for the identification of genes whose knockout leads to cell survival, such as resistance to pathogen infection (Miles, Garippa and Poirier, 2016; Sharma and Petsalaki, 2018).

As such, the remainder of the thesis, when discussing genome wide CRISPR/Cas9 knockout screening, refers to forward pooled positive screening.

1.3.2 Alternative screening approaches and their advantages and disadvantages

Whilst this thesis focusses on the use of CRISPR/Cas9 screening approaches, alternative high throughput techniques can be used to investigate virus-host interactions including, but not limited to, RNA interference (RNAi) and overexpression screening (Jones et al., 2021).

First discovered in *C. elegans* in 1998 (Fire et al., 1998), RNAi has been used in the context of genome wide screening to investigate fields including cancer biology and signalling as well as infectious disease, being first used to study virus-host interactions in 2008 to investigate host dependency factors required for influenza virus replication (Hao et al., 2008). Since, a number of RNAi screens have been undertaken to investigate virus-host interactions. These include, influenza A virus (IAV), West Nile virus (WNV) and hepatitis C virus (HCV) screens identifying antiviral restriction factors (Ng et al., 2007; Brass et al., 2009; Li et al., 2009; 2013; Tai et al., 2009) and a number of studies identifying host dependency factors for replication of viruses including measles virus (MeV), respiratory syncytial virus (RSV) (Anderson et al., 2019a), rotavirus (RV) (Silva-Ayala et al., 2013), and human papillomavirus type 16 (HPV-16) (Lipovsky et al., 2013), amongst many others (Panda and Cherry, 2015).

However, a lack of overlap in hits identified has been observed across RNAi screens investigating virus-host interactions upon infection with the same virus, with the tools used in downstream analysis noted to also contribute to the observed discrepancies (Anderson et al., 2019a). In the case of three independent Vaccinia virus (VACV) screens, no consensus hits were identified in all three studies (Mercer et al., 2012; Sivan et al., 2013; Beard et al., 2014). The lack of overlap in identified hits between screens has been suggested to be due to differences in methodology; however as previously mentioned the choice of analysis can be enough to influence the identified hits leading to inconsistencies. Despite the lack of consistency in observed hits in RNAi screening, pathway analysis is able to show that genes belonging to similar families, or acting within the same pathways, are identified across screens. For example, nuclear pore proteins have been identified as host dependency factors across multiple RNAi screens investigating VACV infection despite the same genes not being identified (Sivan et al., 2013). This allows RNAi to provide a broader overview of virus-host interactions with elevated levels of certainty at the pathway level.

The main distinction between RNAi and CRIPSR/Cas9 screening is that the former results in the transient reduction of gene levels at the mRNA level whilst the latter results in a premature stop codon, resulting in a non-functional gene, at the DNA level, therefore the duration and cell site of the genetic modulation differs with each technology (Kim and Rossi, 2008; Doudna and Charpentier, 2014). The transient knockdown of a gene has its benefits and limitations. It allows for the restoration of gene expression for validation purposes (Gupta et al., 2004) but also results in potential incomplete gene knockdown which can result in an alternative or reduced phenotype compared to complete knockout (Morgens et al., 2016; Kim et al., 2018). A comparison of resulting gene expression following either shRNA knockdown or sgRNA knockout has been investigated by Shalem et. al whereby EGFP expressing 293T cells were transduced with either 6 sgRNAs or 4 shRNAs targeting EGFP. The resulting fluorescence readout was used to assess depletion in gene expression with a lower fluorescence output correlating to a greater reduction in gene expression. Gene knockout by sgRNA resulted in elimination of fluorescence in 93% of cells, to fluorescence levels of non-EGFP expressing cells, indicating complete knockout, whilst transduction with shRNAs resulted in moderate and varied reduction in fluorescence, but higher than that of the control, indicating incomplete knockdown (Shalem et al., 2014). This correlates with other evidence suggesting incomplete knockdown by RNAi, therefore resulting in potential uncertainty in an observed phenotype when compared with sgRNA knockout. As previously discussed, the identification of antiviral restriction factors requires a strong phenotype, due to their low to moderate activity when expressed in isolation. Therefore, sgRNA knockout is better placed for this type of investigation than shRNA knockdown whereby any resulting phenotype may be masked, deemed insignificant compared to a control, and therefore excluded from further analysis.

Another known limitation of RNAi screening is the presence of off target effects (Jackson et al., 2003) which can be caused in three ways: by siRNA sequence similarity (Birmingham et al., 2006; Jackson et al., 2006), by miRNA like events (Doench, Petersen and Sharp, 2003; Sudbery et al., 2010), and by sequence independent effects (Marques and Williams, 2005). This contributes to the difficulty in reproducibility across RNAi screens due to the presence of both false negative and false positive results (Barrows et al., 2010). It is also known that siRNAs are able to induce the IFN response in a sequence independent manner (Marques and Williams, 2005; Saito and Gale, 2008). This phenomenon makes identifying antiviral restriction factors difficult as the cell will be in an unknown antiviral state prior to infection, leading to confounding results. Again, CRISPR/Cas9 screening displays a reduced immune response due to a reduced susceptibility to off target effects but in comparison, overexpression screening completely negates this limitation due to no requirement of knockdown or knockout constructs being introduced into cells.

As previously described, positive screens only select for the extreme phenotypes present in the population, and whilst many antiviral restriction factors have low to moderate activity in isolation, this presents a limitation of all techniques but increased difficulty in identifying hits from RNAi screens where incomplete knockout will have a cumulative effect on missing potentially significant results. Whilst still a limitation of all screening types, due to the redundancy in the antiviral system, CRISPR/Cas9 and overexpression libraries have a greater capacity to identify these factors with low to moderate activity.

Overexpression libraries have been generated and subsequently improved over time for the study of the antiviral response. An overexpression library consisting of 488 different ISGs was released in 2016 being expanded to over 800 genes in 2019 by Rihn et al (Schoggins et al., 2011; Kane et al., 2016; Rihn et al., 2019). The library includes both ISGs of human and Rhesus macaque origin with over 300 genes having variants of both species. This is in comparison to the CRISPR/Cas9 ISG library that encodes for over 1900 genes (OhAinle et al., 2018). The use of a combined human and macaque ISG library in overexpression screening is not uncommon and allows for the identification of potential zoonotic contributors. Such an ISG overexpression screen was used by Feng et. al. to investigate antiviral factors that restrict early stages of the Bunyamwera orthobunyavirus (BUNV) life cycle (Feng et al., 2018). A GFP expressing version of the prototypic virus was used to enable a flow cytometry based readout following infection. From the overexpression library, 20 ISGs were found to have inhibitory properties against the virus with 13 having isoforms in both the human and macaque libraries. The resulting hits were subsequently tested against 15 other bunyaviruses from four different families of both clinical and agricultural significance. Of these, *ISG20*, a well-characterised antiviral factor against many different viruses, was identified as both a human and macaque orthologue, displaying antiviral effects to varying degrees against 9 of the 15 viruses tested against. Feng et. al. observed varying activity between human and macaque ISG orthologues, an effect also seen by Kane et. al. who observed greater than one third of ISGs restricting 11 different retroviruses within the macaque population (Kane et al., 2016; Feng et al., 2018). This indicates that there is species-dependent variation in ISG activity with non-human isoforms exhibiting divergent specificities (Kane et al., 2016). This then poses the question as to whether these species-dependent activities contribute to zoonotic events between hosts and whether sequence differences in the macaque orthologues render some viral counter measures ineffective.

Mechanistic details of the aforementioned screening methods lead to advantages and disadvantages of each technique (Jones et al., 2021). These can be used to influence the choice of screening design based on the experiments aim, with the library choice influencing what genes are identifiable at the end of the screening process. For example, whilst the ISG overexpression library previously described is well placed to identify antiviral factors, it is only able to identify antiviral factors that are already characterised (Schoggins and Rice, 2011), whilst a genome wide library has the ability to identify genes that may be antiviral restriction factors but have yet to be characterised as such, giving the ability to identify novel genes involved in virus-host interactions that are both direct antivirals and regulators of the response. Equally, in order to compare orthologues of the same genes across different species, independent CRISPR/Cas9 screens must be carried out using species specific libraries which is time intensive and costly whist the overexpression library contains both human and macaque orthologues.

1.3.3 The application and advances of CRISPR/Cas9 screening

The screening technique employed in this thesis, is that of genome wide CRISPR/Cas9 knockout screening, used to introduce loss-of-function mutations into cells via the introduction of sgRNAs;

summarised in (Mali et al., 2013; Khan et al., 2018). Pooled screening introduces a library of sgRNAs into Cas9-expressing cells or alongside a Cas9 construct primarily via lentiviral transduction, although other methods such as PiggyBac transposons (Chew et al., 2011) and adeno-associated virus (AAV) delivery (Chow et al., 2017) can be used. Lentiviral transduction is performed at a low multiplicity of infection (MOI) to minimise the chance of cells being transduced by multiple vectors and therefore containing more than one sgRNA. The transduced plasmid containing the sgRNA for the gene of interest also contains a selection resistance marker, such as an antibiotic resistance gene. This allows an appropriate selection pressure to select for successfully transduced cells in the population. A relevant assay to select cells for the phenotype of interest can then be performed followed by extraction of genomic DNA from cells. Next generation sequencing (NGS) can subsequently be employed to identify encoded sgRNAs in each cell and enrichment significance can be calculated (see section 4.2) (Joung et al., 2017; Yau and Rana, 2018).

There are many sgRNA libraries available for use in genome wide pooled CRISPR/Cas9 knockout screening. In the literature, two have been predominantly adopted; the activity-optimised genome wide library by Sabatini and Lander et. al. which has 10 sgRNAs/ gene and 187,535 sgRNAs in total (Wang et al., 2015) and GeCKOv2 by Zhang et. al. which has 6 sgRNAs/ gene and 123,411 sgRNAs in total (Sanjana, Shalem and Zhang, 2014). Many other libraries have been designed to improve the specificity of sgRNAs including the Toronto KnockOut library by Moffat et. al. which has 12 sgRNAs/ gene and 176,500 sgRNAs in total (Hart et al., 2015) and the Brunello genome wide library by Doench and Root et. al. which has 76,441 sgRNAs in total with 4 sgRNAs/ gene (Doench et al., 2016). The library used in this thesis is the Human Improved Genome wide Knockout CRISPR Library produced in the lab of Kosuke Yusa which contains 90,709 sgRNAs in total with 5 sgRNAs/ gene (Tzelepis et al., 2016). However, it is also possible to custom design libraries to only contain genes of interest, such as the antiviral response, or those of non-human species allowing much flexibility in the capabilities of the technique. The flexibility and diversity of the technique can also be impacted by other experimental design choices out with the sgRNA library choice including cell line and vector manipulation. This allows various aspects of the experimental design to be manipulated and studied, in the case of virus-host interactions, different aspects of virus and host interplay, providing a more well-rounded picture of pathogen infection.

There have been many advances in screening experimentally since its development, for example, improving sensitivity and reducing off target effects. However, all screening techniques rely on the subsequent downstream bioinformatic analysis to deconvolute results to which there are still drawbacks as the speed at which CRISPR/Cas9 screening is developing is at a faster rate than that of the bioinformatic analysis methods available. For screening in general, there are no consensus bioinformatic methods for analysis of data with many algorithms having been originally designed for methods such as siRNA screens, RNA-seq and microarrays (So et al., 2019). However, there have been developments in CRISPR/Cas9 screen specific tools such as MAGeCK (Li et al., 2014), CasTLE and BAGEL, each having varying modelling strategies and inputs (Jeong et al., 2019; Schuster et al., 2019). The latter require the input of non-essential gold standard genes whereas MAGeCK does not.

Additionally, the presence or absence of negative control inputted into the analysis have been shown to affect the identification of false positive hits, as these negative controls can vary between screens to either be non-targeting sgRNAs or sgRNAs targeting non-essential genes; a topic on which there is not a consensus in the community (Chen et al., 2018). As previously discussed, there is a large amount of variation within the output of RNAi screens investigating similar questions (Anderson et al., 2019a), however this is only known due to the large volume of RNAi screens performed. As CRISPR/Cas9 screening is still a relatively new field in comparison, there is a lack of data so far allowing for similar comparisons and to identify if the same phenomenon is occurring. However, it should be noted that the use of MAGeCK as the tool for downstream analysis of CRISPR/Cas9 screening data has been predominantly adopted, being used by the majority of studies. This is key in allowing for a more consistent approach compared to other techniques and therefore an advantage of the technique in allowing for a more robust comparison of data from other studies as more screens are performed.

Genetic screens, as previously discussed, are well placed to study virus-host interactions of clinically important pathogens however they can also be utilised to investigate pathogens of agricultural importance. Tan et. al., have developed a bovine sgRNA library in order to study such genes. The library has so far been used to identify over 150 host dependency factors that enable bovine herpes virus type-1 replication, a virus of severe economic burden in the cattle industry (Tan et al., 2020). In future, such libraries will also enable the identification of other virus-host interactions upon infection with other cattle pathogens providing information on livestock disease, which is currently understudied. It may also provide us with answers as to how to improve food security and aid our understanding of how zoonotic events occur as previously mentioned with the overexpression library. As well as bovine sgRNA libraries there are also other species libraries becoming available for the study of other agriculturally important pathogens, with a porcine library having been used to identify host factors required for Japanese encephalitis virus replication (Zhao et al., 2020).

The use of genetic screening to identify antiviral factors also enables clustering analysis, as previously described with RNAi screening. The large number of hits provided within such a screen provides greater insight into not only the genes implicated in virus-host interactions but also the wider pathways involved; something not possible when performing single gene studies. The collation of data from multiple screens also enables this and provides a secondary level of support to the results acquired. Additionally, high-throughput screening has only exemplified the large amount of redundancy within the IFN response providing reasoning for the use of itself. As such, despite the known limitations of such techniques, they are well placed as a tool for studying virus-host interactions, as will be further discussed.

1.3.4 Identification of antiviral factors using CRISPR/Cas9 genome wide screening

As previously mentioned, genome wide CRISPR/Cas9 knockout screening has predominantly been employed to identify host dependency factors involved in virus-host interactions, particularly upon

infection with flaviviruses, however a limited number of pooled screens have been performed to identify antiviral restriction factors of varying viruses.

One example is the identification of interferon alpha-inducible protein 6 (*IFI6*) as a yellow fever virus (YFV) restriction factor (Richardson et al., 2018). Richardson et. al. pre-treated cells transduced with the Brunello genome wide knockout library with IFN-α prior to infection with a number of flaviviruses and identified hits significantly enriched in the population of interest using the MAGeCK computational tool, subsequently identifying *IFI6*, *STAT2* and *IRF9*. Hits were validated using independent knockouts which showed the absence of the selected genes permits viral infection whilst ectopic expression of the genes of interest significantly restricts virus infection. *IFI6* was subsequently shown to be antiviral against additional flaviviruses; West Nile virus (WNV), dengue virus (DENV) and zika virus (ZIKV).

Whilst not a genome wide approach, Ohainle et. al. developed a human ISG CRISPR/Cas9 sgRNA library for the identification of host restriction factors (OhAinle et al., 2018). The knockout library targets 1905 potentially antiviral genes cumulated primarily from existing libraries and uses the same workflow as a traditional genome wide approach, albeit focussing on known antiviral restriction factors. The Ohainle library was first used to identify HIV-1 restriction factors alongside a custom lentiCRISPRv2 vector, modified to maintain a complete HIV-1 LTR in order to maintain transcriptional and packaging competency of the vector whilst also delivering Cas9 and the sgRNA. Using this system, upon infection with HIV-1, cells that show increased replication are assumed to contain sgRNAs targeting antiviral genes and are as such, enriched in the viral supernatant. sgRNAs targeting antiviral genes including *IFNAR1*, *STAT1*, *IRF9*, *MxB*, *IFITM1*, *Tetherin* and *TRIM5α* were identified, therefore validating the screening approach. Interestingly, the screen confirmed the redundant nature of the antiviral response, determining that the cumulative effect of multiple ISGs contributes to the restriction of HIV-1 rather than the action of a single dominant ISG, demonstrating again the need of a technique to elucidate important factors in this highly redundant response (OhAinle et al., 2018). Additionally, the screen was repeated by Ohainle et. al. using alternative HIV-1 isolates, demonstrating a strain dependent effect of ISGs. This finding about how IFN-dependent antiviral restriction factors act, is consistent with results from Schoggins et. al. showing that statistical enrichment of sgRNAs following CRISPR/Cas9 knockout screening is able to recapitulate patterns observed using the well-established overexpression screening for the identification of ISGs (Schoggins et al., 2011; OhAinle et al., 2018). The same ISG sgRNA library, was subsequently used to identify SARS-CoV-2 restriction factors (Mac Kain et al., 2022). Upon IFN-α pre-treatment of A549-ACE2 expressing cells prior to infection with SARS-CoV-2, *APOL6*, *IFI6*, *DAXX* and *HERC5* were all identified as restriction factors. Subsequent validation, transducing the ACE2 expressing A549 cells with three independent sgRNAs, validated the role of *DAXX* in restricting SARS-CoV-2 replication but interestingly not other RNA viruses including YFV, MeV or MERS-CoV. Additionally, despite *DAXX* being identified in an IFN-α pre-treated screen, little increase in *DAXX* gene expression was seen following IFN treatment with SARS-CoV-2 restriction appearing to be IFN independent.

This is not the only time that IFN independence has been observed during an IFN-α pre-treated screen. Bonaventure et. al. transduced cells with the GeCKO sgRNA library prior to IFN-α pre-treating T98G

glioblastoma cells and incubating with HIV-1 based lentiviral vectors (LVs) to identify HIV-1 restriction factors (Bonaventure et al., 2022). Despite little overlap in observed hits with the aforementioned Ohainle screen, they were able to identify and subsequently validate *DDX42* as an IFN independent HIV-1 restriction factor using both independent sgRNAs and siRNAs. The lack of overlap between the two HIV-1 screens (OhAinle et al., 2018; Bonaventure et al., 2022), despite using different library designs, indicated that CRISPR/Cas9 genome wide screening may be subject to the same phenomenon as RNAi screening (detailed in section 1.3.2) as more screens are published. Finally, CRISPR/Cas9 genome wide screening allows the identification of lytic cycle promoting factors within latent DNA virus settings. The GeCKO v2.0 library was used to identify lytic reactivation of KSHV cells in SLK cells latently infected with KSHV expressing a doxycycline-inducible late gene, ORF52, fused to GFP (Tian et al., 2023). By collating cells based on GFP intensity, similar to when cells are infected with a fluorescence expressing virus, genes involved in lytic reactivation can be identified. Using this approach, Tian et. al. identified that *SMCHD1* knockout restricts lytic replication and verified this finding using independent shRNA knockdown.

All screens discussed, performed NGS enrichment analysis using the MAGeCK computational package (Li et al., 2014), indicating a strong consensus for the use of a single analysis process following CRISPR/Cas9 genome wide screening as previously mentioned. Whilst lack of overlap has also been identified using the technique, the use of the same analysis software, compared to other screening techniques, underpinning this route cause to the experimental design.

1.3.5 Limitations to CRISPR/Cas9 genome wide screening and future directions

The redundancy in the IFN system makes using screening methods difficult as deletion of a single gene from a cell may be phenotypically silent or have a minimal effect such that it does not pass the threshold for hit selection. In order to pass the threshold for hit selection, the phenotypic readout must be within the ‘quantitative window of identification’ i.e., within the difference of the non-treated and treated control (figure 1.3.5.1). This is also true when trying to identify restriction factors that target viruses that can efficiently uncouple the IFN response; these might include non-lab adapted clinical isolates. This is because the increased viral expression, particularly if using a fluorescence based readout, prevents the effects of potential restriction factors being identified. Alternatively, overexpression screening does not rely on the restoration of infection so is better equipped to identify these low and moderately acting ISGs. However, as previously mentioned, using an overexpression ISG library takes away the ability to find non-known restriction factors, or factors that work in concert, and so if CRISPR/Cas9 is to become more effective and allow a genome wide approach, the quantitative window of identification needs to be made larger.

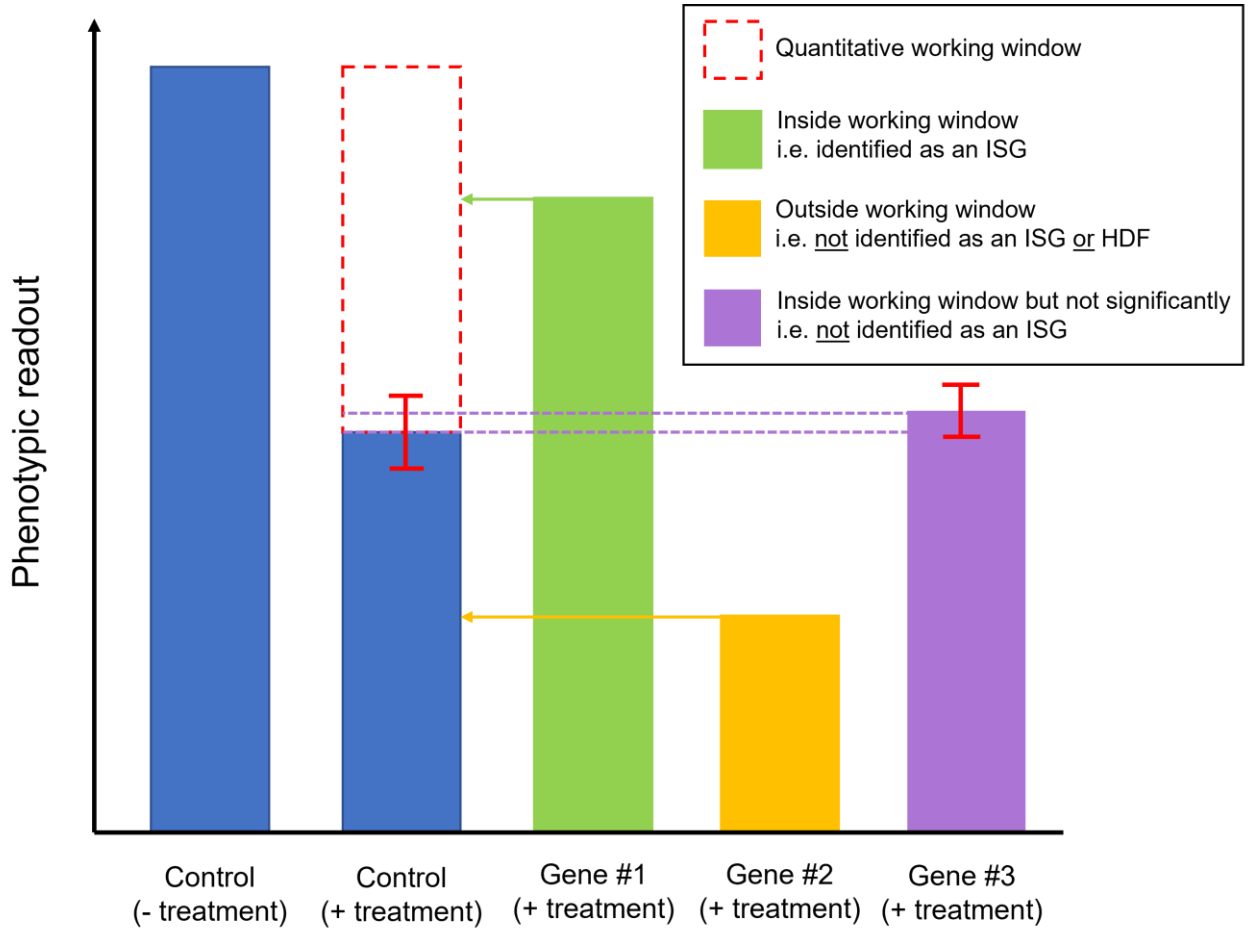

Figure 1.3.5.1: Schematic representation of the quantitative working window for identification of ISGs. The quantitative working window (red dashed box) is defined as the difference of the non-treated and treated control (shown in blue). Following treatment of a cell line deficient in gene #1 (green), the phenotype falls with the working window and so is determined to be an ISG. Following treatment of a cell line deficient in gene #2 (gold), the phenotype falls out with the working window and so is not determined to be an ISG and may be defined as a HDF as the phenotypic readout is reduced compared to the control. Following treatment of a cell line deficient in gene #3 (purple), the phenotype is within the working window but not to a significant degree therefore, it is not identified as an ISG. Broadening the working window would enable statistical significance for the identification of the purple gene.

A possible approach to improve the identification of low-acting restriction factors, or overcome redundancy, might be to use knowledge of negative regulators of the response. Previous work in the lab, and by other research groups, has been shown that cells deficient in IFN stimulated gene 15 (*ISG15*) show a dysregulated IFN response when treated with IFN-α (Speer et al., 2016a; dos Santos and Mansur, 2017; Holthaus et al., 2020). This results in the overexpression of ISGs, compared to a control, and a greater ability to resist viral infection. Unlike most viruses whereby multiple ISGs work in concert to produce an antiviral phenotype, it is known that IFIT1 has the primary role in restricting PIV5 infection (further discussed in section 1.5.6). This information can therefore be utilised in the

development of an improved methodology using ISG15 deficient cells. Work by Holthaus et. al has shown that A549-ISG15$^{-/-}$ cells pre-treated with IFN-α are resistant to PIV5 infection, due to the aforementioned dysregulated response, but viral replication was observed in IFN-α pre-treated A549 naïve cells. However, upon IFIT1 knockdown in both parental cells lines, viral protein expression significantly increased in ISG15 deficient cells but not in A549 naïve cells. The method of using ISG15 deficient cells was then tested following infection of hPIV2 and hPIV3 where IFIT1 has shown to have reduced activity. Results were recapitulated following infection with hPIV2 with a non-significant increase in viral protein expression was seen in single gene knockdowns, but this difference became significant in the double gene deficient cells. Ordinarily, cells deficient in *ISG15* when pre-treated with IFN-α are resistant infection but this shows that this is dependent on their relevant restriction factors being expressed. Therefore, the use of *ISG15* deficient cells within screening may allow the identification of low to moderately acting ISGs, or those that work in concert with others as will be further discussed. However, following infection of hPIV3, whilst there was an increase in viral gene expression, this was calculated to be insignificant thereby resulting in inconclusive evidence that IFIT1 restricts hPIV3. This could be due to the limitations associated with RNAi and incomplete knockdown previously discussed (section 1.3.5) and so CRISPR/Cas9 genome engineering may be better placed to provide proof-of-principle for the utilisation of ISG15 deficient cells in the identification of low to moderately acting ISGs.

1.4 The Reliance of Viruses on Host Genes

Viruses are obligate intracellular pathogens with limited coding capacity and as such, rely on host cells for both machinery and raw materials to complete their replicative cycle (Robinson et al., 2018). Host dependency factors (HDFs) are defined as proteins, encoded by cellular genes, that enable the replication of the virus, therefore performing a proviral role in enhancing or permitting infection in the host cell.

HDFs act at all stages of the virus life cycle from entry to exit with many characterised to act particularly during early phases of infection including attachment, entry, and early trafficking. Additionally, HDFs also play a role in the reactivation of latent to lytic infection. Genome wide CRISPR Cas9 knockout screening has successfully identified virus host dependency factors including pathways required for flavivirus (Ma et al., 2015; Marceau et al., 2016; Zhang et al., 2016; Flint et al., 2019; Li et al., 2019b) and influenza replication and infection (Han et al., 2018; Li et al., 2020; Yi et al., 2022) amongst others which will be further discussed.

The role of HDFs in viral infection can be exploited for drug discovery, and given the nature of global pandemics, the need to rapidly identify HDFs that have this potential is crucial. Currently, the majority of FDA-approved antiviral drugs target viral proteins involved in replication; however, due to the high mutation rate of viruses, particularly RNA viruses, this can lead to antiviral resistance (Kumar et al., 2020; Cakir et al., 2021). Therefore, the targeting of host proteins required for successful virus replication is an alternative tactic.

1.4.1 Identification of viral host dependency factors using CRISPR/Cas9 genome wide screening

Genome wide CRISPR/Cas9 screens are well placed to identify HDFs and as such, have identified host dependency factors for a range of viruses including both RNA and DNA viruses. This has highlighted genes and pathways essential for virus entry, replication and spread and enabled subsequent small molecule testing against such factors as novel therapeutics.

CRISPR/Cas9 screening has been applied to identify host factors involved in severe acute respiratory syndrome coronavirus 2 (SARS-CoV-2) pathogenesis, the virus responsible for the global COVID-19 pandemic that emerged in 2019, with the screening method was used as a high throughput, rapid method. To date, multiple independent screens have been carried out with small molecule inhibitors tested against candidate genes identified. Daniloski et. al. transduced A549 cells, constitutively expressing the angiotensin-converting enzyme 2 (ACE2) receptor, with the GeCKOv2 sgRNA library prior to infection with SARS-CoV-2 (Daniloski et al., 2021). Alongside identification of individual HDFs in the output, multiple gene sets were identified including four members of the endosomal protein sorting retromer complex and four members of the endosomal trafficking commander complex, not only providing confidence in the results but also highlighting key pathways required for SARS-CoV-2 pathogenesis. Seven inhibitors were subsequently tested, resulting in greater than 100-fold reduction in viral load and exhibiting an additive effect in protection when combinatorial therapy was applied (Daniloski et al., 2021). This therefore shows the power of high throughput screening in identifying drug targets allowing for the repurposing of current pharmacological molecules. Additionally, Hoffmann at. al. performed a focused screen upon infection with SARS-CoV-2 at the temperatures of the upper and lower respiratory; 33°C and 37°C respectively. This screen identified a number of pathways specific to either temperature including mammalian mitochondrial ribosomal small subunit (MRPS) genes and Rab GTPases, giving a broader picture of the pathogenesis of this virus (Hoffmann et al., 2020).

Different screening designs have similarly been used to investigate different aspects of a single virus life cycle. For example, different cell lines have been utilised to study various aspects of HIV-1 infection with a CD4+ T cell line used to identify HIV-1 host dependency factors, due to its susceptibility to HIV-1 infection (Park et al., 2017), and a J-Lat 10.6 cell line used to identify novel latency promoting factors in HIV-1 infection (Rathore et al., 2020). Whilst differing cell lines were used, both studies utilised a GFP reporter for virus infection allowing for a FACS based readout and selection of phenotype of interest. For the identification of HDFs, Park et. al. transduced cells with a custom sgRNA and selected for GFP-negative cells following infection. Five gene were significantly enriched for: *CD4*, *CCR5*, *TPST2*, *SLC35B2*, and *ALCAM* (Park et al., 2017). For the identification of latency promoting factors, GFP expression correlated to HIV-1 reactivation and replication. As the J-Lat 10.6 cell line contains a single integrated replication-incompetent HIV-1 with a GFP reporter gene, GFP-positive cells were isolated upon the assumption that deletion of a latency maintaining gene renders the virus susceptible to reactivation. MAGeCK enrichment analysis identified 52 latency promoting genes allowing for validation with small molecule inhibitors (Rathore et al., 2020).

A number of genome wide CRISPR/Cas9 knockout screens have been undertaken to identify HDFs involved in virus-host interactions upon infection with flaviviruses (see section 1.3.4). These include screens that have identified HDFs enabling EBOV, ZIKV and DENV infection alongside other members of the flavivirus family. For example, upon infection on human neural cells with ZIKV, HDFs within the heparan sulfation, endocytosis, endoplasmic reticulum processing pathways were identified. These were subsequently characterised against different strains of the virus, the Uganda strain, and a more recent North American isolate, indicating that these HDFs show broad activity across strains and therefore may be good therapeutic targets (Li et al., 2019b). Additional flavivirus HDFs have also been identified. An independent screen identified *SPCS1*, a member of the endoplasmic reticulum-associated signal peptidase complex. Subsequent independent knockout of *SPCS1* resulted in reduced viral yield of a number of flaviviruses including WNV, DENV, ZIKV, YFV, and JEV, but not other virus families. Further characterisation showed members of the Flavivirus family depend on this signal peptide processing pathway for the cleavage of flavivirus structural proteins and subsequent secretion of newly formed virions whilst other virus families do not (Zhang et al., 2016). Alongside identification of Flavivirus HDFs critical to virion exit, screening has also identified HDFs critical to viral entry. A genome wide CRISPR/Cas9 screen utilising the GeCKOv2 library identified *GNPTAB*, encoding the α and β subunits of N-acetylglucosamine-1-phosphate transferase, as a key HDF for EBOV entry through the modulation of cathepsin B activity. Subsequently, treatment of cells with the small-molecule PF-429242, an inhibitor of the protease on which GNPTAB activity is dependent on, blocks EBOV entry and infection (Flint et al., 2019).

The role of HDFs are not only required for successful RNA virus infection, but also that of DNA viruses. Whilst DNA viruses tend to be larger and encode more of their own proteins, they still rely on host genes and processes to complete their replication cycle. As such, genome wide CRISPR/Cas9 screens have also been employed to study these viruses. One study identified 3′-phosphoadenosine 5′-phosphosulfate synthase 1 (*PAPSS1*) as a host factor for HSV-1 infection (Suzuki et al., 2022). Further characterisation identified a reduced ability of HSV-1 to bind host cells in *PAPSS1* deficient cells as a result of reduced heparan sulphate expression. As many viruses use heparan sulphate for cell surface attachment and entry, it was subsequently shown that knockout of PAPSS1 also reduced binding affinity of other viruses including HSV-2, hCOV and HBV. This indicates that PAPSS1 is a broad acting HDF that plays a role in the pathogenesis of diverse virus families (Suzuki et al., 2022).

HDFs are required for the successful replication and infection of all viruses. This includes those that the Hughes lab is interested in, Paramyxo- and Pneumoviruses which will be further discussed.

1.5 Paramyxoviruses and Pneumoviruses

1.5.1 The pathological significance of Paramyxoviruses and Pneumoviruses

Viruses within the Paramyxoviridae and Pneumoviridae families are of high pathological significance in both the developing and developed world causing extensive lower respiratory tract infections (LRTIs). These result in illnesses including, but not limited to, pneumonia, bronchiolitis, and croup. Research

has shown that in 2010, LRTIs were the primary cause of death in children aged 28-364 days and only second to malaria in number of deaths caused in children aged 1-4 years worldwide (Lozano et al., 2012). As such, children under the age of 5 are particularly susceptible to these illnesses following infection with Paramyxo- or Pneumoviruses which can subsequently result in hospitalisation.

Respiratory syncytial virus (RSV), a pneumovirus, is well-known as one of the leading causes of hospitalisation of children worldwide. Of deaths caused by LRTIs in children aged 28-364 days, 6.7% of total worldwide deaths were attributed to RSV making it one of the most important pathogens in post-neonates (Lozano et al., 2012). Additionally, it has been estimated that in the United States, RSV infections in children <5 years result in ~1 of every 13 visits to a primary care office and ~2.1 million children require medical attention due to RSV annually, with 3% requiring hospitalisation (Hall et al., 2009). In the United Kingdom, it is thought 53% of LRTI hospital admission in children <5 years could be attributed to RSV with this admission rate increasing from 2007/08 to 2011/12 (Reeves et al., 2017).

Whilst RSV is a leading cause of hospitalisation in young children worldwide, it is not the only Paramyxo- or Pneumovirus of medical significance. Two Paramyxoviruses where licensed vaccines are available, measles virus (MeV) and mumps virus (MuV), continue to be of pathological significance. MeV causes encephalitis and blindness alongside pneumonia and croup (Perry and Halsey, 2004) whilst MuV is still a cause of viral encephalitis if left untreated (Rubin et al., 2015).

Additionally, a multi-site study completed in 2019 termed the Pneumonia Etiology Research for Child Health (PERCH) project, investigated causes of pneumonia resulting in hospitalisation of children under the age of 5 years (figure 1.5.1.1) (O'Brien et al., 2019). The multi-site study showed over 60% of severe cases were caused by viruses with over 30% specifically attributed to RSV. However, 7% of cases, rising to 9% of severe cases, were attributed to parainfluenza virus (PIV) infection, a Paramyxovirus (O'Brien et al., 2019). In the United States, it was also found that following RSV, PIV was the next leading cause of hospitalisation due to respiratory illness in children <5 years, with hPIV-3 specifically accounting for 2.8% of pneumonia inpatient stays (Abedi et al., 2015).

Paramyxoviruses are not only of clinical significance but also of agricultural significance, infecting a number of different host species. For example, Newcastle Disease Virus (NDV) causes respiratory, gastrointestinal, neurological, and reproductive illnesses in poultry alongside a high mortality rate (Ganar et al., 2014). Whilst there is a licensed vaccine, it does not prevent virus shedding leading to NDV being of high agricultural significance, resulting in at least four historically panzootic events (Shahar et al., 2018; Hu et al., 2022). The virus also results in severe economic burden upon the necessary implementation of biosecurity measures alongside vaccination (Mayers, Mansfield and Brown, 2017). Another virus of agricultural and subsequent economic burden is that of Atlantic Salmon Paramyxovirus (ASPV). ASPV causes gill disease in Atlantic Salmon, and whilst not the sole cause it was a contributor to the estimated 50 million captive Atlantic salmon that died in Norway in 2019, therefore posing a significant problem for the aquaculture industry (Kvellestad et al., 2005; Oliveira et al., 2021).

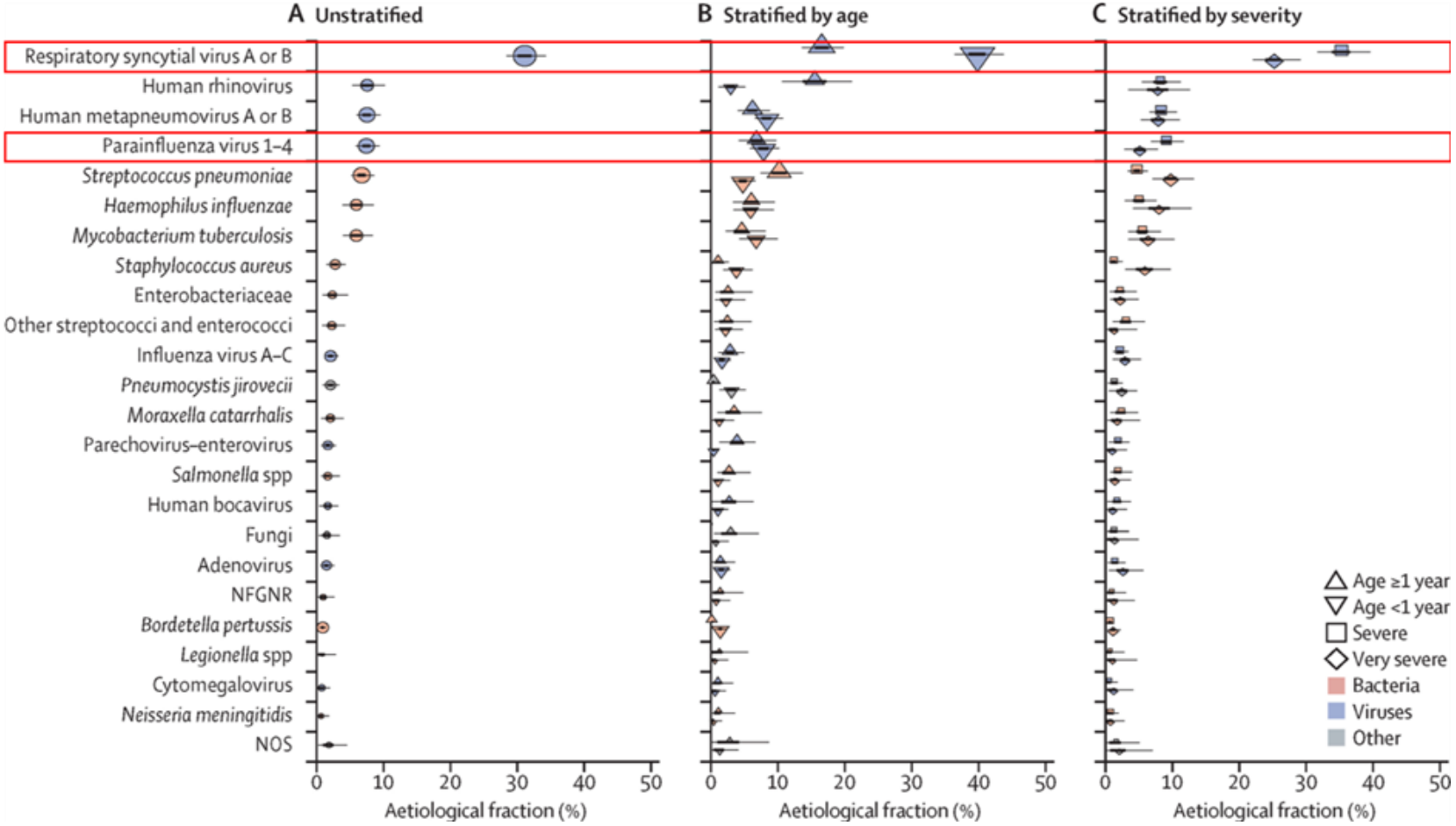

Figure 1.5.1.1: Causes of pneumonia cases by pathogen from multi-site etiological study. The proportion of pneumonia cases diagnosed from positive chest x-ray in multi-site (Bangladesh, The Gambia, Kenya, Mali, South Africa, Thailand, and Zambia) etiological study. (A) Ranked by proportion of cases attributed to pathogen; (B) ranked by age (split into proportion of cases attributed to pathogen in <1yr and >1yr); (C) ranked by severity of disease (split into proportion of cases resulting in severe and very severe disease). RSV and PIV highlighted within red boxes (O'Brien et al., 2019).

As mentioned, Paramyxoviruses contributing to agricultural burden also cause an economic burden, not only in lost earnings but in the necessary biosafety measures to be undertaken. Clinical pathogens also result in an economic burden alongside a disease burden with hospital charges for PIV-associated bronchiolitis, croup, and pneumonia between 1998 and 2010 totalling $257M (Abedi et al., 2015).

1.5.2 Taxonomy, phylogeny, and classification of Paramyxoviruses and Pneumoviruses

The Paramyxo- and Pneumovirus families are found within the Mononegavirales order, an order of negative-stand RNA viruses (figure 1.5.2.1) (Payne, 2017). Viruses within these families are found in varying host species including mammals, birds, reptiles, and fish. Within the Paramyxoviridae family there are four subfamilies: Rubulavirinae, Avulavirinae, Orthoparamyxovirinae, and Metaparamyxovirinae. These subfamilies contain varying numbers of genera within them with 3 further genera remaining unclassified totalling 17 genera within the Paramyxoviridae family (Rima et al., 2019). In total there are currently 78 classified species of Paramyxoviruses, not including species specific strains (Lee et al., 2021b). Known and emerging pathogens are found across all four subfamilies and across various host species as detailed in table 1.5.2.1 (with ICTV accepted taxonomic names). Orthorubulaviruses, within the Rubulavirinae subfamily, contain mumps virus (MuV); parainfluenza virus type 5 (PIV5), the model paramyxovirus; and human parainfluenza virus type 2 (hPIV2). Newcastle disease virus (NDV), a known avian pathogen belongs to the Orthoavaluviruses genus within the Avulavirinae subfamily. The most diverse of the subfamilies is that of the Orthoparamyxovirinae, consisting of 8 genera. Human pathogens such as human parainfluenza virus Type 3 (hPIV3), Nipah virus (NiV) and measles virus (MeV) are found within the Respirovirus, Henipavirus, and Morbillivirus genera respectively. This subfamily also includes non-human viruses such as Atlantic salmon paramyxovirus (ASPV), a Aquaparamyxovirus; Fer-de-Lance virus (FDLV), a Ferlavirus infecting reptiles; hendra virus (HeV), a Henipavirus affecting both horses and humans; and the now eradicated rinderpest virus (RPV), a livestock virus within the Morbillivirus genus (Rima et al., 2019).

Parainfluenza virus Type 5, previously denoted as Simian Virus 5 (SV5) due to its discovery in primary monkey kidney cells, was initially isolated by Hull et. al. in 1956 (Hull, Minner and Smith, 1956). The virus has subsequently been well studied as a model virus for paramyxovirus infection, as whilst it has been isolated from a number of mammals, it is not known to cause acute disease with the exception being that of kennel cough in canines (Wignall-Fleming et al., 2016). It does however maintain the same genome structure of the Rubulaviruses and has similar physical properties and replication strategies of other paramyxoviruses. It is well-characterised and can therefore be used effectively as a Paramyxovirus model.

The Pneumoviridae family was removed as a subfamily of Paramyxoviridae in 2016 and contains two genera; Orthopneumoviruses, of which human Respiratory Syncytial virus (hRSV) belongs, and Metapneumoviruses, of which human Metapneumovirus (hMPV) belongs (Rima et al., 2017). Despite being recategorized, the two families of viruses share many of the same characteristics including similar virion and genome structure. Nevertheless, there are some differences which will be further discussed.

Within virus species, there is also strain diversity at the genome and subsequent phenotype level. Two well utilised hPIV3 strains include the prototype Washington 1957 strain and the wildtype JS strain, isolated from a one-year old infant with LRTI. Whilst there is only an observed 4% difference at the nucleotide level, the start, stop and intergenic sequences remain conserved (Stokes et al., 1992). Despite this, the Washington isolate is more resistant to IFN than its wildtype counterpart, and as such, shows higher levels of virus replication in IFN treated cells. There are also varying strains of bPIV3, clustering into three genotypes: A, B and C. Two of the most well-characterised bPIV3 strains are bPIV3(Shipping Fever) and bPIV3(Kansas) (Bailly et al., 2000).

1.5.3 Paramyxovirus virion structure and the infectious cycle

Paramyxoviruses and Pneumoviruses are enveloped, non-segmented viruses with negative sense ssRNA genomes. Each virion is pleomorphic but spherical in shape and has a diameter of approximately 150 nm (figure 1.5.3.1) (Cox and Plemper, 2017; Rima et al., 2019). The negative sense RNA genome is tightly encapsidated with nucleoprotein monomers (NP) to form a ribonucleoprotein complex (RNP), also called the nucleocapsid. Alongside the ribonucleoside complex, the nucleocapsid also consists of the viral polymerase complex, comprising P and L proteins (Bloyet, 2021). The nucleocapsid associates with the matrix, composed of a layer of M protein subunits at the base of a double-layered lipid envelope with the surrounding membrane containing two transmembrane proteins: the fusion protein (F) and the relevant viral attachment proteins (HN, H or G) (Battisti et al., 2012; Aguilar et al., 2016).

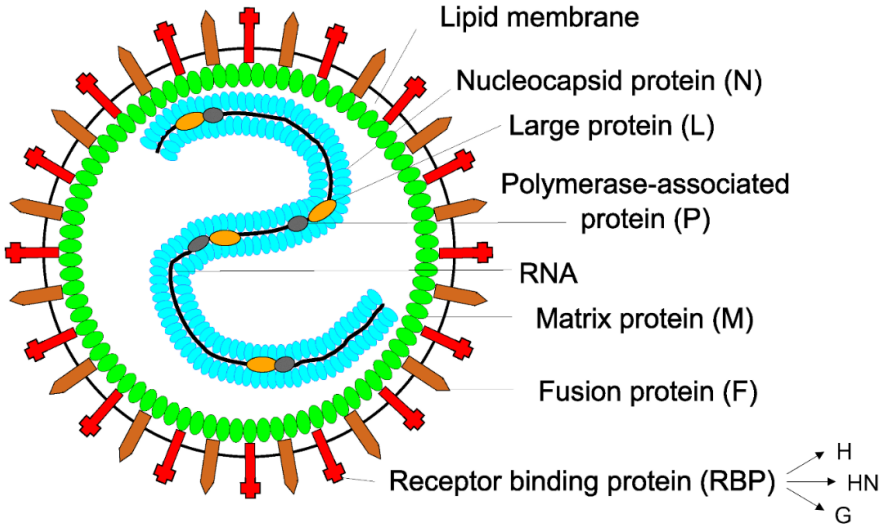

Figure 1.5.3.1: Model Paramyxovirus virion particle. Paramyxoviruses are unsegmented viruses approximately 150 nm in diameter. The envelope consists of fusion (F) and a receptor binding protein (RBP); either H, HN or G. A layer of matrix (M) is found at the base of the lipid envelope and the nucleocapsid is composed of N encapsidated vRNA, P and L proteins (Rima et al., 2019).

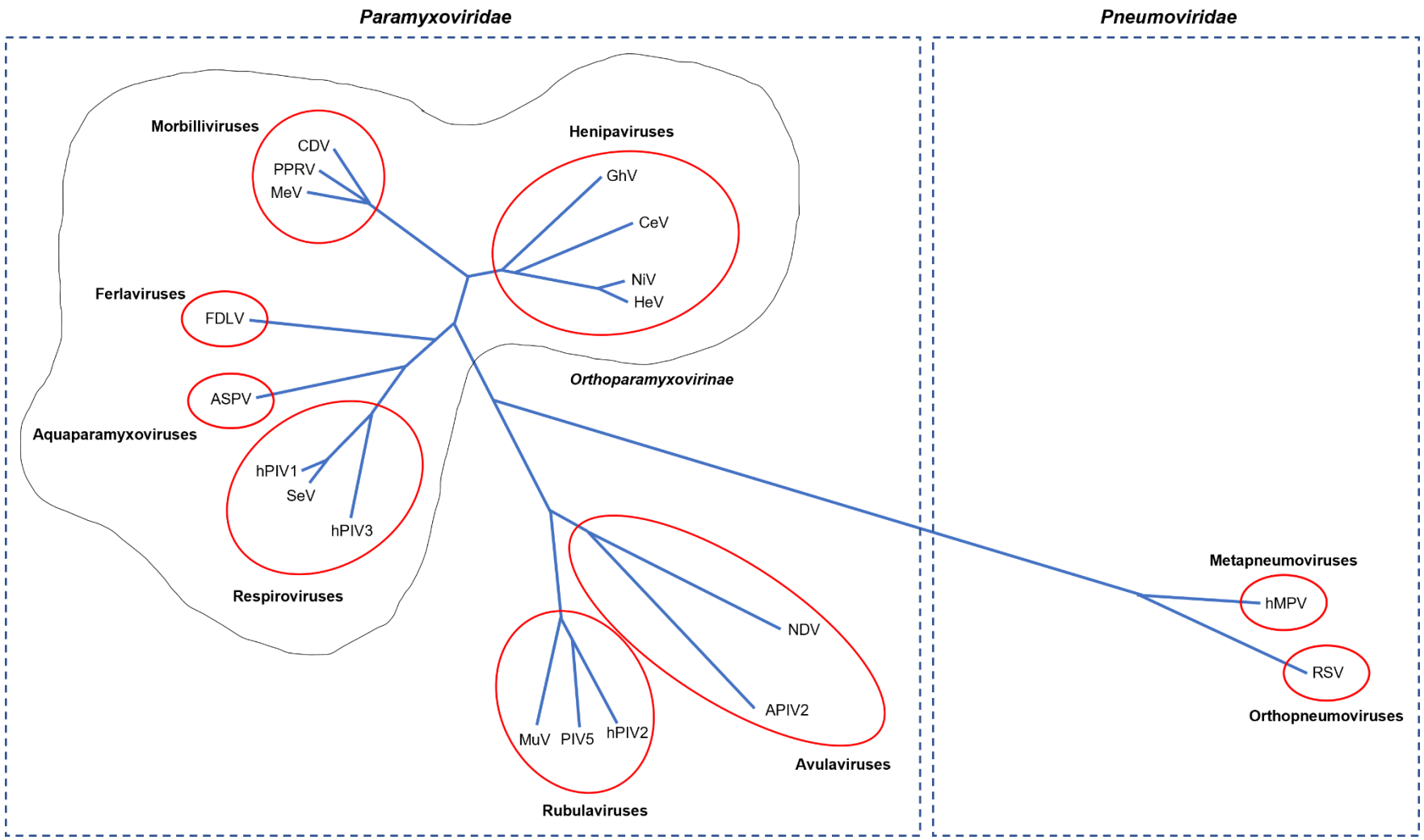

Figure 1.5.2.1: Phylogenetic tree showing the relationship between Paramyxoviridae and Pneumoviridae. Schematic of the relationship (blue lines) between Paramyxoviridae and Pneumoviridae genera (highlighted in red) with example viruses (common names). Orthoparamyxovirinae subfamily, containing Henipa-, Morbilli-, Ferla-, Aquaparamyxo-, and Respiroviruses outlined in grey.

Table 1.5.2.1: Taxonomic summary of the Paramyxovirus and Pneumovirus families. The Paramyxo- and Pneumovirus families are found within the Mononegavirales order with the Paramyxoviridae containing 4 subfamilies and a further 17 genera and the Pneumoviridae family containing 2 genera.

Order	Family	Subfamily	Genus	Example Virus (Common names)	Example Virus (ICTV accepted)
Mononegavirales	Paramyxoviridae	Rubulavirinae	Pararubulavirus		
			Orthorubulavirus	MuV PIV5 hPIV2	Mumps orthorubulavirus Mammalian orthorubulavirus 5 Human orthorubulavirus 2
		Avulavirinae	Metaavulavirus		
			Orthoavulavirus	NDV	Avian orthoavulavirus 1
			Paraavulavirus		
		Orthoparamyxovirinae	Aquaparamyxovirus	ASPV	Salmon aquaparamyxovirus
			Respirovirus	hPIV3 SeV	Human respirovirus 3 Murine respirovirus
			Ferlavirus	FDLV	Fer-de-lance virus
			Henipavirus	NiV HeV	Nipah henipavirus Hendra henipavirus
			Jeilongvirus		
			Narmovirus		
			Morbillivirus	MeV RPV CDV	Measles morbillivirus Rinderpest morbillivirus Canine morbillivirus
			Salemvirus		
		Metaparamyxovirinae	Synodonvirus		
		(Unclassified)	Cynoglossusvirus		
		(Unclassified)	Hoplichthysvirus		
		(Unclassified)	Scoliodonvirus		
	Pneumoviridae		Metapneumovirus	hMPV	Human metapneumovirus
			Orthopneumovirus	hRSV	Human orthopneumovirus

Briefly, Paramyxoviruses attach to host cell receptors through varying glycoproteins. Orthorubulaviruses and Respiroviruses utilise HN, Morbilliviruses utilise H, and Henipaviruses utilise G (as will be further discussed; section 1.5.4.1). For Paramyxovirus entry, the virion must fuse with the host cell membrane; a process dependent on the interaction between the attachment glycoprotein and the fusion protein (F). Interaction between the relevant viral glycoprotein and the F protein causes a conformational change in F resulting in its activation. This leads to the formation of a fusion pore allowing entry of the nucleocapsid into the cytoplasm at the plasma membrane (reviewed; (Chang and Dutch, 2012; Jardetzky and Lamb, 2014). Following release of vRNA into the cytoplasm, transcription and replication of the viral genome occurs (section 1.5.4) cumulating in the assembly of new virions. The matrix (M) protein is the key mediator in this process, mediating the interaction of the nucleocapsid and glycoproteins at the plasma membrane resulting in budding (reviewed; (Battisti et al., 2012; El Najjar, Schmitt and Dutch, 2014).

1.5.4 Paramyxovirus genome structure, transcription, and replication

1.5.4.1 Paramyxovirus genome structure

Members of the Paramyxoviridae share the genes for N, P, M, F and L encoding the nucleocapsid, phosphoprotein subunit of the RNA-dependent RNA polymerase (vRdRP), matrix protein, fusion protein, and the large catalytic subunit of the viral polymerase respectively (figure 1.5.4.1.1). However, there is variation in the expression of attachment glycoproteins with different genera encoding for either G, H, or HN. Viruses within the Morbilli- genus utilise H as their viral attachment protein, and viruses within the Rubula-, Avula-, Respiro-, Ferla-, and Aquaparamyxovirus genera utilise HN. Conversely, Pneumoviridae and members of the Henipavirus genus encode for the G protein instead (Bossart, Fusco and Broder, 2013; Aguilar et al., 2016). This results in differences in receptor binding for entry with those expressing H or HN binding to sialic acid and those expressing G binding to proteinaceous receptors such as heparan sulphate or ephrin B2/B3. HN expressing viruses possess both hemagglutinin and neuraminidase activity for the binding and cleavage of sialic respectively however, Morbilliviruses only have hemagglutinin activity and can also bind cellular proteins additional to sialic acid (Chang and Dutch, 2012; Aguilar et al., 2016).

Variation is also seen in the coding strategies for the evasion of the host innate immune response (Goodbourn and Randall, 2009; Aguilar et al., 2016), as will be further discussed. These differences exist between genera of the same virus family as well as between virus families. Within the Paramyxovirus family, the P gene encodes for more than one polypeptide via alternative initiation and mRNA editing. Morbilli- and Respiro-, Hendra- and Aquaparamyxoviruses encode for the additional V and C genes whilst Rubula-, Avula-, and Ferlaviruses also encode for V (Goodbourn and Randall, 2009). Whilst V is known to play a role in host antagonism, it also plays an important role in RNA stability (Yang et al., 2015). Additionally, Rubulaviruses also encode for the small hydrophobic (SH) protein (Wilson et al., 2006). Conversely, Pneumoviruses solely encode for P with no additional gene products

but do encode for the small hydrophobic (SH) protein with Orthopneumoviruses additionally encoding for NS1 and NS2 at their 3' proximal end (Ribaudo and Barik, 2017).

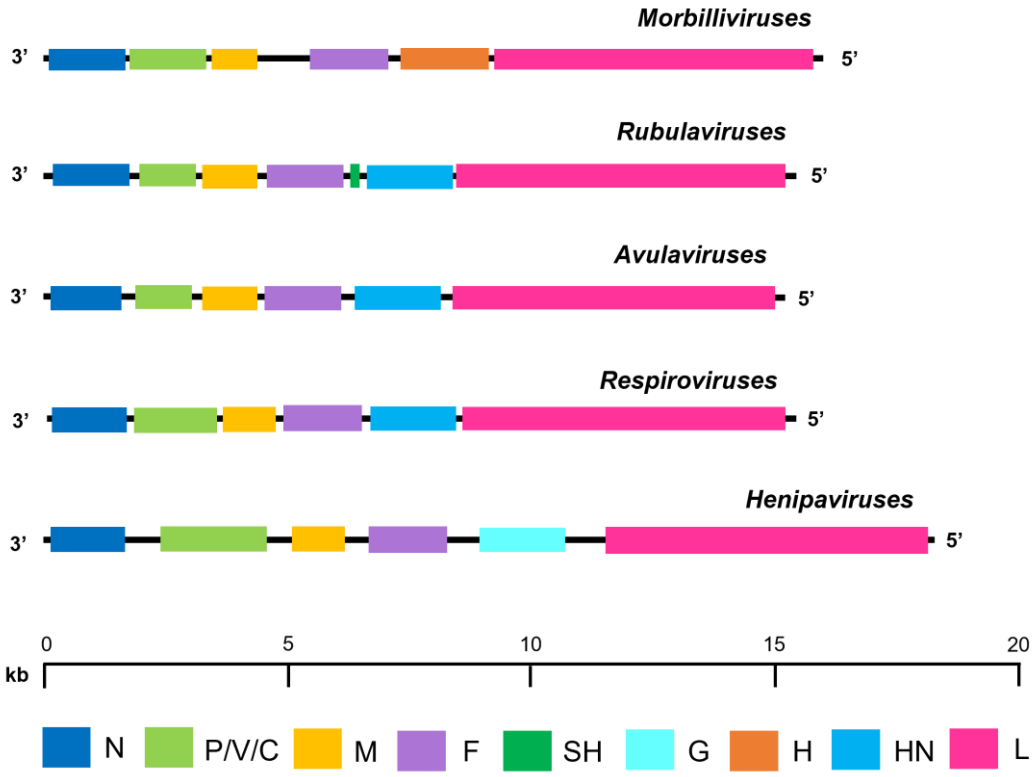

Figure 1.5.4.1.1: Genome structure of Paramyxoviruses across different families. Coding and non-coding regions of Paramyxovirus genomes to scales with the viral proteins shown as follows: N, nucleoprotein (navy); P/V/C, phosphoprotein with alternative gene products (light green); M, matrix protein (gold); F, fusion glycoprotein (purple); SH, small hydrophobic protein (dark green); G (teal), H (orange) and HN (blue) attachment glycoproteins; L, large polymerase protein (pink).

1.5.4.2 Paramyxovirus transcription

As Paramyxoviruses and Pneumoviruses are negative sense single-stranded RNA viruses, their genome cannot be directly transcribed into mRNA for subsequent translation of viral gene products into proteins. At the 3' end of the viral genome is the leader (Le) region, an extracistronic region of between 55 to 70 nt, containing the Le promoter. This region is required for both transcription and replication of the viral genome (Noton and Fearns, 2015).

For the generation of viral mRNA, the vRdRP first binds to the Le promoter element at the 3' end of the genome. Each viral gene is flanked by a gene start (GS) and gene end (GE) site, and so upon the vRdRP encountering a GS site, mRNA synthesis is initiated, beginning with that of NP. Once the RdRP reaches the GS site, the mRNA is polyadenylated at the site of a poly(U) tract downstream of the GE site and released for subsequent translation, this is referred to as start-stop transcription. The vRdRP

then scans the intergenic region between the current GE site and the next GS site to begin the process again; this intergenic site is generally not transcribed into mRNA. Alternatively, the vRdRP can disengage or 'fall off' at any point randomly however, it is thought to occur at a GE site. If this occurs, the vRdRP can only rebind with the viral genome at the Le promoter and so a viral transcription gradient from the 3' and 5' end is observed with the highest mRNA abundance being that of NP (figure 1.5.4.2.1). Failure for the vRdRP to terminate transcription at the GE site results in the transcription of the intergenic readthrough and generation of readthrough mRNA (Noton and Fearns, 2015; Wignall-Fleming et al., 2019).

Paramyxoviruses encode multiple proteins from their P gene. These are transcribed in two ways; RNA editing of the P/V gene by insertion of additional G residues or additional open reading frames (ORF) (Goodbourn and Randall, 2009), as a result of slippage of the vRdRP whilst the transcription of C is a result of an additional ORF upstream of RNA editing site (Wignall-Fleming et al., 2019).

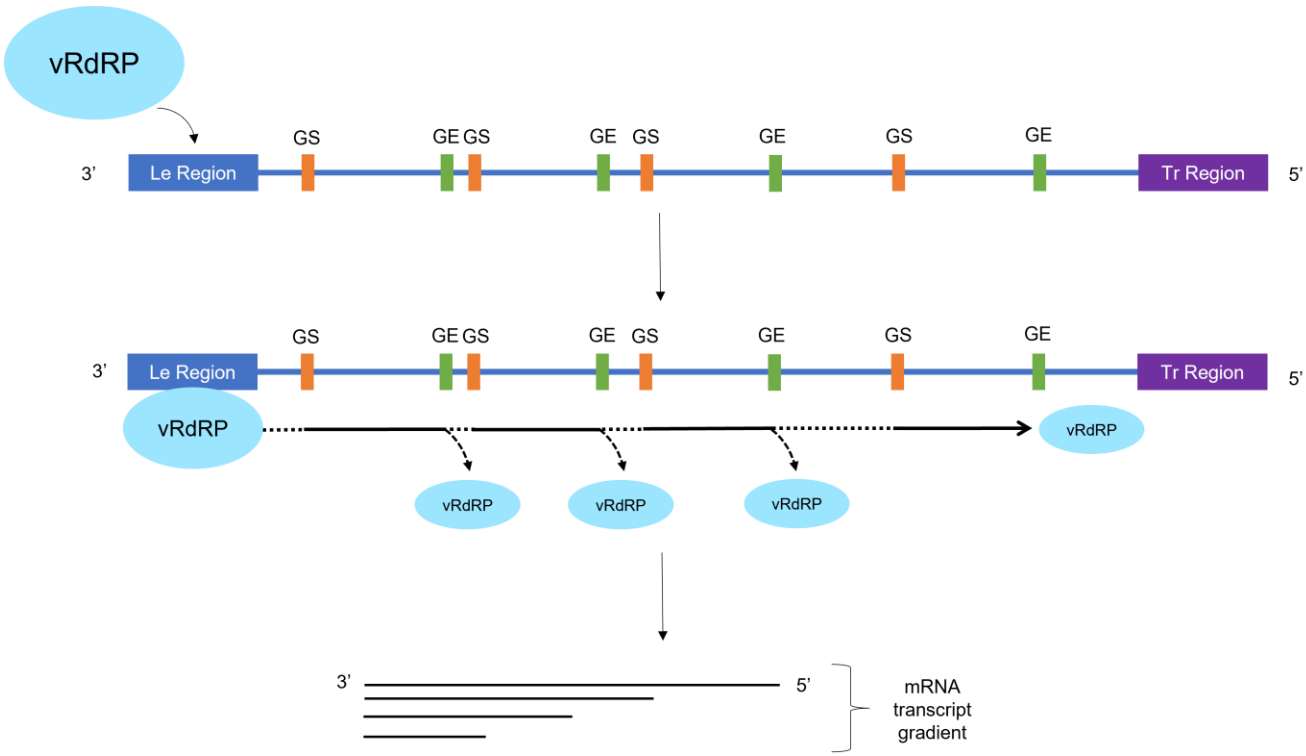

Figure 1.5.4.2.1: Schematic diagram representing Paramyxovirus genome transcription. Genes are illustrated between a GS site (orange) and GE site (green). The vRdRP (light blue) binds to within the Le region (dark blue) at the 3' end of the genome. mRNA transcription is indicated between the GS and GE by solid by black lines with intergenic regions not transcribed (dashed black lines). The vRdRP can 'fall off' at any GE site but must reinitiate back at the Le promoter.

1.5.4.3 Paramyxovirus replication

Whilst mRNA can be generated directly from the viral genome, the replication of the viral genome, either for packaging into newly formed virions, or to provide templates for secondary transcription, requires a two-step process. At the 5' end of the viral genome is the trailer (Tr) region, an extracistronic region of between 21 to 161 nt (depending on the virus). During replication, the viral genome is transcribed in its entirety, ignoring GS and GE sites to produce a positive sense antigenome, the template for the production of new viral genomes. The 3' region of the antigenome is complementary to that of the Tr region in the viral genome and contains a promoter for vRdRP initiation. This then serves as an initiation point for the production of a full-length negative sense viral genome (Noton and Fearns, 2015). However, both the viral genomes and antigenomes require encapsulation in NP and so viral replication can only begin following sufficient NP production (Horikami et al., 1992).

Following translation of NP, it is kept soluble through an interaction with the N-terminal domain of P and V. After sufficient production of NP, as the switch between viral transcription and replication is dependent on the concentration of free NP, newly synthesised genomes can be produced and encapsidated (Nilsson-Payant et al., 2021). This encapsulation is done concurrently, allowing the vRdRP to ignore GE signals and allowing for an extended template resulting in the production of new viral genomes. Encapsidation also prevents detection in the cytoplasm by the host immune response (figure 1.5.4.3.1) (Noton and Fearns, 2015; Wignall-Fleming et al., 2019).

During replication, vRNA synthesis is also modulated by the C protein; it has been postulated that in Ferla-, Avula-, and Rubulaviruses, that do not express a C protein, that the V protein may fulfil the same role. To ensure that antigenome is successfully turned over into genome RNA and does not accumulate in the cell, the C protein has been shown to inhibit RNA synthesis from the Le promoter, but not the Tr promoter (Noton and Fearns, 2015). This not only ensures that new virions can be successfully produced but as genomic RNA is encapsidated, it inhibits detection of the virus by the innate immune response.

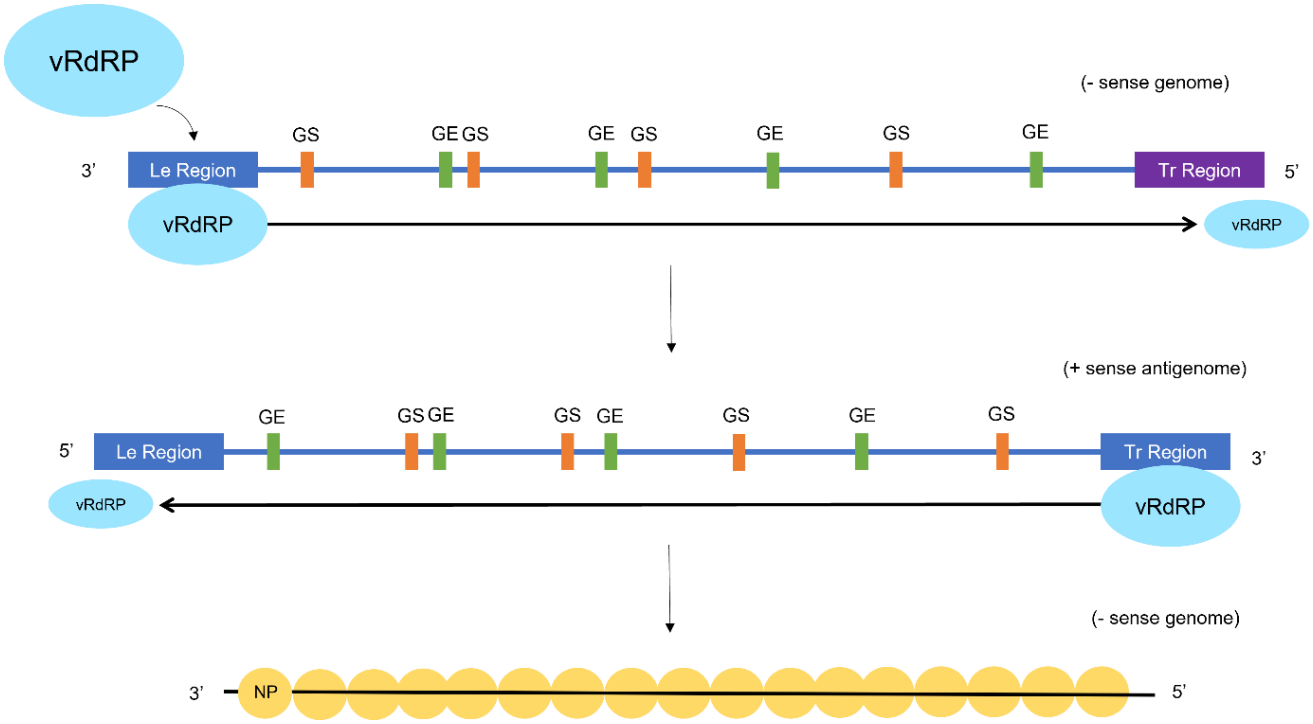

Figure 1.5.4.3.1: Schematic diagram representing Paramyxovirus genome replication. Genes are illustrated between a GS site (orange) and GE site (green). The vRdRP (light blue) binds to within the Le region (dark blue) at the 3' end of the genome. During replication the vRdRP reads through the entire length of the genome (black solid line) to produce a positive sense antigenome. This antigenome acts as a template for genome RNA synthesis with both the antigenome and genome encapsidated in NP protein (yellow, antigenome encapsidation not shown).

1.5.5 IFN antagonism by Paramyxoviruses

Paramyxoviruses, like other viruses, have developed evasion tactics to overcome the IFN response and permit successful infection with the majority of Paramyxoviruses utilising the same strategies to overcome the both the IFN induction and signalling pathways.

Specifically, it is the P/V/C gene products of Paramyxoviruses that target key components of the IFN signalling pathway upon viral infection (Goodbourn and Randall, 2009). Orthorubulaviruses utilise a proteasomal degradation approach to IFN antagonism with the V protein of hPIV2 targeting STAT2 and the V protein of PIV5 targeting STAT1, for proteasomal degradation respectively (Didcock et al., 1999; Parisien et al., 2001; 2002; Ramachandran and Horvath, 2009). Conversely, Respiroviruses cause cytoplasmic sequestration of key IFN signalling components to prevent binding of ISGF3 to the ISRE and the subsequent expression of ISGs. The C protein of hPIV3 inhibits the phosphorylation of STAT1 (Malur et al., 2005) whilst the same protein in hPIV1 blocks the nuclear translocation of STAT1/2 (Schomacker et al., 2012). Additionally, a C-terminal domain in the V protein of all Paramyxoviruses is able to bind MDA-5, a RLR PRR, to prevent downstream activation of the IFN-β promoter (Andrejeva

et al., 2004; Childs et al., 2007). Orthopneumoviruses, such as hRSV, do not produce P/V/C gene products, but the expression of the NS1 and NS2 gene products result in a similar phenotype to that of Paramyxoviruses, specifically the Orthorubulaviruses. Both NS1 and NS2 mediate and promote STAT2 for proteasomal degradation respectively (Lo, Brazas and Holtzman, 2005). Whilst there are differences, this highlights the redundancy in their actions with all resulting in the inhibition of ISG expression, known as IFN antagonism.

It is also known that Paramyxoviruses can establish persistent infections, first being shown by Choppin in 1964, that upon infection with PIV5, no cytopathic effect of virus replication was seen with cells remaining undamaged over an extended period of time (Choppin, 1964). Persistent viral infections are those in which the virus is not cleared by the host and remains either, replicating at a low level or not at all (Boldogh, Albrecht and Porter, 1996). It is now known that Paramyxoviruses are able to repress viral replication in the cell, to become a persistent infection, through a single amino acid change. A phenylalanine to serine substitution at position 157 (F157S) of the P protein is able to switch the infection from lytic to persistent thereby resulting in reduced viral genome transcription and subsequent protein synthesis (Young et al., 2019). Additionally, the NP and P proteins of PIV5 have been shown to localise to cytoplasmic inclusion bodies (Fearns, Young and Randall, 1994). Together this results in a quiescent Paramyxovirus infection that allows evasion of detection by PRRs in the host cell preventing an innate immune response.

Despite the medical and economical significance of the Paramyxoviruses, they are relatively understudied with key information about how they interact with the host not yet understood. As such, implementation of the previously described techniques are well places to further our understanding of this virus family.

1.5.6 Antiviral restriction factors of Paramyxoviruses

Whilst specific ISGs with antiviral activity are unknown for most viruses, an exception is found in PIV5 as previously described in section 1.3.5. It is well established that interferon-induced proteins with tetratricopeptide repeats 1 (IFIT1) is a strong host restriction factor primarily responsible for the antiviral response (Andrejeva et al., 2013).

The IFIT gene family is well characterised within the antiviral immune response, being amongst the most highly expressed genes induced by IFN signalling (Mears and Sweeney, 2018). They are antiviral RNA-binding proteins that act through various mechanisms, including the direct binding to non-self RNA and interaction with eIF3 to inhibit translation. Having coevolved with the IFN system, they are conserved amongst vertebrates with mammals encoding IFIT1, -1B, -2, -3 and -5 in various configurations. A member of the IFIT family, IFIT1 (otherwise known as ISG56), is rapidly induced during early infection following both IFN-α/β or IRF3-dependent signalling (Diamond and Farzan, 2012). It has subsequently been shown to have nucleic acid binding activity with specificity for single stranded ppp-RNA due to its structure (Pichlmair et al., 2006; 2011; Baum and García-Sastre, 2010; Abbas et al., 2013).

IFIT1 is known to be the primary restriction factor of PIV5 infection as previously discussed. It was identified that upon infection of IFN pre-treated cells with PIV5, there was a rapid loss of viral protein synthesis however this was established to not be a result of generic, well characterised ISGs (Carlos et al., 2007). Subsequent investigation revealed the foremost restriction factor to be IFIT1, with IFIT1 deficiency resulting in levels of protein synthesis similar to that of a non-IFN treated control. IFIT1 restriction of viral protein expression was found to be the result of a specific block in translation of viral mRNA (Andrejeva et al., 2013). This corroborates with the earlier findings that IFIT1 recognises and binds ppp-RNA (Pichlmair et al., 2011) as Paramyxovirus transcripts present a 5'-triphosphate group (Laudenbach et al., 2021).

Further work has shown that Rubulaviruses, of which PIV5 belongs, are specifically inhibited by IFIT1 to a higher degree than other Paramyxoviruses due differences in the cap structure of the viral mRNA (Young et al., 2016). Although methylated at the N7 position of the guanine cap (m7Gppp) they are not methylated at the 2' O-position of cap 0 (m7GpppNpRNA). IFIT1 has no dependency on methylation of the N7 cap of ppp-RNA however, the absence of 2' O-position methylation of cap 0 significantly increases sensitivity of IFIT1 to the RNA causing inhibition of translation (Daffis et al., 2010; Habjan et al., 2013; Kumar et al., 2014). Other viruses, including other Mononegavirales, encode 2'-O methyltransferases, a countermeasure to IFIT1, but Rubulaviruses have not evolved this evasion mechanism. It has been suggested by Young et. al. that although a lack of methylation at the 2' O-position of the mRNA cap subjects the virus to inhibition by IFIT1, it may benefit the virus by allowing PIV5 to establish its characteristic persistent infection. Viral proteins M, F and HN are sensitive to IFIT1 whilst NP and L are not therefore allowing for continued replication without spread (Young et al., 2016).

Additional studies investigating PIV5 have suggested no role of either PKR or OAS/ RNase L in antagonising PIV5 transcription and translation (Carlos et al., 2007), otherwise broadly acting ISGs. However, unlike PIV5, other viruses are susceptible to numerous antiviral ISGs with each virus targeted by a unique subset of the 300+ ISGs; combinations of which have been shown to have additive effects (Schoggins et al., 2011). Previous work has shown IFIT1 has some antiviral activity against hPIV2 (Young et al., 2016) and some to little activity against hPIV3 (Rabbani et al., 2016; Young et al., 2016; Holthaus et al., 2020). Upon knockdown of IFIT1, the amount of viral protein is not significantly greater than control (Young et al., 2016; Holthaus et al., 2020) however, alternative work shows that presence of IFIT1 decreases hPIV3 mRNA between 4-8 fold (Rabbani et al., 2016). This suggests IFIT1 is likely a minor antiviral factor against hPIV3 and other ISGs have a more predominant role.

Further work has identified additional ISGs partially responsible for restricting hPIV3 and hRSV infection including IFITM1, PKR and Viperin (Schoggins et al., 2014; Zhang et al., 2015a; Rabbani et al., 2016; Smith et al., 2018). Additionally, using a human interferon-stimulated gene short-hairpin RNA library, Subramanian et. al. identified TDRD7 as a restriction factor of both Paramyxo- and Pneumoviruses, specifically, SeV, RSV and hPIV3. TDRD7 was shown to function by inhibiting the autophagy pathway these virus families use for their replication (Subramanian et al., 2018; 2020). As previously mentioned, Paramyxoviruses are likely to be inhibited by a number of ISGs working in concert and so it is likely far more ISGs than those named here play a role in viral restriction.

1.6 Research Objectives

As viruses are obligate intracellular pathogens, viral infection is dependent on the interplay between a number of host genes; both host dependency factors, that promote viral infection, and antiviral restriction factors, that hinder infection. It is the balance between these two classes of genes that determines whether an infection is successful or not. Therefore, identification of novel host genes that play either role, not only gives us a greater understanding of fundamental virus biology but, on further understanding of their mechanism of action, could provide potential therapeutic avenues to be exploited.

However, an underlying problem faced when trying to answer these questions is the large amount of redundancy within both responses, but especially the antiviral response. Alongside this, multiple restriction factors are often required to work in concert to produce an antiviral response as they exhibit low to moderate activity when expressed in isolation (section 1.3.5). Together, these two factors make studying the response difficult. Current techniques are limited by either; only investigating known ISGs via ISG libraries or lacking the experimental power for the identification of low to moderately acting ISGs due to their weak phenotype in isolation. The former, in particular, potentially misses out on the identification of novel genes or genes that play an important regulatory role in the innate immune response that would not be considered canonical ISGs, therefore limiting the information gained from these approaches.

We are therefore using genome wide CRISPR/Cas9 screening, due to its aforementioned advantages over other genome wide techniques and aim to improve the identification of hits by exploiting known negative regulators of the response (section 1.3.5). This thesis therefore acts as a starting point for not only understanding redundancy but improving the identification of hits for furthering our fundamental understanding of virus biology and identifying new avenues for investigation.

The overall aim of this project was to further identify sets of genes that both promote paramyxovirus infection (host dependency factors) and restrict paramyxovirus infection (antiviral restriction factors) through a genome wide CRISPR/Cas9 screening approach. However, whilst the investigation is focussed on understating paramyxovirus biology, we also question whether restriction factors are virus specific or have broader roles within the innate immune response.

To summarise, the aims of this project were therefore three-fold: (i) to optimise a genome wide CRISPR/Cas9 screening workflow, to include infection, gating and IFN pre-treatment conditions, for the identification of Paramyxovirus HDFs and AFs, (ii) to use this optimised screening workflow to identify novel HDF and AF genes involved in hPIV3 infection through the use of high-throughput sequencing and (iii) to further validate and characterise hit genes, exploring their mechanism of action, and identify if they are also implicated in other virus infections *in vitro*.

Chapter 2: Materials

2.1 Prokaryotic Cell Culture

Table 2.1.1: E. coli strains used within thesis.

Name	Genotype	Source	Notes
NZY5α competent cells	fhuA2Δ(argF-lacZ)U169 phoA glnV44 Φ80 Δ(lacZ)M15 gyrA96 recA1 relA1 endA1 thi-1 hsdR17	nzytech	
NEB 10-beta Electrocompetent *E. coli*	*Δ(ara-leu) 7697 araD139 fhuA ΔlacX74 galK16 galE15 e14- Φ80dlacZΔM15 recA1 relA1 endA1 nupG rpsL* (Str^R) *rph spoT1 Δ(mrr-hsdRMS-mcrBC)*	NEB	DH10B derivative

Table 2.1.2: Reagents for E. coli work.

Name	Composition	Concentration in LB	Source
LB Media	1% (w/v) tryptone, 0.5% (w/v) yeast extract, 0.5% (w/v) NaCl pH 7.0	n/a	St Andrews Media Kitchen
Ampicillin	Ampicillin sodium salt	100 mg/ml	Fisher Bioreagent

2.2 Mammalian Cell Culture

Table 2.2.1: Naïve mammalian cell lines used.

Name	Description
A549	Human carcinomic alveolar basal cell line
HEK 293T	Human embryonic kidney cell line transformed with SV40 large T antigen
293 FT	Human embryonic kidney cell line transformed with SV40 large T antigen
Vero	African green monkey kidney cell lines

Table 2.2.2 Mammalian cell lines generated.

Internal Inventory	Name	Description	Source
2579	A549-Cas9	Derivative of A549 cell line transduced with functional Cas9	N/A Thesis
2928	A549-Cas9.NC1	Derivative of A549-Cas9 cell line transduced with non-cutting control sgRNA (NC1)	N/A Thesis

2296	A549-ISG15$^{-/-}$	A549 cell line expressing a mutant of the *Streptococcus pygenes* Cas9 protein (Cas9n) an sgRNA targetting *ISG15*	Gifted from Connor G.G. Bamford Holthaus, D., et al. 2020. Direct Antiviral Activity of IFN-Stimulated Genes Is Responsible for Resistance to Paramyxoviruses in ISG15-Deficient Cells. J Immunol 205 (1): 261–271
2794	A549-ISG15$^{-/-}$.Cas9	Derivative of A549-ISG15$^{-/-}$ cell line transduced with functional Cas9	N/A Thesis
2929	A549-ISG15$^{-/-}$.Cas9.NC1	Derivative of A549-ISG15$^{-/-}$ cell line transduced with with non-cutting control sgRNA (NC1)	N/A Thesis
2835	A549-Cas9.IFIT1$^{-/-}$	Derivative of A549-Cas9 cell line transduced with sgRNA targeting *IFIT1*	N/A Thesis
2850	A549-ISG15$^{-/-}$.Cas9.IFIT1$^{-/-}$	Derivative of A549-ISG15$^{-/-}$.Cas9 cell line transduced with sgRNA targeting *IFIT1*	N/A Thesis
2975	A549-Cas9.STAT2$^{-/-}$	Derivative of A549-Cas9 cell line transduced with sgRNA targeting *STAT2*	N/A Thesis
3114	A549-Cas9.SLC35A1$^{-/-}$	Derivative of A549-Cas9 cell line transduced with sgRNA targeting *SLC35A1*	N/A Thesis
3115	A549-Cas9.STT3A$^{-/-}$	Derivative of A549-Cas9 cell line transduced with sgRNA targeting *STT3A*	N/A Thesis
3116	A549-Cas9.DHX9$^{-/-}$	Derivative of A549-Cas9 cell line transduced with sgRNA targeting *DHX9*	N/A Thesis
3117	A549-Cas9.UFC1$^{-/-}$	Derivative of A549-Cas9 cell line transduced with sgRNA targeting *UFC1*	N/A Thesis
3118	A549-Cas9.PTAR1$^{-/-}$	Derivative of A549-Cas9 cell line transduced with	N/A Thesis

		sgRNA targeting *PTAR1*	
3118	A549-Cas9.RAD51$^{-/-}$	Derivative of A549-Cas9 cell line transduced with sgRNA targeting *RAD51*	N/A Thesis
3120	A549-Cas9.SMU1$^{-/-}$	Derivative of A549-Cas9 cell line transduced with sgRNA targeting *SMU1*	N/A Thesis
3121	A549-Cas9.IMP3$^{-/-}$	Derivative of A549-Cas9 cell line transduced with sgRNA targeting *IMP3*	N/A Thesis
3122	A549-Cas9.NF2$^{-/-}$	Derivative of A549-Cas9 cell line transduced with sgRNA targeting *NF2*	N/A Thesis
3123	A549-Cas9.HSD17B12$^{-/-}$	Derivative of A549-Cas9 cell line transduced with sgRNA targeting *HSD17B12*	N/A Thesis
3124	A549-Cas9.ZAP$^{-/-}$	Derivative of A549-Cas9 cell line transduced with sgRNA targeting *ZAP*	N/A Thesis
3125	A549-Cas9.P2RY14$^{-/-}$	Derivative of A549-Cas9 cell line transduced with sgRNA targeting *P2RY14*	N/A Thesis
3126	A549-Cas9.ELF1$^{-/-}$	Derivative of A549-Cas9 cell line transduced with sgRNA targeting *ELF1*	N/A Thesis
3127	A549-Cas9.HMOX1$^{-/-}$	Derivative of A549-Cas9 cell line transduced with sgRNA targeting *HMOX1*	N/A Thesis
3128	A549-Cas9.PPA2$^{-/-}$	Derivative of A549-Cas9 cell line transduced with sgRNA targeting *PPA2*	N/A Thesis
3129	A549-Cas9.EIF4EBP3$^{-/-}$	Derivative of A549-Cas9 cell line transduced with sgRNA targeting *EIF4EBP3*	N/A Thesis

Table 2.2.3: Mammalian cell culture media, additives, and supplements.

Solution name	Use	Source	Catalogue Number
Blasticidin	Antibiotic selection of cell lines	Sigma Aldrich	15205-25MG
Dimethyl sulphoxide (DMSO)	Freezing media supplement	Sigma Aldrich	D2650
Foetal calf serum (FCS)	DMEM supplement	Gibco	A5256701
Interferon alpha 2b (Intron A, IFN-α)	Induction of the IFN reponse in cell lines	Merck Sharp & Dohme Corp.	n/a
Penicillin	Antibiotic DMEM supplement	Duchefa Biochemie	P0142
Puromycin	Antibiotic selection of cell lines	InvivoGen	ant-pr-1
Roferon-A (IFN-a)	Induction of the IFN reponse in cell lines	Roche Pharma R&D Labs	n/a
Streptomycin	Antibiotic DMEM supplement	Melford	S62000

Table 2.2.4: Solutions, chemicals, and other reagents used in mammalian cell culture.

Solution name	Composition	Use	Source	Catalogue Number
Avicell 611	Avicell 611 5% w/v in ultra-pure water	Plaque assay overlay	Dupont	n/a
Calcium Chloride Solution	2.5 M $CaCl_2$	Transfection of cells	n/a	n/a
Chloroquine diphosphate	n/a	Transfection of cells	Sigma Aldrich	C6628-25G
Dulbecco's Modified Eagle Medium (DMEM)	n/a	Growth media	Corning	10-013-CV
Formaldehyde	10% v/v formalehyde in PBS	Fixation of cells	Fisher Scientific	11960025
HEPES buffered saline	50 mM HEPES, 0.28 M NaCl, 10 mM KCl, 1.5 mM Na2HPO4, 12 mM D-glucose, pH 7.05	Transfection of cells	Sigma	H887-20ML
Phosphate buffered saline (PBS)	n/a	Washing of cells	University of St Andrews Media Kitchen	n/a
Polybrene (Hexadimethrine bromide)	n/a	Transduction of cells with lentivirus	Sigma Aldrich	H9268-5G
Ruxolitinib	n/a	Inhibition of JAK/STAT IFN signalling in cells	Stratech	S1378-SEL
Trypsin/ EDTA solution	Trypsin 0.05% (w/v) and EDTA 0.02% (w/v) in ultra pure water	Trypsinisation of cell cultures	University of St Andrews Media Kitchen	n/a

2.3 Viruses

Table 2.3.1: List of viruses.

Virus	Host	Strain	Details	Reference
PIV3	Human	Washington/ 47885/57	Wild type strain of PIV3 (prototype)	Durbin, A. P., et al. 1999. Mutations in the C, D, and V open reading frames of human parainfluenza virus type 3 attenuate replication in rodents and primates. Virology 261: 319–330
PIV3	Human	JS	Wild type strain of PIV3 (vaccine strain)	Stokes A, Tierney EL, Murphy BR, Hall SL. The complete nucleotide sequence of the JS strain of human parainfluenza virus type 3: comparison with the Wash/47885/57 prototype strain. Virus Res. 1992 Sep 1;25(1-2):91-103
PIV3	Human	JS GFP	Recombinant strain of PIV3 (GFP)	Zhang L, et al. Infection of ciliated cells by human parainfluenza virus type 3 in an in vitro model of human airway epithelium. J Virol. 2005 Jan; 79(2):1113-24
PIV5	Host unknown	W3 mCherry	Recombinant strain of PIV5 (W3), expresses mCherry, causes persistent infections	Choppin, P. W. 1964. Multiplication of a myxovirus (Sv5) with minimal cyto- pathic effects and without interference. Virology 23: 224–233
PIV5	Canine	CPI^-	Wild type strain of PIV5 unable to block IFN signalling	Didcock, L., et al.1999.TheV protein of simian virus 5 inhibits interferon signalling by targeting STAT1 for proteasome-mediated degradation. J. Virol. 73: 9928–9933

2.4 Plasmids

Table 2.4.1: Table of external plasmids used.

Internal inventory	Name	Vector	Gene	Use	Source
172	pVSV-G	pCMV vector	VSV-G	Packaging plasmid	Addgene: pVSV-G
173	pCMV-DR8.91	pCMV vector	gag, pol, and rev	Lentivirus helper	Addgene: Vector Database - pCMV-dR8.91
183	pLentiGuide-Puro	Custom	Empty	sgRNA cloning backbone	Addgene: 52963
208	pLentiCas9-Blast	pLentiCas9-Blast	Cas9	Cas9 expression in cells	Addgene: 52962
237	pLentiCRISPRv2	pLentiCRISPRv2	Empty	sgRNA cloning backbone	
243	pMD2-G	pMD2-G	VSV-G	Packaging plasmid for lentivirus production. From #691 Nevels group.	https://www.addgene.org/12259/
244	psPAX2	psPAX2	HIV-1 gag, pol	2nd generation lentiviral packaging plasmid. Can be used with 2nd or 3rd generation lentiviral vectors and envelope expressing plasmid (Addgene#12259). From #693 Nevels group.	https://www.addgene.org/12260/

Table 2.4.2: Table of generated plasmids used.

Internal inventory	Name	Vector	Gene	Use	Source
214	pLentiGuide.Puro-NC1	pLentiGuide-Puro	NC1	Non-cutting sgRNA control expression in cells	CGGB
223	pLentiCRISPRv2-sgIFIT1.3	pLentiCRISPRv2	sgIFIT1	CRISPR Cas9 knockout of IFIT1 gene in cells #1	From: Johnson et al., 2018, Immunity, 48(3), pp.487-499.e5.
224	pLentiCRISPRv2-sgIFIT1.4	pLentiCRISPRv2	sgIFIT1	CRISPR Cas9 knockout of IFIT1 gene in cells #2	From: Johnson et al., 2018, Immunity, 48(3), pp.487-499.e5.
235	pLentiCRISPRv2-sgTDRD7.1	pLentiCRISPRv2	sgTDRD7	CRISPR Cas9 knockout of TDRD7 gene in cells #1	
236	pLentiCRISPRv2-sgTDRD7.2	pLentiCRISPRv2	sgTDRD7	CRISPR Cas9 knockout of TDRD7 gene in cells #2	
239	pLentiCRISPRv2-sgSTAT2	pLentiCRISPRv2	sgSTAT2	CRISPR Cas9 knockout of STAT2 gene in cells	
n/a	pLentiCRISPRv2-sgSLC35A1	pLentiCRISPRv2	sgSLC35A1	CRISPR Cas9 knockout of SLC35A1 gene in cells	
n/a	pLentiCRISPRv2-sgSTT3A	pLentiCRISPRv2	sgSTT3A	CRISPR Cas9 knockout of STT3A gene in cells	
n/a	pLentiCRISPRv2-sgDHX9	pLentiCRISPRv2	sgDHX9	CRISPR Cas9 knockout of DHX9 gene in cells	
n/a	pLentiCRISPRv2-sgUFC1	pLentiCRISPRv2	sgUFC1	CRISPR Cas9 knockout of UFC1 gene in cells	
n/a	pLentiCRISPRv2-sgPTAR1	pLentiCRISPRv2	sgPTAR1	CRISPR Cas9 knockout of PTAR1 gene in cells	
n/a	pLentiCRISPRv2-sgRAD51	pLentiCRISPRv2	sgRAD51	CRISPR Cas9 knockout of RAD51 gene in cells	
n/a	pLentiCRISPRv2-sgSMU1	pLentiCRISPRv2	sgSMU1	CRISPR Cas9 knockout of SMU1 gene in cells	
n/a	pLentiCRISPRv2-sgIMP3	pLentiCRISPRv2	sgIMP3	CRISPR Cas9 knockout of IMP3 gene in cells	
n/a	pLentiCRISPRv2-sgNF2	pLentiCRISPRv2	sgNF2	CRISPR Cas9 knockout of NF2 gene in cells	
n/a	pLentiCRISPRv2-sgHSD17B12	pLentiCRISPRv2	sgHSD17B12	CRISPR Cas9 knockout of HSD17B12 gene in cells	

n/a	pLentiCRISPRv2-sgZAP	pLentiCRISPRv2	sgZAP	CRISPR Cas9 knockout of ZAP gene in cells	
n/a	pLentiCRISPRv2-sgP2RY14	pLentiCRISPRv2	sgP2RY14	CRISPR Cas9 knockout of P2RY14 gene in cells	
n/a	pLentiCRISPRv2-sgELF1	pLentiCRISPRv2	sgELF1	CRISPR Cas9 knockout of ELF1 gene in cells	
n/a	pLentiCRISPRv2-sgHMOX1	pLentiCRISPRv2	sgHMOX1	CRISPR Cas9 knockout of HMOX1 gene in cells	
n/a	pLentiCRISPRv2-sgPPA2	pLentiCRISPRv2	sgPPA2	CRISPR Cas9 knockout of PPA2 gene in cells	
n/a	pLentiCRISPRv2-sgEIF4EBP3	pLentiCRISPRv2	sgEIF4EBP3	CRISPR Cas9 knockout of EIF4EBP3 gene in cells	

2.5 Oligonucleotides

Table 2. 5.1: Details of RT-qPCR primers used.

Sequence name	Sequence (5' - 3')	Use	F/R
TDRD7	GCCTGATGCTGAAATGTCT	RT-qPCR primer #1	F
	CATCAGACATCCATGCATC		R
	GTGGAGAAACCTTGCAGTG	RT-qPCR primer #2	F
	CAGAAGGCCATTCTCTATGC		R
IFN-β	GCTTCTCCACTACAGCTCTTTC	RT-qPCR primer	F
	CAGTATTCAAGCCTCCCATTCA		R
NF2	TTCCAGGTGGCTACTCCAGAG	RT-qPCR primer	F
	TACAACTTCTGCCTCCCAGG		R
HSD17B12	CCAGGTAAAGTTCAAGCTGCG	RT-qPCR primer	F
	CAGTGGCATGATCTTGGCTC		R
ZAP	AGCACTGTTCCTCCTTGTAGGG	RT-qPCR primer	F
	GATCAGGAGTTCGAGACCAGC		R
MxA	GCCTGCTGACATTGGGTATAA	RT-qPCR primer	F
	CCCTGAAATATGGGTGGTTCTC		R
HERC5	GACGAACTCTTGCACCGTCTC	RT-qPCR primer	F
	GCGTCCACAGTCATTTTCCAC		R
ISG15	ACCTCTGAGCATCCTGGTGAG	RT-qPCR primer	F
	GAAGGTCAGCCAGAACAGGTC		R
β-Actin	AGCGAGCATCCCCCAAAGTT	RT-qPCR primer	F
	AGGGCACGAAGGCTCATCATT		R

Table 2.5.2: Details of PCR primers for Mycoplasma testing.

Sequence name	Sequence (5' - 3')	Use	F/R
Myco-5-1	CGCCTGAGTAGTACGTTCGC	Mycoplasma testing	F
Myco-5-2	CGCCTGAGTAGTACGTACGC	Mycoplasma testing	F
Myco-5-3	TGCCTGAGTAGTACATTCGC	Mycoplasma testing	F
Myco-5-4	TGCCTGGGTAGTACATTCGC	Mycoplasma testing	F
Myco-5-5	CGCCTGGGTAGTACATTCGC	Mycoplasma testing	F
Myco-5-6	CGCCTGAGTAGTATGCTCGC	Mycoplasma testing	F
Myco-5-7	TGCACCATCTGTCACTCTGTTAAC	Mycoplasma testing	F
Myco-3-1	GCGGTGTGTACAAGACCCGA	Mycoplasma testing	R
Myco-3-2	GCGGTGTGTACAAAACCCGA	Mycoplasma testing	R
Myco-3-3	GCGGTGTGTACAAACCCCGA	Mycoplasma testing	R
Myco-3-7	GGGAGCAAACAGGATTAGATAC	Mycoplasma testing	R

Table 2.5.3: Details of sequencing primers used.

Vector name	Sequence	Use
pLentiGuide-Puro	ATTGTGGATGAATACTGCC	Sequencing of sgRNA clones
pLentiCRISPRv2	GGCAGGGATATTCACCATTATCGTTTCAGA	Sequencing of shRNA clones Sequencing of sgRNA clones

Table 2.5.4: sgRNA oligonucleotides for gene knockout.

Gene	Cell line generated	ENSEMBL ID	sgRNA sequence (5' - 3')	Use	F/R
Non-cutting guide	A549-Cas9.NC1	n/a	caccGTGACGTACCGCTGGAGGTA	Control for knockout cell lines	F
			aaacTACCTCCAGCGGTACGTCAC		R
ISG15	A549-ISG15$^{-/-}$ A549-Cas9.ISG15$^{-/-}$ A549-Cas9.ISG15$^{-/-}$.IFIT1$^{-/-}$	ENSG00000187608	caccgCCTGACGGTGAAGATGCTGG	Independent sgRNA #1	F
			aaacCCAGCATCTTCACCGTCAGGc		R
			caccgCTTCAGCTCTGACACCGACA	Independent sgRNA #2	F
			aaacTGTCGGTGTCAGAGCTGAAGc		R
			caccGACAGCCAGACGCTGCTGGA	Independent sgRNA #3	F
			aaacTCCAGCAGCGTCTGGCTGTC		R
IFIT1	A549-Cas9.IFIT1$^{-/-}$ A549-Cas9.ISG15$^{-/-}$.IFIT1$^{-/-}$	ENSG00000185745	caccgATGACAACCAAGCAAATGTG	Independent sgRNA	F
			aaacCACATTTGCTTGGTTGTCATc		R
STAT2	A549-Cas9.STAT2$^{-/-}$	ENSG00000170581	caccgCTCTGTGCAACCGTACACGA	Independent sgRNA #1	F
			aaacTCGTGTACGGTTGCACAGAGc		R
			caccGCCAGTTCTCGAAACACCTG	Independent sgRNA #2	F
			aaacCAGGTGTTTCGAGAACTGGC		R
SLC35A1	A549-Cas9.SLC35A1$^{-/-}$	ENSG00000164414	caccgTCTGTGATACACACGGCTG	HDF independent sgRNA #1	F
			aaacCAGCCGTGTGTATCACAGAc		R
			caccgTGGAGTTACGCTTGTACAG	HDF independent sgRNA #2	F
			aaacCTGTACAAGCGTAACTCCAc		R
STT3A	A549-Cas9.STT3A$^{-/-}$	ENSG00000134910	caccGTAAGGTGGTACGTGACGA	HDF independent sgRNA #1	F
			aaacTCGTCACGTACCACCTTAC		R
			caccGAGTAGAAACGCCCCGTCC	HDF independent sgRNA #2	F
			aaacGGACGGGGCGTTTCTACTC		R
DHX9	A549-Cas9.DHX9$^{-/-}$	ENSG00000135829	caccGAGCCTCGATGAGTTCAAA	HDF independent sgRNA #1	F
			aaacTTTGAACTCATCGAGGCTC		R
			caccGAGTAGTAATCCTTCAAGT	HDF independent sgRNA #2	F
			aaacACTTGAAGGATTACTACTC		R
UFC1	A549-Cas9.UFC1$^{-/-}$	ENSG00000143222	caccGACAACGATTGGTTCCGAC	HDF independent sgRNA #1	F
			aaacGTCGGAACCAATCGTTGTC		R
			caccGGTGGCAAAATATGCCTGA	HDF independent sgRNA #2	F

			aaacTCAGGCATATTTTGCCACC		R
PTAR1	A549-Cas9.PTAR1$^{-/-}$	ENSG00000188647	caccgCGACTCATACAAGAAGAGA	HDF independent sgRNA #1	F
			aaacTCTCTTCTTGTATGAGTCGc		R
			caccgTACCACTGCATGGAACGTG	HDF independent sgRNA #2	F
			aaacCACGTTCCATGCAGTGGTAc		R
RAD51	A549-Cas9.RAD51$^{-/-}$	ENSG00000051180	caccGTTGCCTATGCGCCAAAGA	HDF independent sgRNA #1	F
			aaacTCTTTGGCGCATAGGCAAC		R
			caccgTATAGCTTCCCATTGACCG	HDF independent sgRNA #2	F
			aaacCGGTCAATGGGAAGCTATAc		R
SMU1	A549-Cas9.SMU1$^{-/-}$	ENSG00000122692	caccGTGCTCGATTTTCTCCAGA	HDF independent sgRNA #1	F
			aaacTCTGGAGAAAATCGAGCAC		R
			caccgTTAGCTGGCGAAGTCAGTG	HDF independent sgRNA #2	F
			aaacCACTGACTTCGCCAGCTAAc		R
IMP3	A549-Cas9.IMP3$^{-/-}$	ENSG00000177971	caccgCCTTGCTCCACAAAGGCCA	HDF independent sgRNA #1	F
			aaacTGGCCTTTGTGGAGCAAGGc		R
			caccgCGCCGCGCCAGCTCACGCA	HDF independent sgRNA #2	F
			aaacTGCGTGAGCTGGCGCGGCGc		R
NF2	A549-Cas9.NF2$^{-/-}$	ENSG00000186575	caccGATTTGGTGTGCCGGACTC	AF independent sgRNA #1	F
			aaacGAGTCCGGCACACCAAATC		R
			caccgAACATCTCGTACAGTGACA	AF independent sgRNA #2	F
			aaacTGTCACTGTACGAGATGTTc		R
HSD17B12	A549-Cas9.HSD17B12$^{-/-}$	ENSG00000149084	caccgAGTACTACCTGTGACAACT	AF independent sgRNA #1	F
			aaacAGTTGTCACAGGTAGTACTc		R
			caccGACTTACATTGTCCAAGTC	AF independent sgRNA #2	F
			aaacGACTTGGACAATGTAAGTC		R
ZAP	A549-Cas9.ZAP$^{-/-}$	ENSG00000105939	caccgTGCGGGTGAGATCGTCCAC	AF independent sgRNA #1	F
			aaacGTGGACGATCTCACCCGCAc		R
			caccgCTGTGACCACTTCACCCGA	AF independent sgRNA #2	F
			aaacTCGGGTGAAGTGGTCACAGc		R
P2RY14	A549-Cas9.P2RY14$^{-/-}$	ENSG00000174944	caccgTCCTACTCAATGGAGTGTC	AF independent sgRNA #1	F
			aaacGACACTCCATTGAGTAGGAc		R
			caccgATTCCGACTTGACTTAAGG	AF independent sgRNA #2	F

			aaacCCTTAAGTCAAGTCGGAATc		R
ELF1	A549-Cas9.ELF1$^{-/-}$	ENSG00000120690	caccgCATGTTCCACAATTACGGC	AF independent sgRNA #1	F
			aaacGCCGTAATTGTGGAACATGc		R
			caccgATATTTGGCGTAGTGGCTG	AF independent sgRNA #2	F
			aaacCAGCCACTACGCCAAATATc		R
HMOX1	A549-Cas9.HMOX1$^{-/-}$	ENSG00000100292	caccgAGGGCCAGGTGACCCGAGA	AF independent sgRNA #1	F
			aaacTCTCGGGTCACCTGGCCCTc		R
			caccgCAGGTAGCGGGTGTAGGCG	AF independent sgRNA #2	F
			aaacCGCCTACACCCGCTACCTGc		R
PPA2	A549-Cas9.PPA2$^{-/-}$	ENSG00000138777	caccGAGCTACTTACTAAAGAAG	AF independent sgRNA #1	F
			aaacCTTCTTTAGTAAGTAGCTC		R
			caccGATGTTAAGAAGTTCAAAC	AF independent sgRNA #2	F
			aaacGTTTGAACTTCTTAACATC		R
EIF4EBP3	A549-Cas9.EIF4EBP3$^{-/-}$	ENSG00000243056	caccgTATACGCCACTACCCCCGG	AF independent sgRNA #1	F
			aaacCCGGGGGTAGTGGCGTATAc		R
			caccgTGAGTTCTTGCACTCCAGC	AF independent sgRNA #2	F
			aaacGCTGGAGTGCAAGAACTCAc		R

Table 2.5.5: Primers used for next generation sequencing of screening gDNA.

Primer	Sequence	Use	F/R
PCR1_F1	TCGTCGGCAGCGTCAGATGTGTATAAGAGACAGTCTTGTGGAAAGGACGAAACACCG	PCR amplification	F
PCR1_F2	TCGTCGGCAGCGTCAGATGTGTATAAGAGACAGATCTTGTGGAAAGGACGAAACACCG	PCR amplification	F
PCR1_F3	TCGTCGGCAGCGTCAGATGTGTATAAGAGACAGGATCTTGTGGAAAGGACGAAACACCG	PCR amplification	F
PCR1_F4	TCGTCGGCAGCGTCAGATGTGTATAAGAGACAGCGATCTTGTGGAAAGGACGAAACACCG	PCR amplification	F
PCR1_F5	TCGTCGGCAGCGTCAGATGTGTATAAGAGACAGTCGATCTTGTGGAAAGGACGAAACACCG	PCR amplification	F
PCR1_F6	TCGTCGGCAGCGTCAGATGTGTATAAGAGACAGATCGATCTTGTGGAAAGGACGAAACACCG	PCR amplification	F
PCR1_F7	TCGTCGGCAGCGTCAGATGTGTATAAGAGACAGGATCGATCTTGTGGAAAGGACGAAACACCG	PCR amplification	F
PCR1_F8	TCGTCGGCAGCGTCAGATGTGTATAAGAGACAGCGATCGATCTTGTGGAAAGGACGAAACACCG	PCR amplification	F
PCR1_F9	TCGTCGGCAGCGTCAGATGTGTATAAGAGACAGACGATCGATCTTGTGGAAAGGACGAAACACCG	PCR amplification	F
PCR1_F10	TCGTCGGCAGCGTCAGATGTGTATAAGAGACAGTACGATCGATCTTGTGGAAAGGACGAAACACCG	PCR amplification	F
PCR1_R	GTCTCGTGGGCTCGGAGATGTGTATAAGAGACAGCTAAAGCGCATGCTCCAGAC	PCR amplification	R
idx_S502	AATGATACGGCGACCACCGAGATCTACAC<u>CTCTCTAT</u>TCGTCGGCAGCGT*C	Barcoding	n/a
idx_S503	AATGATACGGCGACCACCGAGATCTACAC<u>TATCCTCT</u>TCGTCGGCAGCGT*C	Barcoding	n/a
idx_S504	AATGATACGGCGACCACCGAGATCTACAC<u>AGAGTAGA</u>TCGTCGGCAGCGT*C	Barcoding	n/a
idx_S517	AATGATACGGCGACCACCGAGATCTACAC<u>GCGTAAGA</u>TCGTCGGCAGCGT*C	Barcoding	n/a
idx_N701	CAAGCAGAAGACGGCATACGAGAT<u>TCGCCTTA</u>GTCTCGTGGGCTCG*G	Barcoding	n/a
idx_N702	CAAGCAGAAGACGGCATACGAGAT<u>CTAGTACG</u>GTCTCGTGGGCTCG*G	Barcoding	n/a
idx_N703	CAAGCAGAAGACGGCATACGAGAT<u>TTCTGCCT</u>GTCTCGTGGGCTCG*G	Barcoding	n/a
idx_N704	CAAGCAGAAGACGGCATACGAGAT<u>GCTCAGGA</u>GTCTCGTGGGCTCG*G	Barcoding	n/a
idx_N705	CAAGCAGAAGACGGCATACGAGAT<u>AGGAGTCC</u>GTCTCGTGGGCTCG*G	Barcoding	n/a
idx_N706	CAAGCAGAAGACGGCATACGAGAT<u>CATGCCTA</u>GTCTCGTGGGCTCG*G	Barcoding	n/a

Note: 1st round PCR primers (PCR1_F1 to PCR1_R) ordered as regular oligos and index primers (idx_S502 to idx_N706), 2nd round PCR, as Ultramers from IDT with the last base (*) Phosphorothioated. Barcodes within index primers are underlined.

2.6 Enzymes

Table 2.6.1: Restriction enzymes used within thesis.

Name	Use	Source	Catalogue number
*Bsm*BI-v2	Linearisation of vector plasmids	NEB	R0739S
HindIII	Screening of successful cloning vectors	Promega	R6041
HindIII-HF	Digest of non-infected screening DNA	NEB	R3104S

Table 2.6.2: Modifying enzymes used in thesis.

Name	Use	Source	Catalogue number
DreamTaq polymerase	Amplification of DNA in PCR	ThermoScientific	EP0702
FastAP	Dephosphorylation of vector plasmids	ThermoScientific	EF0651
NEBNext Ultra II Q5 Master Mix	Polymerase master mix for second round baroding PCR (screening gDNA)	NEB	M0544S
Proteinase K	Digestion of proteins in gDNA extraction from cells	Qiagen	56404
Q5 Hot Start High-Fidelity DNA Polymerase	Polymerase for first round PCR (screening gDNA)	NEB	M0493S
RNase A	Removal of residual RNA in DNA purification	Omega Bio-Tek	D6945-01
T4 DNA ligase	Ligation of oligonucleotides into linearised vector	Promega	M1801
T4 Polynucleotide kinase (PNK)	Phosphorylation of oligonucleotides maintaining 5' restriction enzyme site overhangs	FisherScientific	10531061

2.7 Standards

Table 2.7.1: List of standards used in thesis.

Name	Use	Source	Catalogue number
1 kb DNA ladder	DNA gel electrophoresis standard	New England Biolabs	N3232S
100 bp DNA ladder	DNA gel electrophoresis standard	Promega	G2101
PageRulerTM Plus Prestained 10-250 kDa Protein Ladder	Acrylamide gel electrophoresis protein ladder	Fisher Scientific	26619

2.8 Buffers and Solutions

Table 2.8.1: Buffers and Solutions used in thesis.

Name	Composition	Source	Catalgue Number
AMPure XP beads	n/a	Beckman Coulter	A63880
Crystal violet	Crystal violet 0.15% w/v/ in ultrapure water	n/a	
FACS Clean	n/a	BD Biosciences	340345
FACS rinse solution	n/a	BD Biosciences	340346
FACS running buffer	PBS, 3% FCS, 0.1% sodium azide	n/a	n/a
Laemmli sample buffer (2x)	4% w/v SDS, 20% glycerol, 0.125 M Tris-HCl pH 6.8, ultrapure water	n/a	n/a
MOPS	0.2 M MOPS free acid, 0.05 M sodium acetate, 0.01 M EDTA	St Andrews Media Kitchen	n/a
PBS with tween (PBS-T)	PBS supplemented with 0.1% v/v tween-20	St Andrews Media Kitchen	n/a
Phosphate buffer saline (PBS)	n/a	St Andrews Media Kitchen	n/a
Sample loading dye	n/a	New England Biolabs	B7024A
TBE	n/a	St Andrews Media Kitchen	n/a
Transfer buffer	14.4% w/v glycine, 3.02% w/v Tris Base, 20% methanol in ultrapure water	n/a	n/a

2.9 Chemicals

Table 2.9.1: Chemicals not previously mentioned.

Chemical	Source	Catalogue number
Agarose	Fisher	BP160-500
B-mercaptoethanol	Fisher Scientific	10303050
Ethanol	Fisher Scientific	10437341
Ethidium Bromide	Invitrogen	15585-011
Glycerol	Sigma Aldrich	G9012-500ML
Isopropanol	Fisher Scientific	10497070
Lipofectamine 2000	Invitrogen	11668027
Methanol	Fisher Scientific	10284580
Non-fat milk powder	Marvel	n/a
SIGMAFAST BCIP/NBT	Sigma Aldrich	B5655-25TAB
Sodium Azide	Sigma Aldrich	S2002-100G
Tween-20	Sigma Aldrich	P1379-500ML
Mercaptoethanol	Fisher Scientific	10265220

2.10 Kits

Table 2.10.1: Commercial kits used in thesis.

Name	Use	Source	Catalogue number
Direct-zol RNA MiniPrep Plus	RNA extraction from cells	Zymo Research	R2072
EZNA Plasmid DNA Maxi Kit	Large scale plasmid isolation from *E. coli*	Omega Bio-Tek	D6922-04
EZNA Plasmid DNA Mini Kit II	Small scale plasmid isolation from *E. coli*	Omega Bio-Tek	D6945-01
LunaScript® RT SuperMix Kit	cDNA synthesis from RNA	New England Biolabs	E3010S
Mix & Go E. coli Transformation Kit	Preparation of competent *E. coli*	Zymo Research	T3001
NucleoSpin Gel and PCR Clean-up Kit	Isolation of gDNA from non-fixed cells	Macherey-Nagel	740609.5
PCR Mycoplasma Kit II	Mycoplasma testing of tissue culture cells	Promokine, VWR	POMOPK-CA20-700-20
QIAamp DNA FFPE Tissue Kit	Isolation of gDNA from foramldehyde fixed cells	Qiagen	56404
Qiagen Plasmid Maxi Kit	Large scale plasmid isolation from *E. coli*	Qiagen	12163
QIAprep Spin Miniprep Kit	Small scale plasmid isolation from *E. coli*	Qiagen	27104
QuantiFluor ONE dsDNA System	Quantification of DNA concentration	Promega	E4871
Wizard SV Gel and PCR Clean-Up system	Gel and PCR clean-up of DNA	Promega	A9281

2.11 Antibodies

Table 2.11.1: Details of primary antibodies used.

Antibody	Manufacturer	Species	Dilution for immunoblotting	Dilution for flow cytometry
anti-IFIT1	Santa Cruz Biotechnology (sc82946)	Goat	1:1000	n/a
anti-ISG15 F9	Santa Cruz Biotechnology (sc166755)	Mouse	1:1000	n/a
anti-MxA	Proteintech	Rabbit	1:500	n/a
anti-PIV3 HN cocktail (4854, 4497, 4477)	(Klippmark et al., 1990)	Mouse	n/a	1:200
anti-PIV5 NP 125	(Randall et al., 1987)	Mouse	1:2000	n/a
anti-STAT1	Santa Cruz Biotechnology (sc-417)	Mouse	1:1000	n/a
anti-STAT2	Santa Cruz Biotechnology (sc-22816)	Rabbit	1:1000	n/a
anti-TDRD7	Novus	Rabbit	1:750	n/a
anti-USP18	Cell Signalling Technology	Rabbit	1:1000	n/a
anti-NF2	Cell Signalling Technology (12888)	Rabbit	1:1000	n/a
anti-HSD17B12	Invitrogen (13446177)	Rabbit	1:1000	n/a
anti-ZAP	Invitrogen (15721361)	Rabbit	1:1000	n/a
anti-IRF3	Cell Signalling Technology (11904)		1:1000	n/a
β-Actin	Sigma AC-15	Mouse	1:2500	n/a

Table 2.11.2: Details of secondary antibodies used.

Antibody	Manufacturer	Species	Dilution for immunoblotting	Dilution for flow cytometry	Dilution for immunostaining
anti-goat HRP	Dako (P0449)	Rabbit	1:5000	n/a	n/a
anti-goat IRDye 800CW	LiCor (926-32214)	Donkey	1:10,000	n/a	n/a
anti-mouse Alexa Fluor 488	Invitrogen (A11001)	Goat	n/a	1:500	n/a
anti-mouse horseradish peroxidase (HRP)	Dako (P0447)	Goat	1:5000	n/a	n/a
anti-mouse IgG conjugated to alkaline phosphatase	Abcam	Goat	n/a	n/a	1:1000
anti-mouse IRDye 800CW	LiCor (926-32210)	Goat	1:10,000	n/a	n/a
anti-rabbit IRDye 800CW	LiCor (926-32211)	Goat	1:10,000	n/a	n/a
anti-rabbit HRP	Dako (P0448)	Goat	1:5000	n/a	n/a

2.12 Instruments and Equipment

Table 2.12.1: Key instruments and laboratory equipment used within thesis.

Product	Manufacturer	Use
CytoFLEX flow cytometer	Beckman Coulter	Flow cytometry
EVOS M5000 cell imaging system	Thermo Fisher Scientific	Imaging of live cells
FACSAria IIIu 4 laser Cell Sorter	BD Biosciences	Fluorescence activated cell sorting
FACSJazz cell sorter	BD Biosciences	Flow cytometry and fluorescence activated cell sorting
GenePulser Xcell electroporation system	BioRad	Electroporation transformation of E. coli
Guava easyCyte HT System	Merck Millipore	Flow cytometry

2.13 Computer Programmes

Table 2.13.1: Details of software and databases used within thesis.

Name	Provider	Use
Excel	Microsoft	Data processing and analysis
Fiji ImageJ	ImageJ, NIH	Image analysis and editing
Flowing Software	Turku Biosciences	Analysis of flow cytometry and cell sorting data
Flowing Sortware	BD Biosciences	Acquiring of flow cytometry and cell sorting data
FlowJo v10	BD Biosciences	Analysis of flow cytometry and cell sorting data
GenBank	NCBI	Retrieval of DNA sequences
GraphPad Prism	GraphPad Software	Data analysis and graphing
Image Studio Lite	LI-COR Biosciences	Aquiring and processing immunoblot images
ImageQuant TL	Cytivia	Analysis of plaque size
Mendeley	Mendeley	Reference management
Powerpoint	Microsoft	Image editing
PubMed	NCBI	Literature search
SnapGene Viewer	GSL Biotech	Analysis of DNA sequences
Ubuntu	Canonical Ltd.	Linux distribution for NGS processing
Word	Microsoft	Thesis writing

Chapter 3: Methods

3.1 Cell culture

3.1.1 Cell maintenance

A549 cells and their derivatives, HEK293T, HEK293FT and Vero cells were cultured in 25 cm^2, 75 cm^2, or 175 cm^2 flasks in Dulbecco's modified eagle media (DMEM, Sigma-Aldrich) supplemented with 10% (v/v) foetal calf serum (FCS, Biowest), subsequently referred to as 10% (v/v) DMEM. Cells were maintained in a humidified incubator at 37°C with 5% CO_2. To passage cells, 90% confluent flasks had DMEM removed and were washed with PBS to remove excess DMEM. Trypsin (trypsin 0.05%, ethylenediaminetetraacetic acid (EDTA) 0.02%) was added proportionally to flasks (1 mL/ T25, 3 mL/ T75, 7 mL/ T175) to cover cells and cells were stored in a humidified 37°C incubator for 1-5 min to allow monolayers to detach. Following incubation flasks were gently knocked to detach cells and thoroughly re-suspended to ensure single cell suspension in 10% DMEM. Cells were transferred to new flasks at differing ratios dependent on use.

3.1.2 Single cell cloning

Cells were trypsinised, resuspended in 10% (v/v) DMEM to halt the trypsinization process, counted and 2 x 10^4 cells seeded in a single well of a 96 well plate. Cells were then serial diluted 1:2 down the column (from A1 to H1) and further 1:2 serial dilutions were made across rows (A1 to A12). Cells were regularly monitored through light microscopy across 7-10 days to determine which wells contained single cells and which contained more than one colony; wells containing single cells or colonies were marked. Single cell clones were grown to 50% confluency in 96 well plates before trypsinisation and subculturing in a 24-well plate. These were again monitored through light microscopy, and once at 90% confluency, cells were trypsinised and transferred to a 6-well plate and subsequently T25 and T75 flasks for freezing and long term storage. Functional validation of single cell clones was performed using immunoblot assay.

3.1.3 Mycoplasma testing of cell cultures

To test cell lines for mycoplasma contamination, 100 µL cell culture media was removed from an 80-100% confluent flask. Cell culture media was centrifuged at 2500 xg for 5 min to pellet cell debris and the supernatant was moved into a fresh 1.5 mL Eppendorf. Sample was heated for 5 min at 95°C prior to centrifuging at 16,000 xg for 2 min. Samples were used for PCR using a pool of 7 forward and 4 reverse primers specific to mycoplasma DNA diluted to a final concentration of 10 µM. PCR reaction mix and cycling conditions are listed in tables 3.1.3.1 and 3.1.3.2 resepectively, with pJET1.2BLUNT plasmid with positive product from PCR Mycoplasma Kit II (Promokine) used as a positive control. Following PCR, samples were run on a 1.5% agarose gel containing 0.2 µg/mL ethidium bromide with a 100 bp molecular weight marker to identify positive samples.

Table 3.1.3.1: Reaction set-up for amplification of mycoplasma DNA

Reagent	Volume per reaction(µl)
10x DreamTaq PCR Buffer	2.5
2mM dNTPs	2.5
Forward primer mix	1.0
Reverse primer mix	1.0
Cell culture supernatant	2.0
DreamTaq polymerase	0.2
dH_2O	to 25 µL

Table 3.1.3.2: Thermocycler conditions for amplification of mycoplasma DNA.

Cycle Number	Denature	Anneal	Extend
1	95°C, 2 min		
2-6	94°C, 30 s	50°C, 30 s	72°C, 35 s
7-36	94°C, 15 s	56°C, 15 s	72°C, 30 s
37			4°C, hold

3.1.4 Cryopreserving and resuscitation of cells

To cryopreserve, cells were trypsinised, resuspended in 10% (v/v) DMEM and pelleted at 300 xg for 5 min at room temperature. Pelleted cells were resuspended at approximately $1x10^6$ cells/ mL in freezing media (45% 10% (v/v) DMEM; 45% FCS; 10% DMSO), aliquoted into cryovials (1 mL) and frozen at -80°C in polystyrene boxes to prevent ice crystal formation. Cryovials were transferred to liquid nitrogen for long term storage.

To resuscitate cells, cells were quickly thawed at 37°C and pelleted at 300 xg for 5 min at room temperature. Cells were then resuspended in 10% (v/v) DMEM, transferred to 25 cm^2 flasks and maintained in a humidified incubator at 37°C with 5% CO_2. 24 h after resuscitation, media was changed on cells to remove any remaining DMSO.

3.1.5 Lentiviral transductions of A549 cell lines

For CRISPR/Cas9-mediated gene knockout, A549 and A549-ISG15$^{-/-}$ cells that stably express Cas9 were generated by lentivirus transduction with lentiCas9-Blast (gift from F. Zhang, Addgene plasmid #52962, (Sanjana, Shalem and Zhang, 2014)) and cells were selected with blasticidin (10 µg/mL). Vectors that expressed either a control non-cutting single guide RNA (sgRNA) sequence (sgNC1: 5'- acgaaaGTGACGTACCGCTGGAGGTA – lowercase BsmBI RE site), or sgRNA sequences targeting genes of interest (table 2.4.2) were generated. Target cells, seeded for 50% confluency into 25 cm^2 flasks 18-24 h prior to transduction, were inoculated with lentiviruses (1 mL) diluted with 1 mL serum-free DMEM and polybrene (8 µg/mL) for 2 h at 37°C, continual rocking, after which, 3

mL DMEM supplemented with 2% (v/v) heat-inactivated FBS (Biowest) was added. When confluent (48 h post-transduction), cells were passaged and plated in antibiotic-containing media for selection. For gene knockout, genes cloned with the pLentiCRISPRv2 or pLentiGuide.Puro, transduced cells were selected with puromycin (1 µg/mL).

For generation of double gene knockout cells lines deficient in both ISG15 and a second gene, A549-A549-ISG15$^{-/-}$ cells, generated through transient transduction, were first transduced with lentiCas9-Blast (as above), and selected for using blasticidin for stable expression. A second round of transduction with a vector expressing a sgRNA sequence targeting genes of interest was then performed and successfully transduced cells were selected for using puromycin treatment (as above).

For generation of independent gene knockouts for hit validation and characterisation (sections 4.5 and 5.3) two sgRNAs were introduced into the same cells targeting two independent gene sites. A549-Cas9 cells (generated as above) were first transduced with lentiviral construct #1 (containing a single sgRNA, table 2.5.4) and selected for with puromycin (as above). Following 1st round transduction, selected cells were bulked for transduction with lentiviral construct #2 (containing a single sgRNA, table 2.5.4) and further selected for successful transduction with puromycin (as above). Transduction with lentiviral construct #2 used to boost efficiency of gene knockout; all cells transduced should express at least one sgRNA.

3.2 Microbiological methods

3.2.1 Preparation of competent E. coli

To generate Mix & Go chemically competent cells lab *E. coli*, manufacturers (Mix & Go E. coli Transformation Kit, Zymo Research) protocol was followed. 50 mL ZymoBroth™ was inoculated with 0.5 mL fresh, overnight *E. Coli* culture and shaken at 37°C, 230 rpm until OD_{600nm} reached 0.4-0.6. The resulting culture was incubated on ice for 10 min prior to pelleting the bacteria at 2500 xg for 10 min at 4°C. The supernatant was removed, and the pellet resuspended in 5 mL ice cold 1X Wash Buffer. This wash step was repeated prior to resuspending the pellet in 5 mL ice cold 1X Competent Buffer. Cell suspension was divided into 100 µL aliquots and stored at -70°C ready for transformation.

3.2.2 Storage of E. coli

Transformed *E. Coli* were picked with a pipette tip and grown overnight in 3 mL of LB broth media containing ampicillin (100 mg/mL) at 37°C and 230 rpm, this was then diluted 1:1 v/v in filter sterilized 50% v/v glycerol in ultrapure water and frozen at -80°C. In order to resuscitate from glycerol stocks, *E. Coli* were picked with a pipette tip and plated on LB agar plates, these were grown at 32°C overnight and colonies picked, these could then be grown for plasmid isolation.

3.3 Molecular biology techniques

3.3.1 Transformation of E. coli by heat shock

Competent NZY5α *E. Coli* cells (NZYTech) were thawed on ice. 20 µL ligated plasmid DNA was added to 50 µL competent cells and mixed. *E. Coli* and DNA were then incubated for 30 min on ice before a heat-shock at 42°C for 45 s and returning to ice for 2 min. Cells were grown in 1 mL LB, not containing antibiotic, for 1-2 h at 32°C and shaking at 300 rpm. Transformed cells were then pelleted at 4000 xg for 1 minute and resuspended in 250 µL LB prior to being plated on LB agar plates in the presence of ampicillin and incubated at 32°C for 24 h. Colonies were then picked with a pipette tip and grown in LB broth containing ampicillin (100 mg/mL) for either plasmid isolation or storage of successful transformations as glycerol stocks.

Competent Mix & Go *E. Coli* cells (Zymo Research) were thawed on ice. 2 µL ligated plasmid DNA was added to 50 µL competent cells and mixed. *E. Coli* and DNA were incubated on ice for 20 min before plating onto pre-warmed (37°C) LB agar plates containing ampicillin and incubated at 32°C for 24 h.

3.3.2 Transformation of electrocompetent cells with DNA library

For DNA library transformation, library DNA (Addgene, 67989) was diluted to a final concentration of 10 ng/µL and 1 µL was added to 25 µL NEB 10-β electrocompetent *E. coli* (catalog no. C3020K; NEB) on ice. Cells were electroporated at 2.0 kV, 200 Omega and 25 µF in 0.1 cm gap electroporation cuvettes (catalog no. 165-2083; BIO-RAD) using BIO-RAD GenePulser Xcell electroporator (catalog no. 165-2662; BIO-RAD). SOC recovery medium (provided with *E. coli*) was pre-warmed to 37°C and 1 mL was immediately added after electroporation and cells were transferred to a 50 mL Falcon tube. Cells were then shaken at 37°C for 1 h before being added to 500 mL pre-warmed LB broth supplemented with ampicillin and shaken at 37°C overnight. Plasmid was purified from culture using Qiagen plasmid maxi kit (catalog no. 12163; Qiagen) as per the manufacturer's instructions.

3.3.3 Small scale plasmid isolation from E. coli

In order to extract small levels of plasmid, *E. Coli* was grown overnight in 3 mL LB broth media containing ampicillin (100 mg/mL), cultures were pelleted at 4200 xg for 10 min and supernatant discarded. Manufacturers (QIAprep Spin Miniprep Kit) protocol was followed. The bacterial pellet was resuspended in 250 µL Buffer P1 and, after transferring to a fresh 1.5 mL Eppendorf tube, 250 µL Buffer P2 was added and gently mixed by inversion, not exceeding a 5 min incubation. Following incubation 350 µL Buffer N3 was added and immediately inverted to mix and then pelleted by centrifugation at 16,000 xg for 10 min. Resulting supernatant was added in 700 µL aliquots to QIAprep spin column, and passed through the column by centrifugation at 16,000 g for 1 min. Once all supernatant has been passed through the column, 750 µL Buffer PE was then passed through the column at 16,000 xg for 1 min. This wash step was repeated twice prior to drying the column by centrifugation at 16,000 xg for 2 min. The column was then transferred to a clean 1.5 mL Eppendorf

tube. DNA was eluted with either 50 µL ultra-pure water or Buffer EB ((10 mM Tris·Cl, pH 8.5) by centrifugation at 16,000 xg for 1 min. DNA concentration and purity was verified through use of a Nanodrop noting concentration and 260/280 values to evaluate purity.

3.3.4 Large scale plasmid isolation from E. coli

For large scale plasmid extraction, *E. Coli* were grown overnight in 250 mL LB broth media at 37°C shaken at 230 rpm overnight. Following the manufacturers protocol (Qiagen Maxi prep kit), *E. Coli* was pelleted at 6000 xg for 15 min at 4°C. Cell pellet was resuspended in 10 mL Buffer P1 and 10 mL P2 added and mixed through inversions and lysis allowed to continue for 5 min. Following cell lysis 10 mL Buffer P3 was added, mixed, and incubated for 20 min. Cell debris was pelleted at 4200 xg for 45 14 min at 4°C and supernatant added to a QIAGEN-tip column that had been equilibrated with 10 mL Buffer QBT. Column was then washed twice with 30 mL Buffer QC and DNA eluted with 15 mL Buffer QF into a 50 mL falcon tube. DNA was precipitated with 10.5 mL isopropanol and pelleted at 4200 xg for 1 h at 4°C and supernatant removed. DNA was then resuspended in 1 mL 70% v/v ethanol, transferred to 15 mL falcon, DNA pelleted at 4200 xg for 5 min. Ethanol was removed and pellet allowed to air dry before resuspending in 100 µL water. DNA concentration and purify was verified as above.

3.3.5 Cloning

Prior to cloning, 10 µg vector plasmid, pLentiGuide.Puro (sgNC1; gift from Feng Zhang, Addgene plasmid # 52963) or pLentiCRISPRv2 (sgIFIT1; gift from Feng Zhang, Addgene plasmid #52961), were linearised using 0.5 µL *Bsm*BI-v2 (NEB) for 1 h at 55°C. Linearisation of vector was confirmed using agarose gel electrophoresis (Section 3.3.7). Vector was subsequently dephosphorylated with FastAP (ThermoScientific, Cat. # EF0651) for 15 min at 37°C. Linearised and dephosphorylated vector was purified using Wizard SV Gel and PCR Clean-Up system (Promega, Section 3.3.8) and concentration of plasmid DNA was measured using a Nanodrop. Purified linear plasmid was used immediately or stored at -20°C for use in subsequent ligations.

Oligonucleotides (100 µM) that maintained 5' restriction enzyme site overhangs once hybridised were phosphorylated using polynucleotide kinase for 20 min at 37°C and the enzyme was inactivated for a further 10 min at 75°C. Sense and antisense oligonucleotides were hybridised using a sequential heating programme; 5 min at 95°C, adjust heat block was adjusted to 70°C using a cooling function, once at 70°C the heat block was turned off allowing the oligonucleotides to cool to at least 30°C (approx. 2.5 h). Hybridised oligonucleotides were stored on ice and used immediately in the ligation reaction. 2.5 ng hybridised oligonucleotides were ligated into 100 ng linearised vector DNA in a 5-fold excess using T4 DNA ligase (Promega, Cat. # M1801) overnight at 4°C. DNA was transformed into *E.* coli and amplified as per Section 3.3.3 and 3.3.4. DNA was sequenced by either Eurofins-GATC or MRC PPU DNA Sequencing and Services for verification of successful insertion in vector plasmid (sequencing primer see Table 2.5.3).

3.3.6 Restriction digest of cloning vectors

Prior to sequencing verification, clones were screened using restriction digest of DNA. Within a 20 µL reaction, 5µL of DNA was incubated with HindIII (Promega, Cat. #R6041) for 20 min at 37°C. Successful digest of DNA was confirmed using agarose gel electrophoresis (Section 3.3.7) and concentration of plasmid DNA was measured using a Nanodrop.

3.3.7 Agarose gel electrophoresis

Agarose gels were cast from 1% w/v agarose in TBE with ethidium bromide (0.4 mg/mL). Prepared agarose was poured into gel tray and appropriate comb used to generate wells. Set gels were loaded into gel tanks containing TBE and samples were diluted 5:1 v/v in 6 x sample loading dye and loaded into wells alongside the appropriate ladder. Electrophoresis was performed at a constant 100 V for 40 min. Gels were visualised through exposure to UV light.

3.3.8 Gel and PCR clean-up

Purification of PCR products was performed using of Wizard SV Gel and PCR Clean-Up system (Promega) according to the manufacturer's protocol. PCR products were mixed 1:1 with membrane binding solution and added directly to the mini-column assembly. DNA was bound to the column by centrifugation at 16,000 xg for 1 min. Column membranes were washed twice by addition of 700 µL and 500 µL membrane wash solution followed by centrifugation of columns at 16,000 xg for 1 min. Residual ethanol was removed through centrifugation of an empty column for 1 min at 16,000 g and DNA was subsequently eluted by centrifugation at 16,000 xg for 1 min with 50 µL ultrapure water into a clean 1.5 mL Eppendorf tube. DNA was then stored at -20°C or used immediately.

3.4 Quantitative PCR

3.4.1 Isolation of cellular RNA

A549 cells and their derivatives were grown in 6 well plates, in the presence or absence of their treatment condition. Samples were harvested in 600 µL TRIzol reagent (Invitrogen) per well and RNA was extracted using Direct-zol RNA Miniprep Plus Kit, including DNase I treatment (Zymo Research), according to the manufacturer's protocol. An equal volume of ethanol (100%) was added to cells harvested in TRIzol reagent and transferred to Zymo-Spin IICR Column in collection tubes and passed through the column at 16,000 xg for 30 s and flow-through discarded. Following transfer of all cellular material through the column, the column was washed with 400 µL RNA Wash Buffer centrifuging at 16,000 xg for 30 s. The column was subjected to DNase I treatment, 5 µL DNase I and 75 µL DNA Digestion Buffer mixed per column, for 15 min at room temperature. 400 µL Direct-zol RNA PreWash was then added, and passed through the column twice at 16,000 xg for 30 s each followed by 700 µL RNA Wash Buffer which was passed through the column at 16,000 xg for 2 min to ensure all ethanol was removed. To elute RNA, 50 µL of ultrapure water was added directly to

column matrix and eluted through centrifugation at 16,000 xg for 30 s into a RNase free eppendorf. RNA concentration was measured using a Nanodrop and RNA frozen at -20°C for short term storage.

3.4.2 cDNA synthesis

To generate cDNA for RT-qPCR, LunaScript RT Supermix (NEB) was used according to the manufacturer's protocol. RNA was diluted to 100 ng/µL and 5 µL was included in the cDNA reaction for a final concentration of 500 ng RNA per reaction. RNA was combined with 4 µL LunaScript RT SuperMix (5x) and the reaction mix was made up to 20 µL with ultrapure water. Reaction mixes were then incubated in a thermocycler for a 2 min primer annealing step at 22°C, a 10 min cDNA synthesis step at 55°C and a heat inactivation step at 95°C for 1 min. cDNA samples were then frozen at -20°C for later use or used directly in RT-qPCR.

3.4.3 RT-qPCR

RT-qPCR reactions were set up with 1 µL cDNA, 10 µL PerfeCTa SYBR green SuperMix (Quanta BioScience), and 10 µM relevant forward/ reverse primers (table 2.5.1), made up to 20 µL total volume with ultrapure water. Cycling was performed in either a ViiA7 real time PCR machine (Applied Biosciences) or QuantStudio1 real time PCR machine (Applied Biosciences) with an initial 2 min step at 95°C followed by 40 cycles of 5 s at 95°C and 20 s at 60°C. Verification of amplicon specificity was performed using melting curve analysis. Average cycle threshold values (CT) of independent triplicates were normalised to their average respective β-actin CT values and relative expression was examined using the ΔΔCT method.

3.5 Lentiviral vectors

3.5.1 Transfection of 293T cells for lentivirus production by calcium phosphate precipitation

Lentiviruses were generated by transfecting 80% confluent HEK293T cells in 75 cm^2 flasks with 10 µg pLentiCas9-Blast, pLentiGuide-Puro or pLentiCRISPRv2 along with 7.5 µg pCMV-dR8.91 and 2.5 µg pVSV-G using the calcium phosphate precipitation method. 48 h post-transfection, lentivirus preparations (10 mL) were filter sterilised (0.45 µm), aliquoted (1 mL), snap frozen and stored at -80°C.

3.5.2 Titration of lentivirus using flow cytometry

For titration, 3 x10^5 A549-Cas9 or A549-ISG15$^{-/-}$.Cas9 cells were plated on a 6-well plate 10 h prior to transduction. Varying volumes of lentivirus supernatant, 100ul, 80ul, 40ul, 20ul, 10ul or 0ul, were mixed separately with 8 ug/mL Polybrene in 1 mL culture media with 10% FCS. The culture media was then aspirated from the 6-well plate and the lentivirus dilutions added to the cells. Transduction media was left on cells for 24 h, after which, the lentivirus was removed and 2 mL of fresh media containing 10% FCS was added to each well. Cells were prepared for analysis using CytoFLEX

(Beckman Coulter) to detect percentage of cells with BFP 24 h after the fresh media change. The quantity of virus used for the well with ≤30% transduced cells was chosen to calculate the amount of virus needed for the screen at a MOI = 0.3. Concentration of lentivirus in TU/mL was calculated using the following formula:

$$Transduction\ Units\ per\ mL\ \left(\frac{TU}{mL}\right) = \frac{number\ of\ cells\ transduced \times percent\ fluorescent \times dilution\ factor}{transduction\ volume\ in\ mL}$$

3.5.3 Titration of lentivirus using colony forming units

For titration, a 10-fold serial dilution of lentivirus was prepared into DMEM 10% v/v FBS containing 10 µg/mL polybrene from 1:10 to 1:100,000 and 150 µL of each viral dilution was added to each well of a 6-well plate. Cells were counted and 1000 cells in 1.35 mL DMEM 10% v/v FBS were added directly on top of the lentivirus, mixed, and placed in an incubator for 48 h. Final dilutions ranged from 1:100 to 1:100,000 included a no lentivirus control well. After 48 h, media was aspirated from cells and 2 mL DMEM 10% v/v FBS containing 2 µg/mL Puromycin was added. Media was replaced on cells with fresh antibiotics containing DMEM every 3-4 days for 2 weeks until un-transduced (negative control) cells had died, and colonies were visible in the transduced wells. After 2 weeks, media was aspirated, and the cells washed with PBS. Cells were fixed with 5% formaldehyde for 10 min and washed with PBS. Plaques were analysed using 0.15% Crystal Violet staining for 30 min and the number of colonies at each dilution counted to determine transduction units/ mL (TU/mL) using the following formula:

$$Transduction\ Units\ per\ mL\ \left(\frac{TU}{mL}\right) = \frac{Number\ of\ colonies}{Total\ volume\ in\ the\ well\ (ml)\ x\ Dilution\ factor}$$

3.6 Virological techniques

3.6.1 Preparation of virus stocks

Virus stocks were prepared by inoculating Vero cells at a multiplicity of infection (MOI) of 0.001 (formula below) in serum-free media with continual rocking at 37 ˚C. Supernatants were harvested at 3 d post-infection, clarified by centrifugation at 2500 g for 15 min, aliquoted, snap frozen in liquid nitrogen and stored at -80°C.

$$Multiplicity\ of\ Infection\ (MOI) = \frac{Volume\ of\ virus\ (mL)\ x\ Titre\ of\ virus\ (pfu/mL)}{Number\ of\ cells}$$

3.6.2 Plaque assay

Viruses were diluted to 20 – 30 PFU in 1 mL DMEM, either serum-free or 2% FBS, and were adsorbed for 1 h onto confluent monolayers of cells in six-well plates while rocking at 37 ˚C. Following

adsorption, 2 mL overlay (DMEM and 2% FBS; Avicel) was added to wells and incubated for 6 d. Cells were fixed with 5% formaldehyde (30 min) and washed with PBS. Plaques were analysed by either: 0.15% Crystal Violet staining for 30 min or permeabilized for 10 min (PBS, 1% Triton X-100, and 3% FBS), washed, and incubated for 1 h with a pool of virus-specific Abs diluted in PBS and 3% FBS (1:1000). Following PBS washes, cells were incubated for 1 h with goat anti-mouse IgG Abs conjugated to alkaline phosphatase (catalog no. ab97020; Abcam) diluted 1:1000 in PBS and 3% FBS. Cells were washed in PBS, and signals were detected using SIGMAFAST BCIP/NBT (Sigma-Aldrich). Alternatively, fluorescent plaques as a result of infection with hPIV3-GFP(JS) were visualised using Amersham Typhoon at wavelength 488 nm.

3.6.3 Titration of virus stocks

For titration of virus stocks, Vero cells were seeded in a 6-well plate for confluency next day. A 10-fold serial dilution of virus was prepared into serum-free or 2% v/v FCS DMEM from 10^{-3} to 10^{-8} and 1 mL of each viral dilution was added to each well of a 6-well plate. Plates were rocked at 37°C for 1 h. Following fixing and imaging as per section 3.6.2, plaque number was counted in the second highest dilution containing plaques and titre was calculated using the following formula:

$$Plaque\ Forming\ Units\ per\ ml\ \left(\frac{pfu}{ml}\right) = \frac{Average\ plaque\ number\ x\ Plaque\ Diltuion\ Factor}{Volume\ dilutant\ added\ to\ well}$$

3.6.4 Measuring plaque size

Plaques were analysed with ImageQuantTL colony counter. Images of individual wells were input into the program with plaque number being manually counted and settings being maintained between technical repeats. Plaques that localised next to each other and merged together were not counted as part of the analysis.

3.7 Protein biochemistry

3.7.1 Western blot

Confluent monolayers in six-well plates were lysed with 250 μl 2x sample buffer (4% w/v SDS, 20% v/v glycerol, 0.004% w/v bromophenol blue, and 0.125 M Tris–HCl (pH 6.8)) with 10% v/v β-mercaptoethanol. Samples were incubated at 95 °C for 10 min, lysed by sonication at an amplitude of 2 μm for 12 s (MSE, Soniprep 150) and centrifuged at 12,000 xg for 10 min. Proteins were separated using a 4-12% NuPage bis-tris acrylamide gel (Invitrogen) in MOPS running buffer (0.2 M MOPS free acid, 0.05 M sodium acetate, 0.01 M EDTA) at 160 V for 1 h and transferred to a methanol-activated PVDF membrane (Amersham) at 20 V or Nitrocellulose (Amersham) at 10 V using wet transfer for 1 h. Membranes were blocked in 7% (w/v) non-fat milk diluted in phosphate buffered saline containing 0.001% v/v Tween 20 (PBS-T) for 1 h at room temperature. Primary antibodies were prepared in 7% (w/v) non-fat milk diluted in PBS-T according to dilutions in table

2.11.1 and membranes were incubated in dilution overnight at 4°C on a tube roller. Following incubation, membranes were washed 3 times for 10 mins in PBS-T to remove unbound primary antibody. For chemiluminescence, membranes were incubated in species specific secondary antibody conjugated to horseradish peroxidase (HRP) at a dilution of 1:5000 for 1 h. Following incubation with secondary antibody, membranes were washed 3 times for 10 min in PBS-T followed by a 10 min wash in PBS. Membranes were incubated with 700 µl enhanced chemiluminescence reagent (EZ-ECL, GeneFlow, K1-0170) and exposed to X-Ray film. For membranes not imaged using chemiluminescence, membranes were incubated in species specific IRDye secondary antibody (LI-COR Biosciences) at a dilution of 1:10,000 for 1 h and washed as previously described. Signal were detected using Odyssey CLx scanner and data were processed and analysed using Image Studio software (LI-COR Biosciences).

3.8 Imaging

3.8.1 EVOS microscopy

Live cells infected with fluorescent-tagged viruses (hPIV3-GFP(JS), rPIV5-mCherry(W3)) were imaged using the EVOS M5000 cell imaging system (Thermo Fisher Scientific). Trans-luminescence images were taken with 4, 10 or 20 x phase-contrast objective with the magnification, light-emitting diode intensity, gain and exposure time settings kept the same across images. hPIV3-GFP(JS) infected cells were imaged using a GFP light cube (470/525 nm, excitation/emission) and rPIV5-mCherry(W3) infected cells were imaged using a Texas Red light cube (585/624 nm, excitation/emission). Images were saved as both individual channels and overlays and visualised in PowerPoint (Microsoft 365).

3.9 Flow cytometry and cell sorting

3.9.1 Flow cytometry (fluorescent reporter virus)

To prepare for flow cytometry, media was removed from cells seeded in 6-well plates at the appropriate time point. Cells were washed with 1 mL PBS and lifted using 300 µL of Trypsin-EDTA and incubating cells at 37°C. Trypsinisation was stopped by adding 800 µL DMEM supplemented with 10% FCS and moved to 1 mL cryovials. Cells were pelleted by centrifuging at 300 xg for 5 min, media removed, and cells were resuspended in 1 mL cold PBS. The wash step was repeated once more and cells resuspended in FACS buffer (PBS, 3% FCS, 0.1% sodium azide) to a concentration of $2x10^5$ cells/ mL. Cells were kept at 4°C until required. Samples were analysed by flow cytometry using either FACSJazz Cell Sorter (BD Biosciences) utilising BD FACS Sortware Application (BD Biosciences, v.1.1.0.84) or Guava easyCyte HT System (Merck Millipore). A negative control was first run to establish the negative cell population and remove doublets from analysis and relevant

gates were set based on protocol. Data was analysed using either Flowing Software 2 (Turku Bioscience) or FlowJo Software for Windows version v10.7.2 (BD).

3.9.2 Flow cytometry (antibody staining)

Approximately 6 x10^5 cells were seeded into each well of a six-well plate 2 days prior to infection. Cells were pre-treated with IFN-α prior to infection with 1000 IU/mL IFN-α (IntronA, Merck Sharp & Dohme or Roferon-A, Roche Pharma R&D Labs) for 18 h. After 18 h, wells were rinsed with phosphate buffered saline (PBS) and infected with hPIV3 diluted in 1 mL DMEM to achieve a MOI of 10. Cells were placed in a gas box to achieve 5% CO_2 and placed at 37°C, continual rocking, until harvest. At 24 h.p.i and 48 h.p.i cells were harvested for flow cytometry analysis. Cells were harvested with 300 µL trypsin and pelleted at 300 xg for 5 min. Cells were resuspended in PBS and pelleted at 300 xg for 5 min to wash. Cells were resuspended at 1 x10^6 cells/ mL in a cocktail of three PIV3 HN antibodies at a dilution of 1:200 (Randall et al., 1987) and incubated for 30 min at 4°C in the dark before being pelleted as before. Following primary antibody conjugation, cells were fixed with 10% formaldehyde at 1 x10^6 cells/ mL for 10 min at room temperature. Following fixation cells were kept at 4°C until secondary antibody conjugation for flow cytometry. Prior to secondary antibody conjugation, cells were washed with PBS as above. Cells were resuspended in Alexa Fluor 488 antibody (Invitrogen, A11001) at a dilution of 1:1000 for 30 min at 4°C before being washed once more and resuspended in FACS buffer (PBS, 3% FCS, 0.1% sodium azide).

3.9.3 Analysis with FlowJo software

FCS files were imported into FlowJo v.10.8.0 (BD Biosciences) for data analysis. Gating was first performed on the negative control cell populations whereby cells were first gated to remove debris by plotting FSC against SSC and gating around the main cell population, termed R1. R1 cells were subsequently singlet gated to remove doublets by plotting trigger pulse width against SSC. Singlet gated cells could then be analysed for fluorescence either by histogram gating or pseudoplot. Dependent on experiment, singlet gated cells were either analysed with hand drawn polygon gates (pseudoplot), hand drawn range gates (histogram) or bisector gates (histogram). Once gates had been set on the negative control population, all gating was copied across to the rest of the files using the ‘Ctrl + Shift + G’ function. Cell gating and ancestry could be viewed within layout editor and data analysis of ‘% Parent’ or ‘Mean Fluorescence Intensity’ could be compiled within the table editor and exported for plotting and statistical analysis.

3.9.4 Fluorescence activated cell sorting

Cells were sorted using FACSJazz Cell Sorter (BD Biosciences) utilising BD FACS Sortware Application (BD Biosciences, v.1.1.0.84). Cells were resuspended to ~ 2x10^5 cells/ mL in PBS and transferred to 5 mL polypropylene tubes with filter caps (Falcon). Cells were loaded onto sample line and sorted using a 1.0 Drop Pure Sort mode into a 2 Tube Holder – 2 way sort. Piezo amplitude and drop frequency (kHz) were adjusted manually throughout to maintain drop frequency and drop delay was determined using BD FACS Accudrop beads (BD Biosciences) as per manufacturer’s protocol.

3.10 Genome wide CRISPR/Cas9 knockout screening

3.10.1 Production of screening library lentivirus

The lentivirus library was packaged in 293FT cells using the calcium phosphate transfection method. One day prior to transfection, 20 15 cm tissue culture treated dished were each seeded with 7 x10^6 early passage 293FT cells. 2 h before transfection, cells underwent media replacement with 10 mL prewarmed media containing 10% FCS for each plate. Cells were then transfected, using a well-established calcium phosphate and chloroquine diphosphate protocol, with the CRISPR library plasmid pool and the two packaging plasmids pMD.2 and psPAX2. After 16 h, the media was removed and 32 mL of fresh media containing 10% FCS was added to each dish. 48 h after transfection, the supernatant from all dishes was combined and centrifuged at 300 xg at 4°C for 10 min to remove cell debris. The resulting supernatant, containing lentiviral particles, was filtered through a 0.45 µm filter, aliquoted into 50 mL conical tubes and stored at -80°C until the day of library transduction.

3.10.2 Transduction of cell with library lentivirus

A549-Cas9 cells were seeded in 14 T175 flasks to be 50% confluent after 10 h. Cells were then transduced at MOI = 0.3 by diluting viral stocks into 7 mL volume per flask using serum-free culture media containing 8 ug/mL Polybrene with continual rocking at 37°C. After 2 h, culture media containing 2% FCS was added up to 35 mL in each flask. Lentivirus was replaced by fresh media containing 2% FCS 24 h after transduction and 48 h after transduction, the cells were passaged into media containing 10% FCS and 2 µg/mL Puromycin. Passaging continued for 8-10 days to obtain a pure population of transduced cells. Each passage was frozen in freezing solution containing 10% DMSO, 45% FCS and 45% culture media containing 10% FCS and stored at -80°C.

3.10.3 Infection of cells with hPIV3-GFP

For the screening, ~7.5 x10^6 cells were plated in each T175 flask (7 flasks per repeat) 1 day prior to infection (passage 4 or 5 with 9-10 days of puro selection and culture post transduction). Cells in each flask were infected with hPIV3-GFP at MOI 5 in serum-free media. After 1 h rocking at 37°C, each flask was topped up to 35 mL with media containing 2% FCS.

3.10.4 Harvesting cells for FACS

To prepare cells for sorting, media was aspirated at 18 h.p.i and cells were dislodged by incubating with 7 mL trypsin (per T175 flask) at 37°C. Trypsin was neutralized with 13 mL media containing 10% FCS and the cell suspension harvested. All cell suspensions were combined and pelleted at 300 xg for 5 min before washing with PBS and recentrifuged. The cell pellet was resuspended in 1% formaldehyde (2x10^6 cells/ mL of formaldehyde) for 10 min at room temperature to inactivate the virus. The pellet was washed once more as above and filtered with a 100 µm nylon mesh cell strainer (Corning, 431752). Cells were resuspended at 1x10^7 cells/ mL in ice cold PBS and kept at 4°C.

3.10.5 Fluorescence activated cell sorting

Cells were sorted into four fractions: GFP-negative, GFP low, GFP Medium, and GFP High using BD FACS Aria IIIu 4 laser Cell Sorter (Roslin Institute). Cells were collected into tubes pre-filled with 200 µL FCS filtered with 0.22 µm syringe filter prior to sort.

3.10.6 Isolation of gDNA

FACS isolated cell fractions were pelleted at 300 xg for 5 min prior to being washed was PBS. Washed, dried pellets were stored at -80°C until gDNA isolation. gDNA was isolated from sorted cells using QIAamp DNA FFPE Tissue Kit (Qiagen) according to the manufacturer's protocol. Cell pellets were resuspended in 180 µL Buffer ATL and 20 µL proteinase K, mix by vortexing and incubated at 56°C for 1 h followed by a 1 h incubation at 90°C to partially reverse formaldehyde modifications. Once cooled to room temperature, 100 mg/mL RNase A was added and incubated at room temperature for 2 min. Following RNase A treatment, 200 µL Buffer AL was added to the sample followed by 200 µL ethanol (96-100%) and the sample was mixed by vortexing. Lysate was transferred to a QIAamp MinElute column and centrifuged at 6000 xg for 1 min. Column was washed with 500 µL Buffer AW1 and 500 µL Buffer AW2, centrifuging at 6000 xg for 1 min and transferring the column to a fresh collection tube between steps. gDNA was eluted with 2 x 25 µL Buffer ATE warmed to 55°C. Elution buffer was allowed to sit on the membrane for 1 min followed by centrifugation at 16,000 xg for 1 min. Concentration of eluted gDNA was assessed using Nanodrop.

For non-infected samples, 300 µg gDNA was digested with 2000 units HindIII-HF overnight in 2 mL total volume. The resulting DNA was run on a 0.7% agarose gel and a gel slice in the in the range 1.2 kb- 1.8 kb was excised under UV light. DNA was extracted from the gel slice using the NucleoSpin Gel and PCR Clean-up Kit (Macherey-Nagel) according to manufacturer's protocol. For each 100 mg gel, 200 µL Buffer NTI was added and the sample was incubated at 50°C for 5 – 10 min until the gel slice was dissolved. Sample was then loaded onto a NucleoSpin Gel and PCR Clean-up Column and centrifuged at 11,000 xg for 30 s, repeated until all sample was loaded. Column was washed twice with 700 µL Buffer NT3 and centrifuged at 11,000 xg for 30 s between additions of wash buffer. Membrane was dried by centrifuging at 11,000 xg for 1 min prior to eluting gDNA with 2 x 15 µL Buffer NE warmed to 55°C. Elution buffer was allowed to sit on the membrane for 1 min followed by centrifugation at 11,000 xg for 1 min. Concentration of eluted gDNA was assessed using Nanodrop.

3.10.7 Preparation of gDNA for NGS

All isolated gDNA was amplified by PCR in 2 µg reactions (table 3.10.7.1) using thermocycler conditions detailed in table 3.10.7.2.

Table 3.10.7.1: Reaction set-up for amplification of isolated gDNA during first round PCR.

Reagent	Volume per reaction	Final concentration
Q5 HS HF	1 µL	0.02 U/mL
dNTPs	2 µL	200 µM
Primer Mix	2 µL	0.1 µM (per primer)
gDNA	2 µg	2 µg
Buffer	20 µL	1 X
Enhancer	20 µL	1 X
dH_2O	to 100 µL	

Table 3.10.7.2: Thermocycler conditions for amplification of isolated gDNA during first round PCR.

Cycle Number	Denature	Anneal	Extend
1	98°C, 30 s		
2-23	98°C, 10 s	61°C, 15 s	72°C, 20 s
24			72°C, 2 min
25			10°C, hold

Following amplification, samples of the same fraction were pooled together and cleaned up using Wizard SV Gel and PCR Clean-Up system (Promega) according to the manufacturer's protocol (section 3.3.8) and eluted in 50 µL water prior to checking DNA quality and size on a 2% agarose gel. PCR amplified cleaned-up DNA was diluted to 0.5 ng/µL for barcoding PCR (table 3.10.7.3) with 2x NEBNext Ultra II containing polymerase, dNTPs and buffer. Each DNA sample was barcoded with a unique combination of one Index 1 (i7) adapter and one Index 2 (i5) adapter, termed the primer mix using thermocycler conditions detailed in table 3.10.7.4. Second round PCR was purified using AMPure XP beads (Beckman Coulter) according to manufacturer's protocol. To purify DNA, 1.8 µL AMPure XP beads were added per 1 µL sample and mixed prior to separation on a magnetic stand. Beads bound to DNA were washed twice with 80% ethanol and left to air dry prior to elution. DNA was eluted with 15 µL EB buffer (Qiagen miniprep kit) pre-warmed to 55°C. PCR DNA quality was again assessed on 2% agarose gel following purification and concentration was measured using QuantiFluor ONE dsDNA System and Quantus Fluorometer (Promega) according to manufacturer's protocol. Samples were all diluted to concentration of the least concentrated sample and pooled together for sequencing. Sequencing was performed on a NextSeq 2000 sequencing platform (100 cycles, 400M reads) with a spike-in of 20% PhiX added to the sample mix to increase sequence diversity.

Table 3.10.7.3: Reaction set-up for barcoding of gDNA fractions during second round PCR.

Reagent	**Volume per reaction**	**Final concentration**
2x NEBNext Ultra II	50 µL	1 X
Primer mix (10 µM each)	5 µL	1 µM
1st PCR product	4 µL	2 µg
dH_2O	41 µL	

Table 3.10.7.4: Thermocycler conditions for barcoding of gDNA fractions during second round PCR.

Cycle Number	Denature	Anneal	Extend
1	98°C, 30 s		
2-10	98°C, 10 s	63°C, 15 s	72°C, 20 s
11			72°C, 5 min
			10°C, hold

3.10.8 Analysis of NGS data (MaGeCK)

Demultiplexed files of NGS data were processed in Linux distribution, Ubuntu. Three packages were utilised; 'cutadapt' for the removal of adaptor sequences from reads, 'mageck' for robust rank aggregation for identification of CRISPR-screen hits and 'fastqc' for quality control of high-throughput sequence data. Cutadapt was first used to trim the 5' and 3' ends of each read leaving only the 19 bp CRISPR sequences for read counting using MaGeCK. Trimmed reads were saved as separate files and subsequently analysed for quality control using fastqc. Trimmed files were analysed using function 'mageck count' to count the number of reads within each fraction sample. Counts for each fraction sample, including plasmid library were combined into a single file, 'counts_files'. Read counts were compared between fractions of interest using the 'mageck test' function to provide rankings and enrichment analysis. The same function was used to compare non-infected samples to the plasmid library to assess library performance. For full code, see appendix. Resulting data was processed and plotted using GraphPad Prism version 9.5.0 for Windows.

3.10.9 Analysis of NGS data (Panther Gene Ontology analysis)

For Panther Gene Ontology Analysis, gene names generated in MaGeCK analysis were first converted to ENSEMBL IDs. The ID list generated was batch uploaded, separated by spaces, into Panther 'Gene List Analysis' tool (http://pantherdb.org/), list type was selected as 'ID List' and organism selected as 'Homo sapiens'. 'Functional classification' analysis was selected, and results were viewed and exported for following ontologies; molecular function, biological processes and pathways.

3.10.10 Analysis of NGS data (DAVID pathway analysis)

For DAVID pathway analysis, gene names as exported by MaGeCK were entered as a list into DAVID Functional Annotation tool (https://david.ncifcrf.gov/summary.jsp). Identifier was selected as 'OFFICIAL_GENE_SYMBOL', List type selected as 'Gene List' and Species selected as 'Homo sapiens'. Following submission, results were viewed and analysed using the 'Functional Annotation Chart' and sorting resulting terms by p-value.

Chapter 4: Optimisation of a genome wide CRISPR/Cas9 screening platform for the identification of hPIV3 host dependency factors

4.1 Introduction

hPIV3 is an important human pathogen in both the developed and developing world with no vaccine that protects against infection or specific antiviral treatment for hPIV illness (CDC, 2015). Viruses require host factors in order to replicate and be successful infectious agents; these are termed host-dependency factors (HDFs) (Robinson et al., 2018). There is a need to better understand these host genes and pathways essential for virus survival as not only does it aid our understanding of the virus but provides potential targets for antiviral interventions. As previously described, many antivirals target viral proteins which are susceptible to rapid mutation whilst antivirals that target host proteins are harder to develop resistance to (Kumar et al., 2020; Cakir et al., 2021; Badia, Garcia-Vidal and Ballana, 2022).

Previous work has shown that knockout of host dependency factors renders the cell unable to permit, or severely impacts, virus replication (Cisneros, Cornish and Hultquist, 2022) and as such, a genome-wide approach using a fluorescence reporter virus can be utilised to identify new host dependency factors (Puschnik et al., 2017). As of yet, such a screen has not been performed to identify hPIV3 HDFs and so we have subsequently optimised and performed a genome-wide CRISPR-Cas9 knockout screen to identify such factors.

4.2 Overview of assay workflow

A number of variations on CRISPR-Cas9 genome-wide screening can be applied using a number of different available libraries (Jones et al., 2021). Our screening workflow utilised the Human Improved Genome-Wide Knockout CRISPR Library from Kosuke Yusa as outlined in figure 4.2.1 (Tzelepis et al., 2016). The library targets 18,010 protein-coding genes with each gene being represented by 5 independent sgRNAs. A549 cells expressing the Cas9 protein were transduced with a lentivirus library such that each sgRNA was represented greater than 500 times (500 X coverage). Transduction was performed at a low MOI of 0.3 in order to ensure each individual cell was only transduced with a single sgRNA; therefore, reducing the likelihood of double gene knockouts.

The screening workflow can be implemented to identify both host dependency factors and antiviral factors (section 4.2) with minimal differences, and so the following overview encompasses the assay workflow for the identification of both.

To identify host dependency factors of hPIV3-GFP(JS), transduced cells were infected at a high MOI (MOI = 5) for 18 h prior to being harvested and formaldehyde fixed for analysis. For the identification of antiviral factors, cells were first pre-treated with IFN-α prior to infection. Cells were then sorted using fluorescence activated cell sorting (FACS) into four fractions: GFP-negative, expected to contain cells deficient in genes that permit virus replication (HDFs); GFP low, expected to contain cells deficient in genes that permit virus replication to a lesser degree than the GFP-negative fraction; GFP medium and GFP high, expected to contain cells deficient in genes that hinder virus replication such as antiviral factors. These sorted cells were stored at -80°C prior to gDNA isolation, library

preparation and NGS analysis. It is presumed that any host dependency factors would be significantly enriched in the negative fraction compared to the high as depletion of a host dependency factor would render the cell unable to permit infection with antiviral factors being significantly enriched in the high fraction compared to the negative as depletion of an antiviral factor would render the cell permissive to infection.

Cells were prepared for NGS using a two-step PCR strategy with gDNA first being amplified with a cocktail of 10 forward primers, each increasing in length by one nucleotide. The generation of PCR products with staggered sequence lengths allows for increased nucleotide diversity during NGS, critical to optimal sequencing (Joung et al., 2017; Illumina, 2020). First round PCR products were then barcoded using unique combinations of i7 and i5 adaptors (section 3.10.7) allowing fractions to be pooled for NGS and subsequently deconvoluted for enrichment analysis. Genes in each fraction were identified using the MaGeCK computational tool (Model-based Analysis of Genome-wide CRISPR-Cas9 Knockout) (Li et al., 2014); a computational tool commonly used to identify genes from genome-wide CRISPR-Cas9 knockout screens by considering frequencies of observed sgRNAs in the NGS data set inputted. MaGeCK is a computational tool developed specifically to identify hits from genome wide CRISPR/Cas9 screening. It utilises an algorithm that identifies positively or negatively regulated sgRNAs in a population suitable for no to a few replicates with high levels of variability, as is the case in many screening platforms. By using a robust rank aggregation (RRA) method, it can detect genes that are ranked consistently significantly higher, between treatment and control, compared to those whose reads are more highly distributed and therefore less significant.

Genes identified through MaGeCK analysis subsequently underwent an iterative refinement process (figure 4.2.2) to generate a final list of genes to undergo validation. Genes within each fraction were first sorted by MaGeCK rank and genes with a rank of 75 or higher were crudely removed. For the identification of antiviral restriction factors, an additional step was undertaken. A cumulative list of known ISGs was generated from both the Ohainle ISG-targeting CRISPR knockout library list (OhAinle et al., 2018) and Interferome (Rusinova et al., 2013) and genes that were not considered ISGs from this cumulative list were removed, with the exception of those that passed the false-discovery threshold.

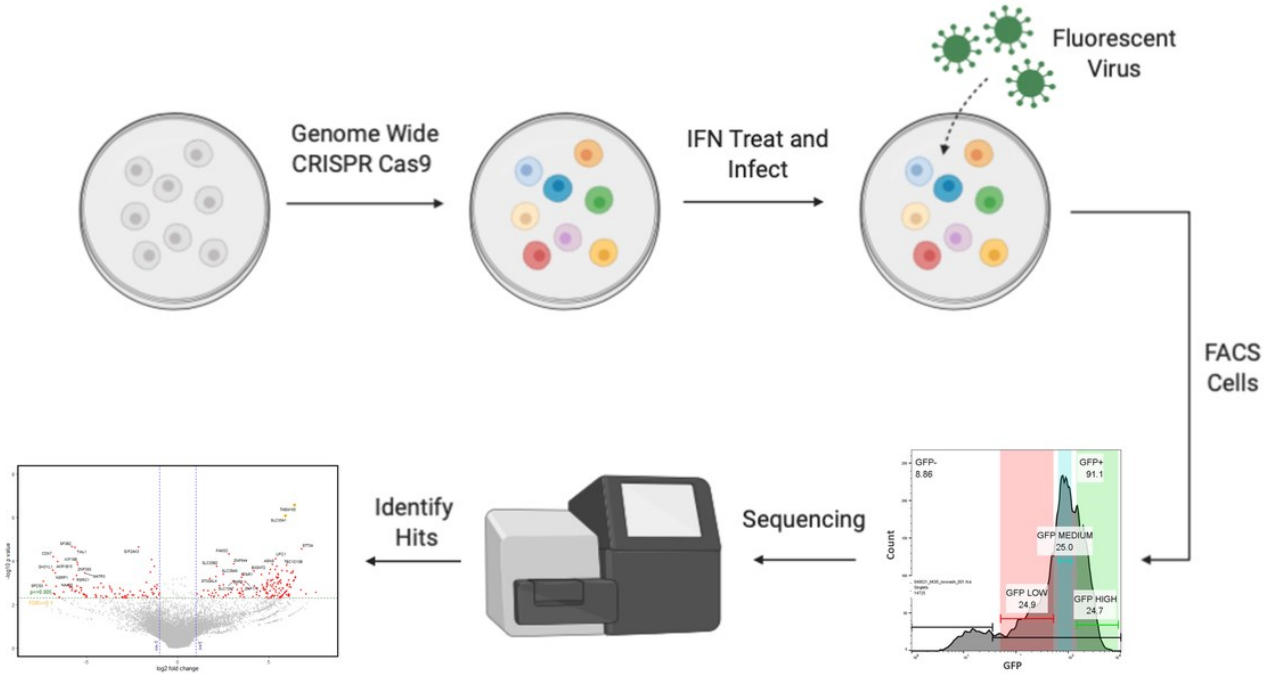

Figure 4.2.1: Workflow outlining the process of genome-wide CRISPR-Cas9 knockout screening.

To prevent unnecessary validation, genes that were known host-dependency factors or antiviral factors were also removed, alongside genes with substantial published literature; these were termed ‘control genes’ as they were genes that provided us confidence in our sorting strategy through their presence in our fractions. Two rounds of literature searching with iterative removal of genes from our starting list rendered us with 8 genes for validation. These selected genes could be placed in three categories; ‘low hanging fruit’ (genes that we expect to play a role with some literature present), ‘medium probability’ (genes that we suspect play a role but there is less literature or non-virus literature present) and ‘potentially novel’ (genes that no to little literature is present or recently identified genes).

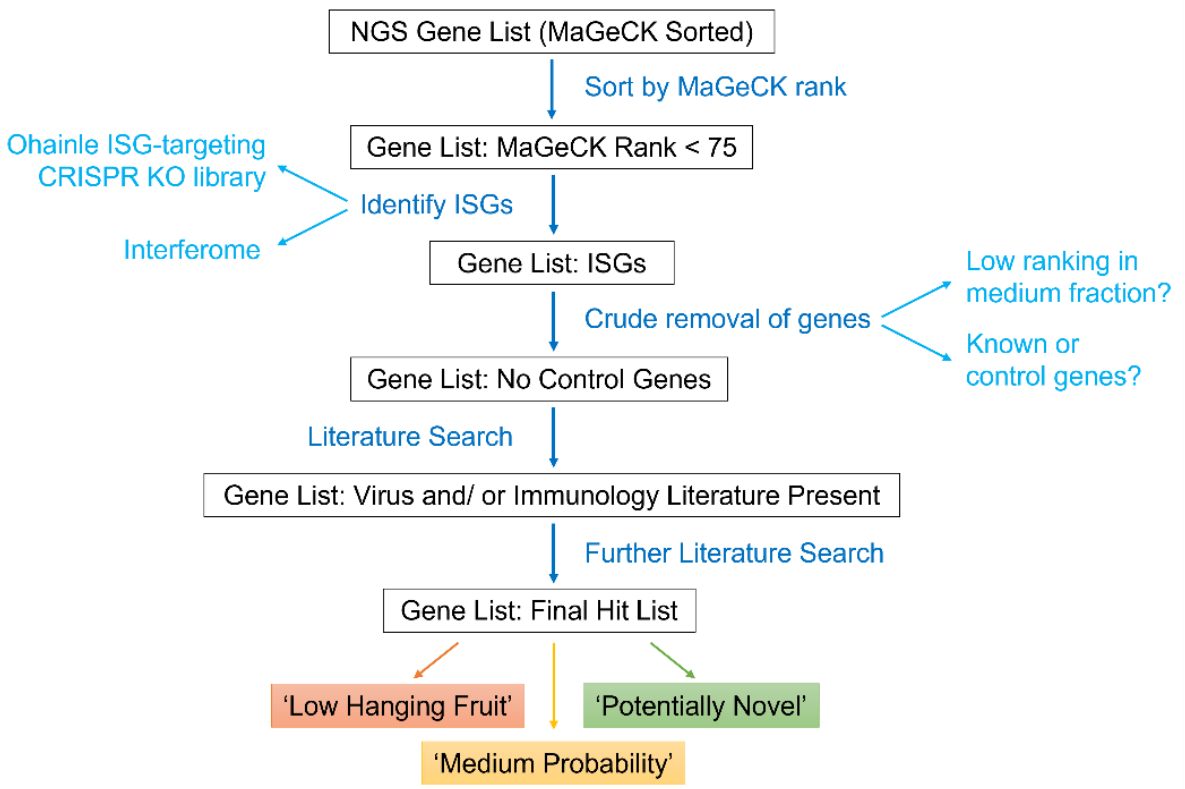

Figure 4.2.2: Flow chart demonstrating the decision process in refining hits identified during screening for further validation.

4.3 Generation of resources for genome-wide screening

Prior to screening, necessary reagents and resources had to be generated including both the hPIV3-GFP(JS) virus and the lentivirus library for transduction of cells. The lentiviral vector used was a pKLV2 vector backbone with improved scaffold and puromycin and BFP markers developed by the Yusa lab (Tzelepis et al., 2016) specifically for CRISPR gRNA expression (figure 4.3.1.a). The gRNA pooled library containing the 90,709 sgRNAs targeting 18,010 genes was acquired from the Yusa lab (Tzelepis et al., 2016). Due to the large scale at which genome wide screening is undertaken, to generate enough sgRNA library DNA for lentivirus production, electrocompetent bacteria were transformed with the library DNA using electroporation, amplified in culture, and the resulting DNA extracted using maxiprep. To ensure coverage of all 90,709 sgRNAs, 30 ng of library DNA was transformed into electrocompetent *E. coli* ensuring > 5 x 10^7 colony forming units, following plating, for reliable library representation. Lentivirus was subsequently generated, using 1.2 mg of library DNA using a calcium phosphate transfection protocol in HEK 293FT cells.

As discussed in section 1.3.5, it has been suggested that the use of ISG15 deficient cells may enable the identification of low to moderately acting antiviral restriction factors and as such, the resulting lentivirus was titrated by transducing onto both A549-Cas9 and A549-ISG15$^{-/-}$.Cas9 cells to assess for any differences between the two cell lines during subsequent use. Due to the need to transduce

the cells at MOI = 0.3, as previously described, the BFP marker within the backbone allowed for titration of the lentivirus generated using flow cytometry. This titration allows for accurate subsequent transductions for the preparation of the library transduced cells for screening.

Using increasing volumes of lentivirus on cells in a 6-well plate from 0 to 100 µl of lentivirus per well, percentage BFP positive cells could be quantified (figure 4.3.1.b). As expected, increasing volume of lentivirus transduced onto cells, increased the percentage of BFP-positive cells as recorded by flow cytometry. Figure 4.3.1.b shows at lower volumes of lentivirus, up to 40 µl, A549-ISG15$^{-/-}$.Cas9 show reduced % BFP positive cells compared to A549-Cas9 cells however by 80 µl lentivirus, the difference in % BFP positive cells in each cell line became non-significant. This may be due to a more robust IFN response in cells unable to express ISG15, a negative regulator of the type I IFN signalling. At higher volumes, where higher MOIs are likely achieved, this effect may be masked. The quantity of virus used for the well with ≤30% transduced cells, 20 µl for each cell line, was used to quantify the amount of lentivirus required for a transduction at an MOI = 0.3 in transduction units/ mL (TU/mL). Based on this, lentivirus concentrations were calculated separately for both A549-Cas9 and A549-ISG15$^{-/-}$.Cas9 cell lines, resulting in concentration of 9.24 x10^{6} TU/mL and 7.11 x10^{6} TU/mL respectively. Despite % BFP positive cells differing at 20 µl lentivirus by 5%, the concentrations of lentivirus calculated differed only by 1.3-fold. As such, the two values were treated as biological repeats and the average of both concentrations, 8.18 x10^{6} TU/mL, was taken and used for the proceeding lentiviral transductions.

(a)

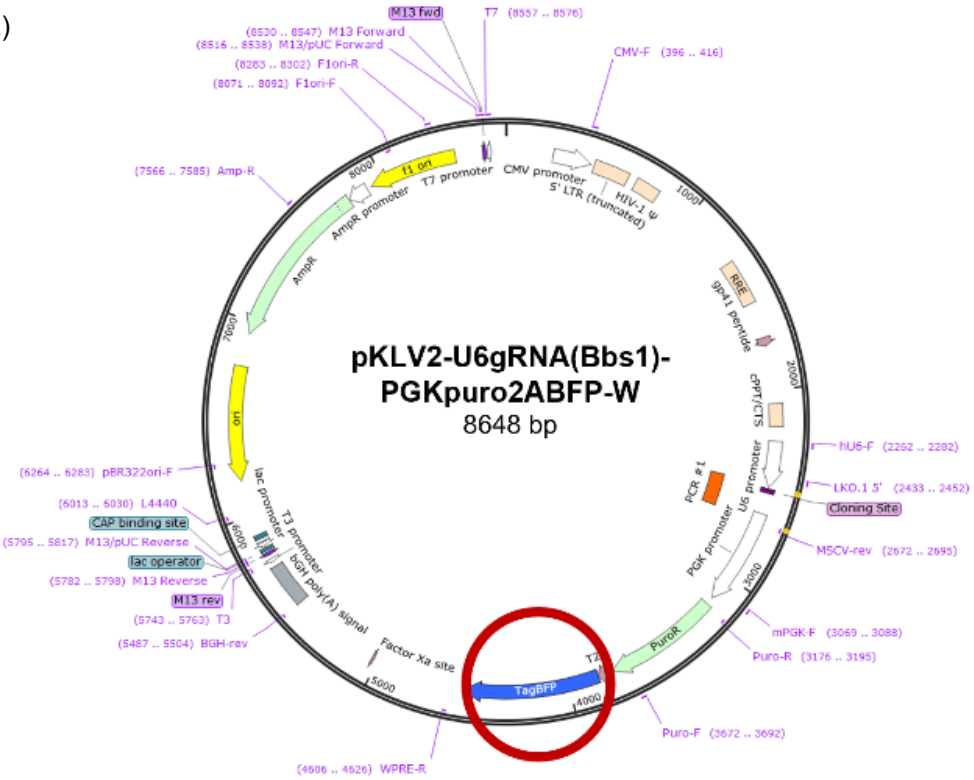
pKLV2-U6gRNA(Bbs1)-
PGKpuro2ABFP-W
8648 bp
M13 fwd
T7 (8557 .. 8576)
(8530 .. 8547) M13 Forward
(8516 .. 8538) M13/pUC Forward
(8263 .. 8302) F1ori-R
(8071 .. 8092) F1ori-F
CMV-F (396 .. 416)
(7566 .. 7585) Amp-R
f1 ori
T7 promoter
CMV promoter
5' LTR (truncated)
HIV-1 ψ
RRE
gp41 peptide
cPPT/CTS
U6 promoter
hU6-F (2262 .. 2282)
LKO.1 5' (2433 .. 2452)
Cloning Site
MSCV-rev (2672 .. 2695)
PCR #1
PGK promoter
PuroR
mPGK-F (3069 .. 3088)
Puro-R (3176 .. 3195)
Puro-F (3672 .. 3692)
T2A
TagBFP
(4606 .. 4626) WPRE-R
Factor Xa site
bGH poly(A) signal
T3 promoter
lac promoter
ori
AmpR
AmpR promoter
(6264 .. 6283) pBR322ori-F
(6013 .. 6030) L4440
CAP binding site
(5795 .. 5817) M13/pUC Reverse
lac operator
(5782 .. 5798) M13 Reverse
M13 rev
(5743 .. 5763) T3
(5487 .. 5504) BGH-rev

(b)

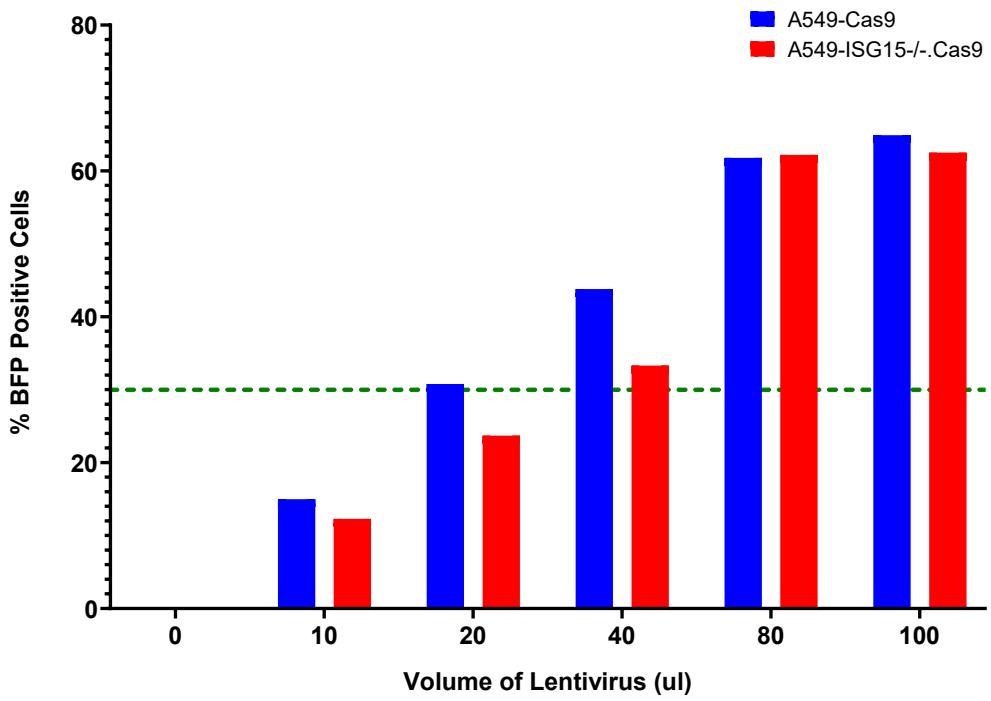
A549-Cas9
A549-ISG15-/-.Cas9
% BFP Positive Cells
0
20
40
60
80
0
10
20
40
80
100
Volume of Lentivirus (ul)

Figure 4.3.1: Generation of sgRNA lentivirus library for genome-wide screening. **(A)** Plasmid map showing vector backbone (pKLV2-U6gRNA5(BbsI)-PGKpuro2ABFP-W) of genome-wide sgRNA library. TagBFP reporter, highlighted by red circle at sequence position 3845 – 4546 bp, used for titration of lentivirus library. **(B)** Lentivirus library was titrated through transduction of A549-Cas9 cells (blue) and A549-ISG15$^{-/-}$.Cas9 cells (red) with increasing volumes of lentivirus library from 0 – 100 µl. Cells were analysed using flow cytometry using violet laser (405 nm) for identification of TagBFP (transduced) positive cells. Data was quantified based on singlet cell gating and percentage BFP positive cells plotted. Green dotted line indicates 30% BFP positive cells with amount of lentivirus required for the screen at a MOI 0.3 calculated from the quantity of virus used for the well with ≤30% transduced cells.

Following the generation of the lentivirus library, A549-Cas9 cells were transduced at an MOI = 0.3 for 500 x coverage; the number identified to result in significant signal over noise in screens with high signal-to-noise ratios and variability such as CRISPR/Cas9 screens (Yau and Rana, 2018). Following transduction, cells were maintained in puromycin selection media for 8-10 days and upon each passage, cells not passaged into new flasks were cryopreserved for future use. In total, four passages of cells were performed with puromycin selection continuing until the end of passage three, allowing for infection of cells at passage four and harvesting of cells for sorting. At each passage 5.4 x 10^7 cells were moved into new flasks to maintain the > 500 X coverage previously described.

To ensure sgRNA library coverage was maintained in the transduced cells, library transduced cells were subject to next generation sequencing alongside the sgRNA DNA library. Comparison of the two populations, via MaGeCK analysis, allowed for identification of gene representation in the transduced cells compared to the sgRNA plasmid library, following lentiviral transduction (figure 4.3.2). Upon comparison of the DNA library and transduced cells it was found that the majority of genes were present in the transduced cells. Of genes that passed the l2fc and p-value thresholds, 4.6% of total genes were downregulated in the library transduced cells and 2.2% upregulated, compared to the DNA library. However, no genes passed the FDR threshold of < 0.1. The 4.6% of genes which were found to be downregulated in the library transduced cells were suggested to be due to dropout as a result of the genes knocked out being essential genes to cell fitness. The knockout of the 2.2% of genes found to be upregulated in the transduced cells compared to the DNA library were postulated to confer a fitness advantage to cells with knockout of the gene leading to increased representation in the cell population. Overall, it was determined that the transduced cells were representative of the sgRNA DNA library and suitable to be used within screening experimentation.

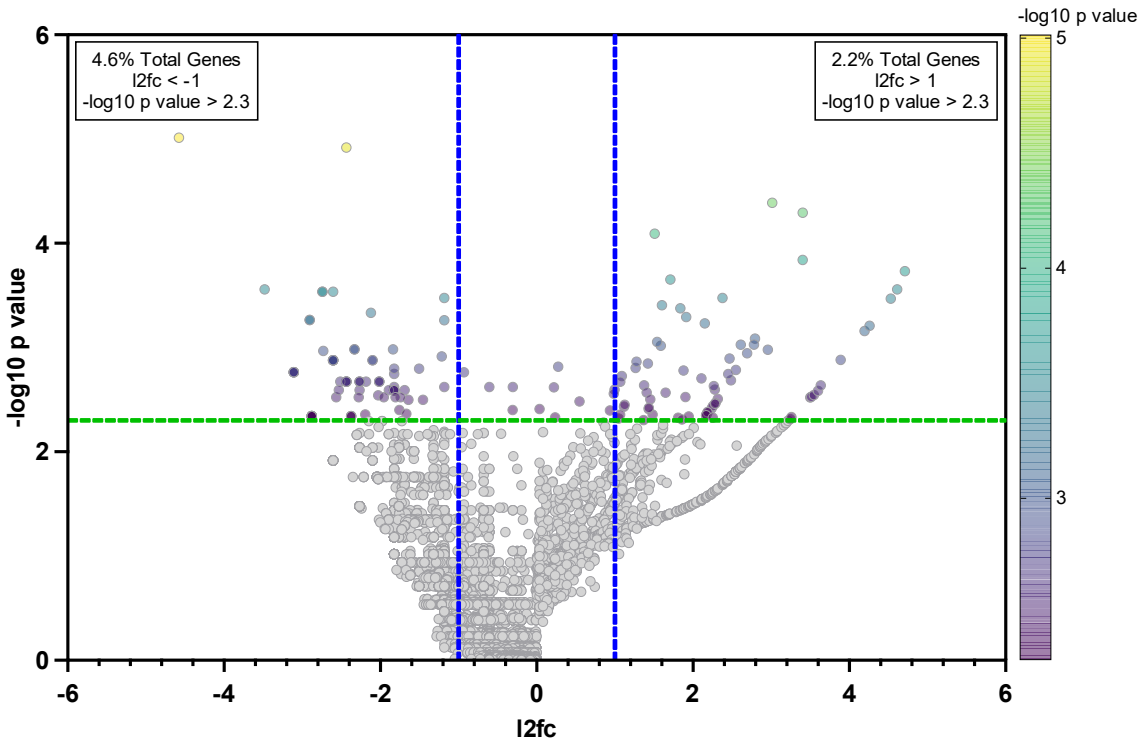

Figure 4.3.2: sgRNA coverage in library transduced cells. gDNA isolated from untreated library transduced A549-Cas9 cells and DNA from the sgRNA plasmid library were subject to next generation sequencing to identify sgRNAs present in each population prior to being subject to MaGeCK computational analysis. Log2 fold change of sgRNAs of all genes present in the untreated transduced cells compared to the DNA library is shown with sgRNAs enriched in the library transduced cells indicated by l2fc ≥ 1 and sgRNA depleted in the library transduced cells indicated by l2fc ≤ -1. Green dotted line indicates p ≤ 0.005 threshold and blue dotted lines indicate l2fc ≤ -1 or l2fc ≥ 1 threshold.

Alongside the generation of a lentivirus stock, a stock of hPIV3-GFP(JS) was also generated. To enable FACS of infected cells, as required in screening, we acquired a GFP expressing version of hPIV3(JS) from Viratree (Zhang et al., 2005), where the GFP open reading frame (ORF) is inserted in the intergenic region between the P/C/D/V ORF and M ORF (figure 4.3.3.a). A stock of hPIV3-GFP(JS) was generated following a MOI = 0.01 infection of Vero cells and harvested 3 d.p.i. The generated virus was subsequently titrated on Vero cells and fixed for analysis 6 d.p.i. Due to the virus expressing GFP when replicating, viral plaques could be identified using Phosphor Imaging using the Cy2 filter, allowing for the identification of viral plaques. Plaques from two technical repeats were counted from the dilution resulting in the second fewest plaques, 10^{-7} (figure 4.3.3.b), and a virus titre of 1.2 x10^{8} pfu/mL was determined.

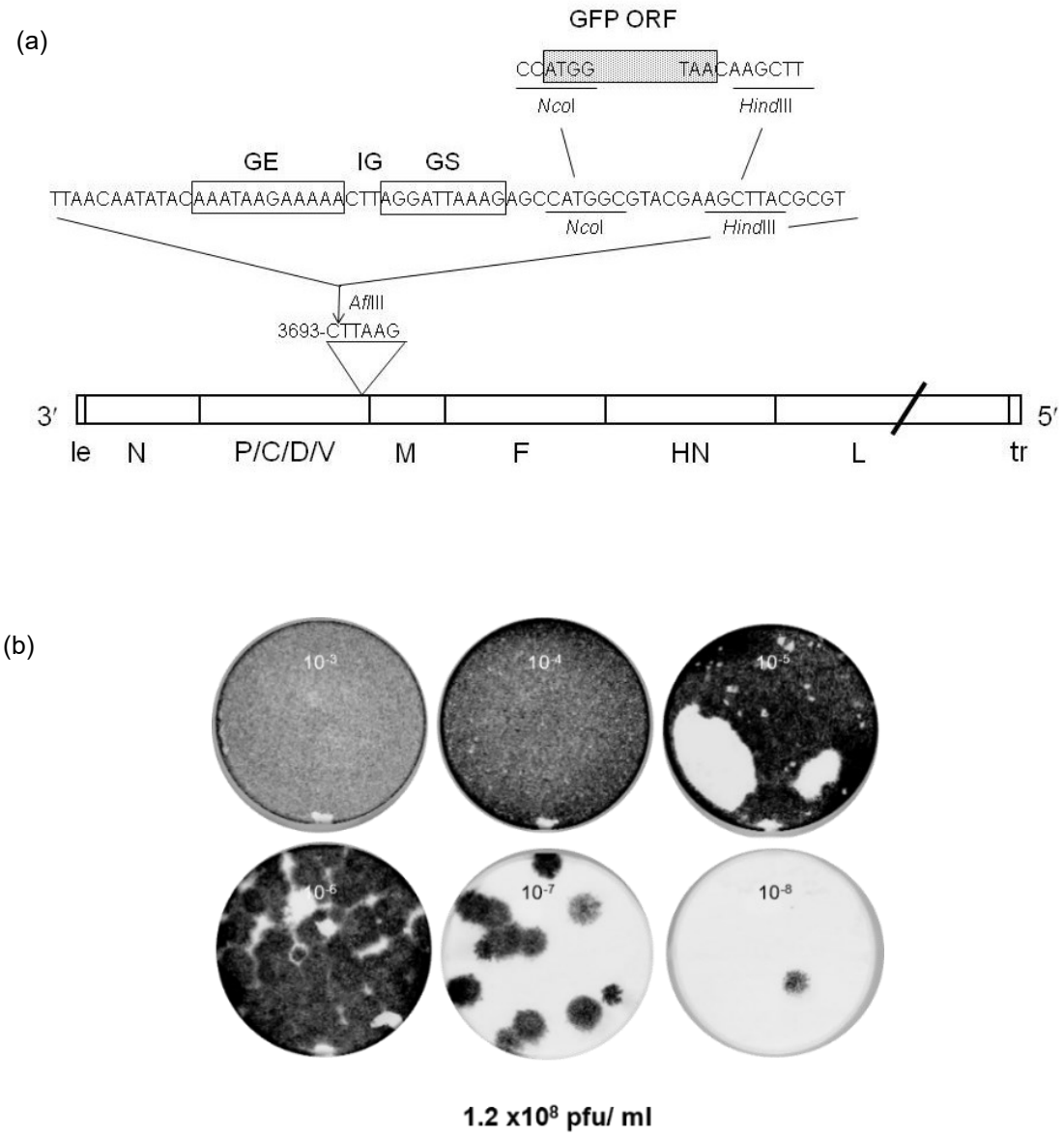

Figure 4.3.3: Generation of hPIV3-GFP(JS) virus stock. **(A)** Genome map showing negative sense RNA genome of hPIV3-GFP (strain JS), which has a 3' end leader (Le) and a 5'end trailer (Tr) region. The insertion region of the GFP ORF is shown in the intergenic region between the P/C/D/V ORF and M ORF. **(B)** Titration of hPIV3-GFP(JS) stocks. hPIV3-GFP(JS) stocks were prepared (MOI 0.01) and titred using Vero cells with monolayers fixed 6 d.p.i. Plaques were detected using Phosphor Imaging, Cy2 for identification of GFP-positive cells. Two technical repeats of plaque assay were performed and virus titre of 1.2 x10^8 pfu/mL calculated from a mean of both plates. Image is representation of repeats.

4.4 Optimisation of experimental conditions for genome-wide screening

Next, conditions for sorting were optimised prior to initiating the screening workflow. Parameters such as sorting strategy and infection conditions (MOI, time of infection) were optimised to allow for efficient isolation of differentially infected cell fractions and subsequent gDNA isolation from sorted cells. Due to external facilities having to be used for cell sorting, formaldehyde fixation conditions were also determined.

To allow for identification of optimal sorting and infection conditions prior to the acquisition of hPIV3-GFP(JS), A549-Cas9 cells were infected with rPIV5-mCherry(W3) at MOI = 1 to result in approximately 60% infected cells (Abedon and Bartom, 2013) with later optimisation being carried out using hPIV3-GFP(JS). Cells were harvested at 24 h.p.i for flow cytometry analysis using the varying sort strategies permitted using the BD FACS Jazz. Cells were sorted into negative and positive fluorophore populations and sorted fractions were reanalysed through the FACS Jazz to establish the efficiency and purity of the sort. Results showed that a 1.0 drop pure sort strategy accurately separated the positive and negative fractions (figure 4.4.1). Upon infection with rPIV5-mCherry(W3), when sorted negative and positive populations were reanalysed through the instrument and the resulting populations overlayed (figure 4.4.1.a/b) there were two distinct populations with both the negative (blue) and positive (red) fractions being enriched from the bulk population. A MOI = 1 infection, termed the ‘sort population’ resulted in 42.2% mCherry negative cells and 57.8% mCherry positive cells. Following a 1.0 drop pure sort, the negative sort was enriched to be 88.2% mCherry negative cells, with the remaining 11.8% showing near to negative mean fluorescence intensity (MFI) rather than being a separate positive population, whilst the positive sort resulted in 98.8% positive cells. The same experiment was subsequently performed with a hPIV3-GFP(JS) infection. Results showed enrichment of the two populations following sorting, however we observed a reduced sort purity compared to infection with rPIV5-mCherry(W3) as shown by breakthrough cells in figure 4.4.1.c. Following sorting, the negative GFP population, the population we expect to see host dependency factors in, consisted of 92.1% GFP-negative cells, compared to 48.8% in the sort population, whilst the positive sort population was enriched from 51.2% to 92.6% GFP-positive cells. Therefore, a sorting 1.0 drop pure sort strategy was determined as the optimal for the screening workflow resulting in > 90% purity following sorting.

To additionally validate our sorting strategy previously determined, we wanted to further challenge the optimised conditions by sorting cells infected with hPIV3-GFP(JS) at MOI = 5 (figure 4.4.2). Challenging the system with a higher MOI infection that results in near to 100% infected cells, compared to a MOI = 1 infection that results in 50-60% infected cells as previously reported, we aimed to see if we could successfully sort and enrich for GFP-negative cells. It is these rare events, particularly those within the GFP-negative fraction, that we are interested in throughout the host dependency screening as previously described. By infecting cells to result in close to 100% infection, we are able to evaluate if our screening design can efficiently isolate these small cell populations for downstream analysis using MaGeCK, reduce the likelihood of high variability and therefore increase significance of resulting hits. Upon infection with hPIV3-GFP(JS), we saw < 10% GFP-negative cells

as shown in the '+ hPIV3-GFP(JS) Sort Population'. On sorting of the infected population into GFP-negative and positive fractions, we reanalysed the negative GFP fraction back through the FACS Jazz to assess for successful isolation of populations as previously described. We saw an enrichment of GFP-negative cells, such that the sorted population was >80% GFP-negative and the remaining GFP-positive. Whist GFP-positive cells were able to get into the GFP-negative population, it was enriched for the negative population of cells we desired to a significant degree, such that downstream analysis would negate the genes contained within these GFP-positive cells. We were therefore confident in our sorting and infection strategy for continuing with the genome-wide CRISPR-Cas9 knockout screen.

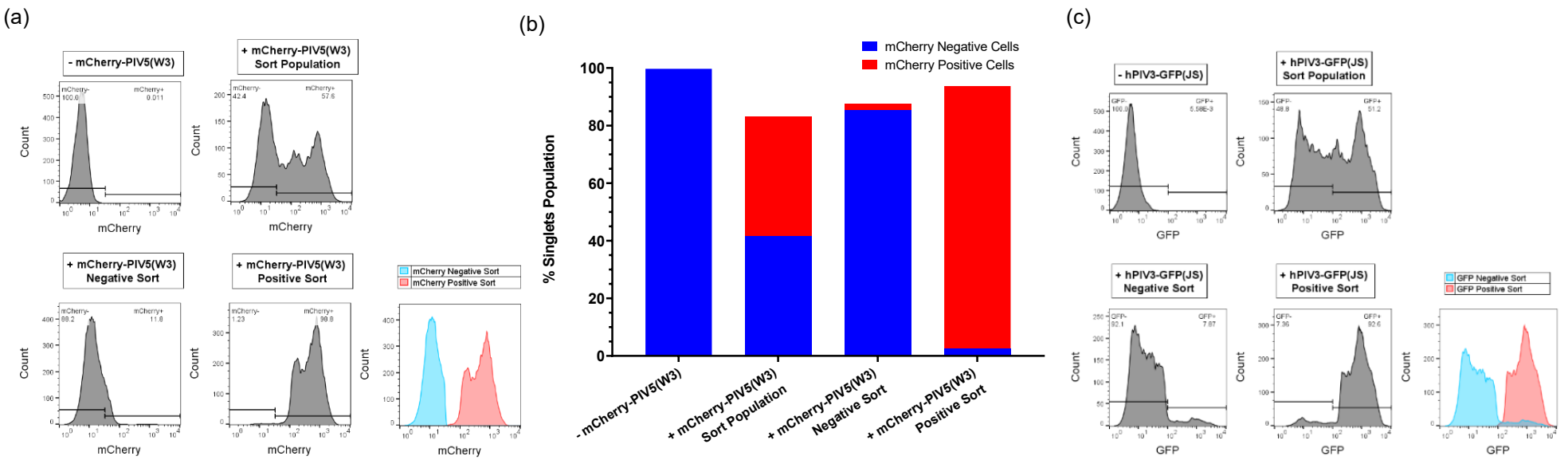

Figure 4.4.1: Optimisation of sorting and infection conditions for genome-wide screening. A549-Cas9 cells were infected with rPIV5-mCherry(W3) (A, B), hPIV3-GFP(JS) (C) (MOI = 1) or mock infected. Cells were harvested at 24 h.p.i for flow cytometry analysis using the yellow/ green (561 nm) or blue (488 nm) laser for the identification of rPIV5-mCherry(W3) or hPIV3-GFP(JS) cells, respectively. **(A)** A549-Cas9 cells infected with rPIV5-mCherry(W3) were sorted by FACS into mCherry negative and positive fractions using a 1.0 drop pure sort strategy. Fractions were re-run through the flow cytometer with the negative sorted fraction (blue) and positive sorted fraction (red) overlayed. Data was analysed using FlowJo v10. **(B)** Data from (A) was quantified based on singlet cell gating and percentage singlet gated cells plotted, mCherry negative cells shown in blue and mCherry positive cells shown in red. **(C)** A549-Cas9 cells infected with hPIV3-GFP(JS) were treated as previously described in (A) with negative sorted fraction shown in blue and positive sorted fraction overlayed in red. Data was analysed using FlowJo v10.

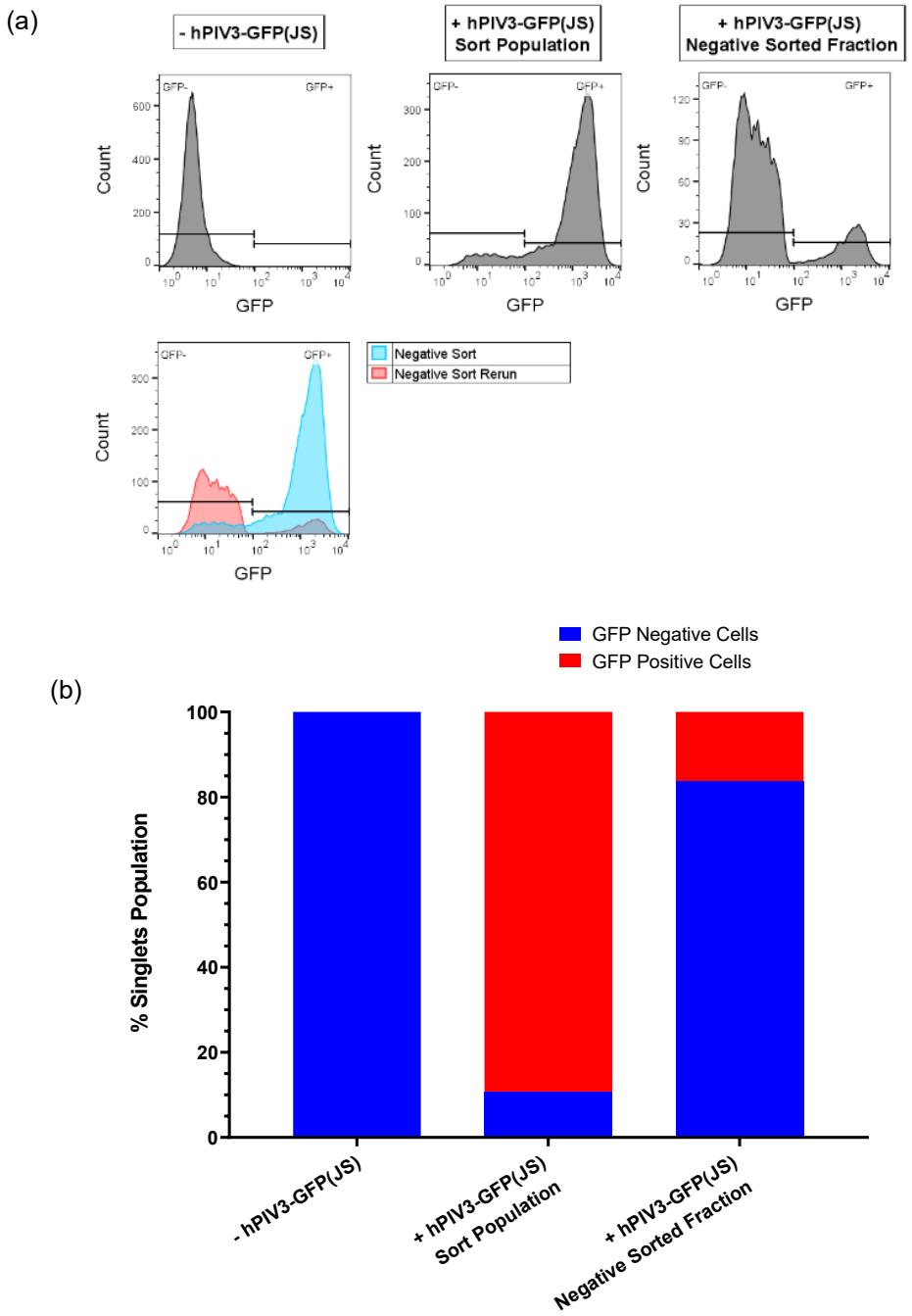

Figure 4.4.2: Sorting strategy effectively isolates hPIV3-GFP(JS) positive cells. A549-Cas9 cells were infected with hPIV3-GFP(JS) (MOI = 5) and harvested at 24 h.p.i for flow cytometry analysis and fluorescence activated cell sorting (FACS) using blue laser (488 nm) for identification of GFP-positive cells. Data was analysed using FlowJo v10. **(A)** Panels represent mock infected A549-Cas9 cells (negative gating control), A549-Cas9 cells infected with hPIV3-GFP(JS) and negative sorted fraction from A549-Cas9 infected cells. Bottom panel shows overlay of input cell population (blue) and GFP-negative sorted population re-analysed (red). **(B)** Data from (A) was quantified based on singlet cell gating and percentage GFP-negative cells (blue) and GFP-positive cells (red) plotted to show enrichment of hPIV3-GFP(JS) negative cells in negative fraction following sort.

Subsequent gating of the sorting population was established by infecting A549-Cas9 cells with hPIV3-GFP(JS) (MOI =5), the MOI used within our screening design, and harvesting cells for flow cytometry analysis 24 h.p.i. (figure 4.4.3). It was established that gates could be set to harvest 20-25% of cells in fractions GFP low, medium, and high whilst allowing for non-overlap of gates to prevent 'leak through' of cells between populations therefore increasing purity of the sorted populations. The percentage of cells in the GFP-negative is dependent on the non-infected gating control used to set the negative population gates; with an MOI = 5 we expect the negative population to account for 5-10% of the population based on infection of A549-Cas9 cells (figure 4.4.3).

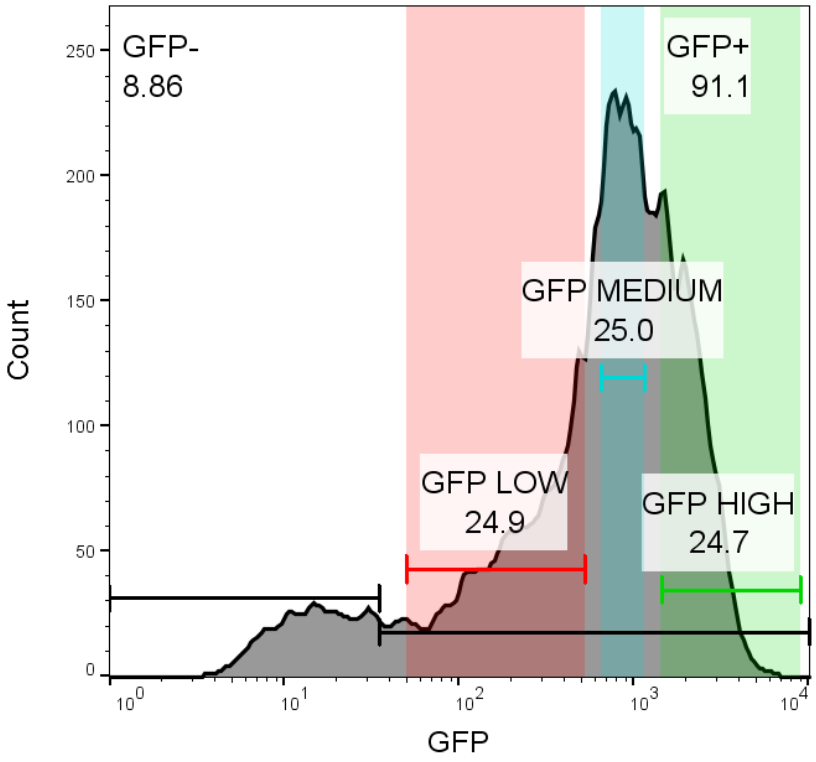

Figure 4.4.3: Gating allows separation of GFP low, medium, and high fractions. Infection and gating strategy was established though infecting A549-Cas9 cells with hPIV3-GFP(JS) (MOI = 5) and harvesting cells for flow cytometry analysis 24 h.p.i. using blue laser (488 nm) for identification of GFP-positive cells. Low, medium, and high gates were set to 25% of total cells each; represented by red, blue, and green boxes, respectively.

To allow for the transportation of infected cellular material to another institution for sorting, cells had to be formaldehyde fixed for virus inactivation. To preserve as much functional material, both cellular for sorting and gDNA for downstream NGS, both the minimum amount of formaldehyde required to inactivate virus and the impact of formaldehyde fixation on the resulting gDNA extracted from fixed cells was established. To determine the minimum amount of formaldehyde required for virus inactivation, A549-Cas9 cells infected with hPIV3-GFP(JS) (MOI = 5) were fixed with 0, 0.5 or 1% formaldehyde at 2 x10^6 cells/ mL of fixative for 10 min. Infected and formaldehyde fixed cells were permeabilised, allowing for the release of any internalised virus in the cells, and the resulting virus

containing media was titrated onto Vero cells with no overlay in a dilution range of 10^{-3} to 10^{-8}. Monolayers were monitored and imaged for GFP expressing virus using the EVOS microscope and fixed for analysis of viral replication after 4 d.p.i (figure 4.4.5.a). As expected, with 0% formaldehyde there was substantial virus infection with the majority of cells being infected at all dilutions up to and including 10^{-8}. We also show that the cellular supernatant contained infectious virus in all dilutions up to 10^{-4} as shown by plaque assay (figure 4.4.5.a). At 0.5% formaldehyde treatment, fluorescence microscopy shows viral infection of cells only at a dilution of 10^{-3}, corroborating with the plaque assay data which shows virus replication only with a 10^{-3} dilution of virus containing cellular supernatant. Whilst a plaque is present in the 10^{-4} dilution, based on the microscopy images which show no infection, it is likely that this is carry over from a higher concentration as a result of pipetting error. We show that 1% formaldehyde treatment of infected cells for 10 min is sufficient to inactivate all virus particles. Resulting supernatant from 1% formaldehyde fixed cells, resulted in the absence of viral replication within cells, as shown by both fluorescence microscopy and the absence of viral plaques at all dilutions of viral supernatant. As 1% formaldehyde fixation resulted in the inactivation of all virus replication, this was determined to be the safest concentration to use. However, it was important to determine how this affected gDNA quality so we wanted to assess whether 1% formaldehyde fixation of cells would affect the gDNA quality extracted from fixed cells compared to non-fixed cells. To investigate this, gDNA was extracted from cells fixed with varying formaldehyde concentrations from 0.5 - 5%. gDNA quality was assessed compared to a non-fixed control by both agarose gel electrophoresis and qPCR. Upon loading 500 ng gDNA, gel electrophoresis showed no difference in gDNA quality compared to a non-fixed control as shown by a single band of the same molecular weight and no breakdown of gDNA into smaller products present on the gel (figure 4.4.5.b). This was seen for formaldehyde concentration up and including 5%, indicating that fixation with 1% formaldehyde does not affect DNA quality. This was further validated by performing qPCR on the same gDNA using primers for IFN-β and TDRD7; genes both known to be expressed upon infection with parainfluenza viruses (Luthra et al., 2011; Subramanian et al., 2018). If gDNA quality was affected by formaldehyde treatment, we would expect to see differences in Ct values of target genes between non-fixed and fixed samples, with 200 ng of each sample used for qPCR analysis. Instead, results show no differences in Ct values between samples, further validating that formaldehyde fixation, up to 5%, does not affect gDNA quality (figure 4.4.5.c).

(a)

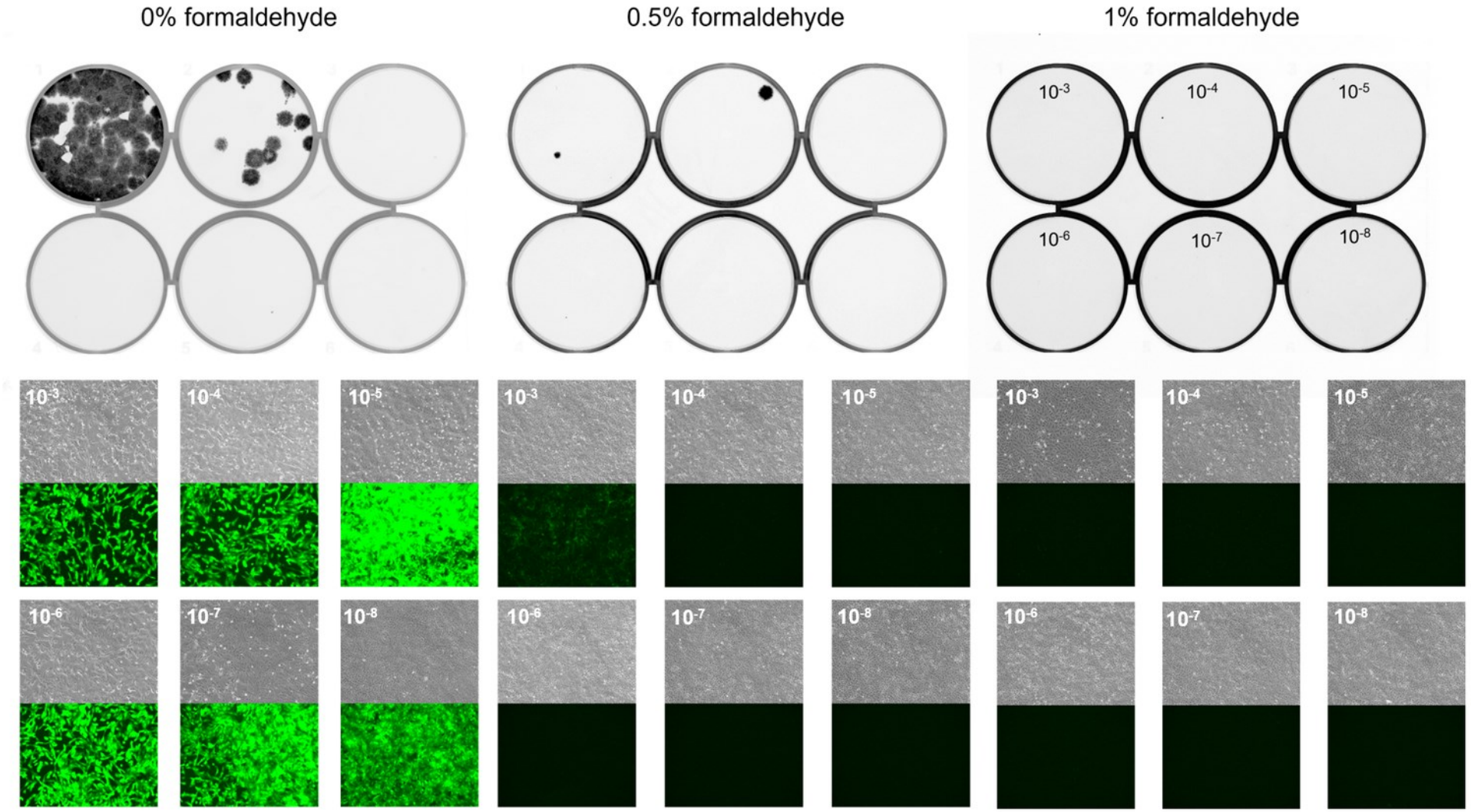
0% formaldehyde
0.5% formaldehyde
1% formaldehyde
10-3
10-4
10-5
10-6
10-7
10-8

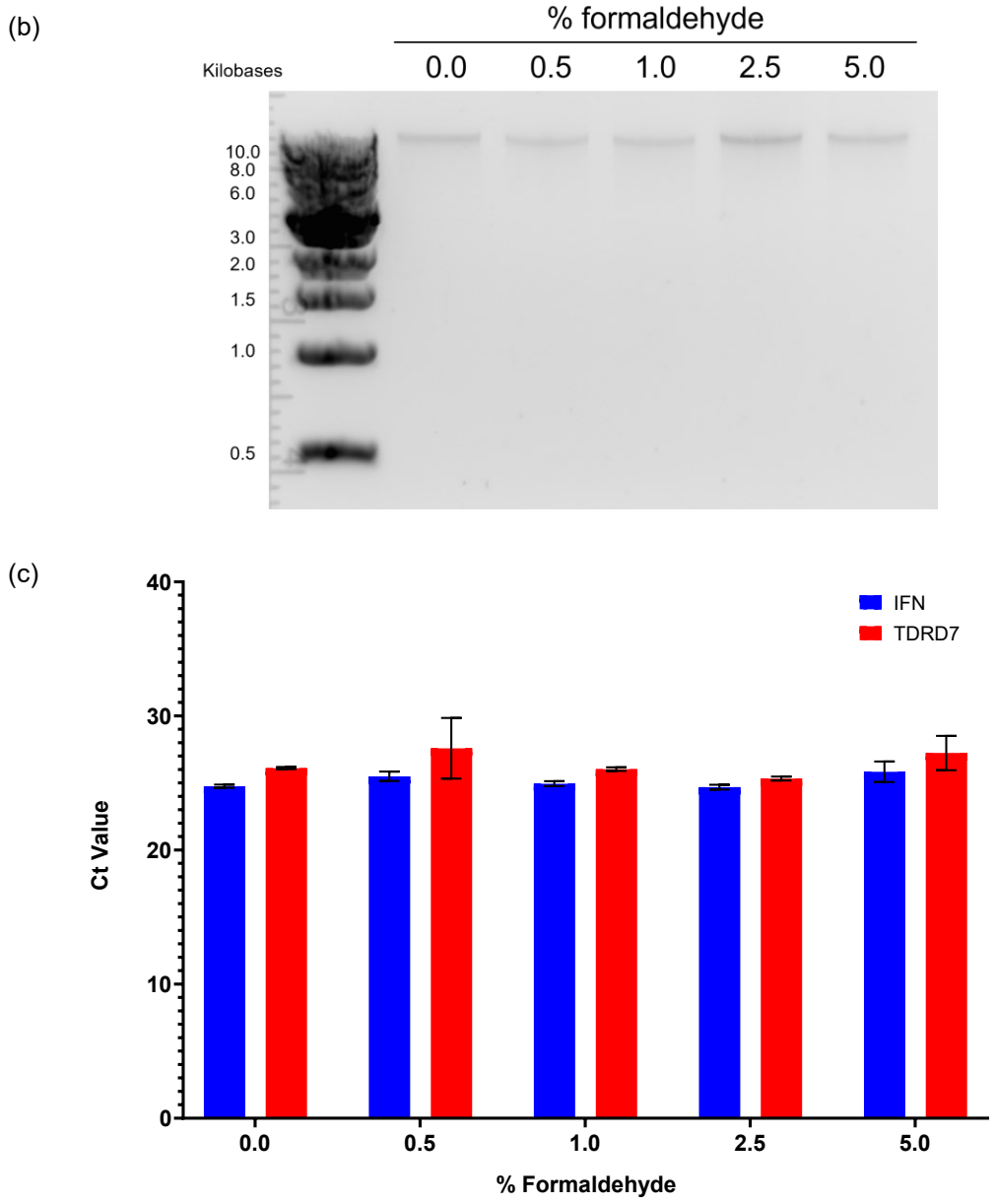

Figure 4.4.5: Formaldehyde inactivation of hPIV3-GFP(JS). **(A)** A549-Cas9 cells were infected with hPIV3-GFP(JS) (MOI = 5). 18 h.p.i, cells were fixed with 0 – 1% formaldehyde for 10 minutes. Cells were permeabilised to release virus particles and viral supernatant was titrated on Vero cells with no overlay. Monolayers were fixed 4 d.p.i. and imaged using GFP filter for visualisation of hPIV3-GFP(JS) virus (bottom panel). Plaques were detected using Phosphor Imaging, Cy2 for identification of GFP-positive cells (top panel). **(B)** To assess gDNA quality following formaldehyde treatment, gDNA was isolated from cells fixed with 0 – 5% formaldehyde for 10 minutes. 500 ng of isolated gDNA was ran on a 1% agarose gel. **(C)** 200 ng of gDNA isolated as per (B) was assessed by qPCR with Ct values for primers specific to IFN-β (blue) and TDRD7 (red) shown. Error bars represent the SD of the mean from two technical repeats.

4.5 Identification of hPIV3-GFP(JS) host dependency factors using genome-wide screening

To identify hPIV3-GFP(JS) host dependency factors, genome-wide CRISPR-Cas9 knockout screening was performed as outlined in section 4.2 (overview of assay workflow) using the conditions optimised as previously described. Gating of GFP-negative, low, medium, and high fractions was established by first running a negative control sample of A549-Cas9 library transduced cells which were fixed but not infected (figure 4.5.1.a) allowing for the gating of the true negative population. Following, gating the negative population, a sample of the infected cells were analysed to gate for the low, medium, and high populations; these gates were set for 5, 20 and 20% of the population respectively with ~5% of the population being GFP-negative.

Upon observing the library transduced cells infected with hPIV3-GFP(JS), the gating strategy from figure 4.4.3 was re-evaluated to capture what we believed to be true low, medium and high populations upon observation of the infected library transduced cells.

In our previous gating optimisation using A549-Cas9 cells, the infection profile of the cells was such that gaps could be left between gates to prevent overlap of gene hits between fractions. However, upon observation of the infected library transduced cells, the negative and low gates had to be positioned side by side to avoid the low gate encroaching on cells with higher GFP intensity. As such, this gating may have resulted in overlap of hits between the negative and low GFP populations and so downstream analysis was performed on both fractions. Additionally, the decision was made to reduce the percentage of cells in the GFP low population from 25 to 5%, as shown in figure 4.5.1.a, to capture a true low population instead of encroaching on cells with a higher MFI, as previously described; a decision that could only be made upon seeing infection of library infected cells.

gDNA isolated from the negative, low and high sorted fractions were subject to next generation sequencing, using NGS primers, to identify sgRNAs present in each fraction. It was decided to not analyse the medium fraction as this represents normal infection and likely would contain genes that have no bearing on infection as host dependency factors. It should be noted that whilst three biological repeats of the screen were performed, only two repeats were processed by NGS due to a low gDNA yield in one repeat. The resulting NGS data was then deconvoluted and subject to MaGeCK computational analysis as previously described (methods section 3.10.8). The log2 fold change of sgRNAs of all genes present in the negative fraction compared to the high fraction of the two combined repeats were plotted (figure 4.5.1.b). Those sgRNAs enriched in the negative fraction have a l2fc ≥ 1 as represented by a blue dashed line and genes with a -log10 p-value of > 2.3 correspond to a significance value of $p < 0.005$, as represented by a green dashed line, were determined to be hPIV3 host dependency factors to varying degrees. Whist 160 genes passed the thresholds of l2fc ≥ 1 and $p < 0.005$, only two genes, TMEM165 and SLC35A1, passed the false discovery threshold (FDR) of 0.1, as shown in the inlay graph highlighted in purple. Based on published studies (section 1.4.1), the number of genes passing the FDR threshold was significantly lower than expected, with only two genes passing this parameter. This is speculated to be due to a number of reasons. We observed only 30% recovery of gDNA from collected cells following sorting, a problem likely to be as a result of fixing cells. The amount of gDNA inputted into the downstream

analysis reduces the number of times genes are identified therefore reducing the chance of passing the FDR threshold.

During fixation optimisation (section 4.4), no difference was seen in the amount of gDNA extracted from 1% formaldehyde fixed cells, as fixed during screening, compared to non-fixed cells with the concentration of gDNA extracted being 91.4 ug/mL and 133.3 ug/mL from each respectively, a 30% reduction. Additionally, during optimisation of sort conditions, cells were not formaldehyde fixed and so the number of cells recovered following sorting was not identified to be a significant factor. It may be possible that the large number of cells used during screening, compared to optimisation, intensified a small decrease in gDNA recovery following fixation that was not observed to be significant during small scale testing.

In addition to identifying individual genes, we were also interested to see if there were conserved pathways within the hits identified. To investigate this, we used a Panther Gene Ontology analysis approach. Many pathways were identified including, transcription regulation and a number of other signalling pathways. However, no pathway was represented by more than 4 genes (figure 4.5.2) indicating that no discrete or conserved pathways were present and that the hits identified are instead diverse. This was surprising however, as manual observation of the MaGeCK analysis identified 6 genes involved in glycosylation and the sialic acid pathway, a pathway essential for paramyxovirus entry: TMEM165, SLC35A1, STT3A, B3GNT2, ST3GAL4, and ALG2.

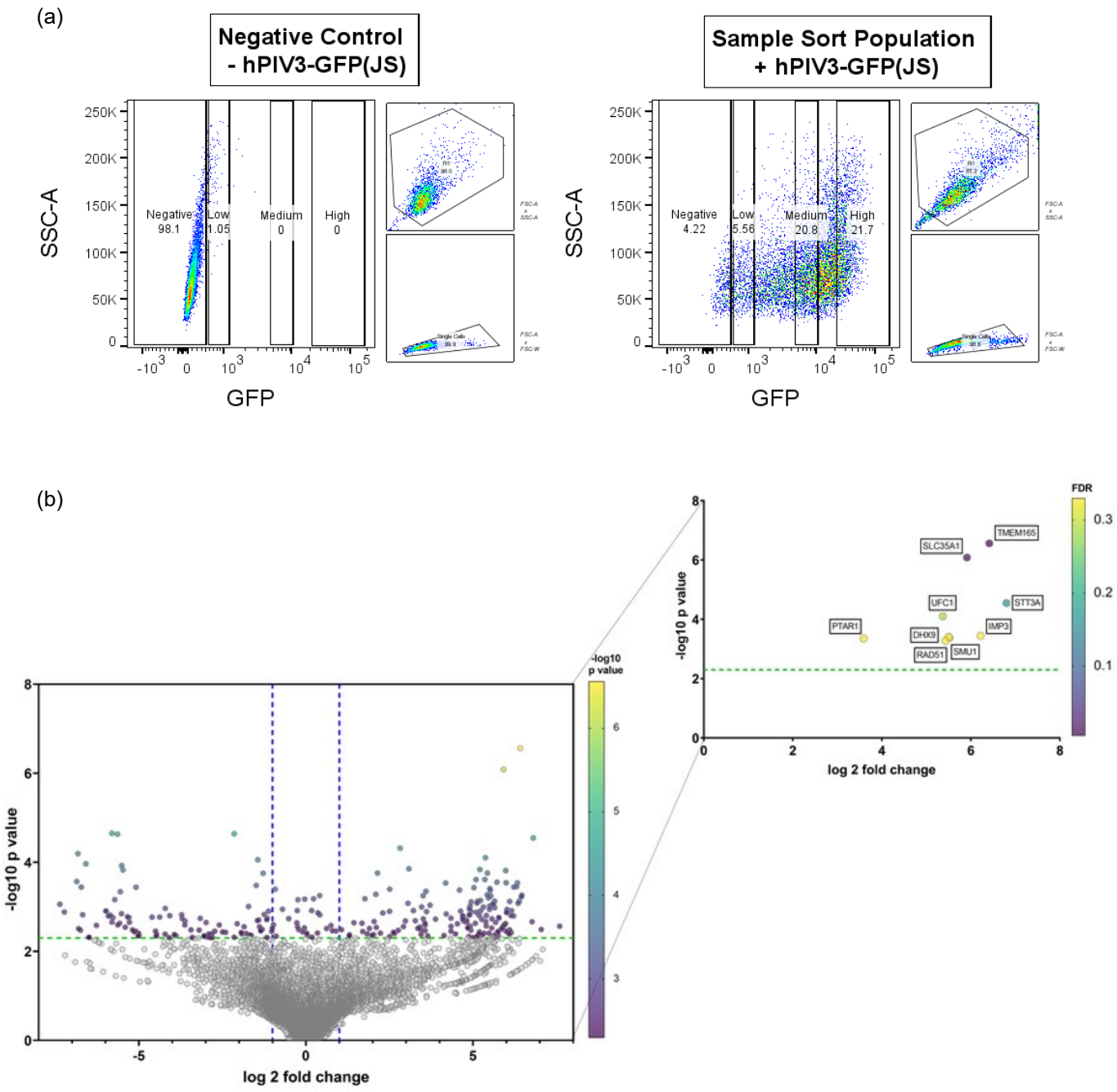

Figure 4.5.1: Identification of genes within hPIV3-GFP(JS) negative population. **(A)** Library transduced A549-Cas9 cells (previously described) were either infected with hPIV3-GFP(JS) (MOI = 5) or mock infected. Cells were harvested at 24 h.p.i and fixed with 1% formaldehyde for FACS. Cells were sorted into GFP-negative, low, medium, and high fractions. Figure is representative of cell populations sorted over 3 independent repeats. **(B)** gDNA isolated from fractions sorted in (A) were subject to next generation sequencing to identify sgRNAs present in each fraction prior to being subject to MaGeCK computational analysis. Log2 fold change of sgRNAs of all genes present in the negative fraction compared to high fraction of 2 combined repeats is shown with sgRNAs enriched in negative fraction indicated by l2fc ≥ 1. Green dotted line indicates p ≤ 0.005 threshold and blue dotted lines indicate l2fc ≤ -1 or l2fc ≥ 1 threshold. Inset graph shows genes of interest with genes passing the FDR threshold of < 0.1 shown in purple.

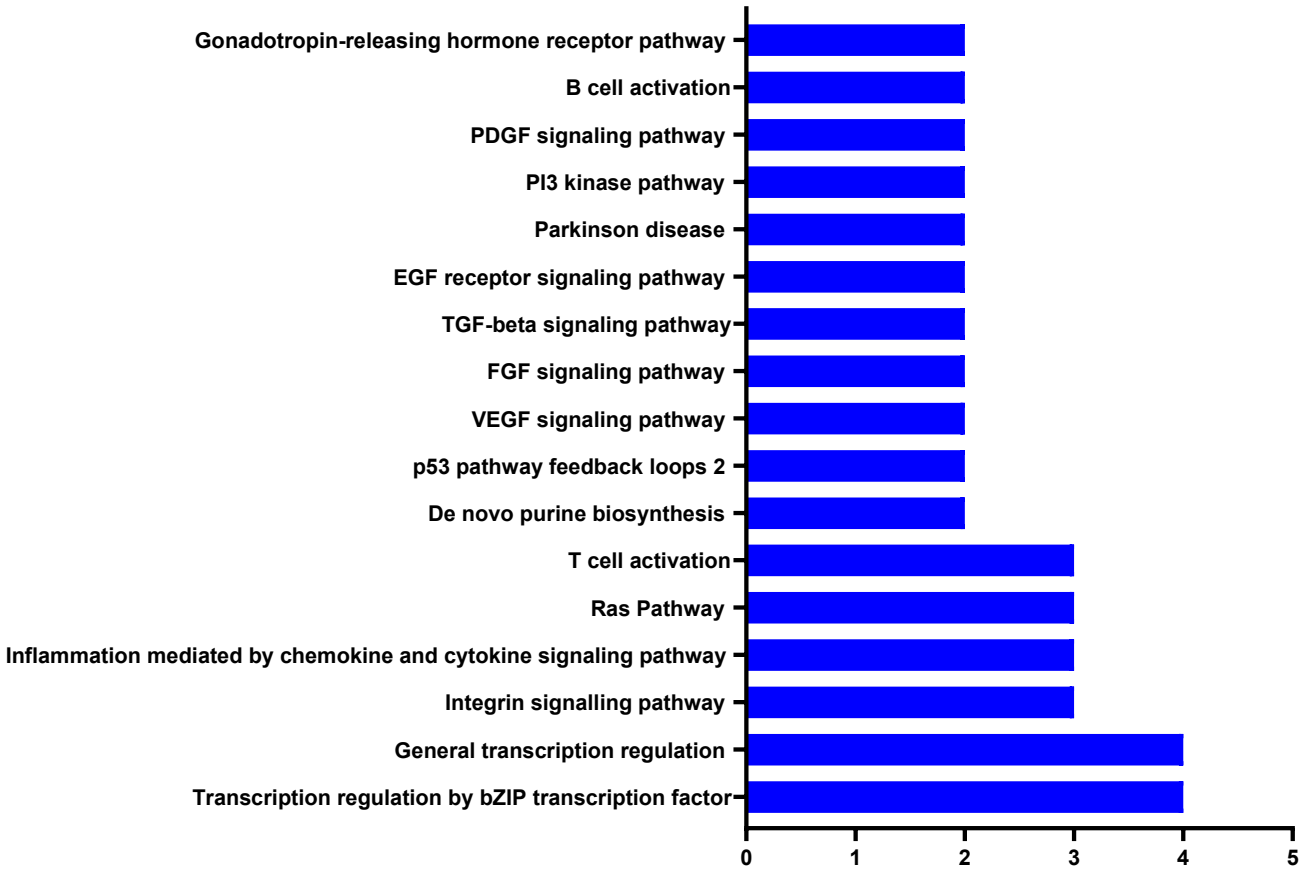

Figure 4.5.2: Gene ontology analysis of genes identified within the hPIV3-GFP(JS) negative population. 160 genes that passed the l2fc ≥ 1 and p < 0.005 thresholds were subject to Panther Gene Ontology Analysis with the number of genes identified in each pathway identified plotted.

From the genes that passed the log fold change and p-value thresholds, hit refinement was carried out as detailed in section 4.5.1.b. Refinement resulted in the identification of 8 genes of interest selected for further validation as shown in figure 3.9.b: SLC35A1, STT3A, DHX9, UFC1, PTAR1, SMU1 and IMP3. The 8 hits selected span a variety of different biological processes and pathways (table 4.5.1). To eliminate redundancy in the validation process, two out the six hits present in the sialic acid pathway were taken forward, one at the beginning of the pathway and one at the end. STT3A is a component of the oligosaccharyltransferase complex (OST), one of the first enzymes in the glycosylation pathway within the endoplasmic reticulum, responsible for transferring an oligosaccharide to a nascent protein (Harada et al., 2019). The second hit selected within this pathway is SLC35A1, a CMP-sialic transporter responsible for taking sialic acid from the cytoplasm to the Golgi for attachment (Hadley et al., 2019). The other hits (outlined in table 4.5.1) include a prenyltransferase, a ubiquitin-like protein transferase spliceosomal factor and small nucleolar riboprotein.

Table 4.5.1: PANTHER gene ontology analysis of hPIV3-GFP(JS) host dependency factors. Results of gene ontology analysis detailing identified Gene Symbols, Gene Names, Molecular Functions and Biological Processes.

Gene ID	Gene Symbol	Gene Name	Panther Molecular Function	Panther Biological Process
ENSG00000164414	**SLC35A1**	Solute carrier family 35 member A1	Molecular function unclassified	Biological process unclassified
ENSG00000134910	**STT3A**	STT3 oligosaccharyltransferase complex catalytic subunit A	Hexosyltransferase activity	Protein N-linked glycosylation wia asparagine; Post-translational protein modification
ENSG00000135829	**DHX9**	DExH-box helicase 9	RNA binding	Biological process unclassified
ENSG00000143222	**UFC1**	Ubiquitin-fold modifier conjugating enzyme 1	Ubiquitin-like protein transferase activity	Protein modification by small protein conjugation
ENSG00000188647	**PTAR1**	Protein prenyltransferase alpha subunit repeat containing 1	Molecular function unclassified	Biological process unclassified
ENSG00000051180	**RAD51**	RAD51 recombinase	ATP hydrolysis activity; ATP-dependent activity, acting on DNA; Double-stranded DNA binding; Single-stranded DNA binding	Reciprocal meiotic recombination; Protein-DNA complex assembly; Double-strand break repair via homolgous recombination; Meiotic telophase; Chromosome organization involved in meiotic cell cycle; Mitotic recombination
ENSG00000122692	**SMU1**	SMU1 DNA replication regulator and spliceosomal factor	Molecular function unclassified	RNA splicing
ENSG00000177971	**IMP3**	U3 small nucleolar ribonucleoprotein protein IMP3	snoRNA binding; Structural contituent of ribosome; rRNA binding	Regulation of biological quality; Positive regulation of translation; rRNA processing; Translational elongation

4.6 Validation of hPIV3-GFP(JS) host dependency factors identified through screening

To validate the 8 selected hits from section 4.5, individual knockout cell lines for each hit were generated using two independent sgRNAs targeting separate sites within the gene. These independent knockout cells were subsequently used to validate hits alongside a A549-Cas9.NC1 control using flow cytometry.

Hit knockout cells were infected with hPIV3-GFP(JS) (MOI = 10) and harvested for flow cytometry analysis after 18 h. A549-Cas9.NC1 cells either infected (blue) or not (red) with hPIV3-GFP(JS) at the same MOI were used to set gates for GFP-negative and positive populations. It would be expected that if the genes were true host dependency factors, deletion of the gene would result in cells being unable to permit virus replication. We would therefore expect knockout cells infected with hPIV3-GFP(JS) (orange) to overlay with the negative control (red). This was only seen for one out of eight hits, SLC35A1 (figure 4.6.1). Quantification of percentage GFP-negative cells shows that A549-Cas9.SLC35A1$^{-/-}$ cells infected with hPIV3-GFP(JS) (red) results in >90% GFP-negative cells when quantified over three biological repeats. However, infection of the other 7 knockout cell lines results in <10% GFP-negative cells, similar to that of the A549-Cas9.NC1 negative control. It was surprising that only one hit resulted in a phenotype, especially as we knew that STT3A was within the same pathway, sialic acid metabolism, as SLC35A1. This could be due to hits not passing the FDR threshold, due to the aforementioned reasons, as SLC35A1 is the only gene of the eight to pass this threshold, or redundancy in the host dependency response as we know that STT3A is one of two isoforms co-expressed in mammalian tissues.

(a)

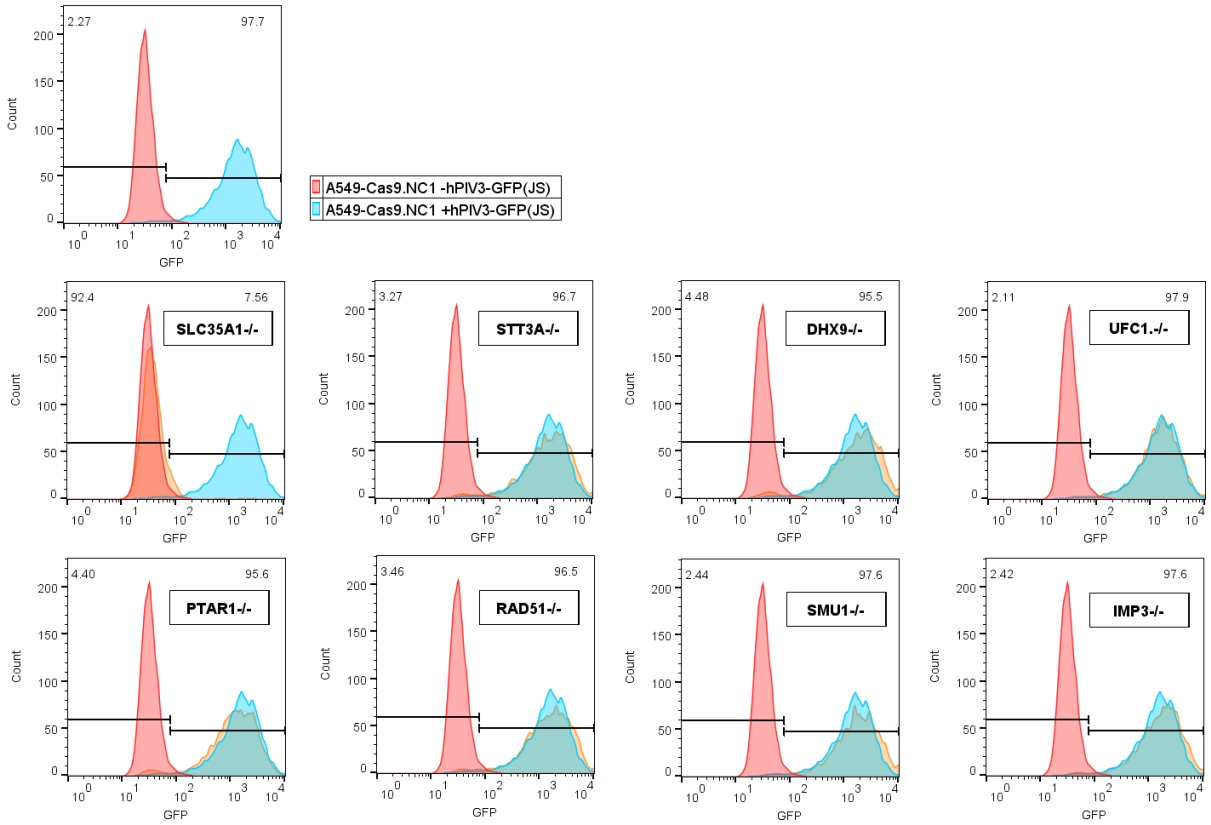
2.27
97.7
A549-Cas9.NC1 -hPIV3-GFP(JS)
A549-Cas9.NC1 +hPIV3-GFP(JS)
92.4
7.56
SLC35A1-/-
3.27
96.7
STT3A-/-
4.48
95.5
DHX9-/-
2.11
97.9
UFC1.-/-
4.40
95.6
PTAR1-/-
3.46
96.5
RAD51-/-
2.44
97.6
SMU1-/-
2.42
97.6
IMP3-/-
Count
GFP

(b)

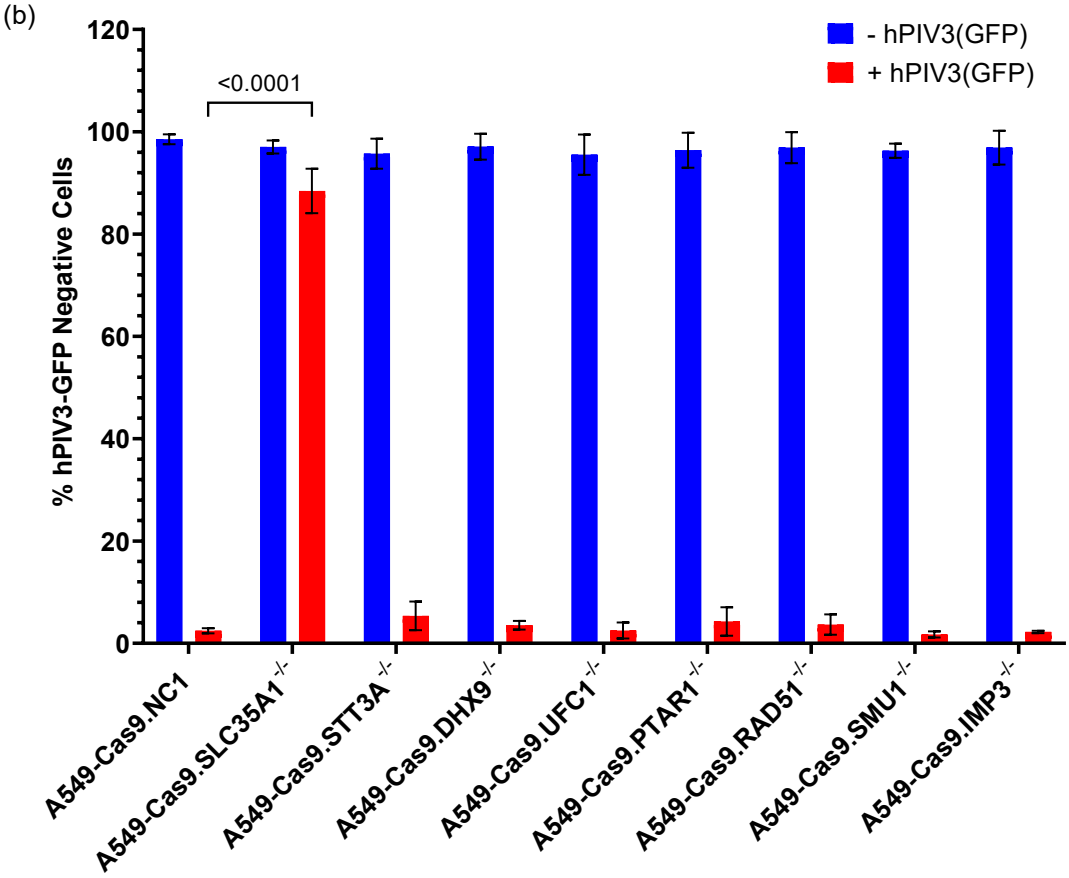
- hPIV3(GFP)
+ hPIV3(GFP)
<0.0001
% hPIV3-GFP Negative Cells
120
100
80
60
40
20
0
A549-Cas9.NC1
A549-Cas9.SLC35A1 -/-
A549-Cas9.STT3A -/-
A549-Cas9.DHX9 -/-
A549-Cas9.UFC1 -/-
A549-Cas9.PTAR1 -/-
A549-Cas9.RAD51 -/-
A549-Cas9.SMU1 -/-
A549-Cas9.IMP3 -/-

Figure 4.6.1: Validation of hPIV3-GFP(JS) host dependency factors. **(A)** CRISPR/Cas9 genome editing was used to knockout gene expression in A549-Cas9 cells of genes identified as hits to validate (Table 3.1); SLC35A1, STT3A, DHX9, UFC1, PTAR1, RAD51, SMU1, IMP3. Knockout cells were infected with hPIV3-GFP(JS) (MOI = 10) or mock infected. Cells were harvested at 18 h.p.i for flow cytometry analysis using blue laser (488 nm) for identification of GFP-positive cells. Data was analysed using FlowJo v10. A549-Cas9.NC1 cells were used as control with non-infected A549-Cas9.NC1 cells shown in red, A549-Cas9.NC1 cells infected with hPIV3-GFP(JS) shown in blue and specified knockout cell infected with hPIV3-GFP(JS) overlayed in orange. Data shown is one repeat, representative of three. **(B)** Data from (A) was quantified based on singlet cell gating and% hPIV3-GFP-negative Cells and plotted. Mock infected shown in blue and hPIV3-GFP(JS) infected shown in red. Error bars represent the SD of the mean from three biological repeats. Statistics performed using two-way ANOVA; p-values denoted on graph.

4.7 Summary

We developed a genome-wide CRISPR-Cas9 knockout screen for the identification of hPIV3-GFP(JS) host dependency factors in A549-Cas9 library transduced cells. Infection and fixation conditions were optimised to enhance the identification of hits following FACS and NGS analysis. MaGeCK analysis identified hits that passed the log-fold change and p-value thresholds as previously described. However, we were unable to identify many hits that passed the fold discovery rate threshold, subsequently suggested to be due to the percentage recovery of cells following fixation that underwent sorting. As the infection and sorting conditions appear optimal, it is proposed that increasing the number of cells subjected to FACS would increase the number of cells passing the FDR threshold and therefore result in the number of hits successfully validated.

Despite this, optimisation of the screen identified hits known to be important for hPIV3 infection, such as those within the sialic acid pathway and successfully validated one such gene within the pathway, SLC35A1, as a host dependency factor. Depletion of SLC35A1, through the generation of independent knockouts, has shown that in the absence of the sialic acid transporter, the virus is rendered unable to permit infection. Additionally, we show that the genes identified through screening are not clustered to a specific pathway and instead are non-discrete indicating the virus relies on a number of host pathways and processes for successful replication.

Chapter 5: A genome wide CRISPR/Cas9 screening platform for the identification of hPIV3 antiviral restriction factors

5.1 Introduction

As previously discussed, the IFN response, a component of the innate immune response, is critical to controlling the rate of infection by providing one of the first lines of defence, especially against viruses, prior to the activation of the acquired immune response (Isaacs and Lindenmann, 1987; Schneider, Chevillotte and Rice, 2014; Fensterl, Chattopadhyay and Sen, 2015). Whilst it is known that the activation of the IFN response results in the expression of hundreds of interferon stimulated genes (ISGs), for many viruses, it is unknown which of these ISGs restrict the virus (Schoggins and Rice, 2011). The large amount of redundancy in this response, and the fact that many ISGs have low activity against any one virus, having to work in concert for full restriction, can make it difficult to untangle which ISGs play a role (Jones et al., 2021).

As with the HDF screen, a genome wide CRISPR/Cas9 screen had not yet been used to identify which ISGs restrict hPIV3, and so we have subsequently performed such a screen to identify restriction factors against this medically and economically important virus.

As many ISGs work in concert, due to their low to moderate activity in isolation, to restrict a virus, it was postulated whether the sensitivity of current screening methods could be improved. Previous work in the Hughes group, has shown that knockout of ISG15, a negative regulator of type-I IFN, results in resistance to virus infection due to the increased expression of ISGs as a result of a dysregulated IFN response (Holthaus et al., 2020). We therefore hypothesised, that by using ISG15 deficient cells, we could augment the working window for the identification of ISGs with low to moderate activity when compared to cells used in current screening methods.

5.2 Optimisation of experimental conditions for genome-wide screening

To identify antiviral restriction factors, the workflow from section 4.2 was followed with the addition of an IFN-α pre-treatment step prior to infection in order to put the cells into an antiviral state. As such, the parameters of IFN-α pre-treatment (time and infection) had to be optimised to ensure the majority of cells were able to restrict virus infection enabling the identification of cells where antiviral factors had been deleted in our screening library. It is assumed that if an antiviral factor has been deleted from a cell, this will render the cell permissive to infection. The majority of cells must therefore be in an antiviral state to identify a minority population of GFP-positive cells and prevent false positive hit identification. To optimise this work flow we utilised two cell lines; A549-BVDV.Npro, a cell line which targets IRF3 for proteasomal degradation therefore preventing IFN induction (Hilton et al., 2006; Chen et al., 2007), and A549-Cas9.STAT2$^{-/-}$, a CRISPR-Cas9 engineered cell line deficient in STAT2, a key component of IFN signalling {Formatting Citation}. The use of these two cell lines enabled the modelling of screening conditions due to their deficiency of a key component of the IFN response, therefore representing library transduced cells deficient in an antiviral restriction factor.

To identify optimal infection conditions, whereby cells deficient in an antiviral factor are as near to 100% infected as possible, A549-BVDV.Npro, alongside A549-Cas9 cells as a control, were infected with hPIV3-GFP(JS) at MOI = 5 for either 18 or 24 hours or left uninfected prior to analysis using flow cytometry (figure 5.2.1.a). As expected, infection of A549-BVDV.Npro cells (orange) resulted in

a greater proportion of GFP-positive cells, indicative of infection, compared to A549-Cas9 cells (red) with mean fluorescence intensity increasing from 151 in A549-Cas9 cells to 201 in A549-BVDV.Npro cells at 18 h.p.i, and 369 in A549-Cas9 cells to 559 in A549-BVDV.Npro cells at 24 h.p.i. A percentage increase in cell infectivity of 33 and 51.5% at each timepoint respectively. This was expected due to the inability of A549-BVDV.Npro cells to produce IFN due to the proteasomal degradation of IRF3. Interestingly, A549-BVDV.Npro cells had higher levels of background fluorescence when mock infected (green) compared to mock infection of A549-Cas9 cells (blue), however this was deemed insignificant. In A549-BVDV.Npro cells, we observed a percentage increase in MFI of 178% between cells infected for 18 and 24 h however the percentage of cells that were determined to be GFP-positive, as gated from A549-Cas9 mock infected cells, remained 93.3 and 96.6% respectively at 18 and 24 h.p.i. This indicated that increasing the time of infection did not lead to any more cells becoming infected and the increase in MFI is likely due to increased viral replication in already infected cells. It should be noted that infection of cells at MOI = 10 (data not shown), did not result in a greater percentage of GFP-positive cells compared to those infected at MOI = 5.

We further observed in the FSC/SSC plot of A549-BVDV.Npro cells both infected and mock infected that there was increased cell debris at 24 compared to 18 h.p.i (figure 5.2.1.b). Forward scatter (FSC) is a representation of a particles size, with larger cells, or cells clumped together, exhibiting a large FSC, and side scatter (SSC) is a measure of the particles complexity; for example cells that are more granular or lobular exhibit a higher SSC than ‘smooth cells’ (Virgo and Gibbs, 2012). This is shown qualitatively by the increasingly scattered distribution of cells in the FSC/SSC plots at 24 h.p.i, as fewer particles exhibit the standard FSC/SSC properties of A549 cells, but also quantitatively by the reduced percentage of cells falling within the R1 gated region, representing the cell population of interest. We observe a reduction from 95% to 88 and 90% of cells falling within the R1 gate for both infected and mock infected respectively. This indicates reduced cell health in cells lacking key components of the IFN response at later time points. Within a screening scenario, each sgRNA is only represented 500 times, and if cell health is poor in cells lacking true restriction factors, this may deplete populations of cells the screen is aiming to identify. Due to similar levels in infection in A549-BVDV.Npro cells at both timepoints but differences in cell morphology, an infection timepoint of 18 h was taken forward for further studies.

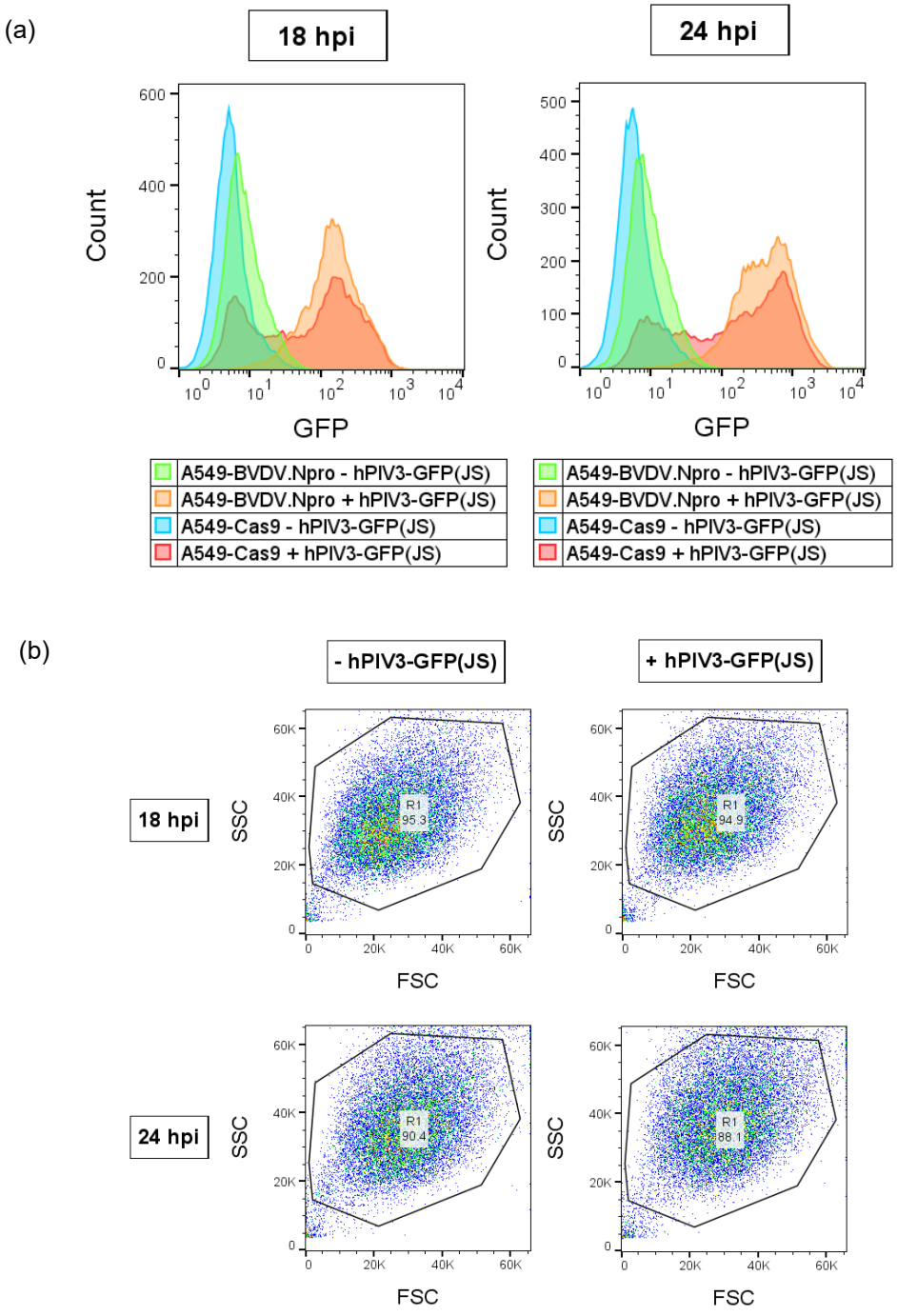

Figure 5.2.1: Optimisation of infection conditions for identification of antiviral restriction factors. **(A)** A549-Cas9 and A549-Npro cells were infected with hPIV3-GFP(JS) (MOI = 5) or mock infected. Cells were harvested for flow cytometry analysis using blue laser (488 nm) for identification of hPIV3-GFP(JS) positive cells at 18 h.p.i (left) and 24 h.p.i (right). GFP intensity for each condition is shown overlayed; A549-Npro –hPIV3-GFP(JS) (blue), A549-Npro +hPIV3-GFP(JS) (orange), A549-Cas9 –hPIV3-GFP(JS) (green), and A549-Cas9 +hPIV3-GFP(JS) (red). **(B)** FSC/ SSC plots of A549-Npro cells infected with hPIV3-GFP(JS) or mock infected at 18 and 24 h.p.i from (A) show increased cell debris at 24 h.p.i.

To assess, whether the previously established sorting and infection conditions (section 4.4) were able to successfully isolate genes deficient an antiviral restriction factor, we generated an A549-Cas9.STAT2$^{-/-}$ cell line using CRISPR-Cas9 genome engineering.

Whilst termed A549-Cas9.STAT2$^{-/-}$, the cell line was left as a 'bulk' cell line and was not single cell cloned, subsequently containing both STAT2 deficient and STAT2 encoding cells. This was used over the A549-BVDV.Npro cell line previously used as sorting and infection conditions could be tested on a heterogenous population. The use of a bulk cell line allowed a closer representation of the screening library whereby cells deficient in antiviral restriction factors are present in smaller numbers alongside cells that are not permissive to infection. A549-Cas9.STAT2$^{-/-}$ (bulk) cells were treated for 24 h with IFN-α or left untreated then either infected with hPIV3-GFP(JS) (MOI = 5) or mock infected prior to being harvested at 18 h.p.i for flow cytometry analysis based on previous data. GFP-negative gates were set based on mock treated (- IFN and – hPIV3-GFP(JS)) cells, representing 100% GFP-negative cells (figure 5.2.2). Infection of non-IFN pre-treated A549-Cas9.STAT2$^{-/-}$ (bulk) cells resulted in ~ 90% GFP-positive cells, indicative of infection. However, addition of IFN-α pre-treatment prior to infection of A549-Cas9.STAT2$^{-/-}$ (bulk) cells resulted in ~ 45% GFP-positive cells with ~ 55% of cells GFP-negative, i.e., not infected. The GFP-negative population indicates the presence of STAT2-expressing cells within the bulk population which are able to restrict virus infection.

The bulk population of IFN-α and hPIV3-GFP(JS)-treated A549-Cas9.STAT2$^{-/-}$ (bulk) cells were sorted using FACS into GFP-negative and GFP-positive populations using the sorting strategy from section 4.4. Sorted cell populations were processed for immunoblot analysis, using antibodies specific for STAT2 and β-actin, to assess for enrichment of cells deficient in antiviral restriction factors in the GFP-positive population. IFN-α pre-treated A549-Cas9.NC1 cells, prior to hPIV3-GFP(JS) infection, were used as a positive control for STAT2. Non-treated A549-Cas9.NC1 cells (- hPIV3, - IFN) were used a negative control, indicating weak endogenous levels of STAT2 (figure 5.2.2.b). Further analysis showed presence of STAT2 in both mock treated and IFN-α and hPIV3-GFP(JS) treated A549-Cas9.STAT2$^{-/-}$ (bulk) cells. However, we observe loss of STAT2 protein signal in the GFP-positive sorted population and enrichment of STAT2 in the GFP-negative sorted population. This is expected because, as previously described, it is assumed that if an antiviral factor (STAT2) has been deleted from a cell, this will render the cell permissive to infection (GFP-positive). These results indicate that the sorting and treatment strategy effectively allows isolation of antiviral factor knockout cells when restriction factor deficient cells are at low levels, in this case 45% of the population, as will be during the antiviral restriction factor screen.

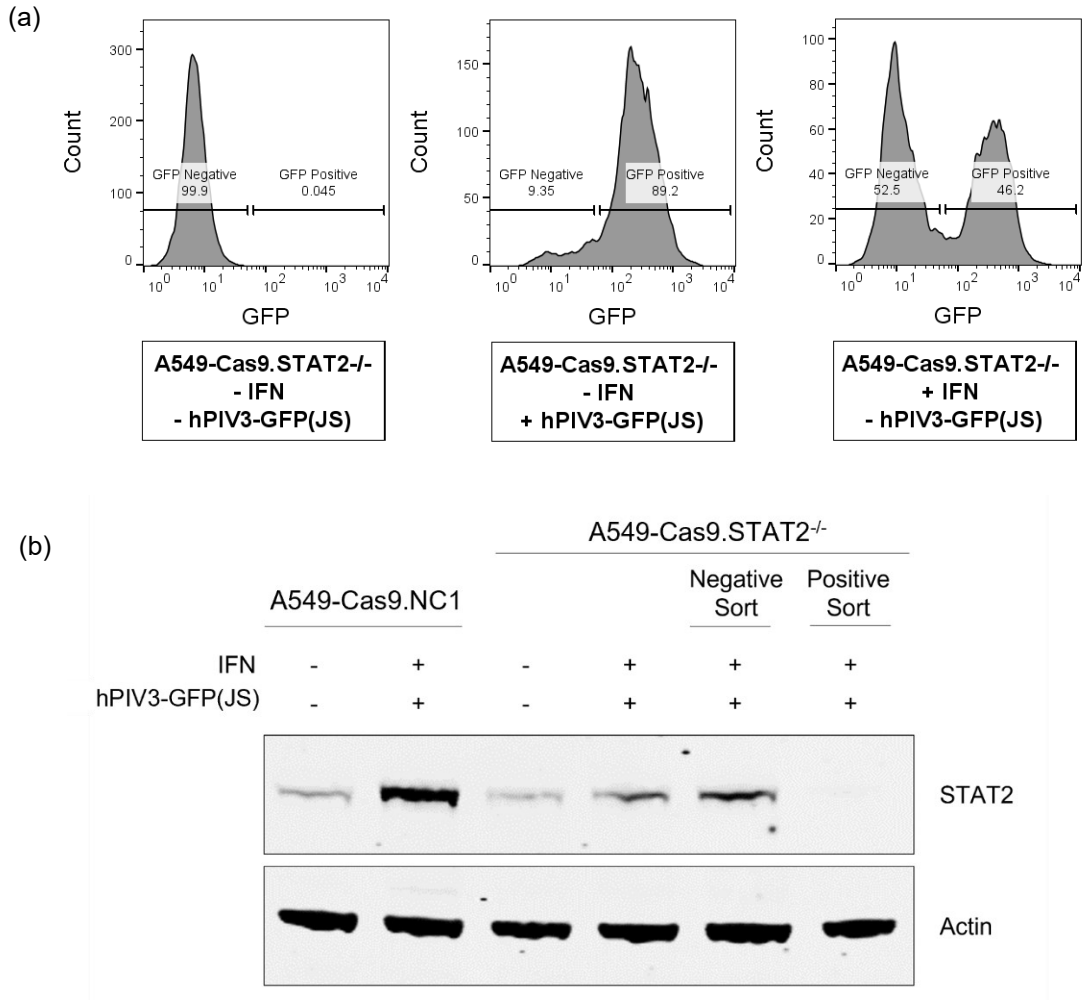

Figure 5.2.2: Sorting and treatment strategy effectively allows isolation of antiviral factor knockout cells. **(A)** A549-Cas9.STAT2$^{-/-}$ (bulk) cells were treated for 24 h with IFN-a or left untreated then either infected with hPIV3-GFP(JS) (MOI = 5) or mock treated. Cells were harvested at 18 h.p.i for flow cytometry analysis and fluorescence activated cell sorting (FACS) using blue laser (488 nm) for identification of hPIV3-GFP(JS) positive cells. Data was analysed using FlowJo v10. **(B)** IFN-α and hPIV3-GFP(JS) infected cells from (A) were sorted into GFP-negative and GFP-positive fractions and processed for immunoblot analysis using Abs specific for STAT2 and β-actin. A549-Cas9.NC1 cells either IFN-α pre-treated and hPIV3-GFP(JS) infected or not were used as STAT2 positive and negative controls, respectively.

5.3 Identification of hPIV3-GFP(JS) antiviral factors using genome-wide screening

To identify hPIV3-GFP(JS) antiviral restriction factors, genome-wide CRISPR-Cas9 knockout screening was performed as outlined in section 4.2 (overview of assay workflow) with the addition of IFN-α pre-treatment using the conditions optimised as previously described. Gating of the GFP-negative fraction was established by first running a negative control sample of A549-Cas9 library

transduced cells which were fixed but not infected (figure 5.3.1.a) allowing for the gating of the true negative population. A sample of IFN-α pre-treated and hPIV3-GFP(JS) infected library transduced A549-Cas9 cells was subsequently ran to gate for the low, medium, and high populations with the medium and high gates, set for 6 and 2% of the population respectively. The medium and high GFP populations are assumed to contain the antiviral restriction factors as deletion of a restriction factor renders the cell able to permit virus replication. Upon observing the sample sort population, the gates representing these two populations were significantly smaller than expected, likely due to the number of restriction factors present within the sgRNA library and the low to moderate activity these genes express in isolation as previously described resulting in fewer cells expressing high levels of GFP. As such, the percentage of cells collected was much lower than previously described in section 5.2. with the number of cells for gDNA extraction and NGS analysis reduced.

gDNA isolated from three biological repeats of the negative, medium, and high sorted fractions were subject to next generation sequencing to identify sgRNAs present in each fraction. The resulting NGS data was then deconvoluted and subject to MaGeCK computational analysis as previously described. The log2 fold change of sgRNAs of all genes present in the high fraction compared to the negative fraction of the three repeats was plotted (figure 5.3.1.b). Those sgRNAs enriched in the high fraction have a l2fc ≥ 1 as represented by a blue dashed line and genes with a -log10 p-value of > 2.3 correspond to a significance value of $p < 0.005$, as represented by a green dashed line, were determined to be hPIV3 antiviral restriction factors. Following analysis, 66 genes passed the thresholds of l2fc ≥ 1 and $p < 0.005$. Hits were further refined from figure 5.3.1, by identifying genes present in the analysis that had previously been described as ISGs, determined by their presence in the Ohainle ISG CRISPR library or on the Interferome server (section 4.2). This resulted in the identification of 26 ISGs that were significantly enriched in the GFP high fraction compared to the GFP-negative fraction. These included a number of genes within the IFN signalling pathway that passed both the significance and FDR thresholds; STAT1, STAT2, IFNAR1, IFNAR2, JAK1 and IRF9 (figure 5.3.1.b). The presence of these genes passing both thresholds, provided an internal control for the success of the screen and confidence in the optimisation of sorting and treatment conditions that had been previously established.

As in section 4.5, we were also interested to see if there were conserved pathways within the 66 hits identified. Using a Panther Gene Ontology analysis approach, many pathways were identified including, JAK/STAT signalling pathway, as would be expected. The pathway containing the largest number of genes was the ‘inflammation mediated by chemokine and cytokine signalling pathway’, containing 5 out of 66 genes. However, all other pathways contained 4 or less genes indicating that no discrete or conserved pathways were present and that the hits identified are instead diverse.

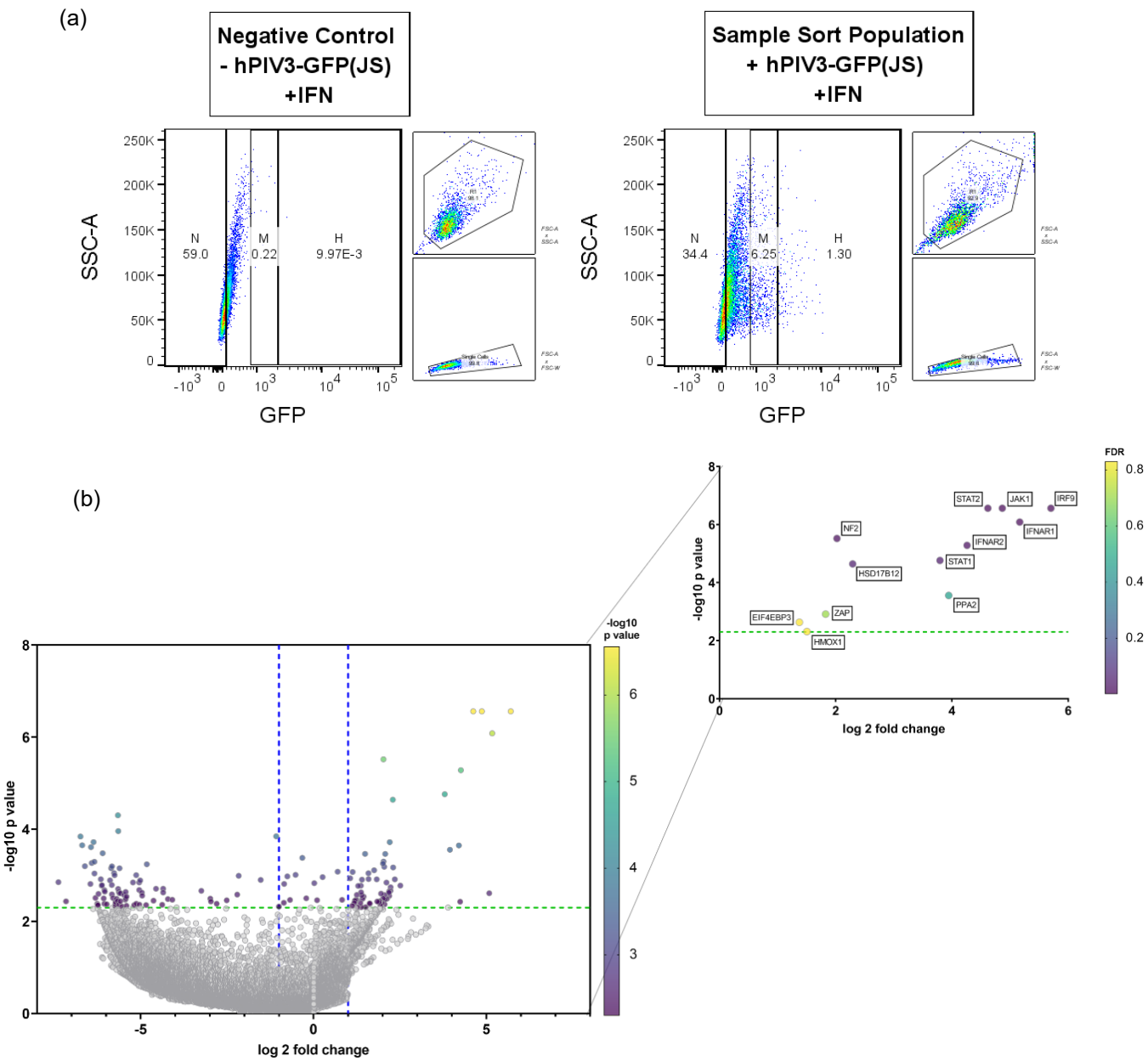

Figure 5.3.1: Identification of genes and processes within hPIV3-GFP(JS) high population within A549-Cas9 cells. **(A)** Library transduced A549-Cas9 cells (previously described) were pre-treated with IFN-α for 24 h prior to being either infected with hPIV3-GFP(JS) (MOI = 5) or mock infected. Cells were harvested at 24 h.p.i and fixed with 1% formaldehyde for FACS. Cells were sorted into GFP-negative, low, medium, and high fractions. Figure is representative of cell populations sorted over 3 independent repeats. **(B)** gDNA isolated from fractions sorted in (A) were subject to next generation sequencing to identify sgRNAs present in each fraction prior to being subject to MaGeCK computational analysis. Log2 fold change of sgRNAs of all genes present in the high fraction compared to negative fraction of 3 combined repeats is shown with sgRNAs enriched in high fraction indicated by l2fc ≥ 1. Green dotted line indicates p ≤ 0.005 threshold and blue dotted lines indicate l2fc ≤ -1 or l2fc ≥ 1 threshold. Inset graph shows genes of interest with genes passing the FDR threshold of < 0.1 shown in purple.

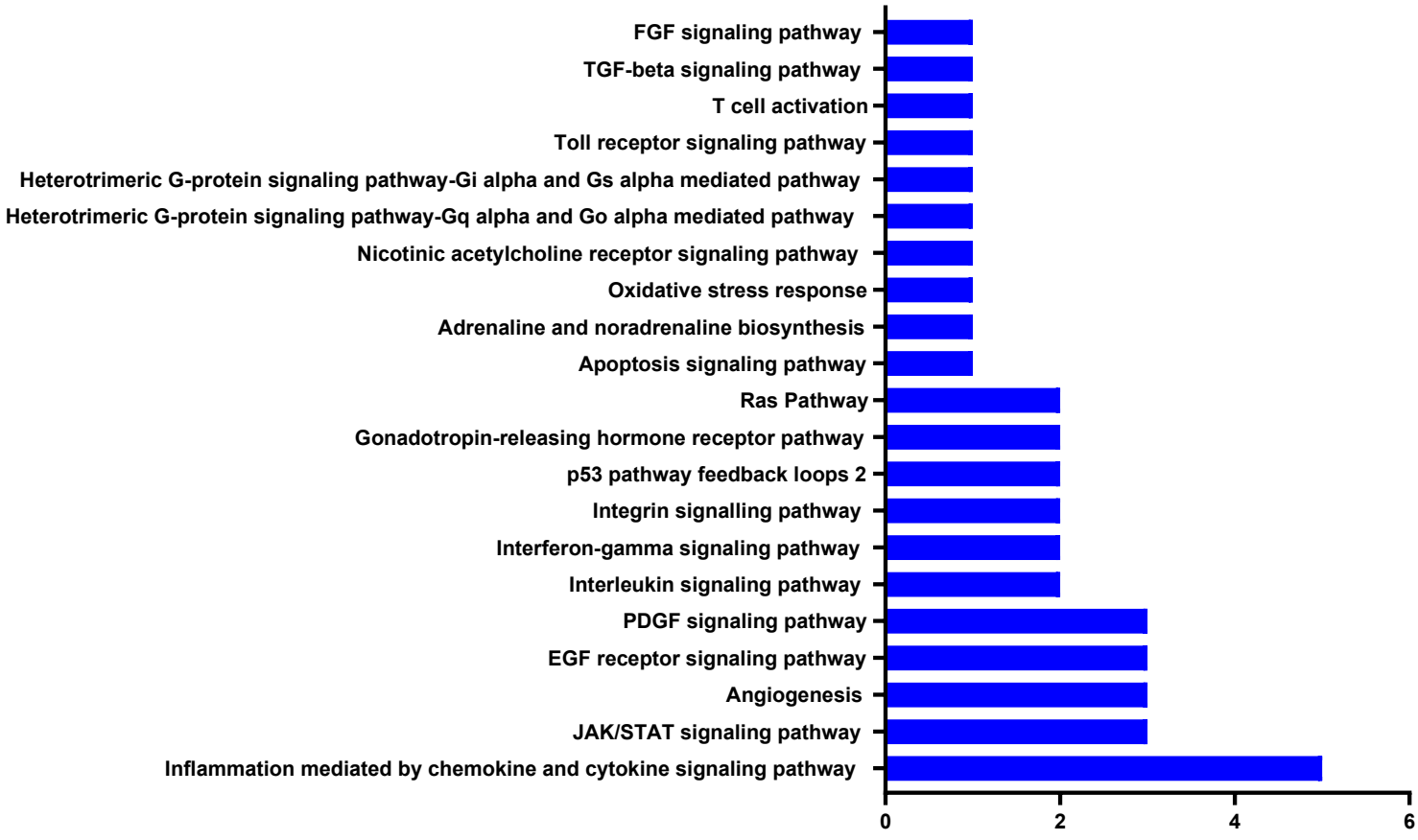

Figure 5.3.2: Gene ontology analysis of genes identified within the hPIV3-GFP(JS) high population. 66 genes that passed the l2fc ≥ 1 and p < 0.005 thresholds were subject to Panther Gene Ontology Analysis with the number of genes identified in each pathway identified plotted.

Due to the low numbers of genes extracted from the analysis in the GFP high population, genes that passed the log fold change and p-value thresholds in both the GFP high and medium (not shown) fraction underwent hit refinement as detailed in section 4.2, with the additional step of ISG identification. Refinement resulted in the identification of 8 genes of interest selected for further validation: NF2, HSD17B12, ZAP (also known as ZC3HAV1), P2RY14, ELF1, HMOX1, PPA2 and EIF4EBP3. Four of the selected genes, HMOX1, ZAP, ELF1 and P2RY14, were identified as ISGs using the tools previously described, whilst PPA2 and EIF4EBP3 showed sufficient literature to warrant further investigation. Two additional genes, NF2 and HSD17B12, were the only two genes, additional to the internal controls that passed both the significance and FDR thresholds, shown in purple, and so were taken forward for further validation. Figure 5.3.1.b shows 6 out of 8 genes taken forward as final hits as P2RY14 and ELF1 were identified in the GFP medium fraction (not shown).

To validate the 8 selected hits from section 5.3, individual knockout cell lines for each hit were generated in A549-Cas9 cells using two independent sgRNAs targeting separate sites within the gene as in section 4.6. These independent knockout cells were subsequently used to validate hits alongside the A549-Cas9.NC1 non-cutting sgRNA cell line control using flow cytometry.

Knockout cells were infected with hPIV3-GFP(JS) at MOI = 2.5 following IFN-α pre-treatment or mock-treatment for 24 h. An MOI of 2.5 was used rather than an MOI of 5, as per the screen, for validation as it enabled the ability of the individual knockout cell lines to result in a GFP-positive phenotype to be further challenged. At MOI = 5, as per the screen, ~ 65% of cells were still observed to be GFP-positive following IFN-α pre-treatment. Conversely, using MOI = 2.5 for validation, < 10% of A549-Cas9.NC1 control cells were GFP-positive (figure 5.3.3), enhancing the effect of IFN treatment and rigorously testing if the individual knockouts could overcome the IFN response. This could also be due to using only single knockout. Cells were harvested at 18 h.p.i for flow cytometry analysis, as per during screening conditions, for the identification of GFP-positive cells. GFP-negative gates were set on A549-Cas9.NC1 cells pre-treated with IFN-α prior to hPIV3-GFP(JS) infection with A549-Cas9.NC1 cells mock-IFN treated used as a positive control. It would be expected that if the genes were true antiviral restriction factors, deletion of the gene would result in cells being able to permit virus replication and therefore show increased GFP intensity, or percentage GFP cells, compared to the negative control. We would therefore expect knockout cells pre-treated with IFN-α (orange) to overlay with the positive control (blue). However, we observe that infection, following IFN-α pre-treatment, of all eight knockout cell lines does not result in cells with a GFP-positive phenotype. Only in three knockout cells lines, A549-Cas9.NF2$^{-/-}$, A549-Cas9.HSD17B12$^{-/-}$, and A549-Cas9.ZAP$^{-/-}$ do we observe a small shift in infection profile to outside the negative control phenotype. As shown in figure 5.3.3.a, cells deficient in either NF2, HSD17B12 or ZAP, when pre-treated with IFN-α (orange), see a shift in their histogram profile to the right indicating increased GFP intensity. This shift moves the peaks away from aligning with A549-Cas9.NC1 cells pre-treated with IFN-α (red), suggesting some of the cell population displays increased susceptibility to infection compared to the control. When quantified for percentage GFP-positive cells, indicative of infection, the results show no difference in levels of infection in the other five hits compared to A549-Cas9.NC1 cells and non-significant increases in percentage GFP-positive cells for the three cells previously described, indicating they are not true antiviral restriction factors (figure 5.3.3.b).

However, a non-significant increase in percentage infection may not be surprising. As previously described, most restriction factors exhibit low to moderate activity when expressed in isolation and so redundancy in the IFN response may be contributing to the phenotype seen. As such, the percentage increase in GFP-positive cells from 6.7% in A549-Cas9.NC1 pre-treated with IFN-α to 14.8, 25.3 and 26.3% in A549-Cas9.NF2$^{-/-}$, A549-Cas9.HSD17B12$^{-/-}$, and A549-Cas9.ZAP$^{-/-}$ respectively was determined sufficient for further validation and characterisation prior to validation of successful knockout (section 6).

Table 5.3.1: PANTHER gene ontology analysis of validated hPIV3-GFP(JS) antiviral factors. Results of gene ontology analysis detailing identified Gene Symbols, Gene Names, Molecular Functions and Biological Processes.

Gene ID	Gene Symbol	Gene Name	Panther Molecular Function	Panther Biological Process
ENSG00000186575	NF2	Moesin-Ezrin-Radixin Like (MERLIN) Tumor Suppressor	Acin binding; Cell adhesion molecular binding	Regulation of cell shape; Regulation of cellular localisation; Organelle assembly; Regulation of protein localisation; Cell morphogenesis; Regulation of organelle organisation; Cell development; Positive regulation of transport; Regulation of vesicle-mediated transport; Positive regulation of cellular process; Regulation of cellular component biogenesis
ENSG00000149084	HSD17B12	Hydroxysteroid 17-Beta Dehydrogenase 12	Oxidoreductase activity	Biological function unclassified
ENSG00000105939	ZAP	Zinc finger CCCH-type antiviral protein 1	Molecular function unclassified	Biological function unclassified
ENSG00000174944	P2RY14	P2Y purinoceptor 14	G protein-couple receptor activity; Purine nucleotide binding	G protein-coupled receptor signalling pathway
ENSG00000120690	ELF1	ETS-related transcription factor Elf-1	RNA polymerase II transcription regulatory region sequence-specific DNA binding; DNA-binding transcription factor activity, RNA polymerase II-specific	Cell differentiation; Transcription by RNA polymerase II; Regulation of transcription by RNA polymerase II
ENSG00000100292	HMOX1		Monooxygenase activity; Heme binding	Cellular nitrogen compound catabolic process; Aromatic compound catabolic process; Iro ino homeostasis; Responser to oxidative stree; Organic cyclic compound catabolic process; Organomitrogen compound catabolic process; Heterocycle catabolic process; Heme metabolic process
ENSG00000138777	PPA2	Inorganic pyrophosphatase 2, mitochondrial	Pyrophosphatase activity	Phosphate-containing compound metabolic process
ENSG00000243056	EIF4EBP3	Eukaryotic translation initiation factor 4E-binding protein 3	Translation initiation factor binding	Regulation of translation initiation; Translational initiation; Negative regulation of translation; Translation elongation

(a)

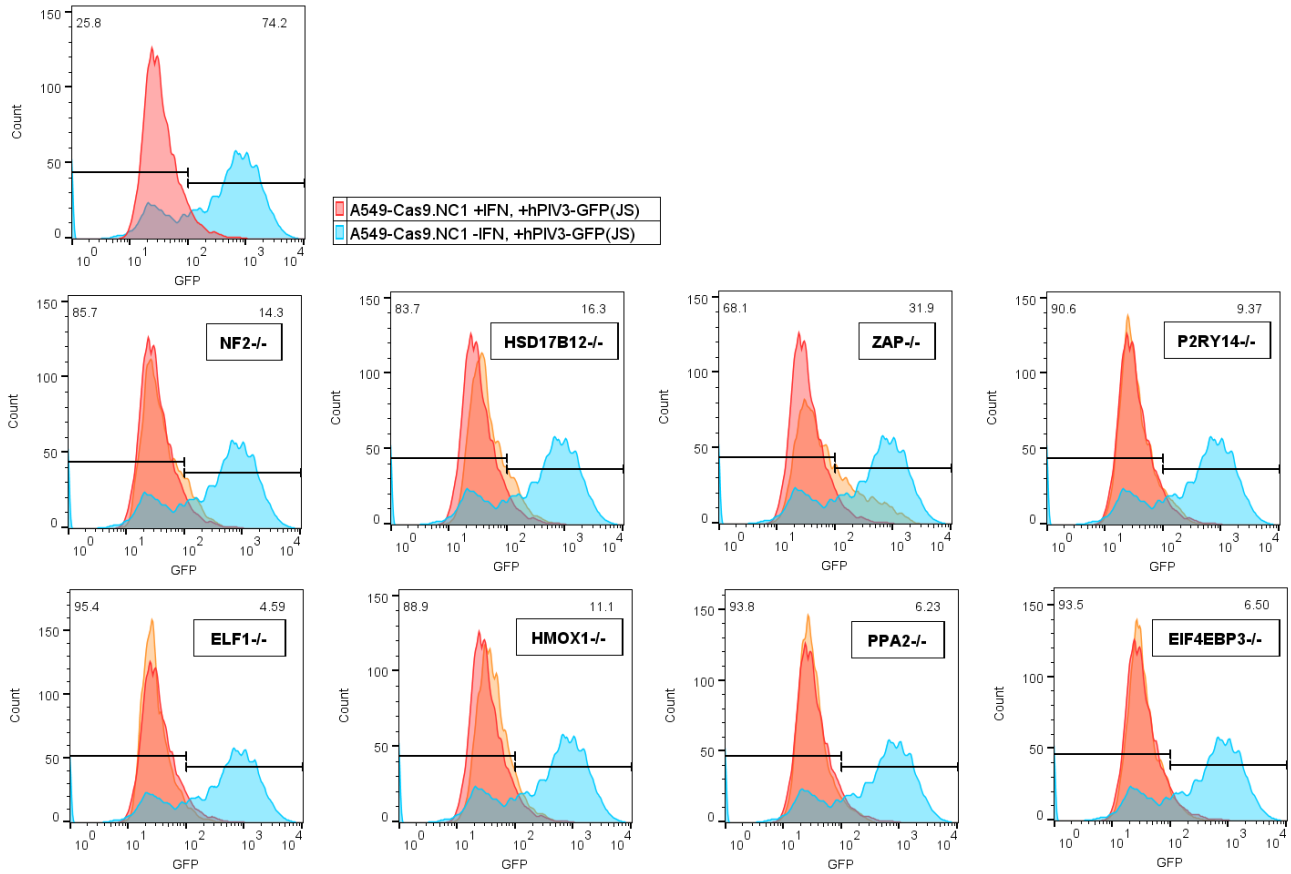
A549-Cas9.NC1 +IFN, +hPIV3-GFP(JS)
A549-Cas9.NC1 -IFN, +hPIV3-GFP(JS)
25.8
74.2
NF2-/-
85.7
14.3
HSD17B12-/-
83.7
16.3
ZAP-/-
68.1
31.9
P2RY14-/-
90.6
9.37
ELF1-/-
95.4
4.59
HMOX1-/-
88.9
11.1
PPA2-/-
93.8
6.23
EIF4EBP3-/-
93.5
6.50
Count
GFP

(b)

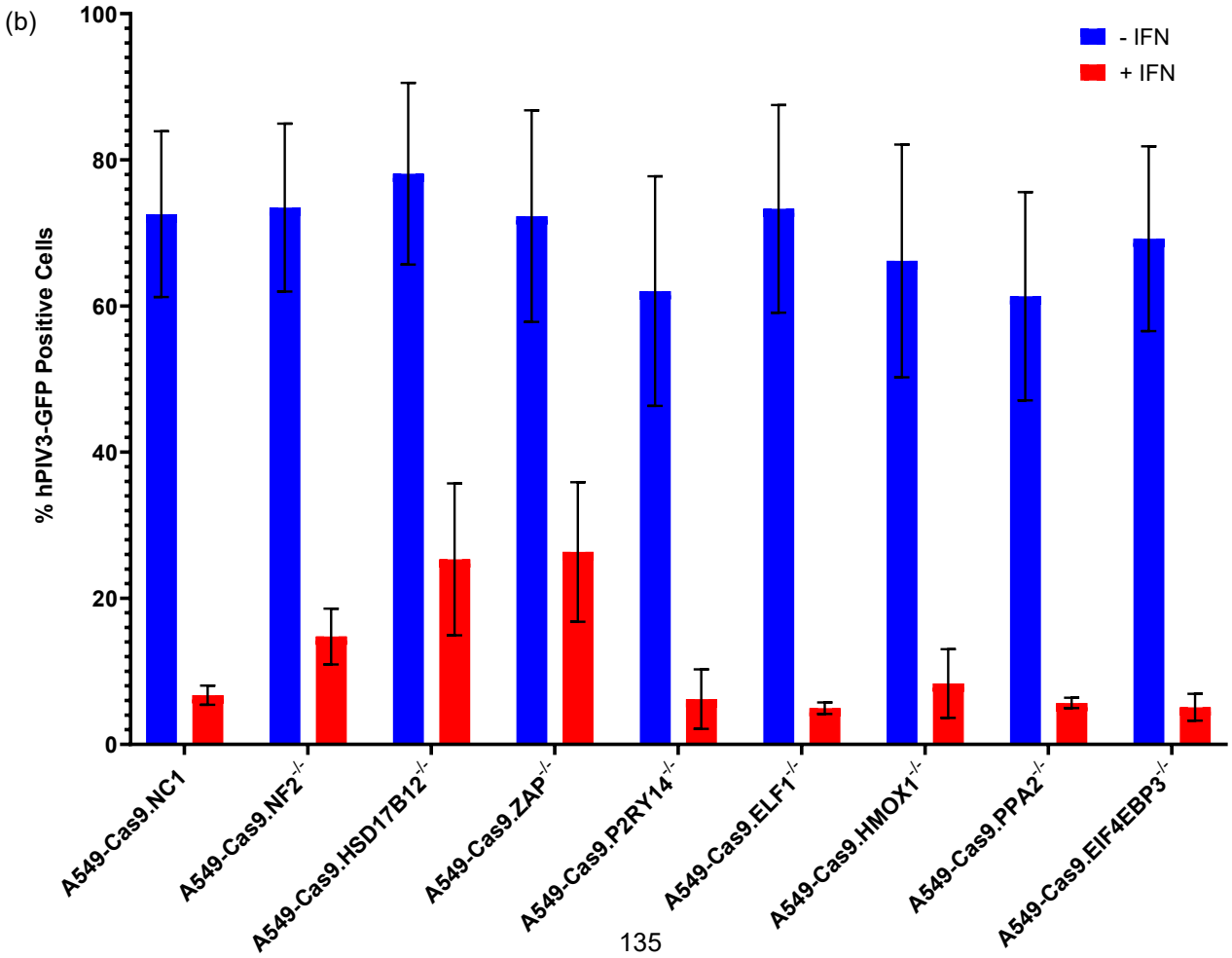
- IFN
+ IFN
% hPIV3-GFP Positive Cells
A549-Cas9.NC1
A549-Cas9.NF2-/-
A549-Cas9.HSD17B12-/-
A549-Cas9.ZAP-/-
A549-Cas9.P2RY14-/-
A549-Cas9.ELF1-/-
A549-Cas9.HMOX1-/-
A549-Cas9.PPA2-/-
A549-Cas9.EIF4EBP3-/-

Figure 5.3.3: Validation of hPIV3-GFP(JS) antiviral restriction factors. **(A)** CRISPR/Cas9 genome editing was used to knockout gene expression in A549-Cas9 cells of genes identified as hits to validate (Table 4.1); NF2, HSD17B12, ZAP, P2RY14, ELF1, HMOX1, PPA2, EIF4EBP3. Knockout cells were infected with hPIV3-GFP(JS) (MOI = 2.5) or mock infected following IFN-α pre-treatment for 24 h (1000 U). Cells were harvested at 18 h.p.i for flow cytometry analysis using blue laser (488 nm) for identification of GFP-positive cells. Data was analysed using FlowJo v10. A549-Cas9.NC1 cells were used as control with non-infected A549-Cas9.NC1 cells shown in red, A549-Cas9.NC1 cells infected with hPIV3-GFP(JS) shown in blue and specified knockout cell infected with hPIV3-GFP(JS) overlayed in orange. Data shown is one repeat, representative of three. **(B)** Data from (A) was quantified based on singlet cell gating and% hPIV3-GFP-positive Cells and plotted. Non-IFN treated shown in blue and IFN-α pre-treated shown in red. Error bars represent the SD of the mean from three biological repeats.

5.4 Development of CRISPR-Cas9 genome-wide screening to improve identification antiviral factors

Previous work has shown that the knockdown of IFIT1 in A549 naïve cells, using shRNA, results in the restoration of PIV5 infection (Young et al., 2016; Holthaus et al., 2020). We therefore aimed to recapitulate these results in IFIT1 knockout cells.

IFIT1 deficient A549-Cas9 and A549-ISG15$^{-/-}$.Cas9 cells were generated using CRISPR-Cas9 genome engineering and single cell cloned for robust gene knockout to generate A549-Cas9.IFIT1$^{-/-}$ and A549-ISG15$^{-/-}$.Cas9.IFIT1$^{-/-}$ cell lines. To assess for successful knockout, cells were treated with IFN-α, or left untreated, and IFIT1 expression levels were determined by immunoblotting (figure 5.4.1). Results show that the expression of IFIT1 was abolished in A549-Cas9.IFIT1$^{-/-}$ cells compared to A549-Cas9.NC1 cells but maintain expression of other ISGs including ISG15 and MxA. We also observed no IFIT1 expression in A549-ISG15$^{-/-}$.Cas9.IFIT1$^{-/-}$ compared to A549-ISG15$^{-/-}$Cas9. Importantly, we still saw increased expression of MxA in the A549-ISG15$^{-/-}$. Cas9.IFIT1$^{-/-}$ compared to the A549-Cas9.IFIT1$^{-/-}$ cells, indicating that the inability of ISG15 deficient cells to regulate to the IFN response is maintained upon IFIT1 knockout.

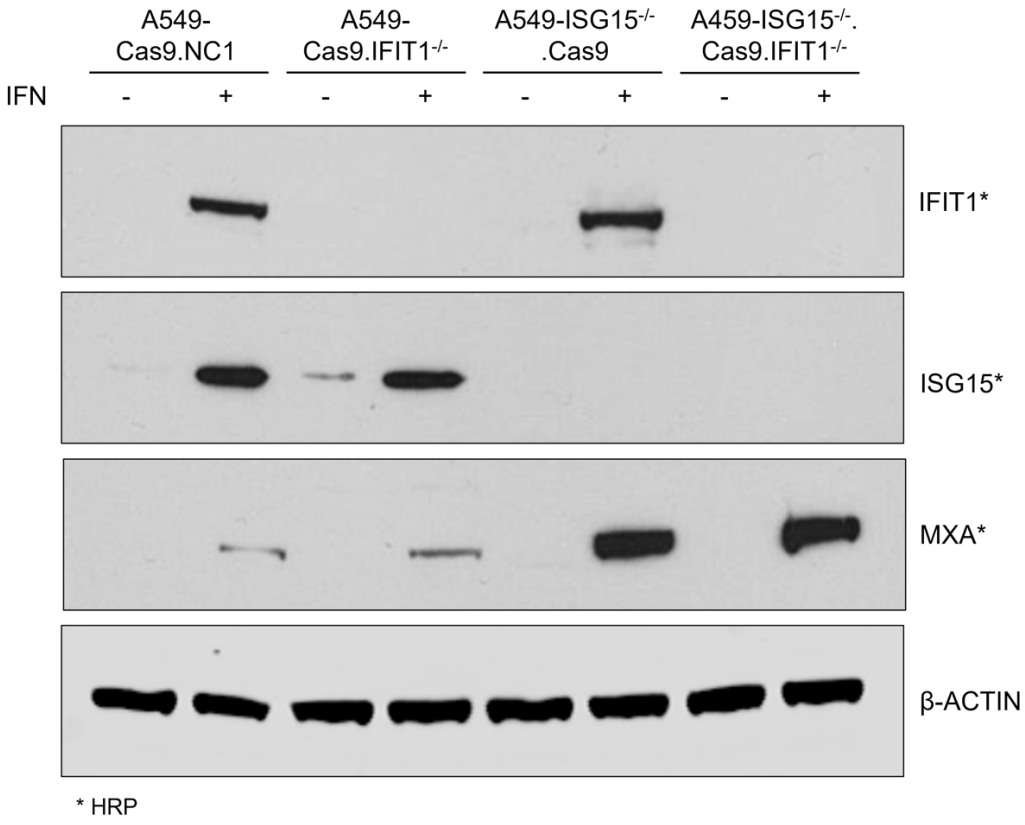

Figure 5.4.1: Functional characterisation of IFIT1-/- clonal cell lines. CRISPR/Cas9 genome editing was used to knockout IFIT1 expression in A549-Cas9 and A549-ISG15$^{-/-}$.Cas9 cells. Cells were either pre-treated for 24 h with 1000 U/mL IFN-α, or left untreated, and protein expression was tested by immunoblot using antibodies specific IFIT1, ISG15, MxA and β-Actin. Visualisation of IFIT1, ISG15, and MxA protein levels was accomplished using secondary antibodies conjugated to horseradish peroxidase (HRP), denoted by '*', whilst β-Actin visualisation was accomplished using IRDye secondary antibody. Control cells were A549-Cas9 and A549-ISG15$^{-/-}$.Cas9 cells.

Pre-treatment of A549-Cas9.NC1 cells with IFN-α 18 h prior to infection of rPIV5-mCherry(W3), resulted in a near complete loss in viral replication and protein synthesis as shown by reduced PIV5 NP levels at 24 h.p.i compared to non-IFN treated control. This result is further supported by the lack of mCherry positive cells in IFN-α treated A549-Cas9.NC1 cells compared to non-IFN treated cells in an independent infection (figure 5.4.2.a). At 48 h.p.i of A549-Cas9.NC1 cells, PIV5 replication begins to recover as shown by increased PIV5 NP levels and increased mCherry expression compared to 24 h.p.i. This is known to be due to the ability of PIV5 to overcome the IFN response through the V protein targeting STAT1 for proteasomal degradation (Didcock et al., 1999).

PIV5 NP immunoblot signal was quantified by normalising to non-IFN treated A549-Cas9.NC1 cells at 48 h.p.i. Results showed significant increase in NP expression in A549-Cas9.NC1 cells at 48 h.p.i compared to 24 h.p.i when IFN-α pre-treated – an increase of approximately 14-fold (figure 5.4.2.b). This corroborates the results seen by fluorescence microscopy indicating that PIV5 is able to begin

overcoming the IFN response at later time points post-infection. Additionally, A549-Cas9.IFIT1$^{-/-}$ cells show increased sensitivity to PIV5 infection, compared to A549-Cas9.NC1 cells, at both time points when both IFN-α pre-treated and untreated. This increased sensitivity to PIV5 infection is amplified in the presence of IFN-α pre-treatment with relative NP expression 26.5-fold higher in IFIT1 deficient cells at 24 h.p.i. This sensitivity to PIV5 infection reduces to a 2.5-fold difference at 48 h.p.i as PIV5 is more able to overcome the IFN response in A549-Cas9.NC1 cells compared to A549-Cas9.IFIT1$^{-/-}$ cells. Moreover, pre-treatment of A549-ISG15$^{-/-}$.Cas9 with IFN-α 18 h prior to infection results in increased viral resistance compared to non-IFN treated cells as shown by no PIV5 NP protein expression at 24 h.p.i or 48 h.p.i, therefore indicating PIV5 is not able to overcome the dysregulated IFN response in these cells at later timepoints, as in the case in A549-Cas9.NC1 cells (figure 5.4.2). This unregulated IFN response in ISG15 deficient cells results in an upregulation of all ISGs, including IFIT1 (Speer et al., 2016b; dos Santos and Mansur, 2017; Holthaus et al., 2020). Whilst IFN-α pre-treatment of A549-ISG15$^{-/-}$. Cas9.IFIT1$^{-/-}$ cells does not result in PIV5 NP expression equivalent to non-IFN treated cells, PIV5 NP expression is increased at both time points compared to A549-ISG15$^{-/-}$.Cas9 cells indicating increased viral susceptibility in the double knockout cells.

(a)

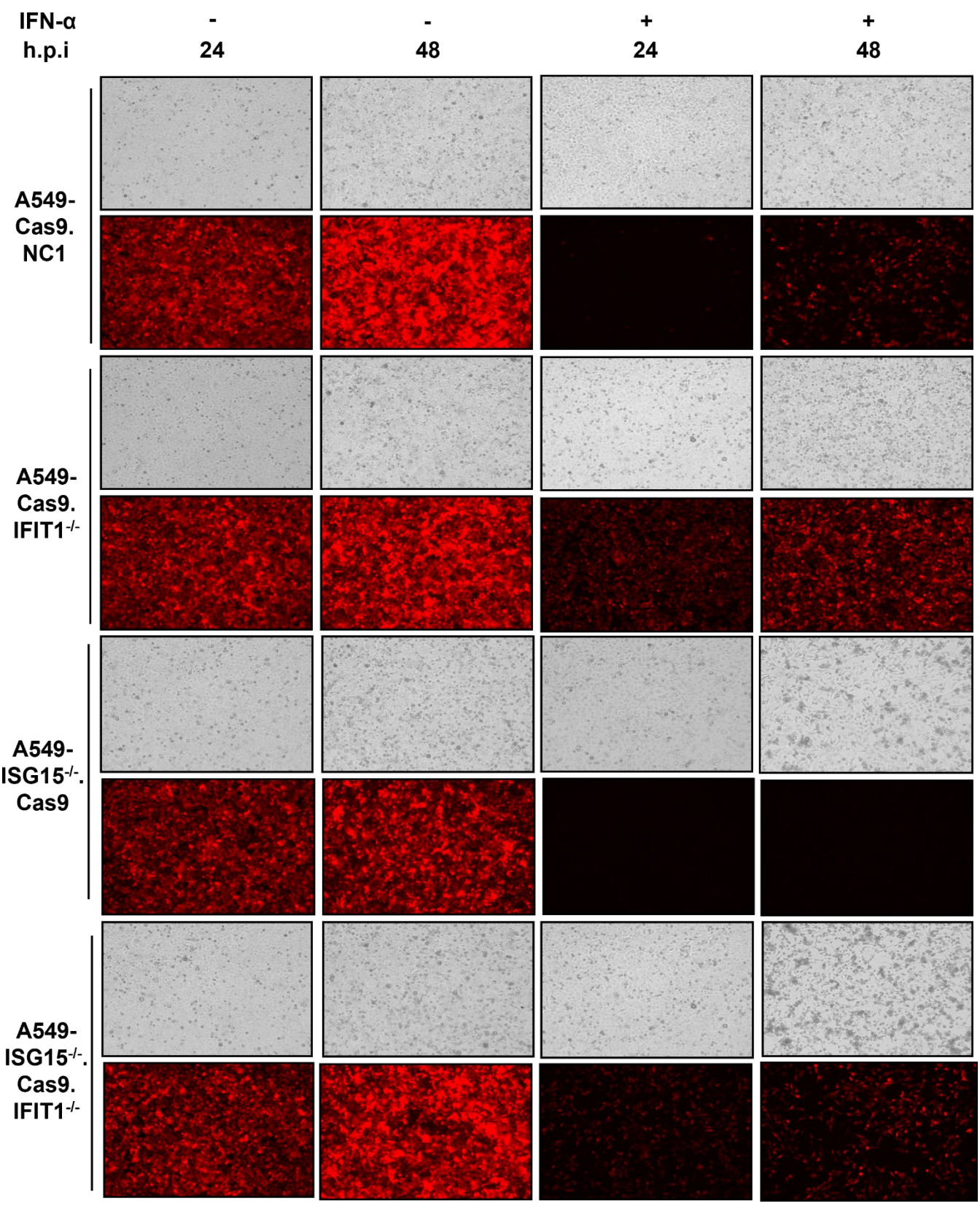
IFN-α
h.p.i
-
24
-
48
+
24
+
48
A549-Cas9.NC1
A549-Cas9.IFIT1-/-
A549-ISG15-/-.Cas9
A549-ISG15-/-.Cas9.IFIT1-/-

(b)

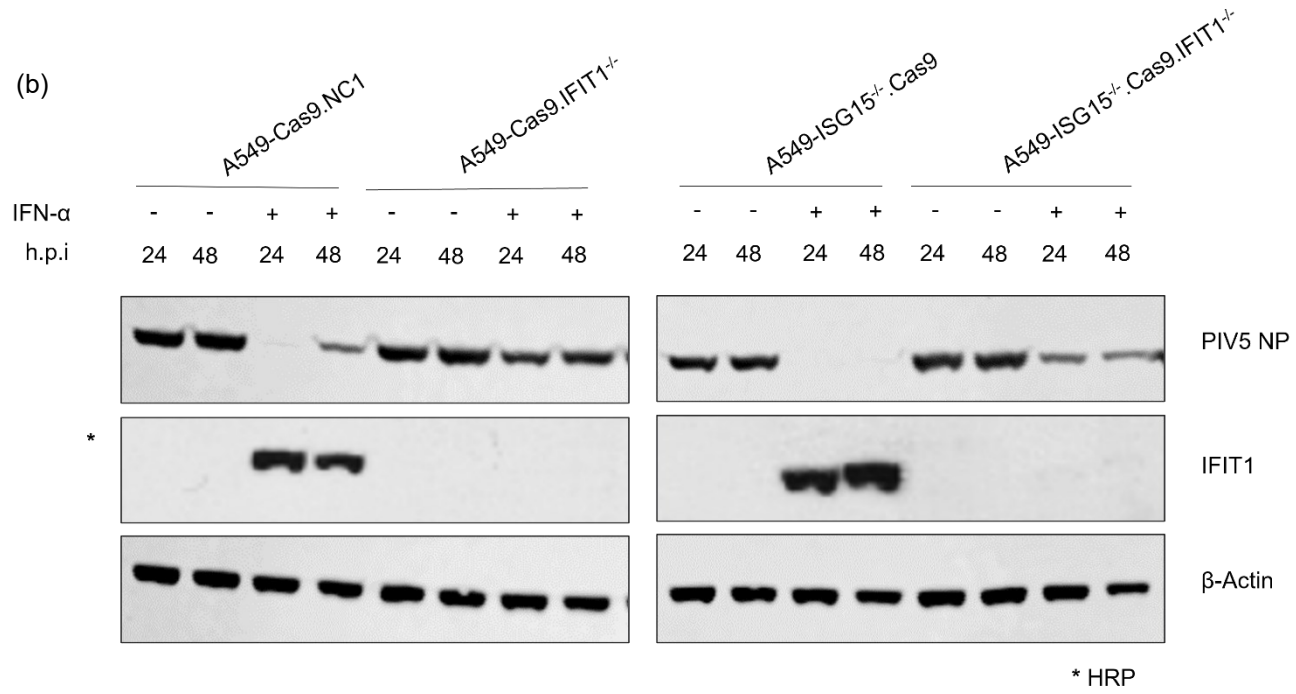
A549-Cas9.NC1
A549-Cas9.IFIT1-/-
A549-ISG15-/-.Cas9
A549-ISG15-/-.Cas9.IFIT1-/-
IFN-α
h.p.i
PIV5 NP
IFIT1
β-Actin
* HRP

(c)

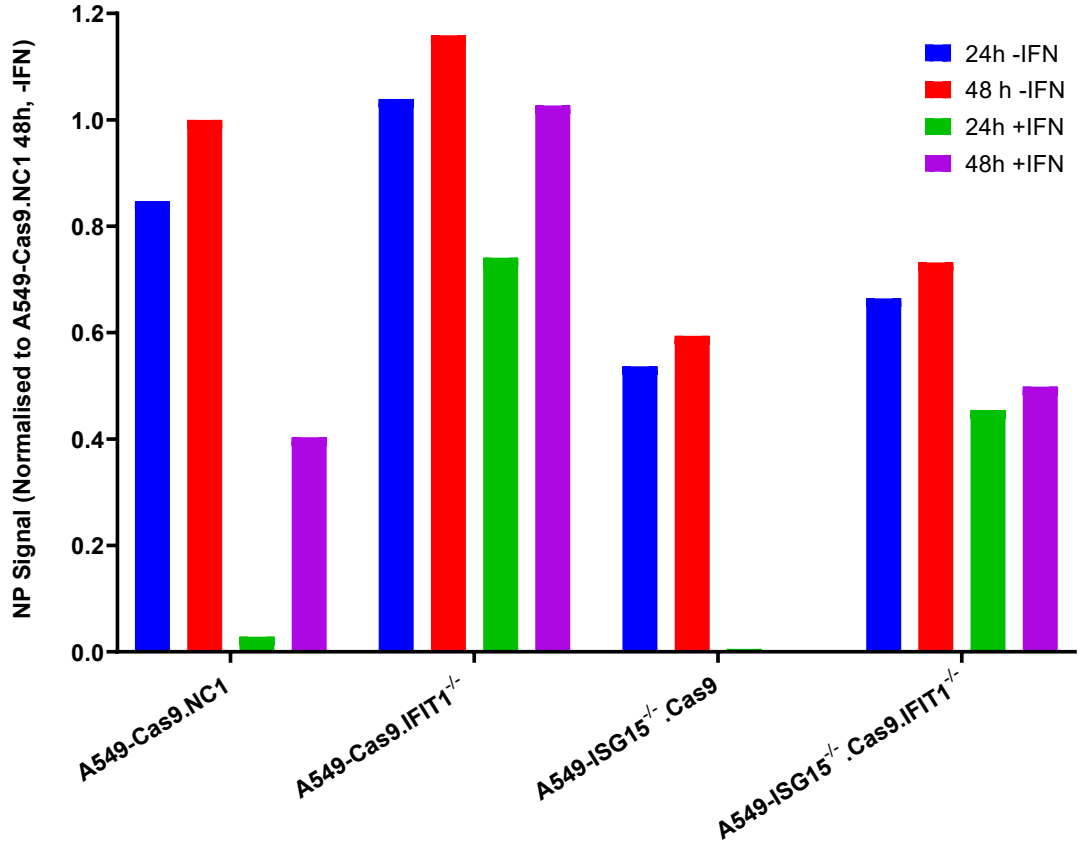
NP Signal (Normalised to A549-Cas9.NC1 48h, -IFN)
24h -IFN
48 h -IFN
24h +IFN
48h +IFN
A549-Cas9.NC1
A549-Cas9.IFIT1-/-
A549-ISG15-/-.Cas9
A549-ISG15-/-.Cas9.IFIT1-/-

Figure 5.4.2: ISG15-/- results in enhanced IFN-dependent virus restriction. **(A)** Control (A549-Cas9 and A549-ISG15$^{-/-}$.Cas9) cells and respective IFIT1 knockouts were treated for 18 h with IFN- α or left untreated and then infected with rPIV5-mCherry(W3) (MOI = 10). Cells were imaged at 24 and 48 h.p.i. using Texas Red filter for visualisation of mCherry virus. Images are representative of three independent experiments. **(B)** Cells were harvested at 24 and 48 h.p.i. and processed for immunoblot analysis using Abs specific for PIV5 NP, IFIT1 and β-actin. Images are representative of three independent experiments. **(C)** Experiments described in (B) were performed independently three times (infections were performed on three separate occasions), and NP and β-actin levels were quantified using Image Studio software. Signals were relative to those generated from IFN-α treated A549-Cas9.NC1 cells infected for 48 h. (set to 1).

Although IFIT1 is known as the primary restriction factor of PIV5, previous work had indicated there may be other moderately acting restriction factors also at play (Holthaus et al., 2020). To verify this, we took A549-Cas9.NC1 (CRISPR control cell line) and the clonal A549-Cas9.IFIT1$^{-/-}$ cell line and infected with PIV5-CPI^{-}, a strain of PIV5 unable to the degrade STAT1 (Didcock et al., 1999), in the absence or presence of Ruxolitinib (figure 5.4.3.a). Ruxolitinib is a JAK inhibitor so inhibits IFN signalling and therefore the expression of ISGs expressed from ISRE-containing promoters. In the presence of Ruxolitinib (and therefore the absence of ISG expression), viral plaques are significantly larger in IFIT1 knockout cells indicating other unidentified ISGs also restrict PIV5 replication (figure 5.4.3.b).

To further validate this finding, we subsequently performed a virus resistance assay in the presence and absence of IFN (figure 5.4.3.c). Cells were pre-treated with IFN-α for 18 h before being infected with rPIV5-mCherry(W3) at MOI = 10 and harvested for flow cytometry analysis at 24 and 48 h.p.i. Data confirms that ISG15$^{-/-}$ enhances IFN-dependent virus restriction as in the absence of ISG15, the% mCherry positive A549-Cas9.NC1 cells (infection) significantly reduces compared to IFN pre-treated A549-Cas9.NC1 control cells. We know this to be due to the aforementioned dysregulated IFN response and increased expression of ISGs in the ISG15$^{-/-}$ condition. Data also supports results from figure 5.4.3.b that suggests additional ISGs restrict PIV5 infection. In our single knockout cells, A549-Cas9.IFIT1$^{-/-}$, we observe no difference in the percentage of mCherry positive cells between the IFN pre-treated and non-treated conditions. However, in our double knockouts, deficient in both ISG15 and IFIT1, we observe a reduced percentage of mCherry positive cells in the IFN pre-treated condition at 48 h.p.i, correlating with a reduced number of infected cells. This suggests that in a ISG15 deficient background where there is enhanced expression of other ISGs, there may be other currently unidentified restriction factors. Additionally, we were able to show that the quantitative working window (as described in section 1.3.5) in which ISGs can be identified is enhanced when using ISG15$^{-/-}$ cells. Results show that the difference between IFN pre-treated and non-treated A549-Cas9.NC1 cells at 48 h.p.i is ~ 30% however, this window increases to nearly 100% in A549-ISG15$^{-/-}$.Cas9 cells. In practice, this means that if a restriction factor were to result in 40% mCherry positive cells, it would not be identified as a restriction factor if the experiment was performed using A549-Cas9.NC1 cells but would be identified if using A549-ISG15$^{-/-}$.Cas9 cells.

(a)

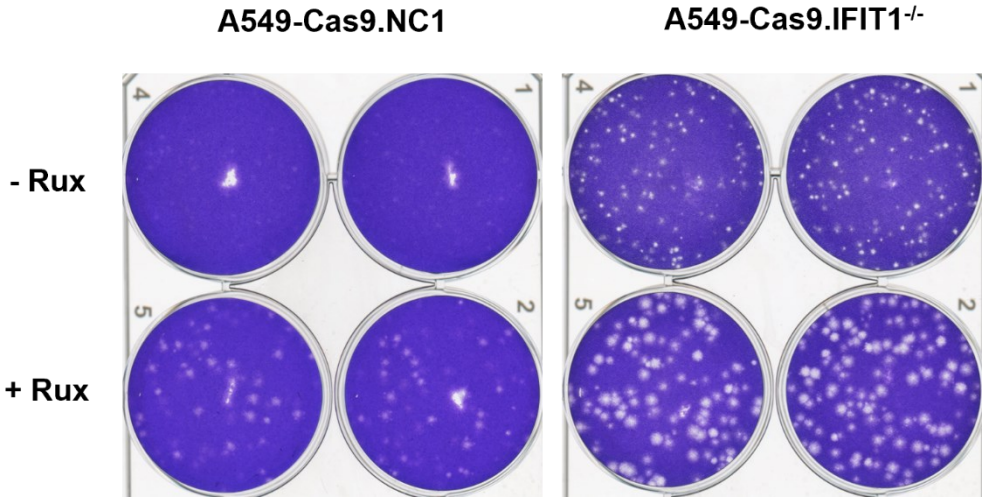
A549-Cas9.NC1
A549-Cas9.IFIT1-/-
- Rux
+ Rux
4
1
5
2

(b)

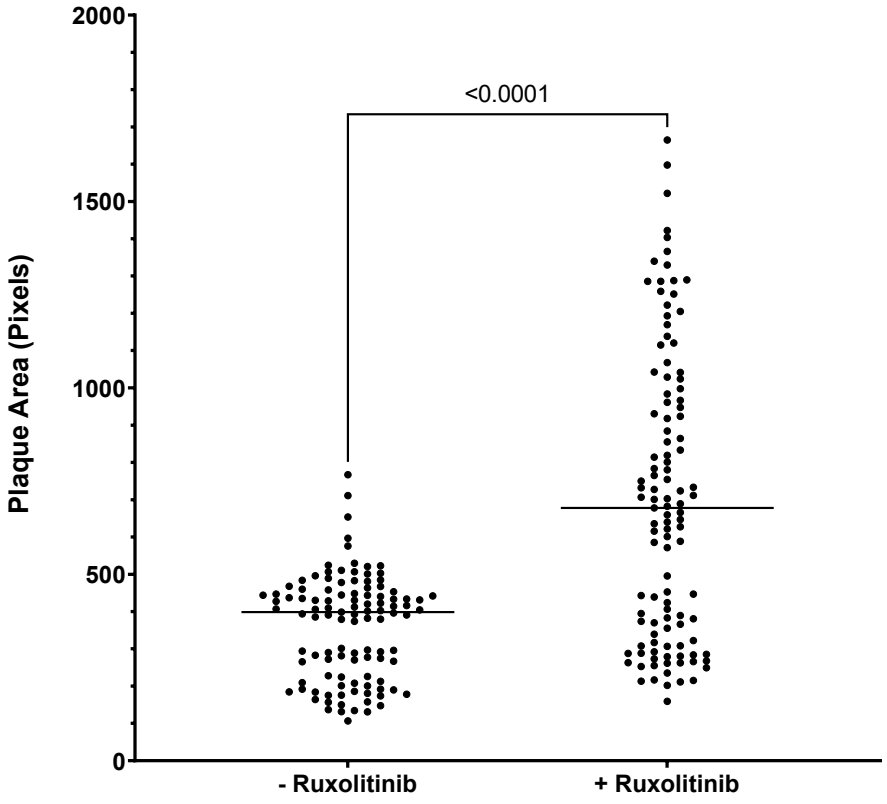
2000
1500
1000
500
0
Plaque Area (Pixels)
<0.0001
- Ruxolitinib
+ Ruxolitinib

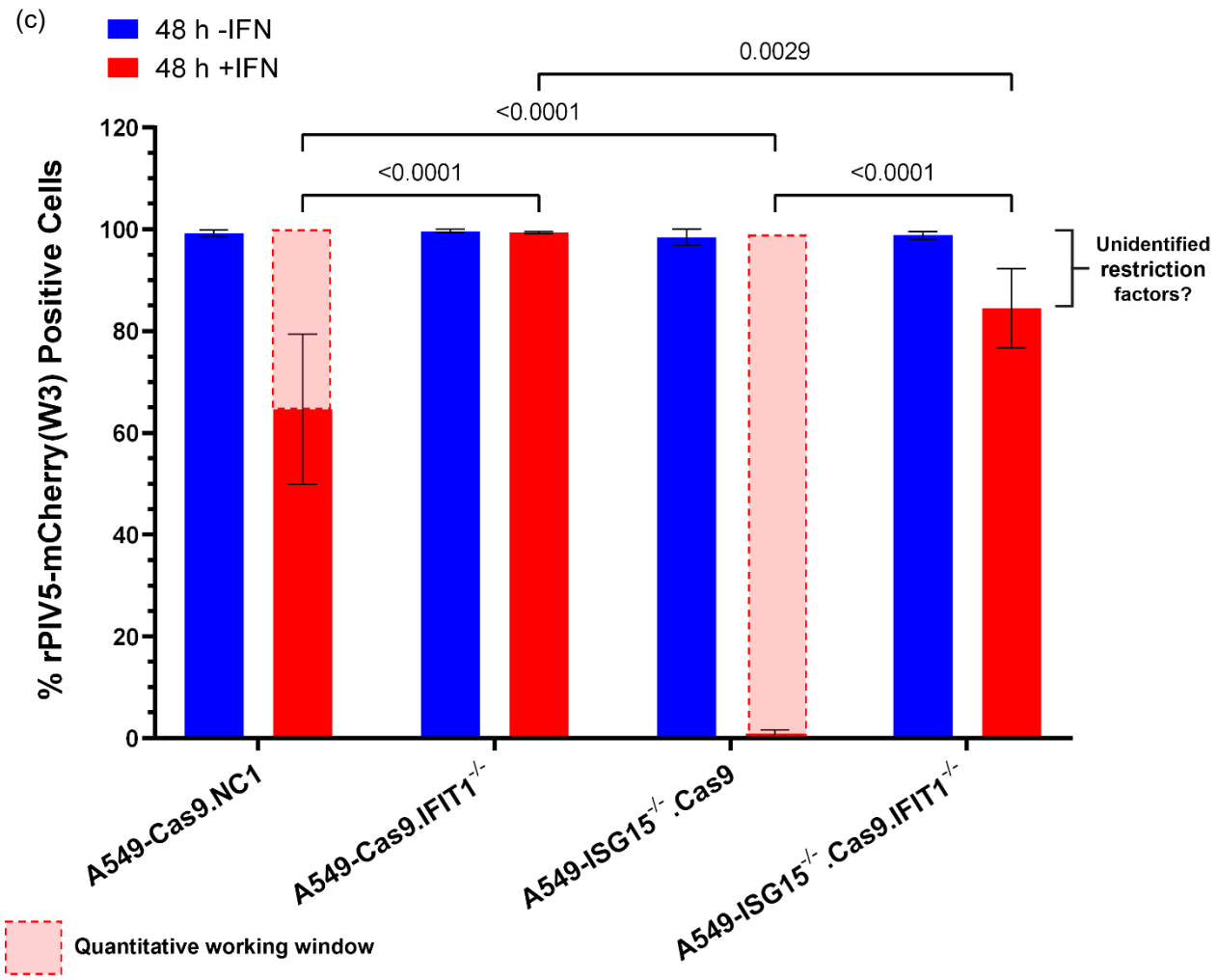

Figure 5.4.3: Multiple restriction factors are required to inhibit PIV5 replication. **(A)** Indicated cells lines were seeded in 10 µM**.** Ruxolitinib or left untreated. Cells were infected for 1 h with 20 - 30 PFU of PIV5 (CPI$^-$) with Ruxolitinib replaced onto cells upon addition of avicell overlay. Monolayers were fixed 6 d.p.i. and plaques were detected using 0.15% crystal violet staining for 30 min. Plaque assays were performed separately on three independent occasions. **(B)** Plaque size of three independent repeats of (A) was quantified using 20 randomly selected plaques of each condition. Statistical analysis completed using Welch's t-test. **(C)** Cells previously described (*4.1*) were either pre-treated for 18 h with IFN-α or left untreated and then infected with rPIV5-mCherry(W3) (MOI = 10). Cells were harvested at 48 h.p.i. for flow cytometry analysis using yellow/green laser (561 nm) for identification of mCherry positive cells. Data was quantified based on singlet cell gating and percentage rPIV5-mCherry(W3) positive cells plotted, IFN-α pre-treated (red) and IFN-α mock treated (blue). Error bars represent the SD of the mean from the three independent experiments. Statistics performed using two-way ANOVA; p-values denoted on graph.

To identify if our method of using ISG15 deficient cells to identify restriction factors would work in a biologically relevant environment, we performed the same virus resistance assay with both hPIV3(JS)

and hPIV3(Washington). The latter, as previously described, is a strain more similar to clinical isolates that have not undergone multiple passages and is subsequently more resistant to IFN (Stokes et al., 1992). Due to hPIV3(Washington) exhibiting increased resistance to IFN, the percentage of infected control cells (A549-Cas9.NC1) is increased compared to other viruses when pre-treated with IFN-α, such as hPIV3(JS), as the virus is able to overcome the IFN response and replicate. As such this makes the difference in percentage of infected cells between non-IFN treated and treated small, therefore making it more difficult to identify restriction factors. Previous work using shRNA knockdown of IFIT1 suggested hPIV3(Washington) was not restricted by the ISG (Holthaus et al., 2020). However, we wanted to see if we could identify IFIT1 as a restriction factor of hPIV3(Washington) using our ISG15$^{-/-}$ model by expanding the quantitative working window previously described (section 1.3.5).

The four cell lines previously described were pre-treated with IFN-α or left untreated prior to infection with either hPIV3 strain at MOI = 5. At 24 h.p.i, cells were harvested and stained with a cocktail of PIV3 HN antibodies followed by AlexaFluor-488 secondary antibody to allow for analysis by flow cytometry. As expected, the percentage of A549-Cas9.NC1 GFP-positive cells was similar between non-IFN treated and pre-treated upon infection with hPIV3(Washington), validating the strain is resistant to IFN. In A549-Cas9.NC1 cells this confined the working window range for identifying restriction factors to between 83.5% and 92.6% GFP-positive cells. When A549-Cas9.IFIT1$^{-/-}$ are pre-treated with IFN-α and infected with hPIV3(Washington) it results in 71.2% GFP-positive cells, therefore falling outside the window for identification, indicating IFIT1 is not a hPIV3(Washington) restriction factor. However, IFN pre-treatment of A549-ISG15$^{-/-}$.Cas9 cells reduced levels of hPIV3(Washington) infection by approximately 50% compared to A549-Cas9.NC1 cells. Subsequently, the observed working window range, between non-IFN treated and IFN pre-treated was between 74.8% to 33.1% GFP-positive cells. hPIV3(Washington) infection of double knockout cells, deficient in both ISG15 and IFIT1, pre-treated with IFN resulted in 55.7% GFP-positive cells. This value subsequently falls within the working window for A549-ISG15$^{-/-}$.Cas9 cells indicating that IFIT1 is a restriction factor against hPIV3(Washington), albeit a low to moderately acting one.

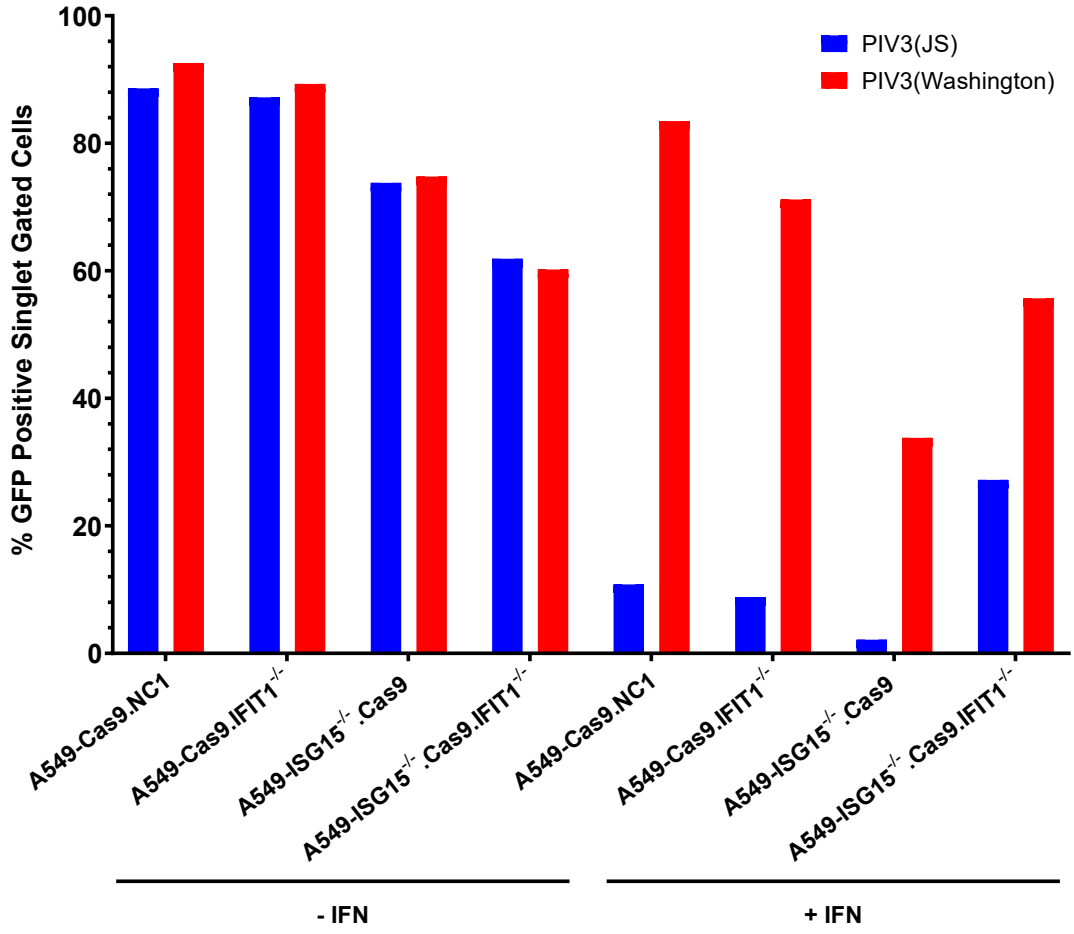

Figure 5.4.4: ISG15-/- cells enable identification of antiviral factors that restrict viruses more resistant to IFN. Cells previously described (*4.1*) were either pre-treated for 18 h with IFN-α or left untreated and then infected with either hPIV3(JS) (blue) or hPIV3(Washington) (red) (MOI = 5). Cells were harvested at 24 h.p.i. and stained with a cocktail of anti-PIV3 antibodies specific for hemagglutinin (HN) followed by Alexa-488. Cells were analysed using flow cytometry using blue laser (488 nm) for identification of Alexa-488 (PIV3) positive cells. Data was quantified based on singlet cell gating and percentage hPIV3 positive cells, either JS or Washington strain, plotted (n=1).

5.5 Summary

Following the optimisation of experimental conditions for infection, we performed a genome-wide CRISPR-Cas9 knockout screen for the identification of hPIV3-GFP(JS) antiviral restriction factors in A549-Cas9 library transduced cells. Following FACS and NGS analysis, 66 hits were identified to pass log-fold change and p-value thresholds as previously described, including 26 previously described ISGs.

We were also able to demonstrate that the use of ISG15 deficient cells enhances the quantitative working window for the identification of low to moderately acting ISGs using a model Paramyxovirus,

PIV5. Using ISG15 deficient cells as a tool we were also subsequently able to identify a restriction factor of hPIV3(Washington), IFIT1, that had previously been shown to not be a restriction factor against this IFN-resistant virus.

Chapter 6: Characterisation of Paramyxovirus antiviral restriction factors

6.1 Introduction

Genome wide CRISPR/Cas9 screening was performed to identify potential antiviral restriction factors of hPIV3 (section 5). Initial refinement of screening hits identified eight genes for further validation with three, NF2, HSD17B12 and ZAP (table 5.3.1), showing restriction of hPIV3-GFP(JS) infection (section 5.3). As such, these three genes were further investigated and characterised in order to (i) assess if they are inducible genes, (ii) evaluate their role in regulating the IFN response, and (iii) investigate their ability to restrict replication of other viruses.

6.2 Characterisation of AF hits as restriction factors of hPIV3-GFP(JS)

Characterisation of NF2, HSD17B12 and ZAP knockout cells were performed in parallel, and as such the controls used during experimentation were the same. For the purposes of this thesis, genes of interest have been separated for clarity, but control data is mirrored across figures throughout this chapter.

6.2.1 Functional characterisation of antiviral restriction factor deficient cell lines

NF2, HSD17B12 and ZAP deficient A549-Cas9 cells were generated using CRISPR-Cas9 genome engineering through the introduction of two independent sgRNAs, targeting separate parts of the gene, to generate A549-Cas9.NF2$^{-/-}$, A549-Cas9.HSD17B12$^{-/-}$, and A549-Cas9.ZAP$^{-/-}$ cell lines as previously described in section 5.3. Two independent sgRNAs were used to negate the need for single cell cloning and to improve the robustness of the gene knockout in our cells. Prior to further characterisation we wanted to assess for successful knockout of our genes of interest in order to have confidence that resulting phenotypes were as a result of gene deficiency. Cells were treated with Sendai virus strain Cantell, a preparation rich in defective interfering particles (DIs), or left untreated, and the relevant protein expression levels were determined through immunoblotting (figure 6.2.1.1). DIs are potent activators of the IFN response, acting as PAMPs, resulting in the expression of IFN and subsequently resulting in the robust expression of ISGs (Genoyer and López, 2019). As genes were identified as antiviral factors, but not yet characterised as ISGs, this allowed us to identify if proteins were induced as a result of the IFN response or constitutively expressed. Results show that the expression of NF2 and ZAP is abolished in A549-Cas9.NF2$^{-/-}$ and A549-Cas9.ZAP$^{-/-}$ cells compared to the A549-Cas9.NC1 control respectively (figure 6.2.1.1). Additionally, immunoblotting shows that both NF2 and ZAP are both constitutively expressed in the absence of DI treatment as shown by the presence of a protein band at 70 kDa and 101 kDa respectively. The expression of short-form ZAP (ZAP-S), shown by a band at 78 kDa, increases upon IFN induction by DI treatment, correlating with the phenotype previously observed in the literature (Li et al., 2019a). However, because of a lack of suitable antibody, we were unable to observe HSD17B12 protein expression in either cell line, including A549-Cas9.NC1 cells, in order to confirm gene knockout. Nevertheless, we were confident that HSD17B12 had been successfully knocked out in our cells, despite not being able to characterise with immunoblotting, as morphological and phenotypic differences were observed in these cells compared to the control. Cells, when viewed under a light microscope, appeared more fibril than naïve A549 cells and showed

increased cell death and slow proliferation; characteristics previously described within the literature (Nagasaki et al., 2009; Heikelä et al., 2020).

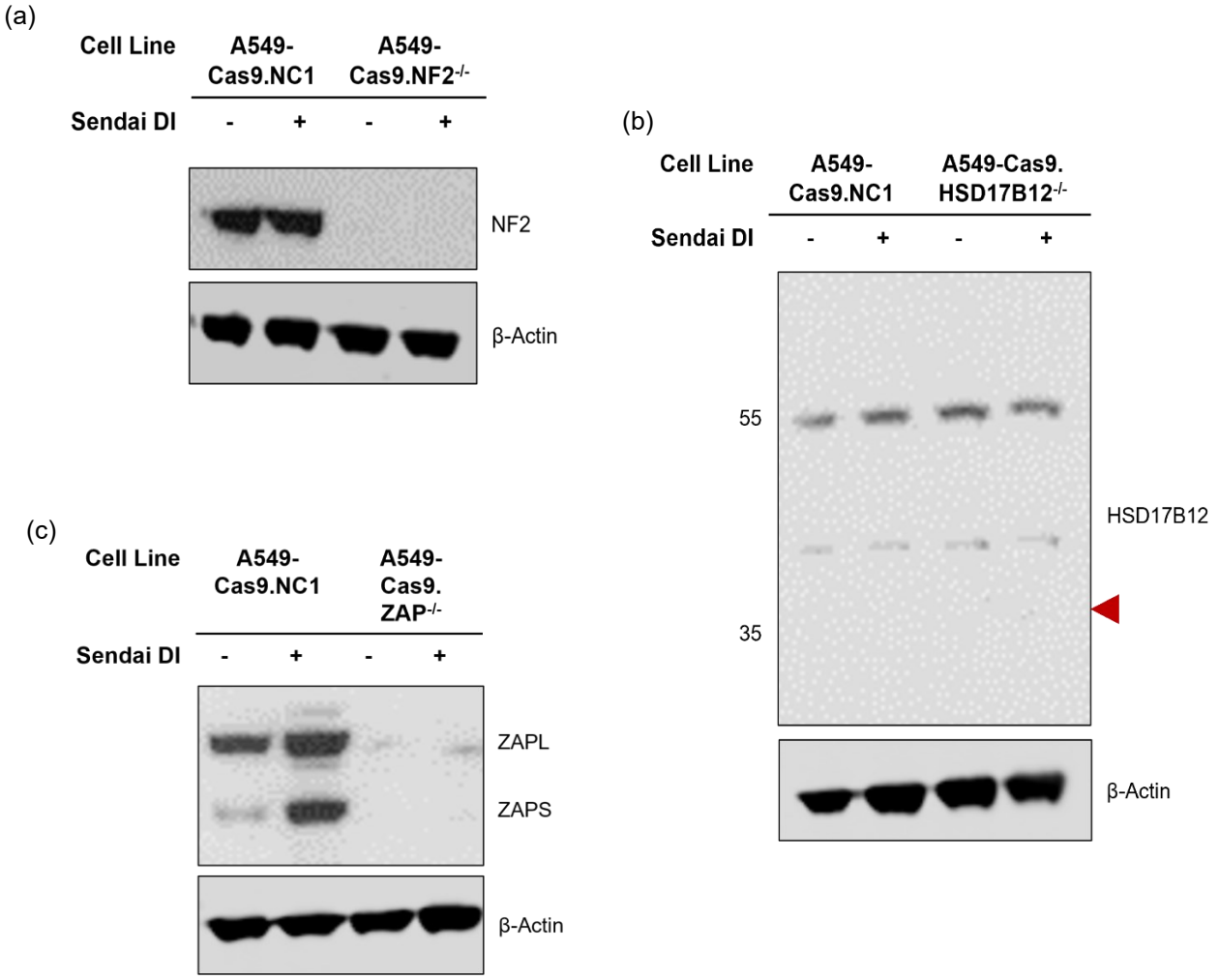

Figure 6.2.1.1: Functional characterisation of antiviral factor deficient cell lines. CRISPR/Cas9 genome editing was used to knockout NF2, HSD17B12 and ZAP expression in A549-Cas9 cells. A549-Cas9.NC1 control cells and knockout cell lines were either pre-treated for 24 h with SeV Cantell DIs or left untreated, and protein expression was tested by immunoblot using antibodies specific for **(A)** NF2, **(B)** HSD17B12 (expected HSD17B12 band denoted by red arrow), **(C)** ZAP (ZAPL and ZAPS isoforms indicated) alongside β-Actin. Visualisation of NF2, HSD17B12 and ZAP protein levels was accomplished using secondary antibodies conjugated to horseradish peroxidase (HRP), whilst β-Actin visualisation was accomplished using IRDye secondary antibody. Control cells were A549-Cas9.NC1 cells.

6.2.2 Low MOI validation of hPIV3-GFP(JS) antiviral restriction factors

Following validation of the genes as antiviral restriction factors at MOI = 2.5 (section 5.3), we wanted to identify if the genes were capable of restricting a low MOI virus infection. A549-Cas9.NC1 cells and knockout cells were infected for 1 h with 20 - 30 PFU of hPIV3-GFP(JS) prior to the addition of an avicell overlay for viral plaque analysis. Due to the aforementioned difficulties of culturing A549-Cas9.HSD17B12$^{-/-}$ cells, only NF2 and ZAP deficient cells could be analysed. Viral plaques were analysed based on three parameters to quantify viral replication: plaque number, area of plaque (pixels), and plaque intensity (a.u.).

For all three parameters, A549-Cas9.NF2$^{-/-}$ cells showed non-significant differences compared to A549-Cas9.NC1 cells whilst A549-Cas9.ZAP$^{-/-}$ cells only showed a significant increase in plaque number, increasing from a mean plaque number of 24.5 plaques in the control cells to 42.5 in the ZAP deficient cells. In order to conduct plaque area and intensity analysis, data on individual plaques were randomised and the number of plaques in the least populated condition was used across all cell lines. This ensured statistical analysis was performed on the same number of plaques across conditions. As such plaque area and intensity calculations were performed on only 16 plaques. Additionally, whilst two technical repeats were performed of all conditions, biological repeats were not performed. This small sample number, and lack of biological repeats may account for the large standard deviations observed and may be responsible for the non-significant results; especially as we have observed restriction of hPIV3-GFP(JS) in these cell lines at a higher MOI (section 5.3).

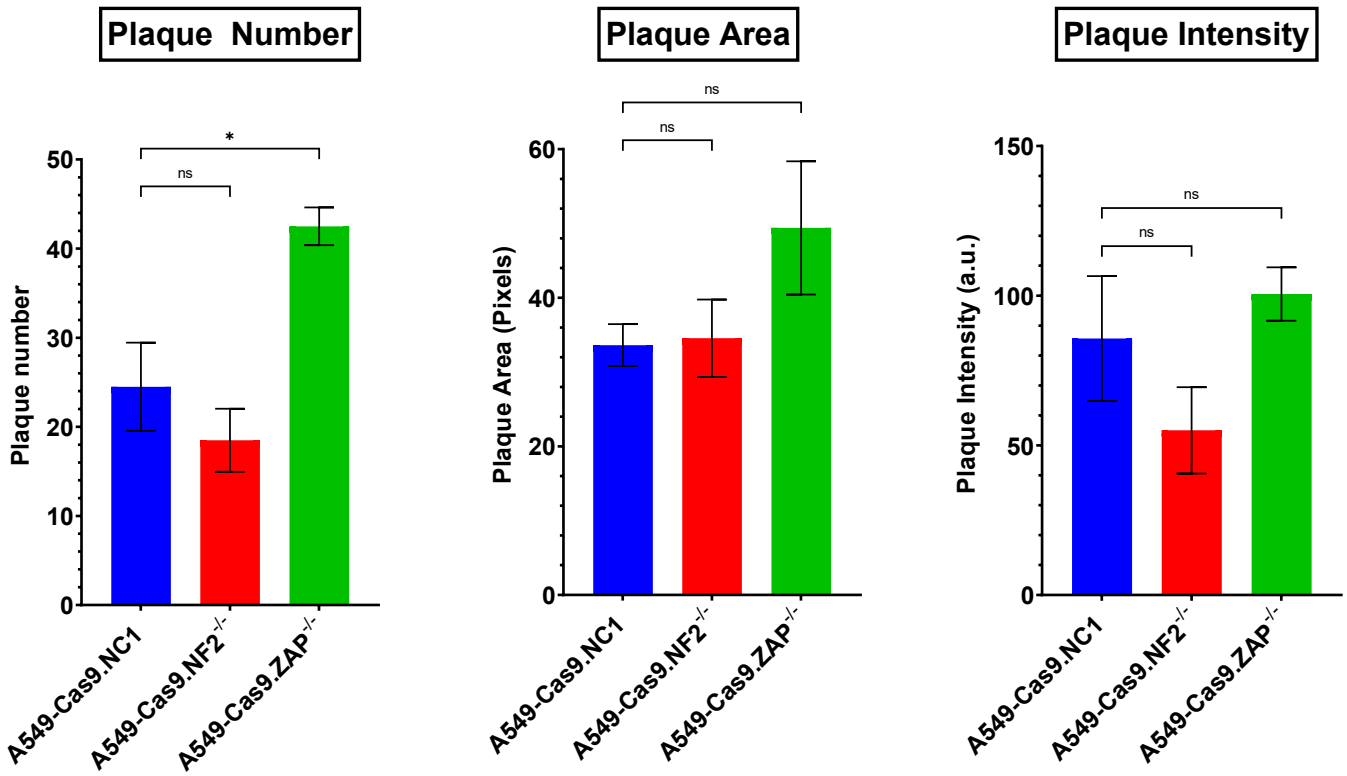

Figure 6.2.2.1: Antiviral restriction factors are able to restrict virus replication at low multiplicity of infection. A549-Cas9.NC1, A549-Cas9.NF2$^{-/-}$ and A549-Cas9.ZAP$^{-/-}$ cells were infected for 1 h with 20 - 30 PFU of hPIV3-GFP(JS) prior to the addition of an avicell overlay. Monolayers were fixed 6 d.p.i. and plaques were detected using Phosphor Imaging, Cy2 for identification of GFP-positive cells. Plaque size of three technical repeats of were quantified using 16 randomly selected plaques of each condition (n = 16). Statistical analysis performed using students t-test; *, p = 0.01 to 0.05, ns, p ≥ 0.05.

6.3 Moesin-Ezrin-Radixin Like (MERLIN) Tumour Suppressor (NF2)

6.3.1 PIV3 NP expression following infection of NF2 deficient cells

To further characterise hPIV3-GFP(JS) infection in NF2 deficient cells, we investigated the effect of NF2 on the transcription kinetics in viral replication by performing a time course analysis. A549-Cas9.NC1 and A549-Cas9.NF2$^{-/-}$ cells were pre-treated with IFN-α prior to infection with hPIV3-GFP(JS) at MOI = 10. Following a 1 h inoculation with the virus, the virus was removed, cells were washed, and the media was replaced with non-virus containing media. By removing the virus containing media after 1 h, we are able to observe replication of a single round of infection and attribute any increase in viral mRNA expression to replication rather than secondary infection. Viral replication was monitored over time by harvesting samples at 1, 6, 12, 18, 24 h.p.i and analysing mRNA expression of a viral transcript, *hPIV3 NP*, using RT-qPCR (figure 6.3.1.1). Analysis of hPIV3 NP transcription showed that both A549-Cas9.NC1 and A549-Cas9.NF2$^{-/-}$ cells were infected, and that viral transcription increased over time. Importantly, the levels of *hPIV3 NP* mRNA expression at 1 h.p.i was equivalent in both cell lines, a time point that likely represents primary infection (figure 6.3.1.1, inset). However, we observed that the rate of *hPIV3 NP* transcription over time was muted in the A549-Cas9.NC1 cells compared to those deficient in NF2. The fold-change of *hPIV3 NP* mRNA expression between the two cell lines increased from 1.3 -fold at 12 h.p.i to 1.9-fold at 24 h.p.i. This indicates that the expression of NF2 is able to reduce viral transcription. It should be noted that throughout this chapter, all RT-qPCR and flow cytometry figures are a representative of two or more biological repeats (as denoted in figures legends) however, variation between biological repeats was such that standard deviations were very high. Despite variation between repeats, the observed phenotype and patterns remained consistent convincing us that the results observed are reliable (additional data from biological repeats within appendix).

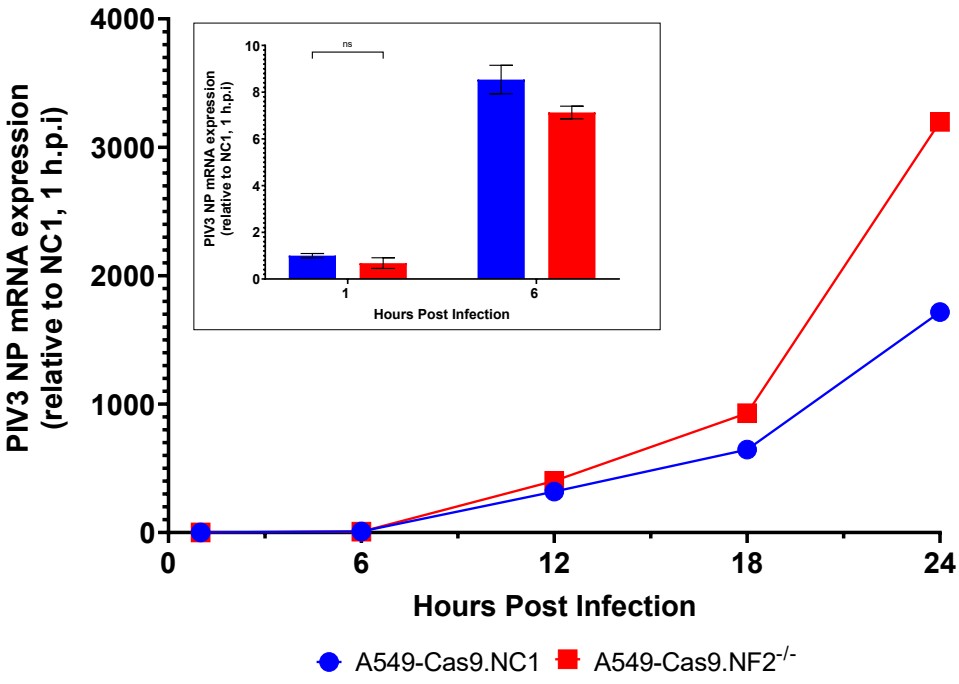

Figure 6.3.1.1: hPIV3(JS) NP expression is increased in NF2 deficient cells over time. A549-Cas9.NC1 control cells and A549-Cas9.NF2$^{-/-}$ cells were infected with hPIV3-GFP(JS) (MOI = 10) for 1 h following IFN-α pre-treatment for 8 h (1000 U). Following 1 h absorption, cells were washed and non-virus containing media added. Cells were harvested at 1, 6, 12, 18 and 24 h.p.i. Expression of viral mRNA was tested using reverse transcription quantitative PCR (RT-qPCR) with primers specific for *PIV3 NP*. Relative expression (compared to 1 h.p.i) was determined following SYBR Green quantitative PCR (RT-qPCR) using ΔΔCt method. *β-Actin* expression was used to normalise between samples. Inset shows 1 and 6 h.p.i with error bars representing the SD of the mean from three independent RNA samples. Data shown is a representation of one of three biological repeats, additional data from biological repeats see appendix 2. Statistics performed using two-way ANOVA; ns, no statistical significance.

6.3.2 Virus resistance in NF2 deficient cells following IFN-α pre-treatment

As the screen was performed in IFN-α pre-treated cells, we wanted to investigate the effect of IFN-α on permissiveness to hPIV3-GFP(JS) infection in A549-Cas9.NF2$^{-/-}$ cells compared to A549-Cas9.NC1 control cells. Both cell lines were treated with IFN-α for 24, 16 or 8 h prior to being infected with hPIV3-GFP(JS) (MOI = 10) for 30 h. hPIV3-GFP(JS) infection was then analysed following different lengths of IFN-α pre-treatment using flow cytometry and looking at mean fluorescence intensity of cells as a measure of infectivity. We observed that virus replication, as indicated by MFI, was equivalent in A549-Cas9.NC1 cells regardless of the time cells had been pre-treated with IFN-α, indicating that longer incubation with IFN-α does not provide more resistance to virus infection. However, in A549-Cas9.NF2$^{-/-}$ cells, at all IFN timepoints, NF2 deficient cells are more permissive to infection, shown by an increased

MFI, compared to NC1 control cells, at all timepoints. This suggests that NF2 is required for full IFN restriction of hPIV3. Additionally, an increase in IFN-α pre-treatment length resulted in reduced virus replication; the MFI in NF2 deficient cells reduced from 206.7 at 8 h IFN-α pre-treatment to 126.8 at 24 h. This shows that cell permissiveness to infection progressively reduced with longer times of IFN-α pre-treatment and that any advantage to hPIV3-GFP(JS) replication has as a result of NF2 knockout is reduced when cells have been IFN-α pre-treated for longer time periods. This potentially suggests that either; NF2 acts at early stages of infection within the IFN response or, the effect of later expressed ISGs is able to overcome the advantage NF2 deficiency provides at later timepoints.

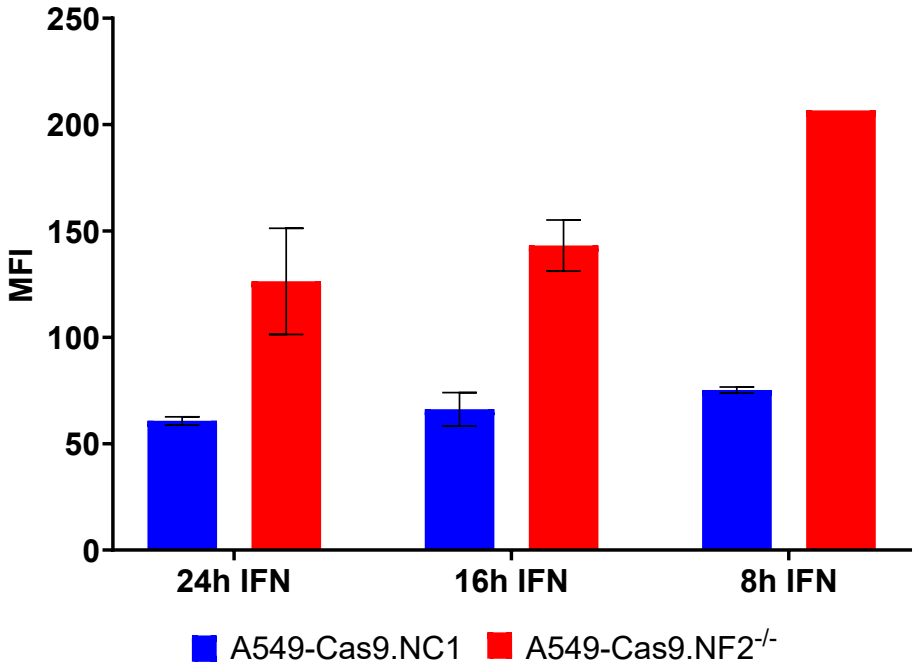

Figure 6.3.2.1: Permissiveness of A549-Cas9.NF2$^{-/-}$ cells to hPIV3(JS) infection reduces with longer IFN-α pre-treatment. A549-Cas9.NC1 control cells and A549-Cas9.NF2$^{-/-}$ cells were treated with IFN-α (1000 U) for 24, 16 or 8 h prior to being infected with hPIV3-GFP(JS) (MOI = 10) for 30 h. Cells were harvested at 30 h.p.i for flow cytometry analysis using blue laser (488 nm) for identification of GFP-positive cells. Data was analysed using FlowJo v10. A549-Cas9.NC1 cells were used as control, shown in blue, with A549-Cas9.NF2$^{-/-}$ cells shown in red. Error bars represent the SD of the mean from two biological repeats, each with three technical replicates.

6.3.3 Induction and regulation of type I IFN induction in NF2 deficient cells

We wanted to investigate whether NF2 is expressed as a result of IFN induction, the half of the IFN response responsible for IFN expression via IRF3 activation, as it has not previously been described as an ISG yet appeared in our IFN-α pre-treated screen. As such, A549-Cas9.NC1 cells were treated with DIs in the presence of Ruxolitinib (Rux). The defective interfering particles acted as PAMPs to initiate the induction cascade (described in section 1.2.2), whilst Rux, a JAK inhibitor, was used to

prevent downstream IFN signalling, and ISG expression from ISRE containing promoters, and ensure any changes in gene expression were solely the result of IFN induction. Gene expression of genes known to be expressed via *IRF3*, *IFN-β* and *ISG15*, and genes known to be expressed via ISRE-containing promoters, *MxA* and *HERC5*, alongside *NF2* were then analysed using RT-qPCR in the presence and absence of DI treatment (figure 6.3.3.1.a). Control genes, *ISG15* and *IFN-β*, showed significant increase in mRNA expression in DI treated compared to mock-treated cells as expected. Interestingly, we also observed a small, but significant, increase in both *MxA* and *HERC5* gene expression in DI treated cells. These data corroborate earlier analyses due to inefficient Rux treatment, however the changes in gene expression were reduced compared to *ISG15* and *IFN-β* so this was deemed acceptable. Also, upon analysing *NF2* expression in A549-Cas9.NC1 cells, no significant difference was observed between DI and mock-treated cells (figure 6.3.3.1.a, insert), with the levels of mRNA expression being extremely low. The indicates that NF2 is not expressed as a result of IFN induction. Potentially not surprising based on the data from figure 6.2.1.1.a, showing constitutive expression of NF2 in non-DI treated A549-Cas9.NC1 cells.

We investigated if NF2 played a role in the regulation of IFN induction (figure 6.3.3.1.b). To such effect, A549-Cas9.NC1 and A549-Cas9.NF2$^{-/-}$ cells were treated with DIs, in the presence of Rux, for 6 h, 24 h or left untreated. The mRNA expression of the above-mentioned IRF3 inducible genes, *IFN-β* and *ISG15*, were analysed using RT-qPCR in control and NF2 deficient cells to compare expression levels. Expression of both genes were reduced in A549-Cas9.NF2$^{-/-}$ cells compared to control A549-Cas9.NC1 cells indicating that the presence of NF2 increases the transcription of genes transcribed as a result of IFN induction. Analysis of *IFN-β* expression showed a mRNA reduction of 6.6-fold in A549-Cas9.NF2$^{-/-}$ cells compared to A549-Cas9.NC1 cells at 6 h post-DI treatment. Whilst *IFN-β* expression declined at 24 h post-treatment, a result of rapid IFN-β mRNA turnover in cells which is well described in the literature (Whittemore and Maniatis, 1990; Peppel and Baglioni, 1991), NF2 deficient cells continued to show a 9.6-fold reduction in *IFN-β* expression compared to control cells at this time point, indicating the effect of NF2 deficiency on *IFN-β* expression is maintained over time. Conversely, whilst *ISG15* expression increases over time in both cell lines, the effect of NF2 deficiency on the expression of *ISG15* increases over time, as with *IFN-β* expression. At both timepoints, *ISG15* mRNA expression is decreased in A549-Cas9.NF2$^{-/-}$ cells compared to A549-Cas9.NC1 cells but the fold change in expression increases with prolonged DI treatment from a 1.65-fold decrease in NF2 deficient cells at 6 h post-treatment to a 3-fold decrease at 24 h post-treatment. Unlike *IFN-β*, *ISG15* mRNA is less rapidly turned over suggesting that a lack of NF2 expression has a prolonged effect in reducing expression of genes as a result of IFN induction, either via the IRF3 or NF-κB pathways. Together these results show that whilst NF2 is not expressed as a result of IFN induction, it does appear to play a role in the regulation of the PAMP sensing response and the expression of other ISGs expressed from the IFN promoter.

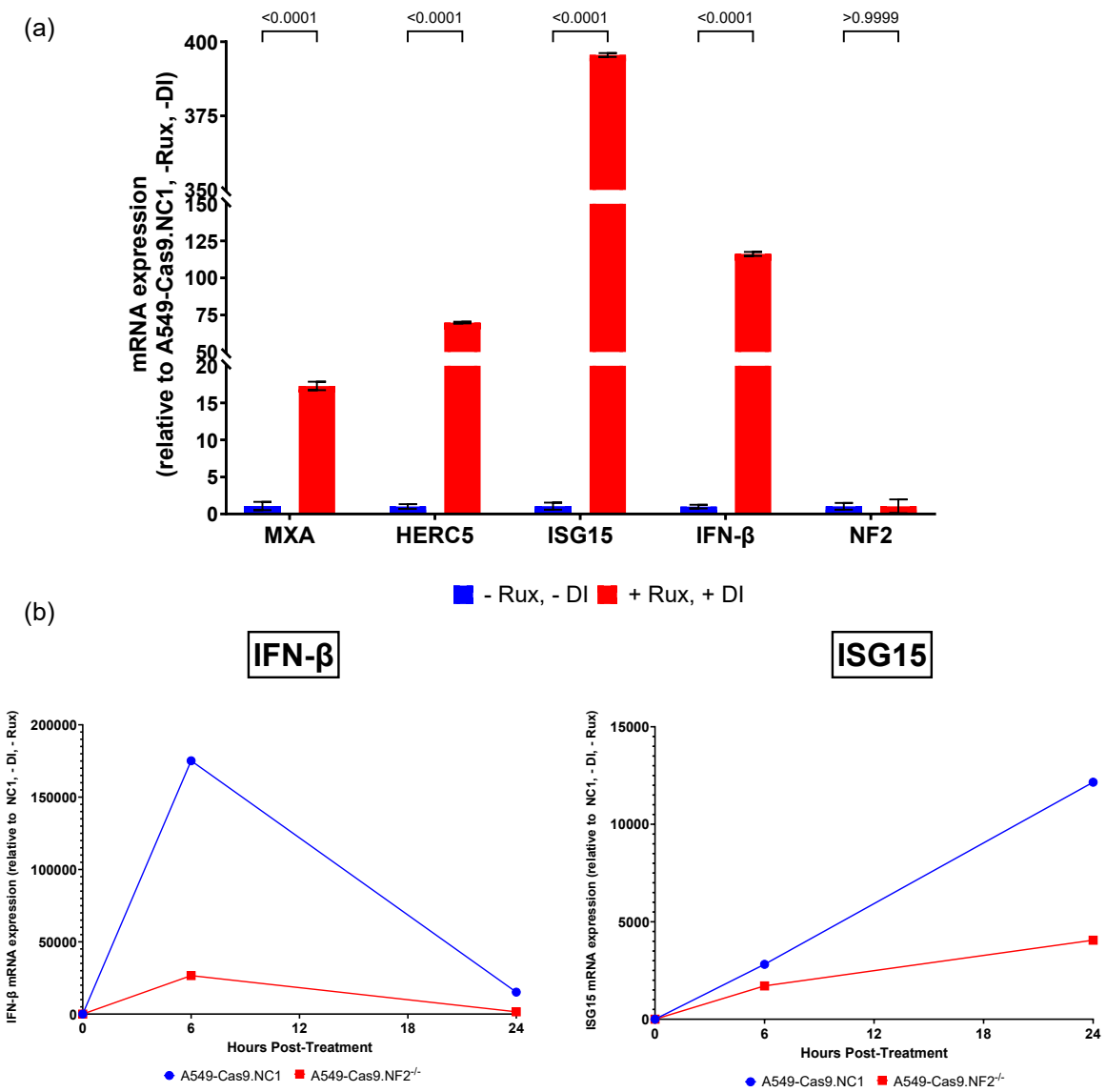

Figure 6.3.3.1: NF2 is not IRF3 inducible but instead, regulates IFN induction. **(A)** A549-Cas9.NC1 control cells were treated with PIV5 DIs in the presence of 10 μM Ruxolitinib for 24 h. Expression of ISGs was tested using reverse transcription quantitative PCR (RT-qPCR) with primers specific for *MxA*, *HERC5*, *ISG15*, *IFN-β*, and *NF2*. Relative expression (compared to - DI, - Ruxolitinib control) was determined following SYBR Green quantitative PCR (RT-qPCR) using ΔΔCt method. *β-Actin* expression was used to normalise between samples. Error bars represent the SD of the mean from three independent RNA samples. Statistics performed using two-way ANOVA; p-values denoted on graph. **(B)** A549-Cas9.NC1 control cells and A549-Cas9.NF2$^{-/-}$ cells were treated with SeV Cantell DIs in the presence of 10 μM Ruxolitinib for 6 h, 24 h or left untreated. Expression of ISGs was tested using reverse transcription quantitative PCR (RT-qPCR) with primers specific for *IFN-β* and *ISG15*. Relative expression (compared to - DI, - Ruxolitinib control) was determined following SYBR Green quantitative PCR (RT-qPCR) using ΔΔCt method. *β-Actin* expression was used to normalise between samples. Error bars represent the SD of the mean from three independent RNA samples. Data shown is a representation of one of three biological repeats, additional data from biological repeats see appendices 3 & 4.

6.3.4 Induction and regulation of type I IFN signalling in NF2 deficient cells

Following identification that NF2 was not induced following IFN induction, we investigated whether it was expressed by IFN binding to IFNAR and activating the JAK-STAT pathway, either directly from ISRE-containing promoters, like other canonical ISGs, or indirectly. We took a similar approach to IFN induction, replacing DI treatment with IFN-α treatment whereby A549-Cas9.NC1 cells were treated with IFN, and the expression of genes known to be expressed via ISRE-containing promoters, *MxA*, *ISG15*, and *HERC5*, were measured alongside *NF2* and an *IFN-β* negative control via RT-qPCR. As expected, we observed no expression of *IFN-β* following IFN treatment but a strong induction of both *MxA* and *ISG15*. As with DI treatment of A549-Cas9.NC1 cells, IFN treatment resulted in no difference in *NF2* expression between IFN and non-IFN treated cells, therefore indicating that NF2 is also not expressed as a result of activation of the IFN signalling pathway. Analysis of NF2 protein expression (figure 6.4.3.1.a) was carried out in DI treated cells in the absence of Rux, allowing for downstream IFN signalling and expression of genes from ISRE-containing promoters. This showed constitutive expression in non-DI treated A549-Cas9.NC1 cells with no upregulation in NF2 expression when DI treated. Therefore, combined, these results support the observation that NF2 is not upregulated as a result of IFN signalling, alongside induction.

As NF2 appeared to play a role in regulating IFN induction, we subsequently investigated if it also played a role in regulation of IFN signalling (figure 6.4.3.1.b). To investigate this, A549-Cas9.NC1 and A549-Cas9.NF2$^{-/-}$ cells were treated with IFN-α for 4 h, 10 h, or left untreated and the expression of three canonical ISGs expressed from ISRE-containing promoters, *MxA*, *ISG15*, and *HERC5*, measured by RT-qPCR. All three genes of interest showed reduced levels of transcription in NF2 deficient cells compared to control cells over time, whilst fold changes remained consistent across time points unlike in figure 6.3.3.1 whereby fold-change increased over time. *MxA* and *ISG15* expression was approximately 2-fold reduced at both time points in NF2 deficient cells compared to control, whilst *HERC5* expression was approximately 3-fold reduced in NF2 deficient cells. This suggests that the presence of NF2 increases transcription of genes transcribed as a result of IFN signalling from ISRE-containing promoters, and points toward a role in NF2 in also regulating the IFN signalling pathway as well as induction.

Interestingly, the increased fold-change in ISG expression levels in A549-Cas9.NF2$^{-/-}$ cells remains consistent over increased IFN-α treatment lengths whilst the fold-change of IRF3 inducible genes increases with prolonged DI treatment. This suggests that regulation of IFN signalling by NF2 either acts early in IFN signalling or the modulation is turned over more quickly, whilst the role of NF2 the regulation of IFN induction has a cumulative effect on the expression genes over time.

(a)

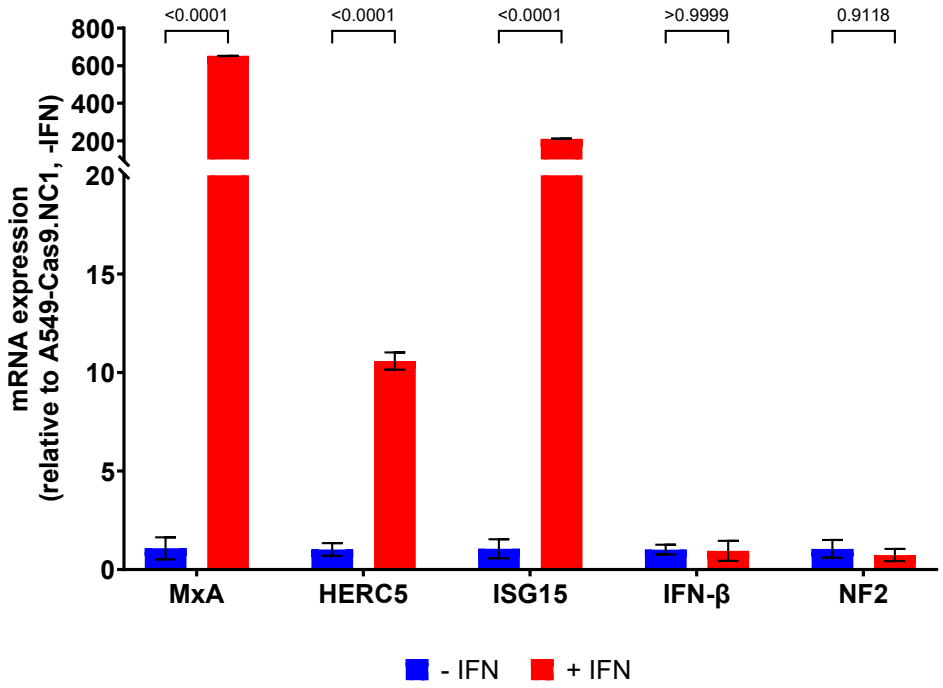
<0.0001
<0.0001
<0.0001
>0.9999
0.9118
800
600
400
200
20
15
10
5
0
mRNA expression
(relative to A549-Cas9.NC1, -IFN)
MxA
HERC5
ISG15
IFN-β
NF2
- IFN
+ IFN

(b)

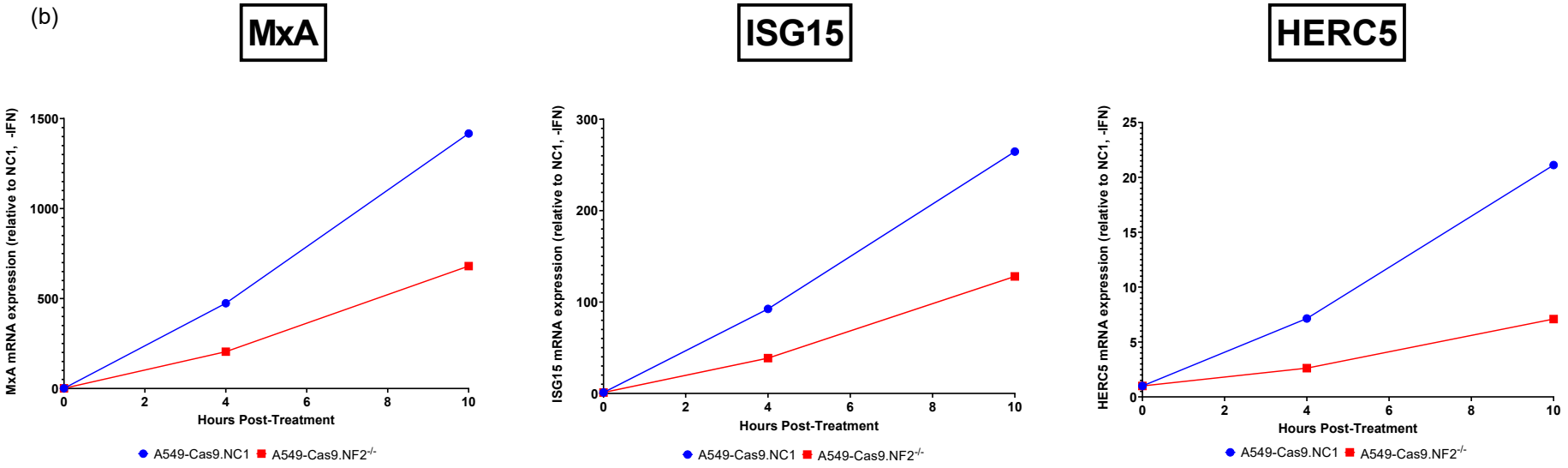
MxA
ISG15
HERC5
MxA mRNA expression (relative to NC1, -IFN)
ISG15 mRNA expression (relative to NC1, -IFN)
HERC5 mRNA expression (relative to NC1, -IFN)
Hours Post-Treatment
A549-Cas9.NC1
A549-Cas9.NF2-/-

Figure 6.3.4.1: NF2 is not IFN inducible but instead, regulates IFN signalling. **(A)** A549-.Cas9.NC1 control cells were treated with IFN-α (1000 1U/ ml) for 24 h. Expression of ISGs was tested using reverse transcription quantitative PCR (RT-qPCR) with primers specific for *MxA*, *HERC5*, *ISG15*, *IFN-β* and *NF2*. Relative expression (compared to - IFN control) was determined following SYBR Green quantitative PCR (RT-qPCR) using ΔΔCt method. *β-Actin* expression was used to normalise between samples. Error bars represent the SD of the mean from three independent RNA samples. Statistics performed using two-way ANOVA; p-values denoted on graph **(B)** A549-Cas9.NC1 control cells and A549-Cas9.NF2$^{-/-}$ cells were pre-treated with IFN-α (1000 1U/ ml) for either 4 h, 10 h or left untreated. Expression of ISGs was tested using reverse transcription quantitative PCR (RT-qPCR) with primers specific for *MxA*, *ISG15* and *HERC5*. Relative expression (compared to - IFN control) was determined following SYBR Green quantitative PCR (RT-qPCR) using ΔΔCt method. *β-Actin* expression was used to normalise between samples. Error bars represent the SD of the mean from three independent RNA samples. Data shown is a representation of one of three biological repeats, additional data from biological repeats see appendices 5-7.

6.3.5 Regulation of IRF3 IFN induction by NF2

Following the observation that NF2 may regulate the IFN response, we aimed to elucidate at which step, or at which protein, this regulation acts. In the literature, one paper showed decreased levels of phosphorylated TBK1 in NF2 knockout cells compared to wild type when infected with VSV, indicating regulation of components of the induction pathway (Meng et al., 2021). We therefore asked if we could observe a similar phenotype in the protein expression of IRF3. To investigate this, A549-Cas9.NC1 and A549-Cas9.NF2$^{-/-}$ cells were treated with DIs for 6 h or left untreated and protein expression of IRF3 was tested by immunoblot analysis (figure 6.3.5.1). Protein expression was chosen to be measured at 6 h post-DI treatment based on results from figure 6.3.3.1.b which showed peak IFN-β expression, and therefore IFN induction, at 6 h post-treatment. Results suggest that IRF3 expression is reduced in NF2 deficient cells compared to A549-Cas9.NC1 control cells, however densitometry analysis would enable confirmation of this when normalised to β-Actin levels. Reduced IRF3 expression in NF2 deficient cells indicates an increased rate of turnover compared to control cells. This finding correlates with the expression of IRF3-inducible genes, IFN-β and ISG15 (figure 6.3.3.1.b), during the activation of the IFN induction pathway. Upon full activation of the IFN induction pathway, as indicated by IFN-β mRNA levels at 6 h post-treatment, reduced total IRF3 protein expression explains the reduction in IFN-β and ISG15 mRNA expression at the same time point. In A549-Cas9.NC1 cells, expression of IRF3 protein, following DI treatment, allows for the downstream phosphorylation and nuclear translocation allowing for the transcription of IFN-β. However, reduced IRF3 would surmount to reduced IRF3 dimerization and subsequent expression from the IRF3 promoter (Lin et al., 1998; Ashley et al., 2019; Duncan et al., 2023). Follow up investigation to analyse proteins levels of components of the IFN induction pathway were performed however, there was insufficient time for optimisation of immunoblot conditions, including that of phospho-IRF3. As such, total protein levels of IRF3 were used as surrogate in order to provide indication of levels of total protein turnover under different conditions.

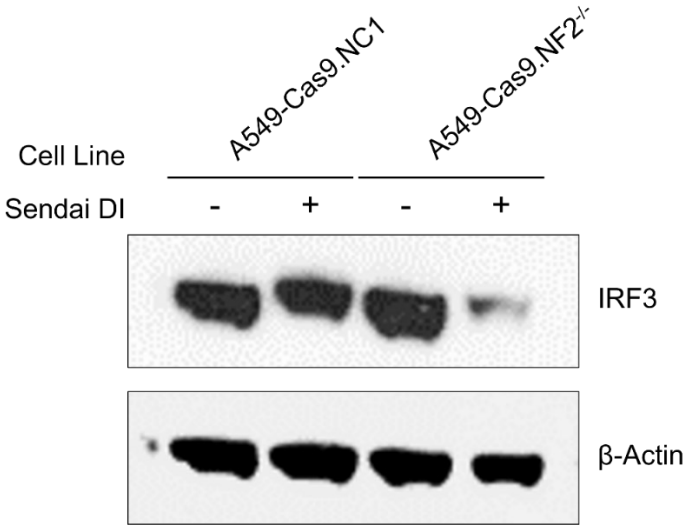

Figure 6.3.5.1: Increased IRF3 turnover in NF2 knockout cells following induction of IFN induction. A549-Cas9.NC1, a sgRNA non-cutting control, and A549-Cas9.NF2$^{-/-}$ cells were treated with DI-rich preparation of Sendai virus for 6 h or left untreated. Protein expression of IRF3 and β-Actin was tested by immunoblot analysis.

6.4 Hydroxysteroid 17-Beta Dehydrogenase 12 (HSD17B12)

6.4.1 PIV3 NP expression following infection of HSD17B12 deficient cells

As per section 6.3.1, to further characterise the effect on hPIV3-GFP(JS) infection in HSD17B12 deficient cells we investigated the effect of HSD17B12 on the transcription kinetics in viral replication. A549-Cas9.NC1 and A549-Cas9.HSD17B12$^{-/-}$ cells were pre-treated with IFN-α prior to infection with hPIV3-GFP(JS) at MOI = 10. Following a 1 h inoculation with the virus, the virus was removed, cells were washed, and the media was replaced with non-virus containing media. Viral replication was monitored over time by harvesting samples and analysing mRNA expression of a viral transcript, *hPIV3 NP*, using RT-qPCR (figure 6.4.1.1). Analysis of *hPIV3 NP* transcription showed that both A549-Cas9.NC1 and A549-Cas9.HSD17B12$^{-/-}$ cells were infected, and that viral transcription increased over time. Again, the levels of *hPIV3 NP* mRNA expression at 1 h.p.i was equivalent in both cell lines, indicating equivalent initial infection (figure 6.4.1.1, inset). However, against what was observed for NF2, both the expression of *hPIV3 NP* and the rate of transcription over time was lower in HSD17B12 deficient cells compared to in A549-Cas9.NC1 cells over time. This is despite results showing that HSD17B12 deficiency enhanced infectivity of hPIV3-GFP(JS) at MOI = 2.5, compared to A549-Cas9.NC1 cells, when analysed by flow cytometry (figure 5.3.3). However, we did not observe the same phenotype when measured by RT-qPCR. This is suspected to be due to the aforementioned, poor proliferation phenotype observed in A549-Cas9.HSD17B12$^{-/-}$ cells. During RNA extraction, RNA yields were always significantly lower than A549-Cas9.NC1 cells and the other two knockout cell lines, despite being seeded at a higher density for infection the following day to account for poorer cell health in the

clonal knockout population. Therefore, the RNA quality in the knockout cells appears to be reporting on the observed cell health.

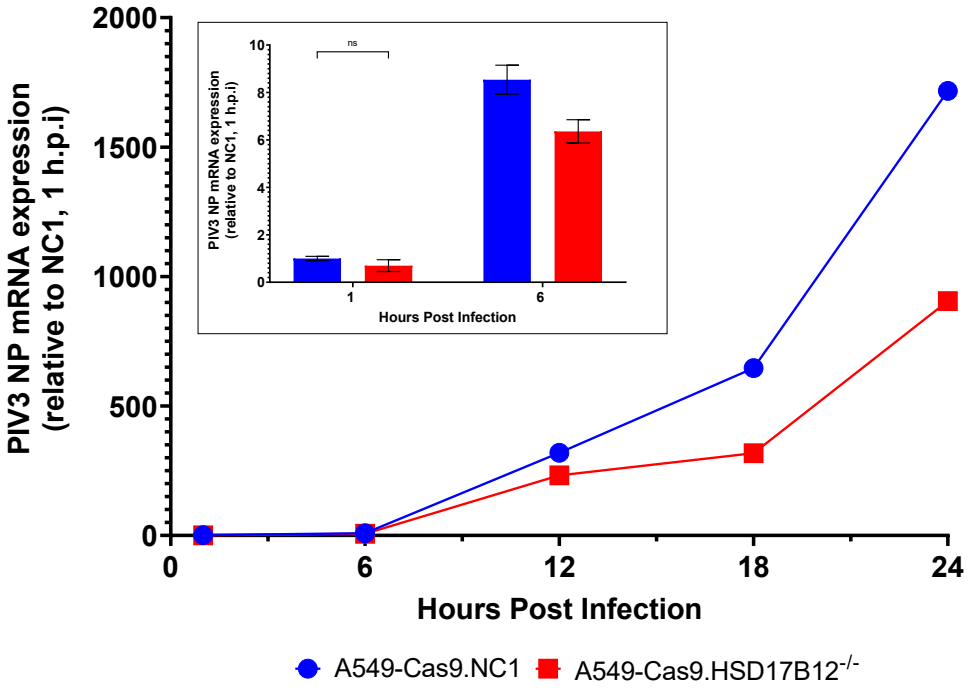

Figure 6.4.1.1: hPIV3(JS) NP expression is increased in HSD17B12 deficient cells over time. A549-Cas9.NC1 control cells and A549-Cas9.HSD17B12$^{-/-}$ cells were infected with hPIV3-GFP(JS) (MOI = 10) for 1 h following IFN-α pre-treatment for 8 h (1000 U). Following 1 h absorption, cells were washed and non-virus containing media added. Cells were harvested at 1, 6, 12, 18 and 24 h.p.i. Expression of viral mRNA was tested using reverse transcription quantitative PCR (RT-qPCR) with primers specific for *PIV3 NP*. Relative expression (compared to 1 h.p.i) was determined following SYBR Green quantitative PCR (RT-qPCR) using ΔΔCt method. *β-Actin* expression was used to normalise between samples. Inset shows 1 and 6 h.p.i with error bars represent the SD of the mean from three independent RNA samples. Data shown is a representation of one of three biological repeats, additional data from biological repeats see appendix 2. Statistics performed using two-way ANOVA; ns, no statistical significance.

6.4.2 Virus resistance in HSD17B12 deficient cells following IFN-α pre-treatment

The effect of IFN-α pre-treatment on infection of hPIV3-GFP(JS) infection in A549-Cas9.HSD17B12$^{-/-}$ cells compared to A549-Cas9.NC1 control cells was investigated using the same protocol as section 6.3.2. Unlike, in A549-Cas9.NF2$^{-/-}$ cells, we observed that virus replication, as indicated by MFI, was equivalent in A549-Cas9.HSD17B12$^{-/-}$ cells regardless of the time cells had been pre-treated with IFN-α, indicating that longer incubation with IFN-α does not provide more resistance to virus infection. It is therefore possible that HSD17B12 has a more fundamental effect on viral replication. Additionally, it

may be that that longer IFN-α pre-treatment impacts the proliferative and cell death effects of HSD17B12 knockout, preventing the effects of other acting ISGs being observed.

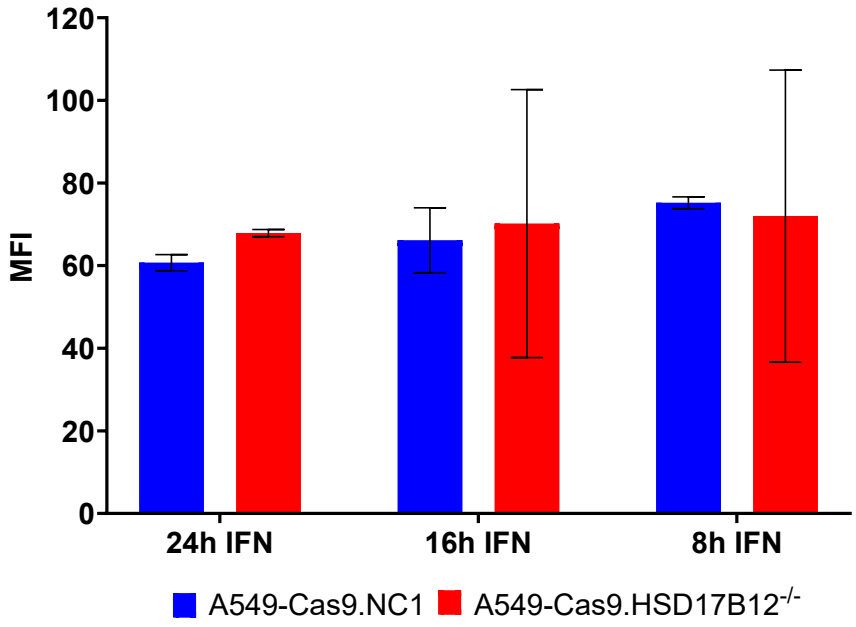

Figure 6.4.2.1: Permissiveness of A549-Cas9.HSD17B12$^{-/-}$ cells to hPIV3(JS) infection does not change with longer IFN-α pre-treatment. A549-Cas9.NC1 control cells and A549-Cas9.HSD17B12$^{-/-}$ cells were treated with IFN-α (1000 U) for 24, 16 or 8 h prior to being infected with hPIV3-GFP(JS) (MOI = 10) for 30 h. Cells were harvested at 30 h.p.i for flow cytometry analysis using blue laser (488 nm) for identification of GFP-positive cells. Data was analysed using FlowJo v10. A549-Cas9.NC1 cells were used as control, shown in blue, with A549-Cas9.HSD17B12$^{-/-}$ cells shown in red. Error bars represent the SD of the mean from two biological repeats, each with three technical replicates.

6.4.3 Induction and regulation of type I IFN induction in HSD17B12 deficient cells

To investigate whether HSD17B12 is expressed as a result of IRF3 activation (IFN induction pathway), A549-Cas9.NC1 cells were treated with DIs in the presence of Ruxolitinib (Rux) as per section 6.3.3, with *IRF3*, *IFN-β*, *ISG15*, *MxA* and *HERC5* expression, alongside *HSD17B12*, being analysed using RT-qPCR in the presence and absence of DI treatment. Analysis of *HSD17B12* expression showed no significant difference between DI and mock-treated cells (figure 6.4.3.1.a, insert), with the mRNA expression being extremely low, indicating that HSD17B12 is not expressed as a result of activation of the IFN induction pathway.

The regulation of IFN induction by HSD17B12 was subsequently investigated, as per section 6.3.3, with *IFN-β* and *ISG15* mRNA expression being compared in A549-Cas9.NC1 and A549-Cas9.HSD17B12$^{-/-}$ cells following DI treatment in the presence of Rux. Expression of both genes was reduced in A549-Cas9.HSD17B12$^{-/-}$ cells compared to control A549-Cas9.NC1 cells at 6 h post-treatment; *IFN-β* by 4.7-fold and *ISG15* by 4.7-fold. This suggests that the presence of HSD17B12 increases the transcription

of genes transcribed as a result of IFN induction. This fold-change in *IFN-β* expression is lowered to a 1.4-fold reduction 24 h post-DI treatment. Like in NF2 deficient cells, the effect of HSD17B12 deficiency on the expression of *ISG15* increases over time. At both timepoints, *ISG15* mRNA expression is decreased in A549-Cas9.HSD17B12$^{-/-}$ cells compared to A549-Cas9.NC1 cells but the fold change in expression increases with prolonged DI treatment from 1.9-fold decrease in HSD17B12 deficient cells at 6 h post-treatment to a 3.7-fold decrease at 24 h post-treatment. It should be noted that whilst the concentration of RNA extracted from HSD17B12 deficient cells was reduced compared to other cell lines, the amount of cDNA used within RT-qPCR is consistent and so the two cell lines can be reliably compared. However, it may be that cells healthy enough to allow for RNA extraction may show different expression profiles to those which do not proliferate and die and so results, in this case, may still require further validation. Together these results show that whilst HSD17B12 is not induced as a result of IFN induction, it does appear to play a role in the regulation of the response and the expression of ISGs from the IFN-β promoter.

(a)

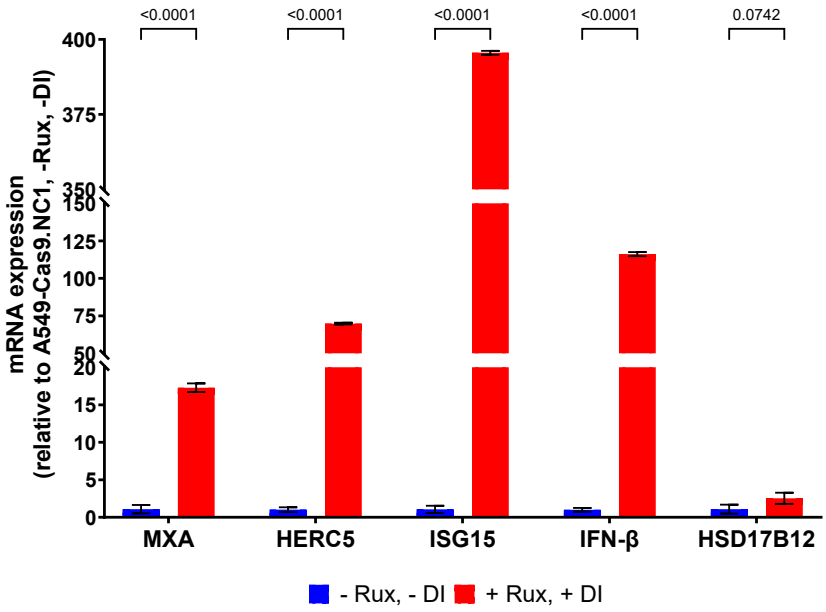

(b)

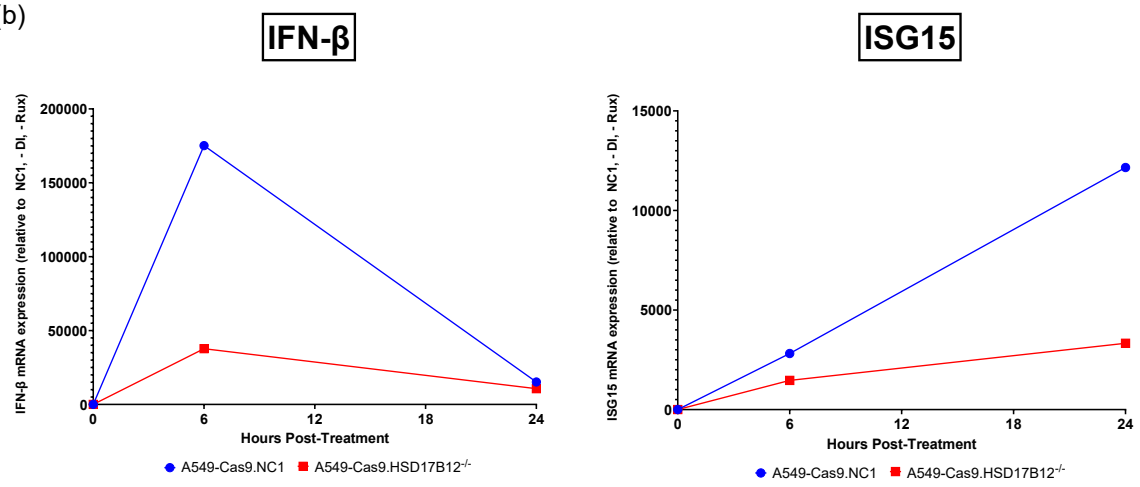

Figure 6.4.3.1: HSD17B12 is not IRF3 inducible but instead, regulates IFN induction. **(A)** A549-Cas9.NC1 control cells were treated with PIV5 DIs in the presence of 10 μM Ruxolitinib for 24 h. Expression of ISGs was tested using reverse transcription quantitative PCR (RT-qPCR) with primers specific for *MxA*, *HERC5*, *ISG15*, *IFN-β*, and *HSD17B12*. Relative expression (compared to – DI, - Ruxolitinib control) was determined following SYBR Green quantitative PCR (RT-qPCR) using ΔΔCt method. *β-Actin* expression was used to normalise between samples. Error bars represent the SD of the mean from three independent RNA samples. Statistics performed using two-way ANOVA; p-values denoted on graph. **(B)** A549-Cas9.NC1 control cells and A549-Cas9.HSD17B12$^{-/-}$ cells were treated with SeV Cantell DIs in the presence of 10 μM Ruxolitinib for 6 h, 24 h or left untreated. Expression of ISGs was tested using reverse transcription quantitative PCR (RT-qPCR) with primers specific for *IFN-β* and *ISG15*. Relative expression (compared to – DI, - Ruxolitinib control) was determined following SYBR Green quantitative PCR (RT-qPCR) using ΔΔCt method. *β-Actin* expression was used to normalise between samples. Error bars represent the SD of the mean from three independent RNA samples. Data shown is a representation of one of three biological repeats, additional data from biological repeats see appendices 3 & 4.

6.4.4 Induction and regulation of type I IFN signalling in HSD17B12 deficient cells

As HSD17B12 was shown to not be inducible as a result of IFN induction, like NF2, we also investigated whether it was expressed as a result of IFN signalling and IFN binding to IFNAR and activating the JAK-STAT signalling cascade. Taking the same approach, A549-Cas9.NC1 cells were treated with IFN, and the expression of *MxA*, *ISG15*, *HERC5*, and *IFN-β* were measured alongside *HSD17B12* via RT-qPCR. Analysis of *HSD17B12* mRNA expression (figure 6.4.4.1.a) showed no significant difference in IFN-α and mock-treated cells indicating that HSD17B12 is also not upregulated as a result of IFN signalling, alongside induction.

The role of HSD17B12 in the regulation if IFN signalling was subsequently investigated as previously described. Upon analysis of the three genes of interest, *MxA*, *ISG15*, and *HERC5*, the expression profile in A549-Cas9.NC1 and A549-Cas9.HSD17B12$^{-/-}$ cells was equivalent for both *MxA* and *HERC5* indicating that HSD17B12 deficiency does not affect expression levels. Conversely, we observed an average fold decrease of 1.7-fold in *ISG15* expression across both timepoints in HSD17B12 deficient cells compared to control.

Whilst ISG15 is expressed from ISRE-containing promoters, it is also expressed as a result of IRF3 dimerization and nuclear translocation, as previously described (Lin et al., 1998; Ashley et al., 2019; Duncan et al., 2023). It is known that genes expressed from ISRE-containing promoters can enter a feedback loop for the production of type-I IFN, as expressed from the IFN induction pathway. As such, it may be that the observed effect on *ISG15* expression may be due to this feedback loop, and the observed role of HSD17B12 in regulating IFN induction, as previously described (figure 6.4.4.1.b). This may explain the lack of change in expression of *MxA* and *HERC5* which are not IRF3 inducible genes. Together, these data suggest that whilst HSD17B12 plays a role in regulation of IFN induction, it does not play in role in the regulation of IFN signalling.

(a)

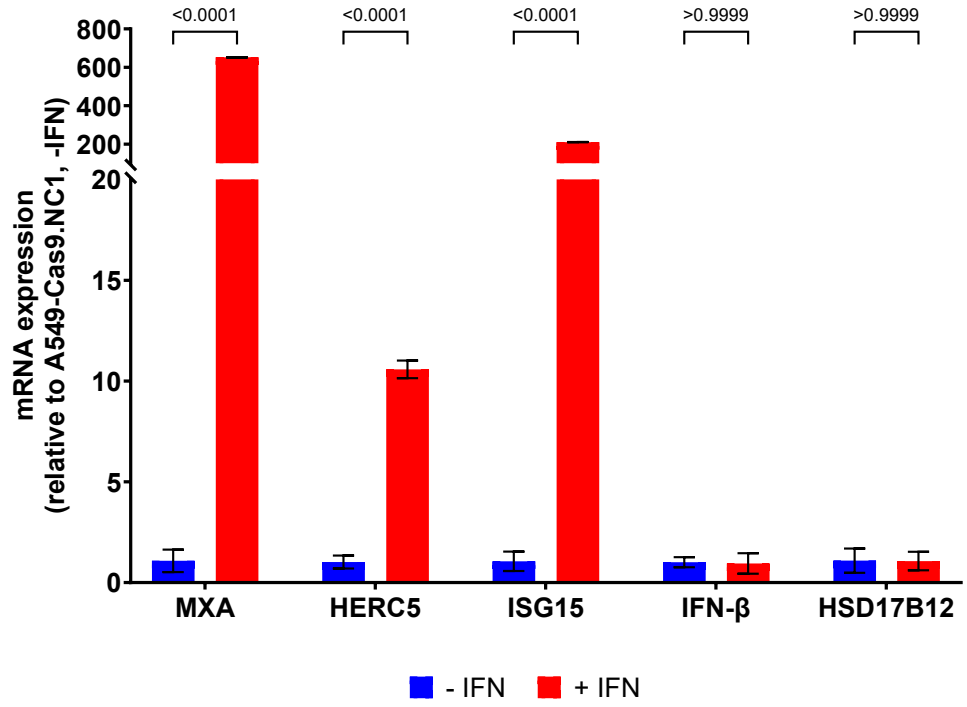
<0.0001
<0.0001
<0.0001
>0.9999
>0.9999
800
600
400
200
20
15
10
5
0
mRNA expression
(relative to A549-Cas9.NC1, -IFN)
MXA
HERC5
ISG15
IFN-β
HSD17B12
- IFN
+ IFN

(b)

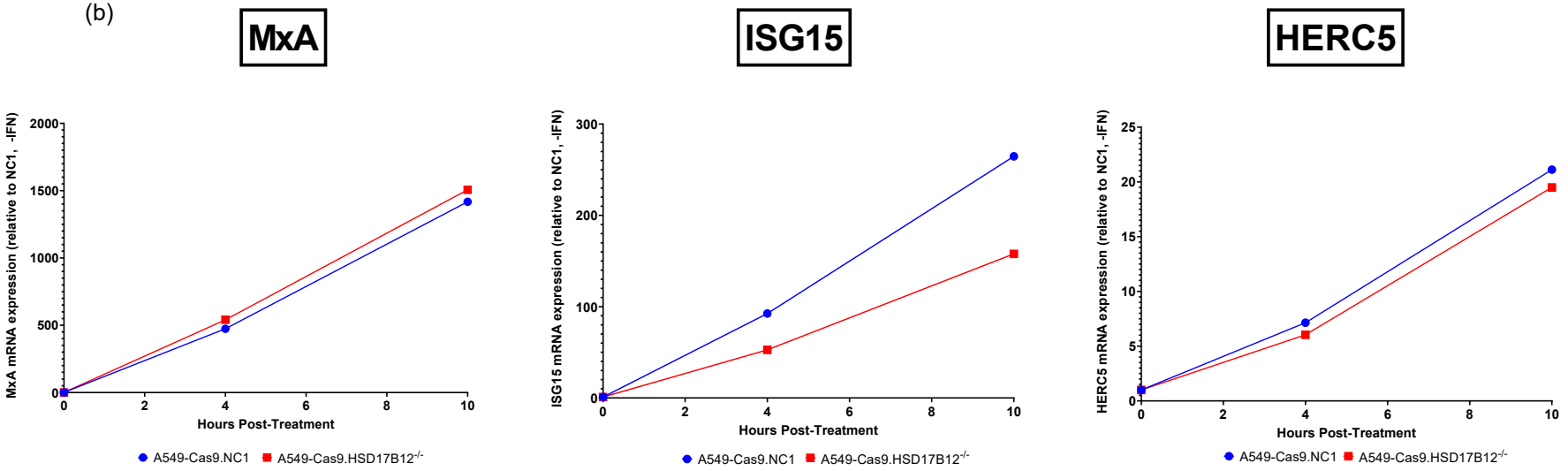
MxA
ISG15
HERC5
MxA mRNA expression (relative to NC1, -IFN)
ISG15 mRNA expression (relative to NC1, -IFN)
HERC5 mRNA expression (relative to NC1, -IFN)
Hours Post-Treatment
A549-Cas9.NC1
A549-Cas9.HSD17B12-/-

Figure 6.4.4.1: HSD17B12 is not IFN inducible but instead, regulates IFN signalling. **(A)** A549-.Cas9.NC1 control cells were treated with IFN-α (1000 1U/ ml) for 24 h. Expression of ISGs was tested using reverse transcription quantitative PCR (RT-qPCR) with primers specific for *MxA*, *HERC5*, *ISG15*, *IFN-β* and *HSD17B12*. Relative expression (compared to - IFN control) was determined following SYBR Green quantitative PCR (RT-qPCR) using ΔΔCt method. *β-Actin* expression was used to normalise between samples. Error bars represent the SD of the mean from three independent RNA samples. Statistics performed using two-way ANOVA; p-values denoted on graph. **(B)** A549-Cas9.NC1 control cells and A549-Cas9.HSD17B12$^{-/-}$ cells were pre-treated with IFN-α (1000 1U/ ml) for either 4 h, 10 h or left untreated. Expression of ISGs was tested using reverse transcription quantitative PCR (RT-qPCR) with primers specific for *MxA*, *ISG15* and *HERC5*. Relative expression (compared to - IFN control) was determined following SYBR Green quantitative PCR (RT-qPCR) using ΔΔCt method. *β-Actin* expression was used to normalise between samples. Error bars represent the SD of the mean from three independent RNA samples. Data shown is a representation of one of three biological repeats, additional data from biological repeats see appendices 5-7.

6.5 Zinc Finger CCCH-Type Containing, Antiviral 1 (ZAP)

6.5.1 PIV3 NP expression following infection of ZAP deficient cells

As with sections 6.3.1 and 6.4.1, the effect on hPIV3-GFP(JS) infection in ZAP deficient cells was further characterised by investigating the effect of ZAP on the transcription kinetics in viral replication. As before, A549-Cas9.NC1 and A549-Cas9.ZAP$^{-/-}$ cells were pre-treated with IFN-α prior to infection with hPIV3-GFP(JS) at MOI = 10. Viral replication was monitored over time by analysing mRNA expression of *hPIV3 NP* using RT-qPCR (figure 6.5.1.1). Analysis of *hPIV3 NP* transcription showed that both A549-Cas9.NC1 and A549-Cas9.ZAP$^{-/-}$ cells were infected, that viral transcription increased over time, and the expression levels of *hPIV3 NP* mRNA at 1 h.p.i were equivalent in both cell lines (figure 6.5.1.1, inset). Similar to in A549-Cas9.NF2$^{-/-}$ cells, we observed that both the rate of *hPIV3 NP* transcription over time and *hPIV3 NP* expression levels were muted in A549-Cas9.NC1 cells compared to those deficient in ZAP. The fold-change of *hPIV3 NP* mRNA expression between the two cell lines increased from 1.9-fold at 12 h.p.i to 2.6-fold at 24 h.p.i. This indicates that the expression of ZAP is able to reduce viral transcription and to a more significant degree than NF2, as shown by a large fold change in *hPIV3 NP* mRNA expression at all time points in ZAP deficient cells compared to A549-Cas9.NC1 control cells. Additionally, ZAP appears to be functioning at earlier time points as indicated by a significant difference at 6 h.p.i in ZAP deficient cells compared to control cells (figure 6.5.1.1, inset); a time point that does not show a significant increase in NF2 deficient cells (figure 6.3.1.1).

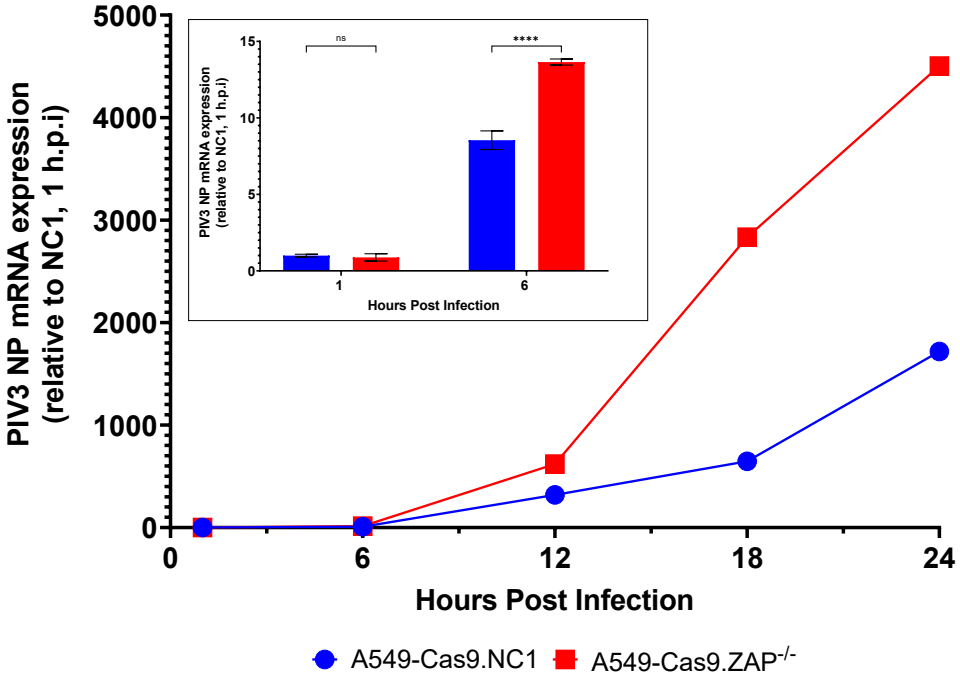

Figure 6.5.1.1: hPIV3(JS) NP expression is increased in ZAP deficient cells over time. A549-Cas9.NC1 control cells and A549-Cas9.ZAP$^{-/-}$ cells were infected with hPIV3-GFP(JS) (MOI = 10) for 1 h following IFN-α pre-treatment for 8 h (1000 U). Following 1 h absorption, cells were washed and non-virus containing media added. Cells were harvested at 1, 6, 12, 18 and 24 h.p.i. Expression of viral mRNA was tested using reverse transcription quantitative PCR (RT-qPCR) with primers specific for *PIV3 NP*. Relative expression (compared to 1 h.p.i) was determined following SYBR Green quantitative PCR (RT-qPCR) using ΔΔCt method. *β-Actin* expression was used to normalise between samples. Inset shows 1 and 6 h.p.i with error bars represent the SD of the mean from three independent RNA samples. Data shown is a representation of one of three biological repeats, additional data from biological repeats see appendix 2. Statistics performed using two-way ANOVA; p-values denoted on graph, ns, no statistical significance.

6.5.2 Virus resistance in ZAP deficient cells following IFN-α pre-treatment

The effect of IFN-α pre-treatment on infectivity of hPIV3-GFP(JS) was further investigated in A549-Cas9.ZAP$^{-/-}$ cells as before. As with HSD17B12 deficient cells (section 6.4.2), we observed that virus replication, was equivalent in A549-Cas9.ZAP$^{-/-}$ cells regardless of the time cells had been pre-treated with IFN-α, indicating that longer incubation with IFN-α does not provide more resistance to virus infection. Large standard deviations are observed with 16 h and 8 h IFN pre-treatment compared to 24 h. This could suggest that the effect of IFN is more profound at 24 h or that there is a more sustained effect compared to earlier timepoints where there may be more heterogeneity in the phenotype between cells.

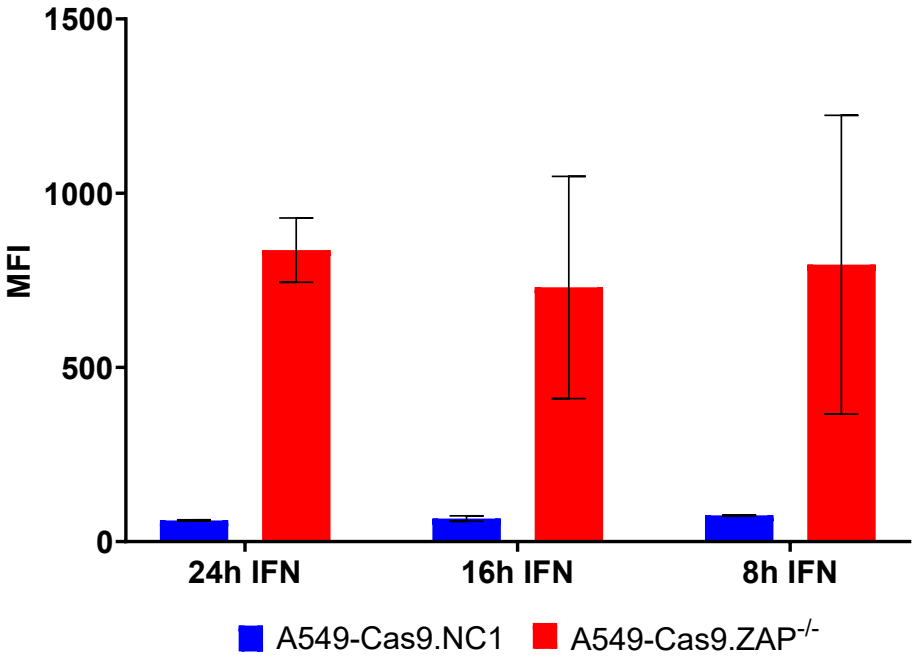

Figure 6.5.2.1: Permissiveness of A549-Cas9.ZAP$^{-/-}$ cells to hPIV3(JS) infection does not change with longer IFN-α pre-treatment. A549-Cas9.NC1 control cells and A549-Cas9.ZAP$^{-/-}$ cells were treated with IFN-α (1000 U) for 24, 16 or 8 h prior to being infected with hPIV3-GFP(JS) (MOI = 10) for 30 h. Cells were harvested at 30 h.p.i for flow cytometry analysis using blue laser (488 nm) for identification of GFP-positive cells. Data was analysed using FlowJo v10. A549Cas9.-NC1 cells were used as control, shown in blue, with A549-Cas9.ZAP$^{-/-}$ cells shown in red. Error bars represent the SD of the mean from two biological repeats, each with three technical replicates.

6.5.3 Induction and regulation of type I IFN induction in ZAP deficient cells

ZAP was further investigated to see if it is expressed as a result of the IFN induction pathway. Upon analysing *ZAP* expression in A549-Cas9.NC1 cells following PIV5 DI and Rux treatment, we observed a significant increase in *ZAP* expression in treated compared to mock-treated cells. This indicates that ZAP is expressed as a result of DI stimulation, likely due to the activation of the IFN induction pathway leading to IRF3 activation. An increase in *ZAP* mRNA expression following DI treatment is supported by immunoblot data from figure 6.2.1.1.c which showed an increase in ZAP expression, in particular ZAP-S, following DI treatment in A549-Cas9.NC1 cells. However, during immunoblot analysis, A549-Cas9.NC1 cells were DI treated, but unlike figure 6.5.3.1, were not treated with Rux alongside. This therefore meant that the increase in protein expression could not be attributed to either to IFN induction or signalling pathways. This supporting evidence, at the mRNA level, suggests that induction of ZAP expression is happening at the IFN induction stage.

Whilst it was observed that ZAP is expressed as a result of IRF3 activation following PAMP stimulation (IFN induction pathway), we also investigated whether ZAP additionally played a role in the regulation

of IFN induction as ZAP will regulate and/ or suppress any gene with high CpG content including cellular host genes (Gonçalves-Carneiro et al., 2021). As such, A549-Cas9.NC1 and A549-Cas9.ZAP$^{-/-}$ cells were treated with SeV DIs, in the presence of Rux, for 6 h, 24 h or left untreated, as before, with the mRNA expression of *IFN-β* and *ISG15* being analysed by RT-qPCR in control and ZAP deficient cells to compare expression levels. We observed reduced expression of both genes in A549-Cas9.ZAP$^{-/-}$ cells compared to control A549-Cas9.NC1 cells however the fold reduction observed was smaller than that for NF2 and HSD17B12 deficient cells. At 6 h post-DI treatment, *IFN-β* expression only saw a modest reduction of 1.6-fold in ZAP deficient cells compared to A549-Cas9.NC1, returning to equivalent levels of mRNA expression at 24 h. Upon analysis of *ISG15* expression, at 6 h post-treatment A549-Cas9.NC1 showed to have reduced *ISG15* expression compared to A549-Cas9.ZAP$^{-/-}$ cells, the opposite of what was observed in the other knockout cell lines. At 24 h post-treatment, *ISG15* expression became reduced in A549-Cas9.ZAP$^{-/-}$ cells compared to A549-Cas9.NC1 but only by 1.5-fold.

These results suggest that whilst ZAP may play a small role in dampening the IFN induction response, it is likely not its main role and instead, its subsequent functions as an ISG are its predominant antiviral mechanism of action. However, these data were generated using the non-truncated isoform of ZAP and so it may be that ZAP-S plays an independent role in regulation if expressed in isolation.

(a)

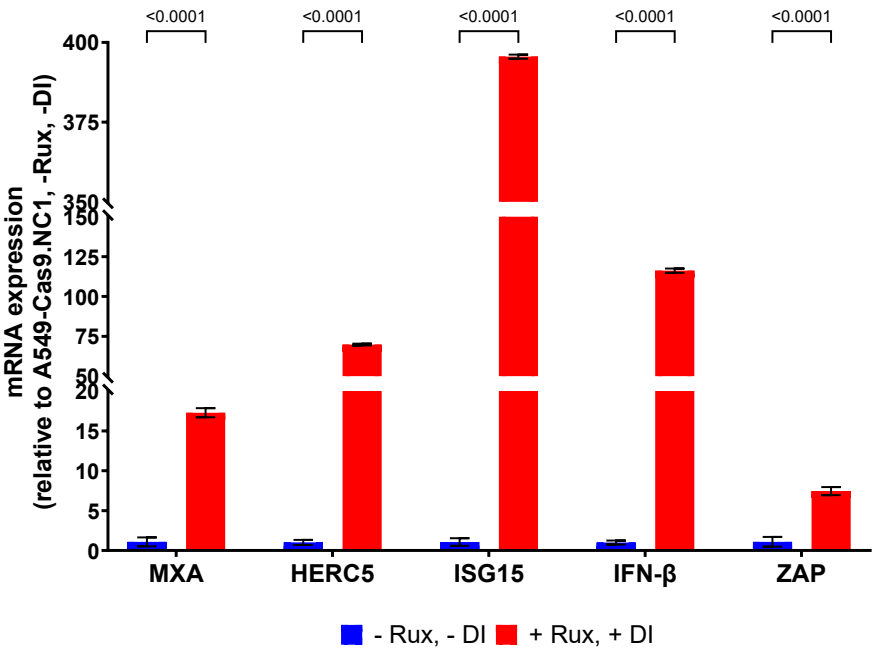

(b)

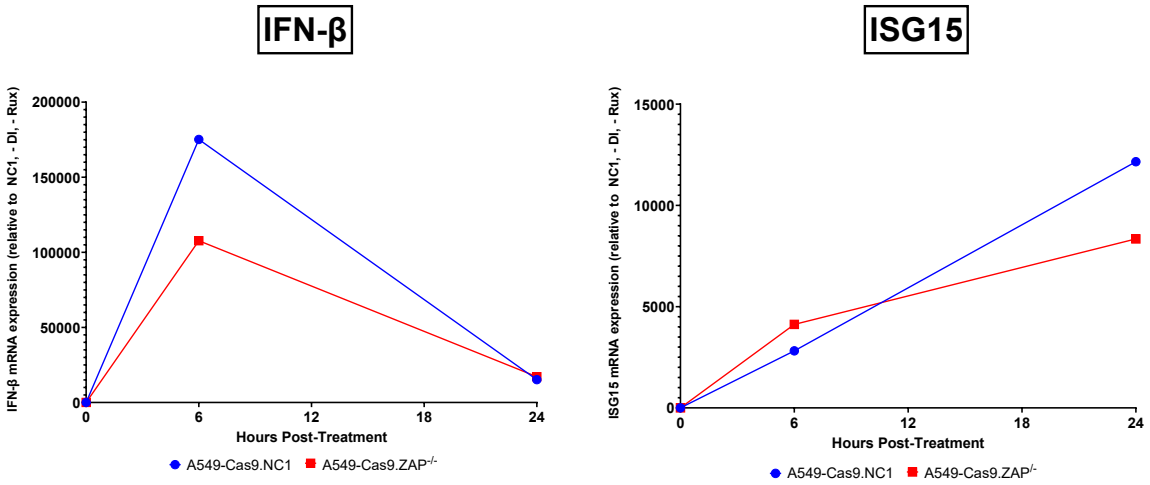

Figure 6.5.3.1: ZAP is IRF3 inducible and regulates IFN induction. **(A)** A549-Cas9.NC1 control cells were treated with PIV5 DIs in the presence of 10 μM Ruxolitinib for 24 h. Expression of ISGs was tested using reverse transcription quantitative PCR (RT-qPCR) with primers specific for *MxA*, *HERC5*, *ISG15*, *IFN-β*, and *ZAP*. Relative expression (compared to – DI, - Ruxolitinib control) was determined following SYBR Green quantitative PCR (RT-qPCR) using ΔΔCt method. *β-Actin* expression was used to normalise between samples. Error bars represent the SD of the mean from three independent RNA samples. Statistics performed using two-way ANOVA; p-values denoted on graph. **(B)** A549-Cas9.NC1 control cells and A549-Cas9.ZAP$^{-/-}$ cells were treated with SeV Cantell DIs in the presence of 10 μM Ruxolitinib for 6 h, 24 h or left untreated. Expression of ISGs was tested using reverse transcription quantitative PCR (RT-qPCR) with primers specific for *IFN-β* and *ISG15*. Relative expression (compared to – DI, - Ruxolitinib control) was determined following SYBR Green quantitative PCR (RT-qPCR) using ΔΔCt method. *β-Actin* expression was used to normalise between samples. Error bars represent the SD of the mean from three independent RNA samples. Data shown is a representation of one of three biological repeats, additional data from biological repeats see appendices 3 & 4.

6.5.4 Induction and regulation of type I IFN signalling in ZAP deficient cells

As it was observed that ZAP is induced following IRF3 activation, we also wanted to investigate if it was further upregulated following activation of the IFN signalling pathway. Again using A549-Cas9.NC1 cells either treated with IFN-α or mock-treated, we analysed the expression of *ZAP* using RT-qPCR. Unlike following DI treatment, IFN-α treatment resulted in no upregulation of *ZAP* mRNA expression indicated it is not induced as a result of type I IFN signalling.

ZAP was also shown to have a minimal role in the regulation of IFN induction, so as with NF2 and HSD17B12, we subsequently investigated its role in the regulation of IFN signalling. A549-Cas9.NC1 and A549-Cas9.ZAP$^{-/-}$ cells were treated with IFN-α for 4 h, 10 h, or left untreated and the expression of three canonical ISGs, *MxA*, *ISG15*, and *HERC5*, measured by RT-qPCR. Analysis of *ISG15* and *HERC5* expression showed no significant differences between ZAP deficient cells and control cells over time, with the average fold reduction between cells lines being 1.2-fold and 1.1-fold for *ISG15* and *HERC5* respectively. This suggests that ZAP also does not play a role in the regulation of IFN signalling.

Interestingly, A549-Cas9.NC1 cells exhibited reduced *MxA* expression over time compared to A549-Cas9.ZAP$^{-/-}$ cells. This result suggests that the presence of ZAP may therefore be playing a proviral role by downregulating the expression of a canonical ISG, MxA, the opposite phenotype we have previously observed in the inhibition of hPIV3-GFP(JS) replication (figure 6.5.4.1). As previously described, ZAP will regulate and/ or suppress any gene with high CpG content including cellular host genes. As such it may be possible that ZAP is suppressing MxA, resulting in the observed phenotype.

Together these results indicate that whilst ZAP displays antiviral functions, it does not have a fundamental role within the IFN signalling pathway. However, it may have gene specific effects based on the CpG content of genes, including cellular host genes such as MxA. To investigate this, an RNA-seq time course would be required.

(a)

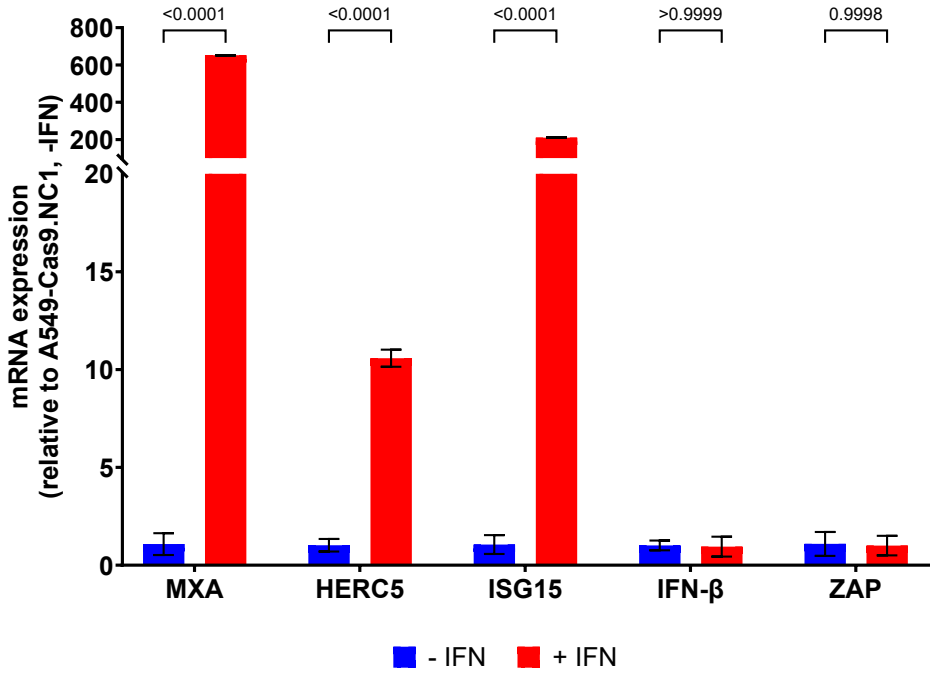
<0.0001
<0.0001
<0.0001
>0.9999
0.9998
800
600
400
200
20
15
10
5
0
mRNA expression
(relative to A549-Cas9.NC1, -IFN)
MXA
HERC5
ISG15
IFN-β
ZAP
- IFN
+ IFN

(b)

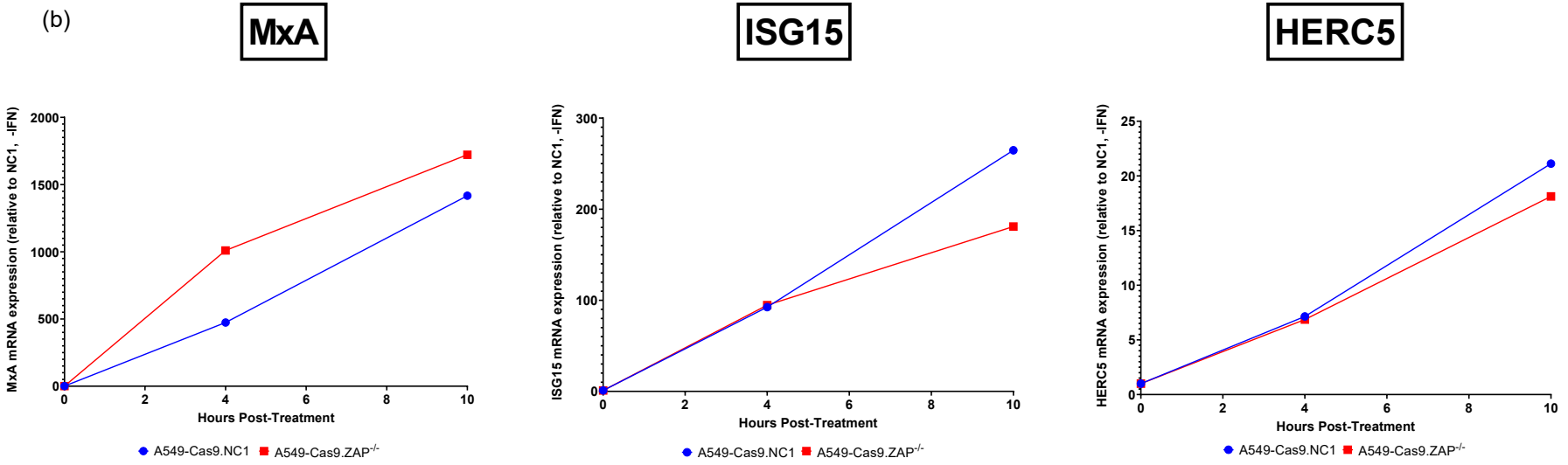
MxA
ISG15
HERC5
MxA mRNA expression (relative to NC1, -IFN)
ISG15 mRNA expression (relative to NC1, -IFN)
HERC5 mRNA expression (relative to NC1, -IFN)
Hours Post-Treatment
A549-Cas9.NC1
A549-Cas9.ZAP-/-

Figure 6.5.4.1: ZAP does not play a fundamental role during IFN signalling. **(A)** A549-.Cas9.NC1 control cells were treated with IFN-α (1000 1U/ ml) for 24 h. Expression of ISGs was tested using reverse transcription quantitative PCR (RT-qPCR) with primers specific for *MxA*, *HERC5*, *ISG15*, *IFN-β* and *ZAP*. Relative expression (compared to - IFN control) was determined following SYBR Green quantitative PCR (RT-qPCR) using ΔΔCt method. *β-Actin* expression was used to normalise between samples. Error bars represent the SD of the mean from three independent RNA samples. Statistics performed using two-way ANOVA; p-values denoted on graph. **(B)** A549-Cas9.NC1 control cells and A549-Cas9.ZAP$^{-/-}$ cells were pre-treated with IFN-α (1000 1U/ ml) for either 4 h, 10 h or left untreated. Expression of ISGs was tested using reverse transcription quantitative PCR (RT-qPCR) with primers specific for *MxA*, *ISG15* and *HERC5*. Relative expression (compared to - IFN control) was determined following SYBR Green quantitative PCR (RT-qPCR) using ΔΔCt method. *β-Actin* expression was used to normalise between samples. Error bars represent the SD of the mean from three independent RNA samples. Data shown is a representation of one of three biological repeats, additional data from biological repeats see appendices 5-7.

6.5.5 CpG dinucleotide analysis of PIV3

To further elucidate the role of ZAP in restricting hPIV3-GFP(JS) infection, we analysed the observed to expected ratio (O:E) for each dinucleotide by hPIV3 ORF (figure 6.5.5.1.a) and by host species (figure 6.5.5.1.b).

ZAP is known to act as an antiviral PRR through sensing high CpG frequencies and so we would expect to observe high CpG frequencies in our hPIV3 genome due to our previously identified restriction of the virus by ZAP. Conversely, upon analysis, we observe a strong CpG suppression in all hPIV3 ORFs, a known ZAP evasion tactic of many viruses due to the two co-evolving (Lin et al., 2020; Gaunt and Digard, 2022; Nguyen et al., 2023). As we observe restriction of hPIV3 by ZAP, the strong CpG suppression of hPIV3 ORFs therefore suggests that ZAP is acting as an antiviral through the suppression of non-viral targets rather than viral. We have previously proposed that ZAP may be responsible for downregulating, either by mRNA degradation or inhibition of translation (Abernathy and Glaunsinger, 2015), components of the IFN response including other ISGs as its recognition of CpG motifs is unspecific. Therefore, the observed antiviral effect of ZAP may be due to the downregulation of other negative regulators of the IFN response itself rather than the suppression of the virus itself. However, observation of CpG suppression itself may suggest a role of ZAP in the direct restriction of hPIV3, however the observed suppression is not enough to circumvent the antiviral role of ZAP, hence observing increased permissiveness to hPIV3 infection in ZAP deficient cells. Additionally, we observed some GpC suppression in all hPIV3 ORFs, a suppression that is not observed in the genomes of other RNA viruses (data unpublished).

Additionally, the overall dinucleotide content of the PIV3 genome was analysed across different host species: human, bovine, other undulate, as well as the average of all species together. Analysis showed that there were no differences in the dinucleotide O:E content between species, including that of CpG.

This suggests that all variants of the virus are equally as susceptible to ZAP suppression, likely by the same mechanism of action, with the degree of ZAP antiviral activity reduced to due to CpG suppression. We do not observe full CpG suppression across genomes and this is likely a trade-off to prevent compromising viral fitness.

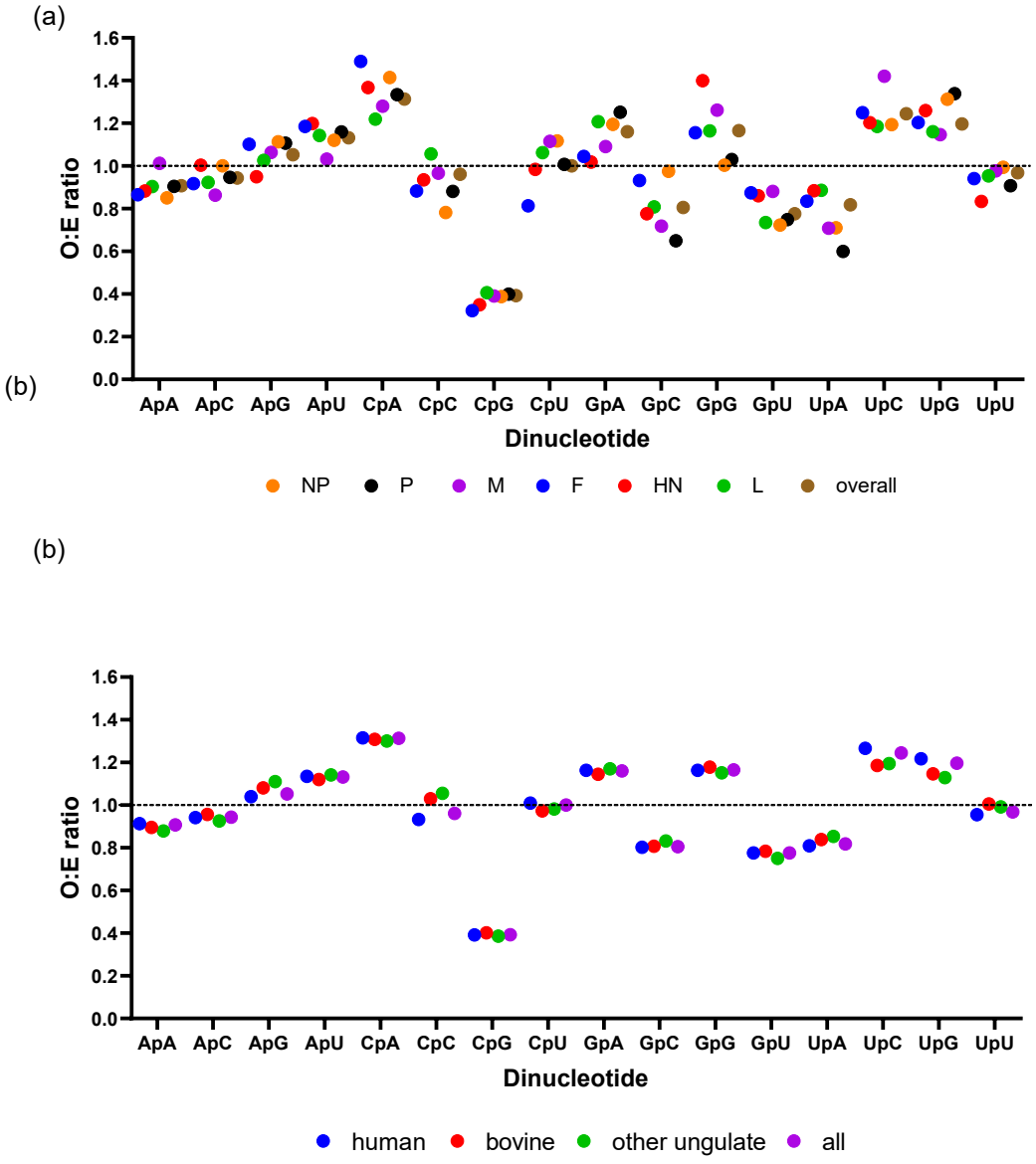

Figure 6.5.5.1: Analysis of dinucleotide O:E ratios within PIV3 genomes. Analysis of the observed to expected ration (O:E) for each dinucleotide within the PIV3 genome. (A) O:E ratios of dinucleotides were analysed within each individual ORF of hPIV3. Each ORF is represented by the following colour: F (blue), HN (red), L (green), M (purple), NP (orange), P (black), average (brown). (B) Average O:E ratios of dinucleotides across whole PIV3 genomes were analysed across host species. Each host species is represented by the following colour: human (blue), bovine (red), other ungulate (green), average (purple).

6.6 Effect of hPIV3(JS) antiviral restriction factors on other Paramyxo- and Pneumoviruses

Following characterisation of NF2, HSD17B12 and ZAP as antiviral factors restricting hPIV3-GFP(JS) infection, we wanted to investigate the effect our three genes of interest had on related Paramyxo- and Pneumoviruses. As such, we performed low MOI plaque assays to assess viral replication in our knockout cell lines compared to our A549-Cas9.NC1 control cell line and evaluated virus replication against three parameters: plaque number, area and intensity (as per section 6.2.2). Plaque analysis was carried out following infection with three viruses: hRSV, a closely related Pneumovirus; PIV5, the model Paramyxovirus; and hPIV3(Washington), a different strain of hPIV3 that is more resistant to IFN.

Analysis of plaque phenotype in NF2 deficient cells showed a significant increase in at least one parameter against all viruses tested when compared to control cells. We observed a significant increase in plaque number and intensity following hRSV infection, a significant increase in plaque area when infected with PIV5, and a significant increase in both plaque area and intensity when infected with hPIV3(Washington) (summarised in table 5.1). These data indicate that NF2 has broad antiviral effect against other related Paramyxo- and Pneumoviruses either through a direct antiviral effect yet to be elucidated or through its regulation of the IFN response (section 6.3.3 and 6.3.4).

Analysis of plaque phenotype in HSD17B12 and ZAP deficient cells showed no significant increases in any parameter measured, when compared to A549-Cas9.NC1 control cells, upon infection with either hRSV, PIV5 or hPIV3(Washington). This suggests no role of either of the two genes in the restriction of other related viruses. However, non-significant increases, compared to A549-Cas9.NC1 control cells, (table 5.1) were observed for the following: an increase in plaque area and intensity in A549-Cas9.HSD17B12$^{-/-}$ when infected with PIV5, an increase in plaque number in A549-Cas9.ZAP$^{-/-}$ when infected with PIV5, and an increase in both plaque number and area in A549-Cas9.ZAP$^{-/-}$ when infected with hRSV.

It is possible we observe non-significant differences between knockout cell lines and control cells due to the limited sample size inputted into the analysis method with an increased sample size overcoming this limitation. As we observe increased means in two out of three parameters in HSD17B12 and ZAP deficient cells, compared to control, upon infection of PIV5 and hRSV respectively, it provided increased confidence that deletion of these genes may be affecting viral replication of viruses related to hPIV3-GFP(JS). We observe high levels of variations in plaques on the same plate and so increasing the number of plaques available for analysis may reduce the standard deviation observed upon statistical analysis. For example, whilst the sample size of A549-Cas9.NF2$^{-/-}$ cells was small (n = 10), we observed significant differences compared to control cells, but the standard deviations of each parameter were smaller than those for plaques identified on HSD17B12 and ZAP deficient cells. In the case of HSD17B12, the lack of significant results could also be a combination of small sample size and known reduced cell health. Further repeats to increase total number of plaques available for analysis may enable to further elucidate the role of our genes of interest in replication of other viruses.

(a)

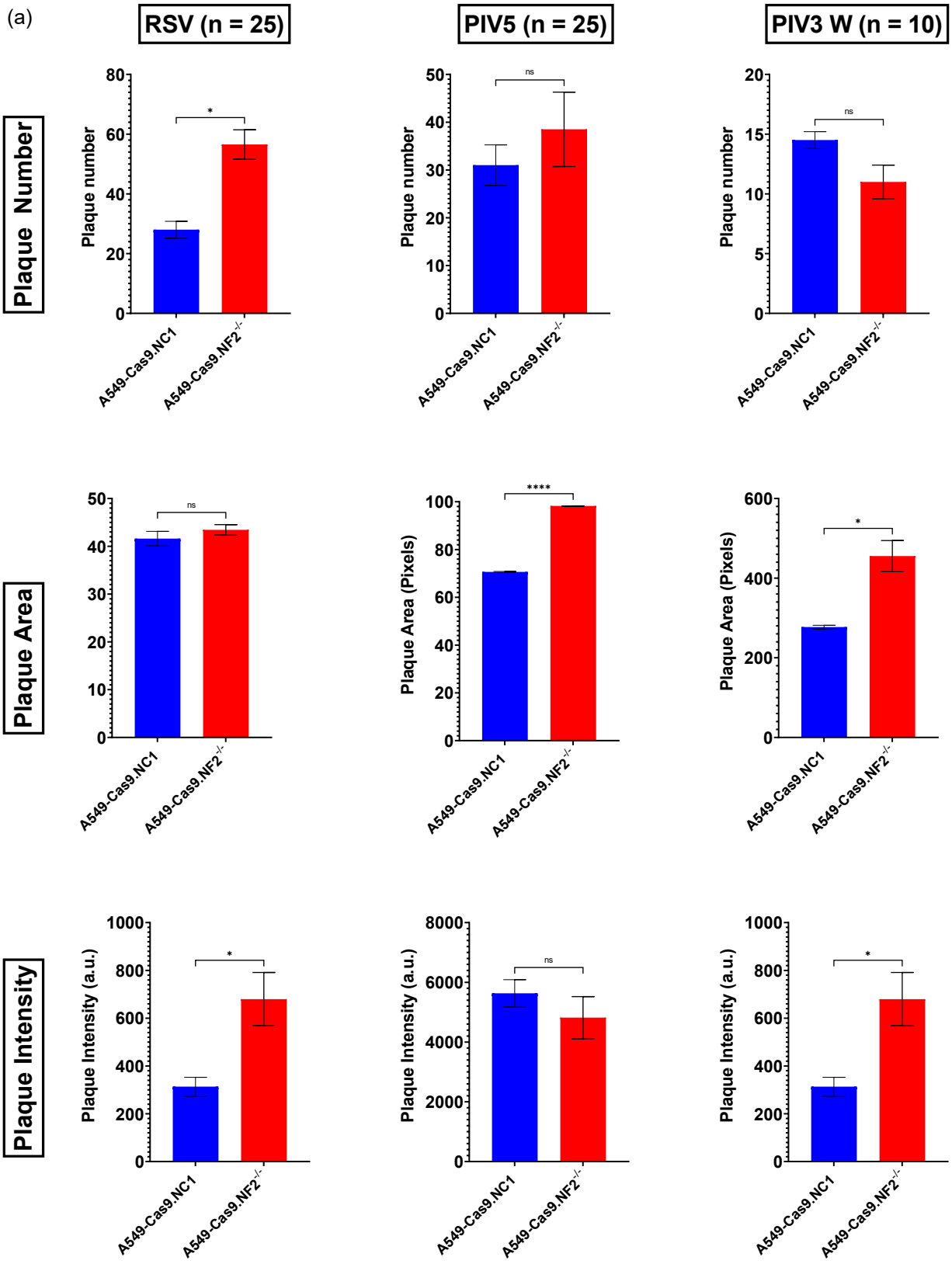
RSV (n = 25)
PIV5 (n = 25)
PIV3 W (n = 10)
Plaque Number
Plaque Area
Plaque Intensity
Plaque number
Plaque Area (Pixels)
Plaque Intensity (a.u.)
A549-Cas9.NC1
A549-Cas9.NF2-/-
*
ns
****

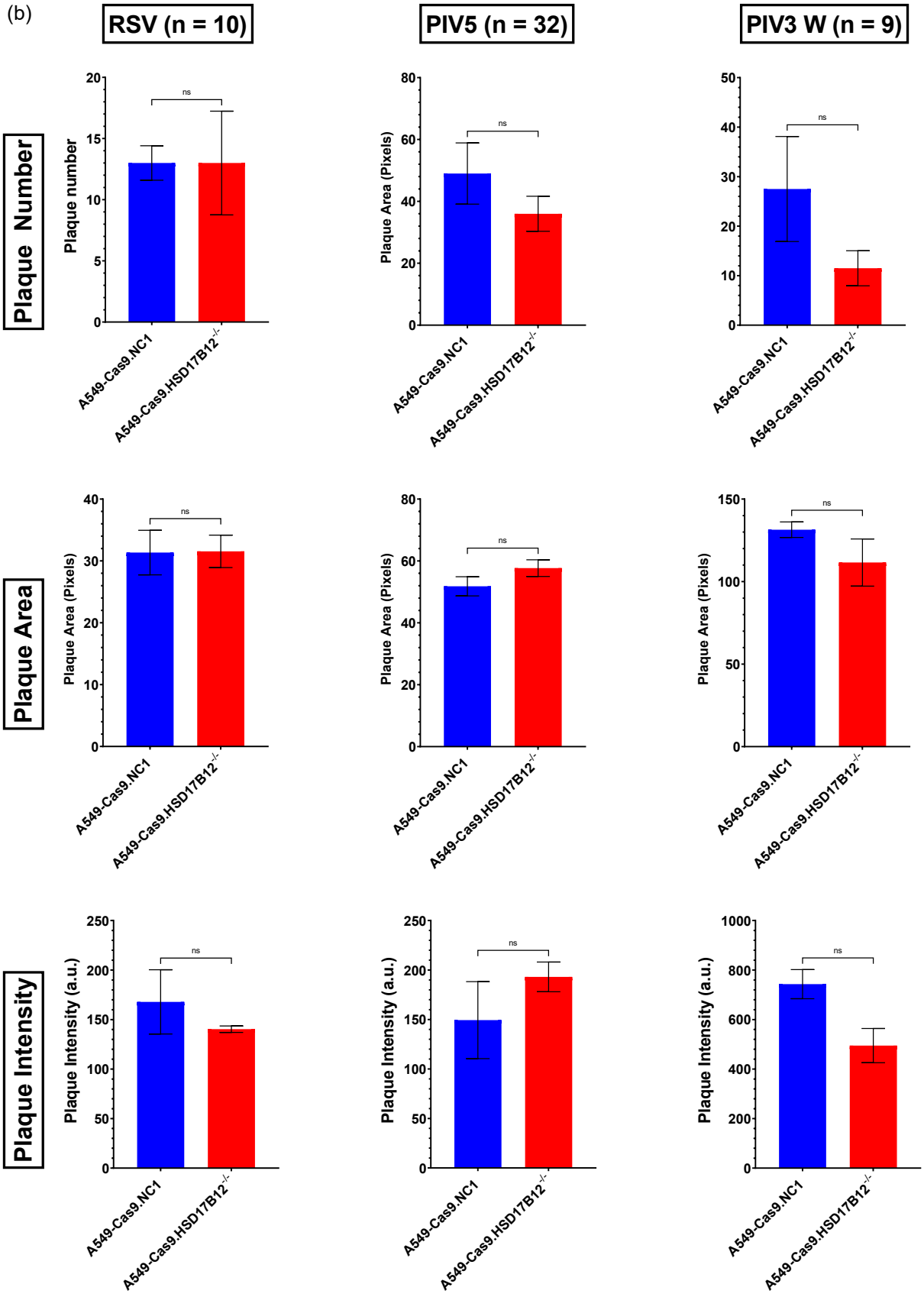
(b)
RSV (n = 10)
PIV5 (n = 32)
PIV3 W (n = 9)
Plaque Number
Plaque Area
Plaque Intensity
Plaque number
Plaque Area (Pixels)
Plaque Intensity (a.u.)
ns
A549-Cas9.NC1
A549-Cas9.HSD17B12-/-

(c)

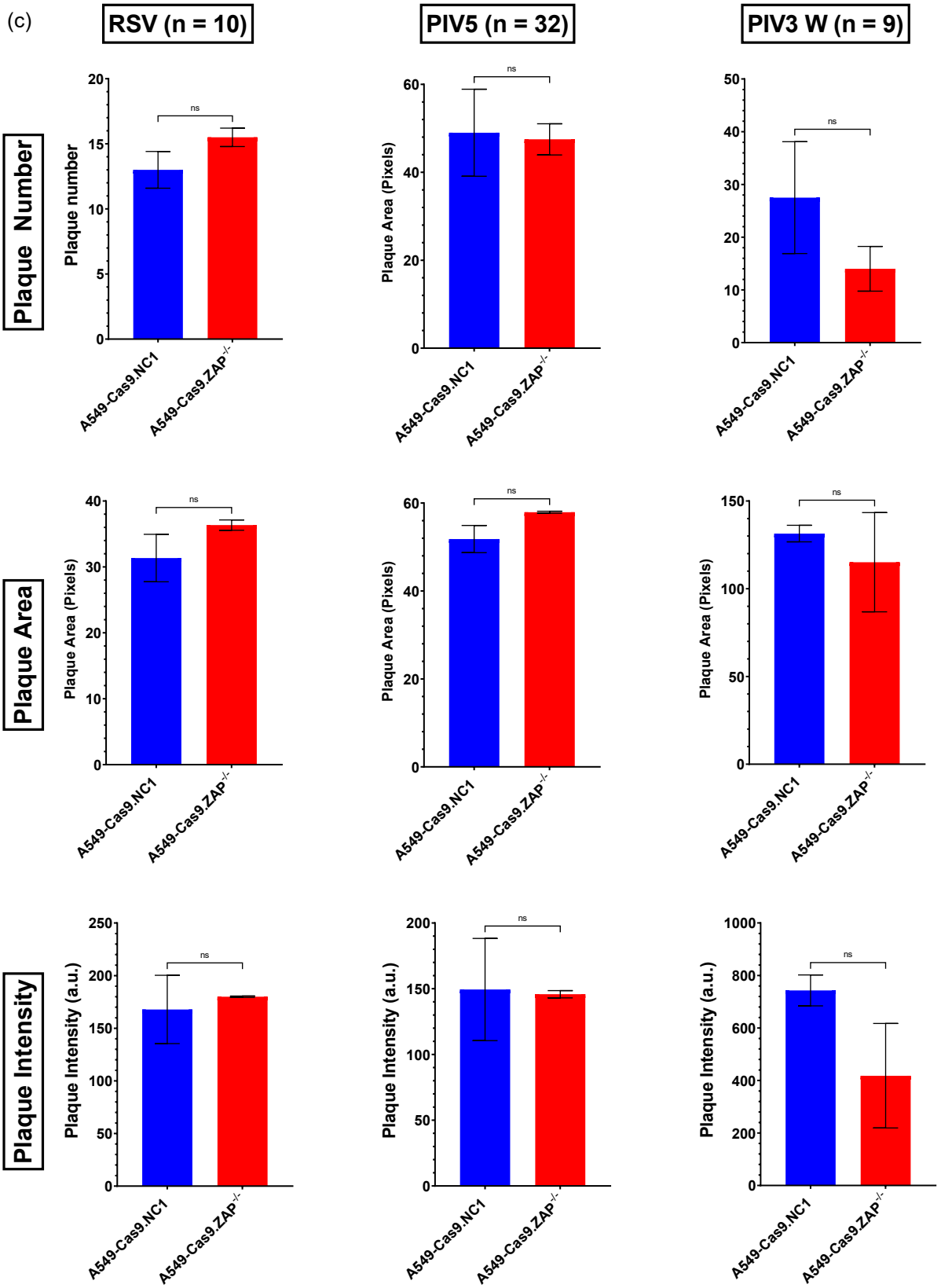
RSV (n = 10)
PIV5 (n = 32)
PIV3 W (n = 9)
Plaque Number
Plaque Area
Plaque Intensity
Plaque number
Plaque Area (Pixels)
Plaque Intensity (a.u.)
ns
A549-Cas9.NC1
A549-Cas9.ZAP-/-

Figure 6.6.1: NF2, HSD17B12, and ZAP are able to restrict other Paramyxo- and Pneumoviruses additional to hPIV3(JS). Knockout cell lines and A549-Cas9.NC1 cells were infected for 1 h with 20 - 30 PFU of hRSV-GFP, PIV5 (F157), and hPIV3(Washington) prior to addition of avicell overlay. Monolayers were fixed 6 d.p.i. Cells infected with PIV5(F157) were stained with a cocktail of anti-PIV5 antibodies specific for hemagglutinin (HN) followed by Alexa-488. Cells infected with PIV3(Washington) were stained with a cocktail of anti-PIV3 antibodies specific for hemagglutinin (HN) followed by Alexa-488. or hPIV3(Washington). Plaques were detected using Phosphor Imaging, Cy2 for identification of GFP-positive cells. Plaque number, area, and intensity of three technical repeats was quantified using randomly selected plaques (denoted by n) for infection with **(A)** hRSV-GFP, **(B)** PIV5(F157), and **(C)** hPIV3(Washington). Error bars represent the SD of the mean from three technical replicates. Statistical analysis performed using students t-test; ****, $p < 0.0001$, ***, $p = 0.0001$ to 0.001, **, $p = 0.001$ to 0.01, *, $p = 0.01$ to 0.05, ns, $p \geq 0.05$.

Table 6.6.1: Summary of data from figure 6.6.1. Data from figure 6.6.1 was summarised to highlight significant parameters by cell line. Significant differences denoted by '✓ and non-significant differences denoted by '×'. Parameters that are not significant but show an increased phenotype in knockout cells compared to A549-Cas9.NC1 are denoted by (*).

Cell Line	Virus	Plaque Number	Plaque Area	Plaque Intensity
A549-Cas9.NF2$^{-/-}$	hRSV	✓	×	✓
	PIV5	×	✓	×
	hPIV3(Washington)	×	✓	✓
A549-Cas9.HSD17B12$^{-/-}$	hRSV	×	×	×
	PIV5	×	× (*)	× (*)
	hPIV3(Washington)	×	×	×
A549-Cas9.ZAP$^{-/-}$	hRSV	× (*)	× (*)	×
	PIV5	×	× (*)	×
	hPIV3(Washington)	×	×	×

To further elucidate the potential role of NF2, HSD17B12 and ZAP as antiviral restriction factors, we took a data mining approach and looked for their presence in publicly available MaGeCK datasets from genome wide CRISPR/Cas9 screens investigating antiviral restriction factors for non-Paramyxovirus and Pneumovirus infections. Literature searching provided four available datasets to probe from IFN-α treated screens, identifying antiviral factors restricting the following viruses: YFV (Richardson et al., 2018), HIV-1 (OhAinle et al., 2018), SARS-CoV-2 (Mac Kain et al., 2022), and IAV (Sharon et al., 2020). NF2 and HSD17B12 were only observed in two data sets whilst ZAP was identified in all four. Data by Ohainle and Mac Kain was generated using a CRISPR/Cas9 sgRNA library of interferon stimulated

genes. As NF2 and HSD17B12 are not described as such, they were not included in experimentation and therefore do not appear in subsequent analysis.

Upon identification of the three genes of interest in these data sets (table 6.6.2), we observed highly varied rankings of all genes. Only the Ohainle (2018) screen investigating HIV-1 identified one of our genes as having a significant antiviral effect with ZAP receiving a MaGeCK ranking of 5. It was surprising that ZAP did not receive higher MaGeCK rankings in additional screens probed as it is known to be antiviral against many viruses. Instead, ZAP received MaGeCK ranking upon investigation of YFV, SARS-CoV-2, and IAV of 6145, 1479, and 18111 respecitively.

We see no significant effect of HSD17B12 restricting either YFV or IAV based on MaGeCK rankings from other studies. Additionally, the highest MaGeCK rank for NF2 is 421 against IAV. This suggests no observed antiviral role of these two genes of interest against other viruses based on other genome wide CRISPR/Cas9 screens. However, based on the observed inconsistencies seen with ZAP, a known antiviral factor, this demonstrates the large amount of discrepancy between studies, as detailed in section 1.3.4, and indicates that screen results should be individually validated and characterised.

Table 6.6.2: MaGeCK rankings of NF2, HSD17B12 and ZAP in genome wide CRISPR/Cas9 screens within the literature. MaGeCK rankings of NF2, HSD17B12 and ZAP were extrapolated from genome wide CRISPR/Cas9 screens in the literature looking at antiviral restriction factors targeting a wide range of viruses.

Virus	MaGeCK Rank			Reference
	NF2	HSD17B12	ZAP	
YFV	6724	9909	6145	(Richardson et al., 2018)
HIV-1			5	(OhAinle et al., 2018)
SARS-CoV-2			1479 (full length) 200 (long isoform)	(Mac Kain et al., 2022)
IAV	421	17735	18111	(Sharon et al., 2020)

6.7 Summary

We have further characterised three hPIV3-GFP(JS) antiviral restriction factors that also demonstrate potential in restricting other viruses. Following data that showed NF2, HSD17B12 and ZAP are able to restrict hPIV3-GFP(JS) infection at an MOI = 2.5, we subsequently investigated whether they were inducible genes or if they played a role in regulating the IFN response to answer the aims set out in section 6.1.

We identified that of the three genes of interest, ZAP was inducible as a result of IFN induction but not signalling. However, neither NF2 or HSD17B12 were inducible by either IFN induction stimuli or IFN-α,

with NF2 constitutive expression supported by immunoblot blot data showing equivalent protein expression in DI treated and non-treated A549-Cas9.NC1 cells.

Whilst only ZAP was found to be upregulated following IFN induction, we show that all three genes of interest appear to play a role in the regulation of the IFN induction pathway with knockout cell lines showing a reduction in mRNA expression of IRF3 inducible genes, IFN-β and ISG15, following DI treatment compared to A549-Cas9.NC1 control cells. In comparison, only NF2 was shown to have a significant role in the regulation of IFN signalling, with HSD17B12 deficiency having a minimal effect on expression of MxA, ISG15 and HERC5, and ZAP having no effect when compared to control cells.

However, we observed high levels of variability between repeats when looking at both plaque assay parameters and mRNA expression levels leading to a number of non-significant results despite the phenotype pattern of restriction being present. As previously described, this could be due to a number of factors including sample size and, in the case of HSD17B12 deficient cells, poor cell health. It has been proposed that variability in DI treated cells could be improved by using IFN-β reporter A549 cells, as opposed to looking at IFN-β mRNA expression using RT-qPCR. Nevertheless, our results, observed over multiple biological repeats (as previously described), convince us that the data shown is valid and the results observed are true.

Chapter 7: Discussion

7.1 Introduction

Viruses are obligate intracellular pathogens which have co-evolved with their hosts and as such, there is a large interplay between the two. The equilibrium of virus-host interactions determines the success or failure of a viral infection as the host provides both the machinery the virus requires to replicate, whilst also encoding counter measures against the virus to inhibit infection.

Genome wide screening is a powerful tool to study these virus-host interactions (section 1.3.3) and as such we developed and performed a genome wide CRISPR/Cas9 screen to study the interplay between Paramyxovirus infection and the host. We were interested to see if we could perform a genome wide CRISPR/Cas9 screen for the identification of both host dependency and antiviral factors influencing hPIV3(JS) infection; of which screening to investigate these questions has not previously been performed. The use of these screening methods not only allows the investigation of complex biological systems, but the identification of host genes involved in either helping or hindering hPIV3 infection provides us with novel information about this medically important virus. Information about genes that impact hPIV3 infection and elucidating their mechanism of action also allows the identification of potentially therapeutic targets.

Prior to performing the screen, conditions were first optimised to allow for the efficient isolation of genes of interest following infection of cells with hPIV3(JS). This led to the development of a screening platform that allowed for the identification of both host dependency and antiviral factors.

We also provided proof-of-principle for the use of ISG15 deficient cells in the identification of low to moderately acting ISGs by screening. As previously discussed in section 1.3.5, whilst it is known that hundreds of ISGs are expressed as a result of IFN signalling, and that they have diverse roles targeting every stage of the viral life cycle, for many viruses, which ISGs result in inhibition of viral replication is unknown. This is accompanied by a large amount of redundancy within the response, with many ISGs having low activity when expressed in isolation, requiring a combination of many to result in an antiviral phenotype. As such, the development of a method to improve the identification of low to moderately acting ISGs will enable an enhanced understanding of the antiviral response against many viruses and allow further utilisation of this technique for the identification of antiviral restriction factors.

7.2 Analysis of hPIV3(JS) host dependency factors

Following screening for the identification of hPIV3(JS) host dependency factors, eight hits were selected for further validation (section 4.6). However, validation of our host dependency screen confirmed only one selected hit, SLC35A1, as a true restriction factor out of the eight tested. This was surprising as all selected hits had varying amounts of literature citing them as potential host dependency factors, they all ranked within the top 35 MaGeCK rankings (table 6.2.1), and STT3A, in particular, is within the same pathway as SLC35A1.

Table 7.2.1: MaGeCK rankings of eight host dependency factor hits selected for validation.

Gene	MaGeCK Ranking
SLC35A1	2
STT3A	3
DHX9	23
UFC1	6
PTAR1	21
RAD51	31
SMU1	16
IMP3	24

7.2.1 Glycosylation and virus entry

We identified six hits required for glycosylation and sialic acid metabolism: STT3A, TMEM165, ALG2, ST3GAL4, and SLC35A1 (figure 7.2.1.1). Whilst sialic acid metabolism was not identified during gene ontology analysis, this provided us with confidence that sialic acid metabolism is crucial for successful hPIV3(JS) replication but also that our screen was able to identify key pathways, even with a limited cell number for NGS analysis. Our screen was not the first to identify SLC35A1 as a HDF for viral infection and so the literature was able to provide a strong case for subsequent validation of the hit. Moskovskich et. al performed a SLC-focussed CRISPR/Cas9 screen and identified both SLC35A1 and SLC35A2 as genes necessary for IAV infection with independent knockout of either resulting in increased resistance to IAV infection due to their non-redundant roles as CMP-sialic acid transporter and UDP-galactose/ UMP antiporter respectively (Moskovskich et al., 2019). Two additional genome wide CRISPR/Cas9 screens also identified SLC35A1 as an IAV HDF, with knockout resulting in decreased viral receptor expression and subsequent reduced IAV entry. The identification of SLC35A1 in multiple IAV screens, establishes the gene as a crucial component of viral entry via the sialic acid pathway. As mentioned, this provided confidence that SLC35A1 also plays a key role as a host dependency factor in hPIV3(JS) replication as our virus also uses sialic acid for viral entry (Suzuki et al., 2001). Another hit we took forward from the glycosylation pathway was STT3A; an oligosaccharyltransferase which is a key component in catalysing the first step of the glycosylation pathway (Harada et al., 2019). STT3A inhibitors have been shown to result in an antiviral phenotype of two viruses suggesting that upstream components, as well as downstream components, including SLC35A1, play a role in successful viral entry and replication. SARS-CoV-2 requires glycosylation of its S protein and inhibition of this step results in reduced infectivity (Huang et al., 2021). Similarly, use of a STT3A inhibitor, NGI-1, results in dysfunctional HSV-1 infection (Lu et al., 2019). The evidence of STT3A in promoting infectivity of both RNA and DNA viruses, alongside the known requirement of glycosylation and sialic acid presentation for hPIV3 infection, led us to believe that STT3A would also be a HDF for hPIV3, like SLC35A1, but this was not the case following validation (figure 4.6.1). STT3A is one of two isoforms co-expressed in mammalian tissues (Ruiz-Canada, Kelleher and Gilmore, 2009; Lu et al., 2018; Harada et al., 2019) and so it could be that the other isoform is able to complement its

role in its absence, so it does not result in a strong phenotype. Conversely, SLC35A1 is the only gene that performs sialic acid transport, as identified in the literature, and so knockout cannot be complemented.

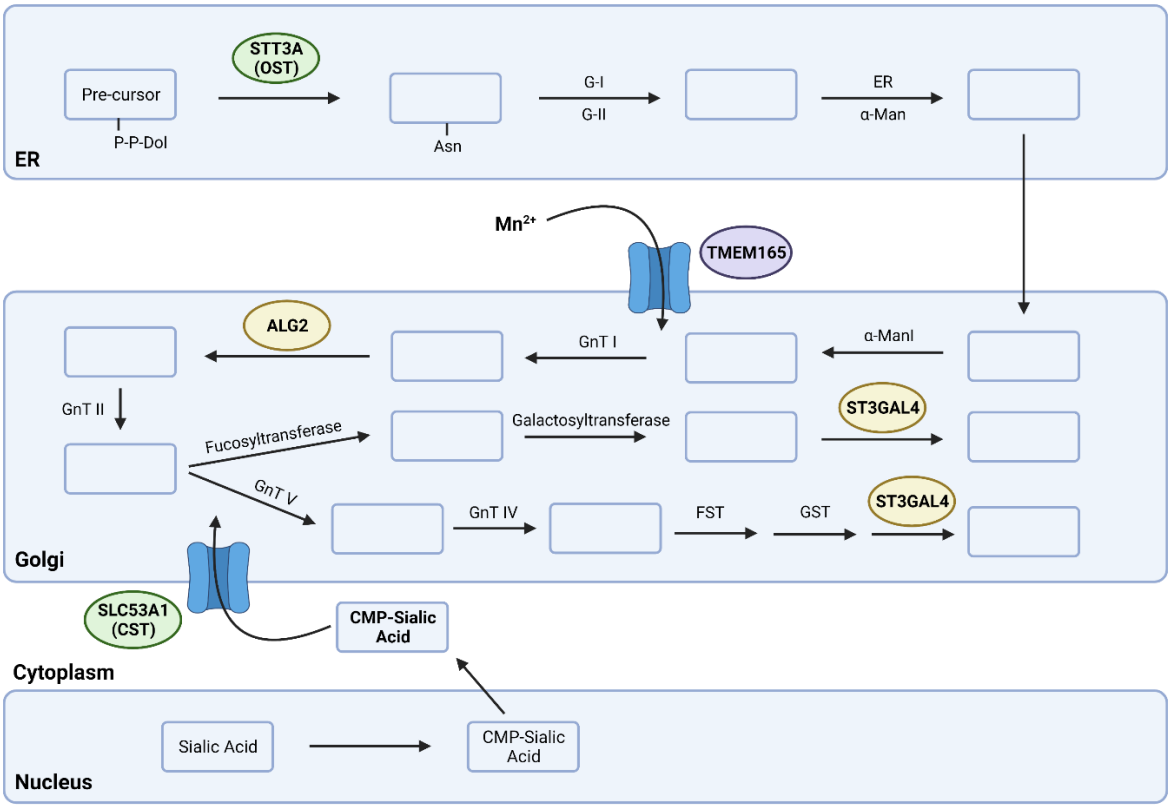

Figure 7.2.1.1: Host dependency hits within the glycosylation pathway. Illustration of five of the hits identified to be within the glycosylation pathway: STT3A, TMEM165, ALG2, ST3GAL4, and SLC35A1. Hits taken forward for validation (green), hits to pass the false discovery threshold (purple), and others (yellow).

Preliminary data suggested that PTAR1 was validated as a true host dependency factor however, upon biological repeats the difference from control became non-significant. This potentially indicates a very weak role of the gene in supporting hPIV3(JS) infection, supporting the idea that there is redundancy in the system and that other genes are able to fulfil the role of PTAR1 in its absence. PTAR1 is a prenyltransferase subunit required for post-translational modifications of proteins. Knockout results in inhibition of glycosylation pathways alongside a decrease in cell surface heparan sulphate (Jae et al., 2013; Blomen et al., 2015) with studies showing that PTAR1 is important for RVFV infection with disruption resulting in RVFV resistance (Riblett et al., 2016).

It is known that some members of the Paramyxovirus and Pneumovirus families utilise heparan sulphate for cell entry. For example, the G protein of Henipaviruses, HeV and NiV, bind to Ephrin B2/B3 dependant on cellular heparan sulphate (Holen et al., 2011; Xu, Broder and Nikolov, 2012; Mathieu et al., 2015), and RSV G proteins and HMPV F, interact with and bind to heparan sulphate proteoglycans (Chang et al., 2012; De Pasquale et al., 2021). Additionally, it has also been shown that hPIV3 is able

to use heparan sulphate for cell entry alongside sialic acid (Bose and Banerjee, 2002), suggesting that PTAR1 may be necessary for successful virus entry and subsequent replication. However, upon inhibition of proteoglycan sulfation, virus entry was not completely blocked. We have shown that SLC35A1 deficiency, a gene required for sialic acid entry, inhibits hPIV3(JS) replication, when investigated by flow cytometry and RT-qPCR, and so it is possible that the role of PTAR1 in the role proteoglycan sulfation is not prominent enough, without the abolition of other entry routes, to provide a phenotype when looking at single knockout, with the expression of other genes supplementing its role. However, this does not provide explanation for it being picked up by MaGeCK in the original screening data. PTAR1 had five good sgRNAs identified within MaGeCK analysis, a threshold that only 20% of significantly positive genes passed in the negative compared to high fraction. As such, it may be that due to the limited number of guides identified, this enabled PTAR1 to rank higher than it would have otherwise done if more cells were sorted thereby being put on our radar for further validation. Together, this suggests a level of redundancy within host dependency factors, as well as antiviral restriction factors, with moderately acting genes not presenting a strong enough phenotype for their true validation.

7.2.2 Limitations in validating host dependency factors

Seven out of eight hits were not validated as true host dependency factors despite being identified from the literature. SLC35A1, the only gene to be successfully validated of the eight, was also the only gene that passed the false discovery rate threshold, a threshold we have identified to be important for the identification of true hits from our genome wide CRISPR/Cas9 screens. The importance of this threshold was further supported following validation of our AF hits (section 4.3), in which two of the three validated to be true hits were the only two hits, besides from internal control genes, that passed the FDR threshold.

As previously mentioned, the lack of genes passing this threshold could be due to a multitude of reasons. Far fewer cells than anticipated were recovered following sorting leading to a low number of cells inputted into downstream processing and gDNA extraction. This was due to the implementation of smaller gates to prevent overlap of fractions (section 4.5). Additionally, the amount of gDNA extracted from sorted cells for NGS preparation was much less than expected, with approximately 30% of gDNA recovered, based on 6 pg DNA/ cells, and 70% of DNA being lost. The reduced number of sgRNAs subsequently extrapolated from the samples and put through the MaGeCK package would reduce the statistical power of the algorithm. As described in section 3.2, the algorithm works by assessing variability within the same sgRNAs and performing a robust rank aggregation, assessing whether genes are consistently clustered or more highly distributed in a positive or negative direction (Li et al., 2014). As such, fewer analysed cells will result in a reduced gDNA extracted, and a reduced number of sgRNAs identified, observed as a low number of ‘good sgRNAs’ during MaGeCK analysis. This enhances the effect of the variability observed and prevents genes from passing the threshold. Whilst all hits passed the significance threshold, they did not all pass the FDR threshold; the FDR threshold being a more stringent threshold that considers the ratio of false positive results to the number of total positive results,

a ratio that increases as sample size decreases. The ability of our screen to identify genes that pass the FDR threshold is therefore a clear limitation of our investigation. However, the observed loss of gDNA extracted could be attributed to fixation of cells prior to sorting. During small scale optimisation (figure 4.4.5), the reduced amount of gDNA extracted was not identified as having a significant impact on results. However, at larger scales, such as our screen, this impact became evident. Therefore, future screens should primarily be performed using non-fixed cells unless unavoidable.

7.3 NF2

Following screening for the identification of hPIV3(JS) antiviral restriction factors, eight hits were selected for further validation (section 5.3). Three hits were validated as true restriction factors and were taken forward for further characterisation: NF2, HSD17B12, and ZAP.

Upon knockout of NF2 we observed an increase in infectivity of hPIV3-GFP(JS) by flow cytometry and RT-qPCR (section 6.3), identifying the gene as an antiviral factor. We have shown that NF2 is a constitutively expressed gene that is not upregulated by IFN induction or signalling but it does play a role in regulating both components of the IFN response, and so we wished to begin elucidating its mechanism of action from the literature.

7.3.1 NF2 and the Hippo-YAP pathway

NF2 is a known component of the Hippo-YAP pathway (reviewed; (Wang et al., 2020)), facilitating the phosphorylation, and subsequent activation, of LATS1/2 by MST1/2. Activation of LATS1/2 results in the phosphorylation of YAP/TAZ, leading to its cytoplasmic retention, due to an interaction with 14-3-3, or poly-ubiquitination and subsequent degradation; this puts YAP/TAZ into its inactive form (Poltorak et al., 1998; Lallemand et al., 2003; Yin et al., 2013). When in its active form, YAP/TAZ is a negative regulator of IFN induction and so its inactivation, dependent on NF2, means NF2 is a positive regulator of IFN induction (figure 7.3.1). This regulation by NF2 is multifaceted with YAP/TAZ and upstream components having well established roles in the regulation of IFN induction. It has previously been shown IRAK1 can inhibit RIG-I-induced IFN-β expression through its kinase activity (An et al., 2008). However, MST1/2 has been shown to inhibit IRAK1, through phosphorylation, to prevent this negative regulation. This leads to enhanced IFN-β expression via increased IRF3 activation (An et al., 2008; Bruni et al., 2013; Li et al., 2015). YAP/TAZ is known to inhibit TBK1 by inhibiting its interaction with MAVS, STING and IRF3 leading to a decrease in type I IFN (Zhang et al., 2017). It has also been shown to directly inhibit the dimerization and nuclear localisation of IRF3 (Wang et al., 2017). However, upon activation of MST1/2, LATS1/2 is able to inhibit these functions of YAP/TAZ. The IFN response also enters a positive feedback loop with Hippo-YAP signalling, with phosphorylated IRF3 inducing the expression of MST1 from the MST1 promoter to further upregulate its antiviral effector functions (Yuan et al., 2017). However, there is an internal control switch to prevent over expression of IFN-β as MST1 is additionally able to inhibit both TBK1 and IRF3 (Meng et al., 2016). As MST1 can be expressed from

the MST1 promoter as a result of IRF3 binding, this activity is NF2 independent. Because NF2 inactivates the YAP/TAZ pathway, cells deficient in NF2 will be more susceptible to viral infection, as observed in section 5.3. This is because MST1 will not be activated, resulting in the negative regulation of RIG-I by IRAK1. Additionally, in the absence of NF2, LATS1/2 is not activated by MST1/2 and so YAP/TAZ phosphorylation is reduced, thereby preventing its degradation and cytoplasmic retention. This results in inhibition of TBK1 and IRF3 by YAP/TAZ, a diminished IFN response, and subsequent uninhibited viral replication.

We observed that IRF3 protein expression was reduced in DI-treated (RIG-I agonist) NF2 deficient cells compared to control by western blot. This correlated with decreased IFN-β and ISG15 mRNA expression in NF2 deficient cells compared to control, both genes that are expressed as a result of IRF3 dimerization and nuclear translocation. We therefore postulated if IRF3 degradation was linked to YAP/TAZ regulation of TBK1 and IRF3. In NF2 expressing cells, YAP/TAZ is inhibited and so TBK1 can activate IRF3 for binding to the IFN-β promoter. However, in cells deficient in NF2, YAP/TAZ is able to inhibit both TBK1 and IRF3 in mechanisms previously described. It has previously been shown that RBCK1 is able to negatively regulate the IFN response by mediating degradation of IRF3 resulting in upregulated viral infection (Zhang et al., 2008). Therefore, it may be possible that an increase in non-phosphorylated IRF3 accumulation in the cytoplasm in NF2 deficient cells results in a more rapid turnover by proteins such as RBCK1.

7.3.2 A novel role of NF2 in IFN signalling

Whilst the role of NF2 in regulating IFN induction has been well characterised, its role in IFN signalling is less so. Previous work has described the role of a TAZ isoform, cTAZ, that contains a C-terminal domain but not TEAD binding or WW domains. However, as it lacks a WW domain, it is unable to interact with LATS1/2 and as such, it is not regulated by and lacks Hippo-YAP functions (Fang et al., 2019). Instead, it is an isoform transcribed by an alternative promoter induced by type I IFN JAK-STAT signalling. cTAZ then acts as a negative regulator of JAK-STAT signalling by disrupting the dimerization and nuclear translocation of STAT1 resulting in the decreased expression of ISGs from ISRE-containing promoters. However, as cTAZ is not regulated by Hippo-YAP signalling, NF2 does not play a role within negative regulation of IFN signalling by cTAZ. As such, the regulative role of NF2 in IFN signalling, observed in section 5.3.4, is still not fully explained. Currently, there is no evidence in the literature of NF2 regulating IFN signalling, and so further experimental investigation may elucidate a novel role of NF2 in within innate immunity.

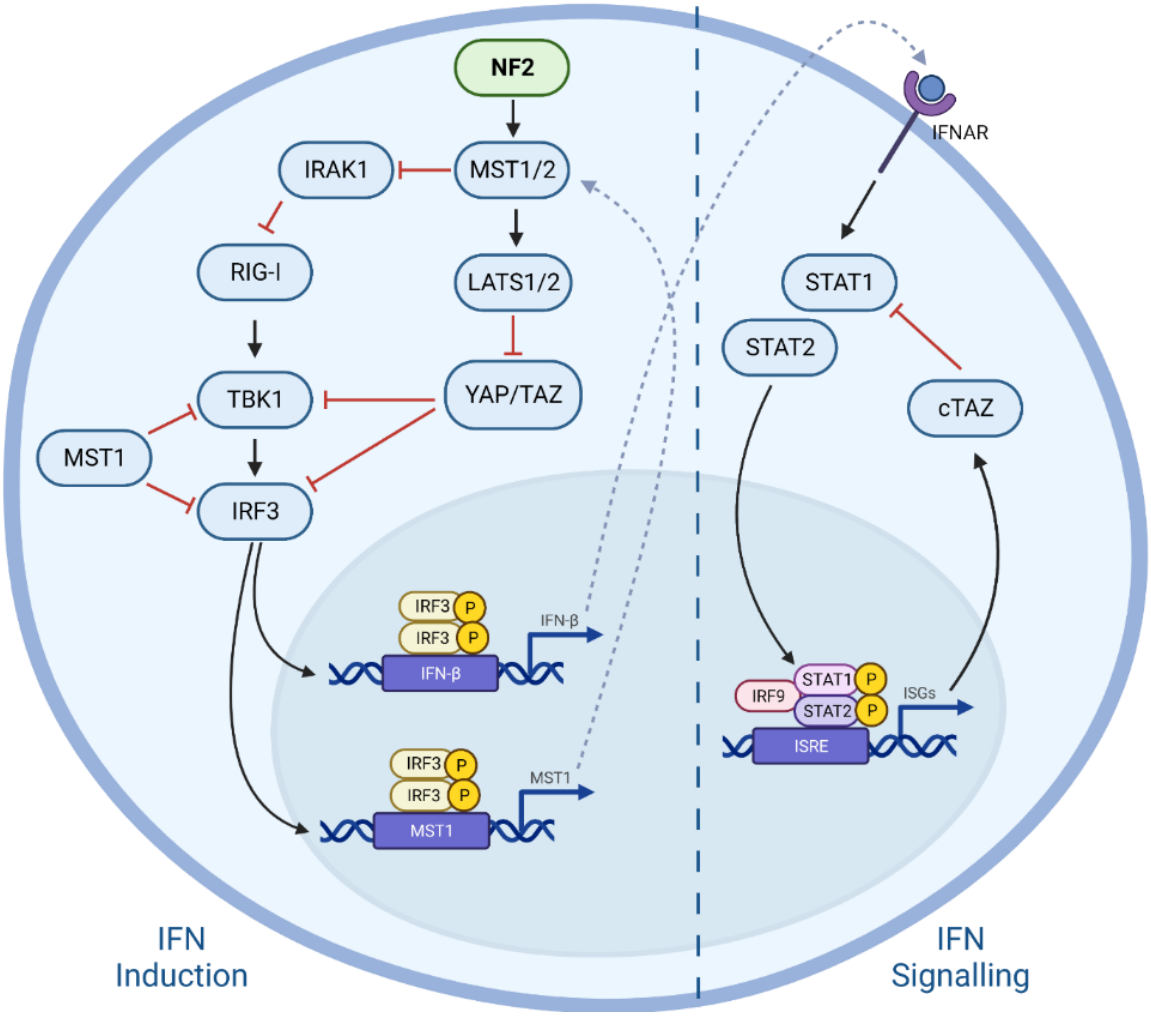

Figure 7.3.1: Mechanisms of NF2 in regulating the IFN response. NF2 (green) is an upstream regulator of the Hippo/YAP pathway resulting in the inactivation of YAP/TAZ. YAP/TAZ is a negative regulator of IFN induction in an NF2-depndent manner, and a differentially expressed isoform is a regulator of IFN induction in an NF2-independent manner.

7.4 HSD17B12

We identified HSD17B12 to provide an antiviral phenotype through the regulation of IFN induction, but not signalling, as shown through its knockout in A549 cells. Results showed decreased expression of IRF3-dependent genes in HSD17B12 deficient cells compared to control, but not those expressed from ISRE-containing promoters (section 6.4). HSD17B12 is a crucial enzyme in the steroid metabolism pathway, catalysing the second step in fatty acid elongation beyond palmitic acid (Mohamed et al., 2020). It is therefore essential for very long chain fatty acid (VLCFA) synthesis.

7.4.1 HSD17B12 and lipid droplets

Lipid droplets (LDs) are intracellular storage organelles composed of triglycerides and VLCFAs, such as oleic and stearic acids, and HSD17B12 is essential to their formation and maintenance (Mohamed et al., 2020; Monson et al., 2021a; 2021b). As such, it has been shown that HSD17B12 knockdown results in a decrease in number, area, and density of LDs due to the decrease in oleic acid and subsequent increase in abundance of its palmitic acid precursor with supplementation of oleic acid able to rescue the formation of LDs in HSD17B12 knockdown cells (Rohwedder et al., 2014; Mohamed et al., 2020; Monson et al., 2021a). Lipid droplets have three predominant functions: lipid storage and transport, metabolism, and protein storage and degradation (Monson et al., 2021b). They have been shown to perform various roles during infection with previous work showing that an increase in LDs can protect against bacterial infection in cell culture and zebrafish fish models (Monson et al., 2021a). They are also known to act as signalling platforms to regulate signalling and interact with other organelles (Monson et al., 2021a). However, their role in viral infection is still to be fully understood with research showing both an antiviral and proviral role of these cytoplasmic organelles (Mohamed et al., 2020; Monson et al., 2021b; 2023).

Flaviviruses and other positive sense RNA viruses lack their own enzymes for lipid synthesis and as such, require host machinery and lipid droplets for virion assembly and successful replication. For example, DENV utilise LDs as a scaffold for the assembly of nucleocapsids alongside using LDs as energy substrates to boost metabolism by upregulating lipophagy (Monson et al., 2021b). Additionally, it has been shown that that a reduction in the number of LDs in a cell, reduces the number of infectious HCV particles produced (Mohamed et al., 2020). However, use of LDs for successful virion assembly has so far only been described in the literature for (+) ssRNA viruses (Altan-Bonnet, 2017; Zadoorian, Du and Yang, 2023). Conversely, it is known, and well described that (-) ssRNA viruses, including Paramyxoviruses, RSV, and Rabies, utilise liquid-liquid phase separation replication compartments rather than LDs (Lahaye et al., 2009; Risso-Ballester et al., 2021; Su et al., 2021).

Additionally, previous work has shown an interplay between LDs and innate immunity, specifically the IFN response (figure 7.4.1). An increase in LD number has been shown to increase expression of type I and type III IFN with increased expression of IFN also resulting in increased abundance of LDs (Monson et al., 2021a). This has been demonstrated by both infecting cells with virus and by using PAMP mimics to induce the IFN response. Upon infection of primary astrocytes with either HSV-1, IAV, DENV or ZIKV, increased LD accumulation was observed as soon as 2 h.p.i, decreasing 72 h.p.i, and resulted in decreased viral replication of all viruses. This has also been shown *in vivo* in mice, with an increase in large LDs observed in bronchioles following IAV infection as well as increased LD accumulation in mice infected with LCMV at both 2 and 4 d.p.i compared to controls (Monson et al., 2021a). As previously mentioned, studies investigating the interplay between innate immunity and LD formation have also used PAMP mimics, specifically poly I:C, an RNA mimic that engages RLR and TLR receptors. It was shown that activation of TLRs by poly I:C recapitulated the results seen upon infection with an increase in LD number but not size (Monson et al., 2021a).

Work by multiple groups has shown that the accumulation of LDs is biphasic; first in an IFN-independent manner and then IFN-dependent (Rohwedder et al., 2014; Monson et al., 2021a). In response to a PAMP, TLR activation engages the EGFR, the predominant activation route, resulting the in the accumulation of LDs independent of IFN. Through a mechanism yet to be determined, this accumulation of LDs results in an increase in type I and III IFN production. Work in Vero cells, deficient in a functioning IFN response, has shown that when stimulated with dsRNA, an IFN independent increase in LD size and number was observed. This IFN independent response has been additionally shown following infection with both HSV-1 and ZIKV with inhibition of the EGFR, resulting in a decrease in IFN-β at both the mRNA and protein level alongside reduced LD formation and subsequent increased viral replication at 24 and 48 h.p.i (Monson et al., 2021a). Correlation between LD accumulation and type I and III IFN expression has also been observed in HeLa and Huh-7 cells as well as the previously describe primary astrocytes (Monson et al., 2021b). Release of IFN from the cell and binding to the IFN receptor, results in a secondary wave of LD accumulation that is IFN dependent. This IFN dependent mechanism was shown through conditioned media, containing secreted IFN, being placed onto Vero cells resulting in increased LD accumulation; however, blocking of IFNAR1 is able to reverse this effect. Additionally, LD accumulation was seen to mimic the known high turnover of IFN mRNA with a sharp increase between 2 and 8 h post-treatment and back at baseline by 72 h (Monson et al., 2021a). A biphasic pattern is also seen in an increase in LD number following oleate treatment of Huh-7 cells. Infected cells treated with oleate show a sharp increase in LD number at early timepoints, followed by a plateau and a continuous but slower rate of increase at later timepoints. It has been proposed that the first stage of rapid LD formation is oleate-independent and a result of a signalling response, with LDs generated from existing cellular lipids, and at later time points oleate is incorporated into LDs (Rohwedder et al., 2014). This correlates with the biphasic model proposed whereby the first stage in IFN-independent, suggesting to be as a result of EGFR signalling, and the second stage IFN-dependent by a yet uncharacterised mechanism. This is further supported by evidence that addition of oleic acid can further upregulate the number of LDs and subsequent transcription of IFN and ISGs following infection with HSV-1, IAV, DENV or ZIKV (Mohamed et al., 2020; Monson et al., 2021a).

7.4.2 The interaction between lipid droplets and ISGs

As well as interplay between IFN and LDs, ISGs have also been shown to localise to LDs. These include viperin, members of the IRGM family, STAT1/2, RIG-I and MDA5 (Monson et al., 2021b; 2023). Upon infection of mice with LCMV, a proteomics approach to look at components of LDs and LD associated proteins at 4 d.p.i found differently upregulated genes within ‘cellular defence response to virus’ and ‘response to IFNs’ pathways. Of the proteins found within these pathways, the percentage of proteins associated with LDs was analysed. This analysis showed that Viperin, a known LD associated ISG, localised to 54.8% of LDs, STAT1 to 44.9%, and STAT2 to 29.9%. Further investigation at 8 h.p.i showed that phosphorylated STAT1 was localised to a higher percentage of LDs than its non-phosphorylated form (Monson et al., 2023). Outside of infection models, viral RNA mimics have been utilised to identify additional components of the IFN response that localise to LDs. Through this method,

RIG-I, MDA5 and MAVs have all been identified. Mitochondria, with MAVS associated, has been shown to localise to LDs alongside RIG-I to form a signalosome complex for IFN induction upon infection with ZIKV or dsRNA stimulation (Monson et al., 2023). These proteomic changes in LDs are dynamically changed following viral infection showing the organelles are sites for enhanced interactions important for IFN induction and antiviral phenotype. Additionally, work in a *C. elegans* model has shown a lipid dependent effect on infection outcome. In mutants deficient in oleate production, expression of irg-4, a known immune effector, is reduced compared to controls resulting in increased susceptibility to bacterial infection. This phenotype was shown to be the result of fatty acid availability with oleate supplementation complementing the phenotype and knockdown of pathways upstream of oleate synthesis resulting in the same bacterial susceptibility phenotype.

It was shown that infection susceptibility in oleate deficient mutants was further exacerbated upon knockdown on the Toll/IR-1 protein domain in *C. elegans* (Anderson et al., 2019b). Within mammalian cells, TLR adaptor proteins contain TIR domains and so this may suggest a link between TLR activation of LDs in cell culture models and *C. elegans* supporting TLR activation of LDs and their antiviral function. Furthermore, it has been found that members of the IRGM family, IRGM1 and IRGM3, localise to LDs (Monson et al., 2021b). These are ISGs that regulate autophagy, with their autophagy and host response regulation dependent on LD interaction. Whilst autophagy is known to have an antiviral effect through destroying infectious virions or activating an innate or adaptive immune response, some viruses use it to promote replication, for example MeV (Grégoire et al., 2011). It has been shown that a siRNA depletion of IRGM expression, results in decreased MeV replication with the C protein shown to interact with IRGM to exploit autophagy. Whilst it might not be the activity of IRGM, as a result of LD accumulation, resulting in an antiviral activity against Paramyxoviruses, it has not yet been investigated whether additional ISGs, other than those previously described, use LDs to enhance their activity or activation.

7.4.3 Other implications of HSD17B12 deficiency

HSD17B12 may also be playing an antiviral role outside of lipid droplet formation as it is also required for the synthesis of arachidonic acid (AA), the precursor of prostaglandin E2 (PGE_2) (Kemiläinen et al., 2016). Prostaglandins are lipid compounds derived from AAs that are involved in a number of cellular processes and pathways (Pettipher, 1998). However, their role in regulation of viral infection is still under debate with contradicting literature indicating both proviral and antiviral roles; reviewed in (Sander, O'Neill and Pohl, 2017). However, it has previously been shown that PGE2, the downstream product of AA, inhibits PIV3 replication in a mechanism not characterised (Luczak et al., 1975).

The role of HSD17B12 in VLCFA synthesis has large effects on host cell processes and subsequent viability. Validation and characterisation of HSD17B12 has therefore been difficult due to poor cell health in our knockout cells. Whilst cell viability has been poor in HSD17B12 knockout out cells, previous work has shown that HSD17B12 knockdown, rather than knockout, does not affect the viability of proliferation of Huh-7 cells (Mohamed et al., 2020) and so knockdown, inducible or not, may allow characterisation

of this gene of interest. Additionally, it may be that supplementation of oleate or oleic acid, as previously described, may preserve knockout cells in general passage until required for experimentation. These changes may allow us to further elucidate the mechanism of action of HSD17B12 as an antiviral factor.

Based on literature analysis, it is likely the role of HSD17B12 in lipid droplet formation that is resulting in the observed regulation of IFN induction. However, the role of lipids in both host processes and viral infection is vast and implicated in many pathways. As such, the role of HSD17B12 in the formation of VLCFAs and restriction of hPIV3(JS) may be multitudinous. It is therefore perplexing as to how HSD17B12 was identified from the IFN screen if, as previously described, it does not display a strong antiviral phenotype in isolation. A possible explanation is that screens, and initial validation of hits, were performed at a low passage, and we observe that cell health in HSD17B12 deficient cells decreases over time. Therefore, it may be possible that cell health of the knockout cells was viable enough for its mechanism of action to have an antiviral effect. Nevertheless, it is likely to be a true result, not amplified by the lack of other gene passing the false discovery threshold, as statistical outputs were calculated from only two good sgRNAs out of five. This suggests that results were not due to a higher number of sgRNAs being extrapolated from the NGS dataset than other genes. As such, characterisation at very low passage number, or HSD17B12 knockdown, may allow further investigation of this antiviral factor.

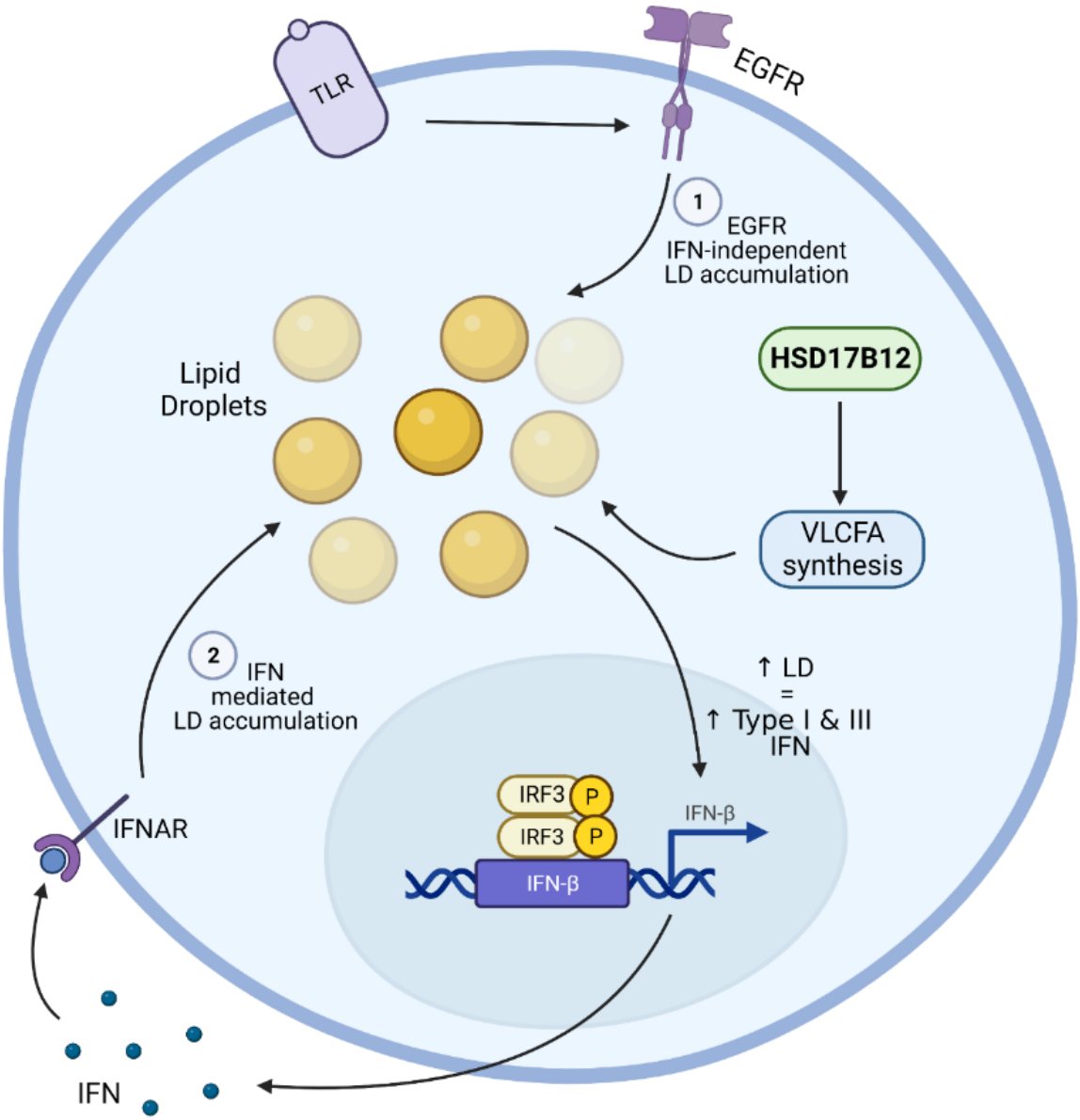

Figure 7.4.1: Role of HSD17B12 is regulating IFN induction. HSD17B12 is a key component of very long chain fatty acid synthesis, a key component of lipid droplet formation which is a biphasic process resulting in (1) the accumulation of lipid droplets following PAMP stimulation and an increase in type I and III IFN expression and (2) IFN mediated LD accumulation resulting in enhanced IFN induction.

7.5 ZAP

We identified ZAP (identified as ZC3HAV1 in our MaGeCK analysis) to be a hPIV3-GFP(JS) restriction factor. Results showed that ZAP was both IRF3 inducible and plays a role in the regulation of IFN induction whilst not playing a role within IFN signalling, unlike NF2. It was not surprising that we identified ZAP to play an antiviral role against hPIV3(JS) as it is a known broad antiviral factor described to target several viruses, both with RNA and DNA genomes (Ficarelli, Neil and Swanson, 2021). These include IAV, SeV, NDV, Alphaviruses, SINV, JEV, SARS-CoV-2 and HBV (Bick et al., 2003; Hayakawa et al., 2011; Mao et al., 2013; Gaunt et al., 2016; Li et al., 2017; Chiu et al., 2018; Zhang et al., 2020).

Multiple ZAP isoforms are present as a result of alternative splicing, the most common being the short form (ZAPS) and the long form (ZAPL). Whilst all isoforms contain a N-terminal RNA binding domain with four CCCH-type zinc finger motifs, they differ in their C-terminal domains with ZAPL also possessing a C-terminal PARP-like domain with no ADP-ribosyltransferase activity (figure 7.5.1). These two isoforms have been shown to differ in their cellular localisation and activity with ZAPS shown to have a regulatory role and ZAPL a more direct antiviral role (Ficarelli, Neil and Swanson, 2021). This difference in subcellular localisation is determined by prenylation of the C-terminal CaaX motif and farnelysation present in the ZAPL PARP-like domain which targets ZAPL to endolysosomal membranes (Chemudupati et al., 2019; Schwerk et al., 2019).

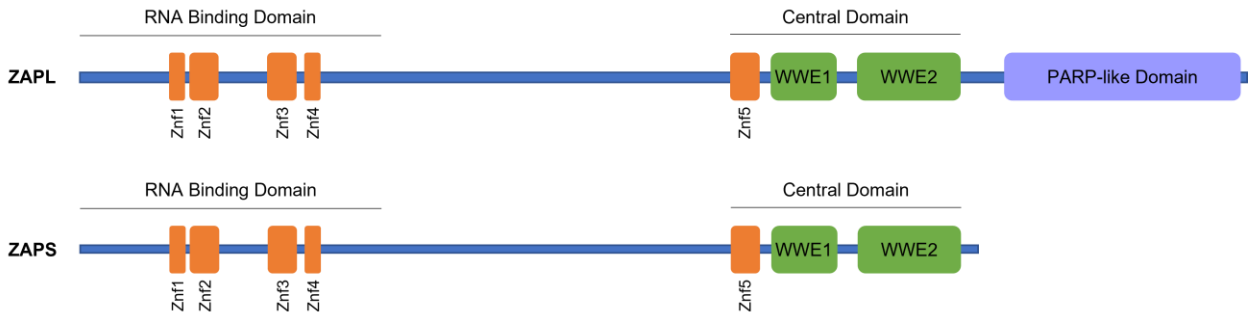

Figure 7.5.1: Schematic of ZAP isoform gene structures. Both ZAPS and ZAPL contain an N-terminal RNA binding domain, able to bind CpG motifs, and a central domain. ZAPL additionally contains a catalytically inactive PARP-like domain which results in differential cellular localisation. (Adapted from (Ficarelli, Neil and Swanson, 2021)).

7.5.1 ZAPS

ZAPS has been shown to have a role in the regulation of IFN induction; however, this is still contested with opposing literature (Ficarelli, Neil and Swanson, 2021). The short isoform has been shown to enhance production of type I IFN by mediating RIG-I, NF-kB and IRF3 (Hayakawa et al., 2011). Following NDV infection, ZAPS has been shown to interacts with RIG-I via its carboxy-region domain resulting in enhanced IFN production by promoting RIG-I oligomerisation. Additionally, knockdown of

ZAPS was shown to result in reduced IRF3 dimerization and subsequent nuclear localisation. This is described to be as a result of ISRE and IRF-binding elements within the ZAP promoter region (Hayakawa et al., 2011). Similarly, ZAP knockdown results in the reduction of phosphorylated IRF3 following IAV infection resulting in suppression of IFN-β mRNA in A549 cells (Zhang et al., 2020). This effect was ZAPS-dependent and ZAPL-independent indicating that ZAPS is a positive regulator of the IFN response in an IRF3-depdent manner, not requiring the PARP domain (Hayakawa et al., 2011; Li et al., 2019a). Conversely, ZAPS has also been shown to interact with the 3'-UTR of IFN mRNAs with ZAP knockout resulting in increased IFN-(β, λ1, λ2, and λ3) mRNA and subsequent increase in IFIT1 and ISG15 expression in knockout cells. Therefore, suggesting that ZAPS targets host IFN mRNA for a negative regulatory response and prevent autoinflammation (Schwerk et al., 2019). We observe a reduction in IFN-β expression in ZAP knockout cells compared to control, thereby supporting the argument that ZAP is a positive regulator of the IFN induction pathway. However, our data was produced following the knockout of full-length ZAP and so confirmation is required following the ectopic expression of each isoform in our knockout cells.

We observed that ZAP expression is induced following DI treatment but not IFN-α treatment indicating that expression is IFN induction but not signalling dependent. In particular, western blot data showed a significant upregulation of ZAPS compared to ZAPL, which is instead shown to be constitutively expressed. Expression following IFN induction is supported by the literature which shows ZAPS expression is enhanced following viral infection, including IAV, and is IRF3-dependent following PAMP stimulation. Upon stimulation with a RIG-I ligand, ZAPS expression was not observed in IRF3 deficient cells suggesting IRF3-dependency (Schwerk et al., 2019). Additionally, Zhang et al. showed by immunoblot that upon knockdown of ZC3HAV1, the gene encoding ZAP, there is reduced protein expression of phospho-IRF3 following IAV infection, with the reverse observed following overexpression (Zhang et al., 2020). However, when IRF3 deficient cells are treated with IFN-α, they have been shown to exhibit robust expression of ZAPS, whilst IFNAR1 deficient cells do not, indicating ZAPS expression may be a downstream consequence of IRF3 deficiency resulting in inhibited expression (Schwerk et al., 2019). Moreover, ZAPS, but not ZAPL, has been shown to be upregulated in response to IFN-β treatment (Zhang et al., 2020). These findings differ to our results in that we do not observe expression of full-length ZAP, by RT-qPCR, to be IFN signalling dependent following IFN treatment. However, as we extrapolated findings following RT-qPCR of primers designed against the full-length form of ZAP following IFN-α treatment. It may be that IFN signalling leads to ZAPS through alternative polyadenylation, and so an alternative isoform is not observed unless IFN signalling is activated. Repetition of RT-qPCR, or analysis by western blot, specifically for ZAPS will allow us to compare data more closely to that in the literature.

7.5.2 ZAPL

On the other hand, ZAPL has been shown to act as a more direct antiviral. Previous work has shown that following alphavirus infection, ZAPL is localised to viral RNA (Schwerk et al., 2019) whilst

prenylation at the C-terminus of ZAPL enhances antiviral activity in mice (Li et al., 2019a). The direct antiviral phenotype of full-length ZAP is thought to function via two mechanisms: targeted RNA degradation and inhibition of translation. Both of which rely on ZAP cofactors with RNA binding activity including TRIM25 and KHNYN (Wang et al., 2010; Mao et al., 2013; Ficarelli et al., 2019). Activation of ZAP relies on the interaction of its N-terminal domain with the SPRY domain of TRIM25. The mechanism of this interaction is still not fully understood but it is known that both ZAPS and ZAPL are ubiquitylated at multiple sites and deletion of TRIM25 reduces this modification. Another ZAP cofactor, KHNYN, is responsible for the mediation of viral mRNA degradation by ZAP with its NYN domain thought to have endonuclease activity. As such, KYNYN depletion has been shown to increase HIV-1 virion production (Ficarelli, Neil and Swanson, 2021). As ZAP activity relies on these cofactors for its activity, we would therefore expect them to appear significant within our MaGeCK analysis however this is not the case with TRIM25 and KHNYN, ranking 2274 and 7944 respectively. However, observation shows that each gene has only one good sgRNA present in the analysis. Due to the limitations previously described and the algorithm used, we would therefore expect these genes to rank more highly and even become significant following repeating with a greater number of cells. ZAP is also able to inhibit virus replication by inhibiting translation initiation. Interaction with eIF4A and eIF4G prevents their recognition of the 5’ cap structure on mRNA, therefore preventing initiation of translation (Ficarelli, Neil and Swanson, 2021). Together it is these two mechanisms of directly binding RNA that are thought to be the main drivers in ZAP antiviral activity (figure 7.5.2).

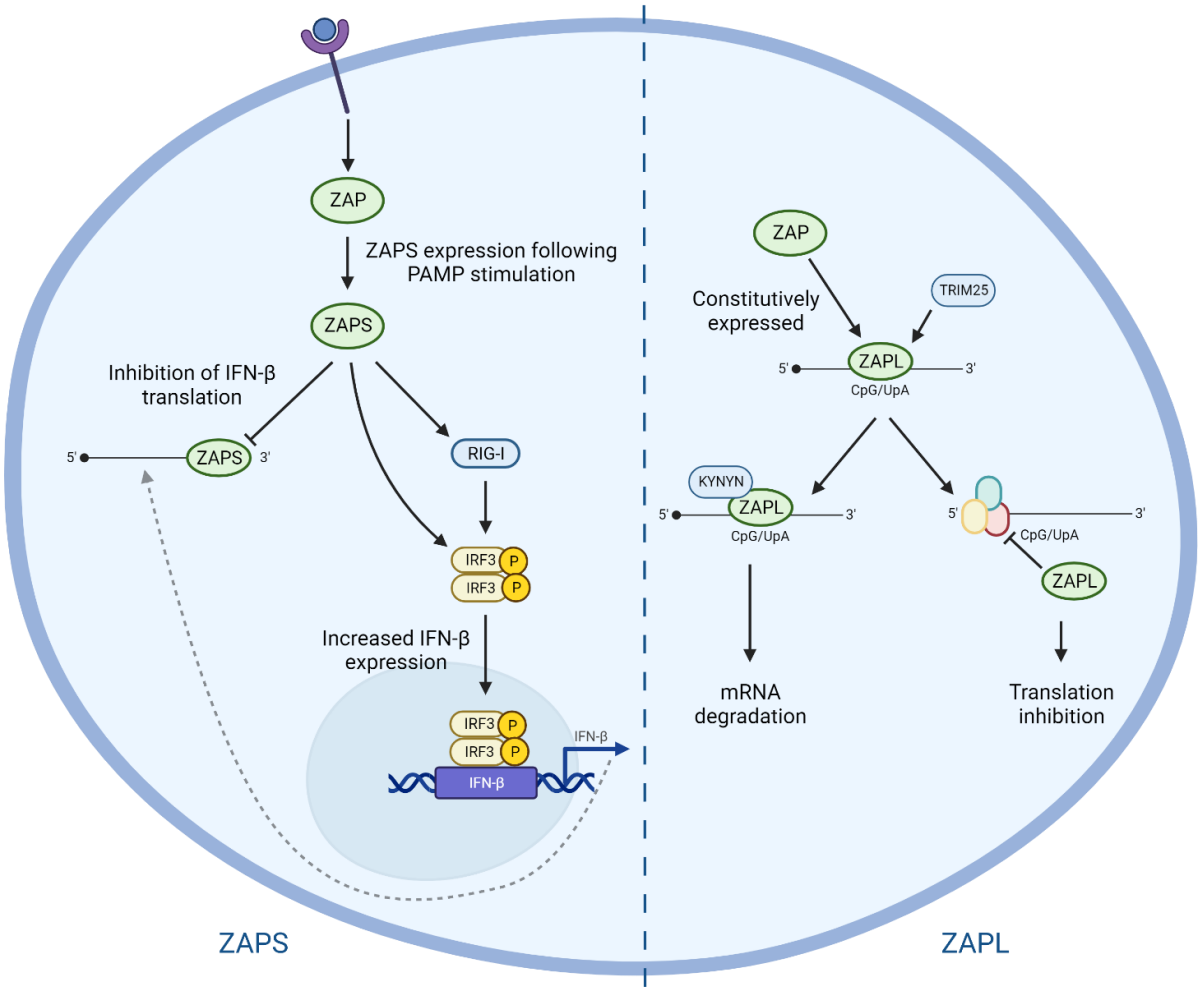

Figure 7.5.2: Mechanism of action of two ZAP isoforms. ZAPS (left) has a regulatory role within IFN induction, promoting RIG-I and IRF3 activation resulting in enhanced IFN-β expression. It is also able to negatively regulate and control for autoinflammatory responses by binding the C-terminal of IFN-β mRNA and inhibit its translation. ZAPL (right) plays a more direct role in in inhibiting viral replication by either (i) directly binding vRNA resulting in mRNA degradation, or (ii) inhibiting binding of eIF4A/G to 5' cap structure on mRNA thereby inhibiting translation. ZAPL adapted from (Ficarelli, Neil and Swanson, 2021).

7.5.3 The relationship between ZAP function and RNA dinucleotide content

ZAP is known to function by sensing CpG motifs and targeting RNA with high CpG frequencies irrespective of whether it is of viral or host origin. However, vertebrate genomes have evolved to suppress CpG dinucleotide frequency to enable ZAP discrimination between self and non-self RNAs. Despite this, ZAP has still been shown to regulate host gene expression with ZAP depletion in HeLa cells shown to change the expression of IFN response proteins (Ficarelli, Neil and Swanson, 2021). Following CpG sensing, ZAP can then mediate inhibition of translation or target the mRNA for degradation as previously described (section 7.5.2). If the RNA source is of viral origin, this then results

in CpG dependent inhibition of viral infection (Odon et al., 2019). To this effect, we analysed the dinucleotide frequencies within the PIV3 genome of three species, including human. As we observe virus restriction by ZAP, we expected to see a lack of CpG suppression in the PIV3 genome like in viruses such as IAV, Ebola and Sindbis virus (figure 7.5.3.1) (Ficarelli, Neil and Swanson, 2021). Conversely, we observe suppression of CpG O: E frequencies across all ORFs of the PIV3 genome, regardless of host species.

CpG suppression of other viruses, such as CMV, can be observed in only certain ORFs, unlike PIV3 in which suppression is universal. ZAP has been shown to specifically target transcripts from the UL4-UL6 gene locus, resulting in antiviral restriction (Gonzalez-Perez et al., 2021). This is likely to do with the evolutionary arms race between ZAP and viruses. ZAP is known to be an ancient ISG which viruses have co-evolved with and so viruses have co-evolved CpG suppression as a ZAP evasion mechanism. CMV is a large virus, with a 236 kbp genome and approximately 170 ORFs based on canonical protein genes (Murphy and Shenk, 2008), compare to PIV3 which is a small virus of only 8 genes and approximately 15 kb (Marsh et al., 2012). As such CpG suppression is more evolutionary simple for PIV3 than other larger and more complex viruses. Therefore, this may explain the universal suppression of CpG's across the genome. It may be considered surprised that we observe CpG suppression whilst also observing ZAP dependent restriction of hPIV3(JS) replication. However, we did not observe a strong antiviral response, with only a 2-3 fold reduction compared to control in IFN-treated cells, when investigated by RT-qPCR (figure 6.5.1.1). Therefore, this is not inconsistent with CpG suppression. Observation of CpG O:E ratios of other viruses restricted by ZAP, such as SARS-CoV-2 which is inhibited by both ZAPS and ZAPL, show similar levels of CpG suppression suggesting this is not a limiting factor to ZAP restriction (Lee et al., 2021a). However, we also observe that ZAP appears capable of regulating IFN induction and so CpG independent regulation of IFN induction, rather than direct antiviral effects (as previously described) may be having a larger effect.

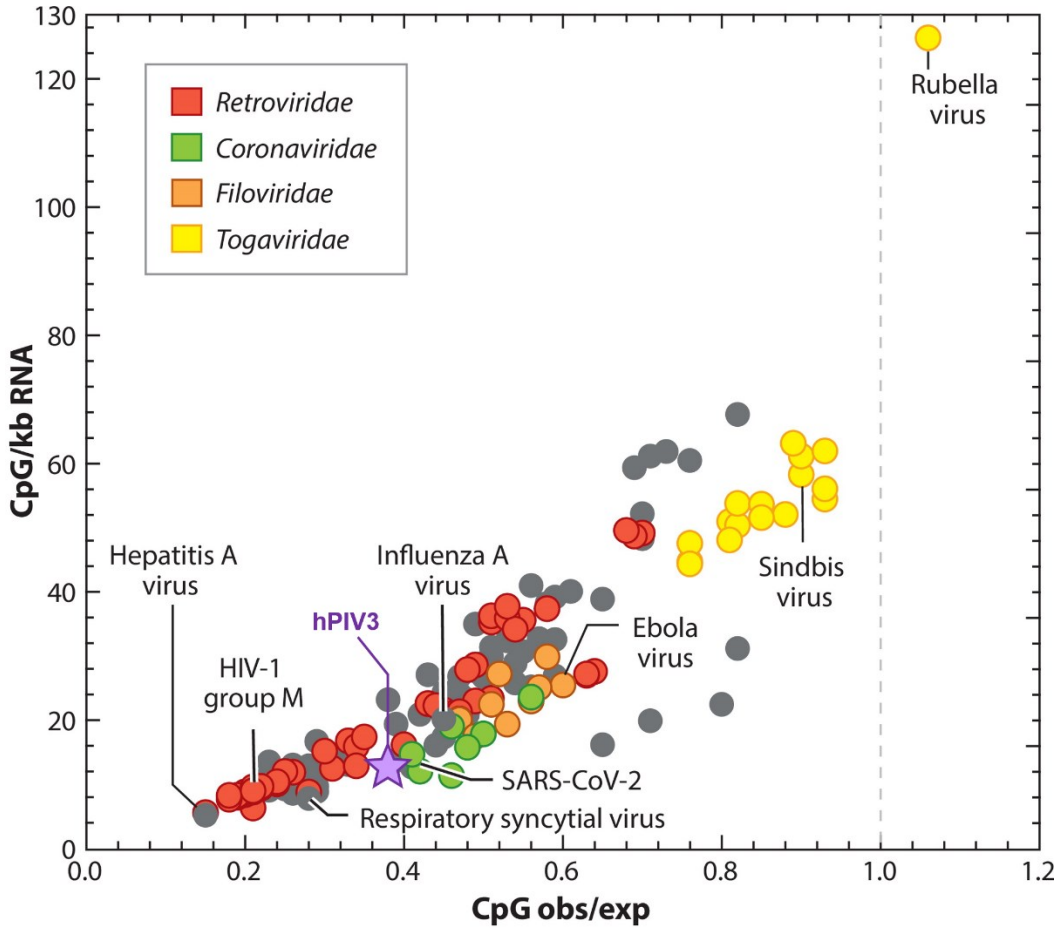

Ficarelli M, et al. 2021
Annu. Rev. Virol. 8:265–83

Figure 7.5.3.1: CpG dinucleotide content across viruses. Ratio of CpG O:E plotted against CpG per genome size (kb RNA). Viruses are clustered into approximately three groups with varying levels of ZAP susceptibility with hPIV3 (purple) falling within the base of group two. Viruses within Retroviridae (red), Coronaviridae (green), Filoviridae (orange), and Togaviridae (yellow) additionally highlighted. Adapted from (Ficarelli, Neil and Swanson, 2021).

In addition to CpG suppression, we also observed GpC suppression, a phenomenon not observed in other viruses (data unpublished). For analysis, ORFs are annotated in the 5' to 3' direction and so dinucleotide frequencies are observed in the same direction. For example, during transcription, a 3' - 5' GpC dinucleotide on the genome results in ZAP suppression of the resulting CpG on the 5' – 3' mRNA transcripts. Whereas, during replication, a GpC on the 5' - 3' antigenome results in ZAP suppression of the resulting CpG on the 3' – 5' genome (figure 7.5.3.2). We hypothesise that GpC suppression could be due to three possible explanations: stochastic coincidence, RNA genome protection, or to protect transcripts in the opposite direction. We observe moderate GpC suppression in comparison to CpG suppression whilst CpG suppression is enhanced compared to other viruses (figure 7.5.3.1). This suggests the GpC suppression is a stochastic coincidence. Alternatively, it may be that we observe GpC suppression as the virus has evolved to protect the 3' – 5' RNA genome during replication of the 5' to 3' antigenome. However, this is unlikely as genomes are packaged and the coating process is

tightly linked to replication, so ZAP is not likely to ever see nascent RNA (Bloyet, 2021). Finally, it is possible that GpC suppression is present to protect transcripts in the 5' to 3' direction but this is again unlikely as Paramyxovirus transcription is known to begin from a 3' Le promoter. Consequently, it is likely that GpC suppression is stochastic, and it may have no effect on ZAP restriction of hPIV3(JS).

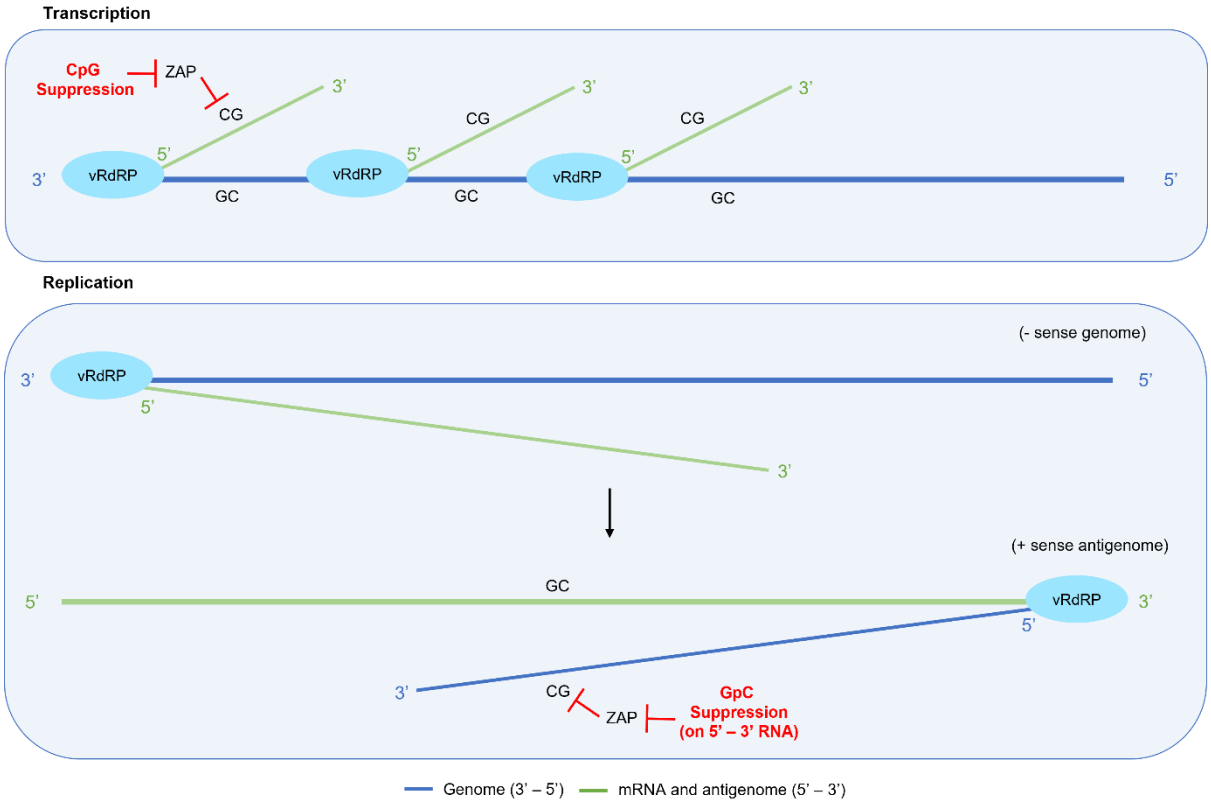

Figure 7.5.3.2: Mechanism of ZAP evasion by dinucleotide suppression. CpG and GpC dinucleotide suppression inhibits the action of ZAP at both the transcription and replication stage. CpG suppression (top box) prevents ZAP inhibition of nascent, uncoated 5' to 3' mRNA (green) during viral gene transcription. GpC suppression (bottom box) on the 5' to 3' antigenome (green) prevents ZAP inhibition of the 3' to 5' genome (blue).

We also observe moderate UpA suppression in our hPIV3 genome, a phenomenon observed across the vertebrate RNA virus group (Odon et al., 2019). ZAP has previously been shown to bind to both CpG and UpA sequences upon infection with Echovirus 7 (E7), with attenuation of E7 observed in UpA-high mutants. Additionally, mutation of IAV segment five to be UpA-high also results in virus attenuation in both cell culture and mice models. Therefore, UpA suppression may be another evasion strategy by hPIV3(JS). However, this effect may be a ZAP-independent evasion technique as RNaseL is also known to target single-stranded RNA sequences at UpA dinucleotides (Odon et al., 2019).

Together, our data supports the majority of that found in the literature showing ZAP regulation of the IFN response alongside a potential direct antiviral effect. However, further elucidation of the mechanism of action occurring is required using individual isoforms of ZAP.

7.6 Exploiting the role of ISG15 as a negative regulator of the IFN response

There is a need to improve the identification of ISGs and other antiviral restriction factors, as information not only provides us with information about how the host responds to virus infection, but information about their mechanism of action may elucidate novel pathways for therapeutic treatment. However, as described in the introduction (section 1.3.5), we observed a need to improve the identification of low to moderately acting restriction factors and overcome redundancy within the IFN response when employing screening technology. Improved identification of restriction factors would not only be useful within genome wide screening, and further their use in the field, but also within single gene studies.

Previous work in the lab suggested that known negative regulators of the IFN response could be exploited to achieve enhanced identification, namely ISG15, whereby ISG15 deficiency results in the overexpression of ISGs in IFN-treated cells (section 1.3.5) (Holthaus et al., 2020). We subsequently performed proof-of-principle studies in ISG15 deficient cells to successfully broaden the window for identification, detailed in figure 1.3.5.1, to enable the identification of low acting ISGs previously described as not having virus restricting capabilities in A549 naïve cells.

During proof-of-principle studies, we were able to demonstrate four key findings: (i) ISG15 deficiency enhances IFN-dependent virus restriction, (ii) multiple ISGs are required to restrict PIV5, (iii) we are able to broaden the quantitative working window for the identification of low acting ISGs, and (iv) IFIT1 restricts hPIV3(Washington) infection. The latter two of these findings are crucial to implementing the use of ISG15 deficient cells within an experimental workflow.

Previous work by Holthaus et. al had suggested that hPIV3(Washington) was not restricted by IFIT1 (Holthaus et al., 2020). However, this was investigated using shRNA knockdown of IFIT1 and so we therefore aimed to see if this was a true phenotype following CRISPR/Cas9 knockout. Upon, IFN-α pre-treatment, followed by hPIV3(Washington) infection, of A549-Cas9.IFIT1$^{-/-}$ cells, this phenotype was recapitulated, and results suggested that IFIT1 was not a hPIV3(Washington) restriction factor. However, upon infection of our A549-ISG15$^{-/-}$.Cas9.IFIT1$^{-/-}$ cells, this phenotype changed. The percentage of cells infected in our double knockouts compared to ISG15-deficient-only cells was higher, therefore suggesting that IFIT1 does play a role in restricting hPIV3(Washington). This observation was only permissible due to the exploitation of a negative regulator of the IFN response to expand the quantitative window. As hPIV3(Washington) is more resistant to the effects of IFN, IFN-α pre-treatment of control cells prior to infection does not reduce the percentage of cells infected to a significant degree compared to non-IFN treated cells and so phenotypes upon depletion of an ISG cannot be identified. Conversely, upon deletion of ISG15, the IFN response becomes dysregulated and the expression of ISGs upregulated. Whilst hPIV3(Washington) is more resistant to the effects of IFN, the ability of the virus to overcome this dysregulated response is more difficult and so IFN-α pre-treatment in ISG15 deficient cells results in a reduced percentage of cells becoming infected, therefore broadening the working window for the identification of antiviral restriction factors, such as IFIT1. This finding, that hPIV3(Washington) is indeed restricted by IFIT1 to a moderate degree, therefore suggests that ISG15

deficient cells may enable the identification of ISGs that target other viruses more resistant to IFN, or low to moderately acting ISGs against a range of viruses. Excitingly, whilst the dysregulation of the IFN response in ISG15 deficient cells is known, this is the first time it has been tested as a method development tool with applications in future research.

Future work would use these ISG15 deficient cell lines within a genome wide CRISPR/Cas9 screen and compare the output with sgRNA transduced naïve cells to see, in a screening context, if we are able to either (i) increase the numbers of genes identified compared to infection in naïve cells and/ or (ii) enhance either the significance or FDR of genes in the ISG15 deficient screen compared to the naïve.

7.7 Conclusion

This work has led to the development of a genome wide CRISPR/Cas9 screening platform that has enabled the identification of Paramyxovirus host dependency and antiviral restriction factors. Alongside the utilisation of the genome wide screening, we have also provided proof-of-principle for the use of ISG15 deficient cells in the discovery of low and moderately acting antiviral restriction factors, overcoming current limitations in regard to phenotypic power of current methods and redundancy with the IFN response.

Despite the limitations observed in the lack of genes passing the false discovery rate threshold, suggested to be due to the reduced amount of gDNA recovered from cells following sorting, potentially due to fixing, and the downstream effect on MaGeCK analysis, we were still able to characterise known and novel genes that affect hPIV3(JS) replication. The approach was validated through the successful identification of non-novel and control genes in both screens. Well characterised genes involved in sialic acid metabolism, such as SLC35A1, were identified in the host dependency screen. These are genes described to play a vital role in the replication of many viruses, including hPIV3. Similarly, genes involved in JAK/ STAT signalling were observed in the results of the antiviral restriction factor screen, acting as internal controls for our experimental conditions. The presence of these genes and pathways therefore provided us with confidence that our screening strategy was sound.

We were also able to successfully validate additional hPIV3(JS) antiviral restriction factors: NF2, HSD17B12, and ZAP. We were able to begin elucidating their mechanisms of action, assessing their expression alongside regulatory roles, and identify broader restriction against other related viruses. Most interestingly, this provided evidence for novel regulation of IFN signalling by NF2 that had not previously been described, with further work required to elucidate the mechanism of action.

Further work will enable the implementation of ISG15 deficient cells within a screening workflow, aiding the identification of more ISGs against not only hPIV3(JS) but also other viruses. Further investigation into the mechanism of action of our identified restriction factors, especially NF2, may also provide novel mechanisms of virus restriction that could be exploited for therapeutic purposes. Additionally, it would be interesting to see if our identified restriction factors are capable of restricting non-related viruses,

including both other RNA and DNA viruses. Based on evidence suggesting they play a regulatory role, rather than a direct antiviral role, we hypothesise that they will be broad acting restriction factors.

References

Abbas, Y.M., Pichlmair, A., Górna, M.W., Superti-Furga, G. and Nagar, B., 2013. Structural basis for viral 5′-PPP-RNA recognition by human IFIT proteins. *Nature*, 494(7435), pp.60–64. https://doi.org/10.1038/nature11783.

Abedi, G.R., Prill, M.M., Langley, G.E., Wikswo, M.E., Weinberg, G.A., Curns, A.T. and Schneider, E., 2015. Estimates of parainfluenza virus-associated hospitalizations and cost among children aged less than 5 years in the United States, 1998-2010. *Journal of the Pediatric Infectious Diseases Society*, 5(1), pp.7–13. https://doi.org/10.1093/jpids/piu047.

Abedon, S.T. and Bartom, E., 2013. Multiplicity of Infection. *Brenner's Encyclopedia of Genetics: Second Edition*, pp.509–510. https://doi.org/10.1016/B978-0-12-374984-0.00989-X.

Abernathy, E. and Glaunsinger, B., 2015. Emerging roles for RNA degradation in viral replication and antiviral defense. *Virology*, 479, p.600. https://doi.org/10.1016/J.VIROL.2015.02.007.

Aguilar, H.C., Henderson, B.A., Zamora, J.L. and Johnston, G.P., 2016. *Paramyxovirus Glycoproteins and the Membrane Fusion Process*. *Current Clinical Microbiology Reports*, https://doi.org/10.1007/s40588-016-0040-8.

Altan-Bonnet, N., 2017. Lipid Tales of Viral Replication and Transmission. *Trends in Cell Biology*, 27(3), pp.201–213. https://doi.org/10.1016/J.TCB.2016.09.011.

An, H., Hou, J., Zhou, J., Zhao, W., Xu, H., Zheng, Y., Yu, Y., Liu, S. and Cao, X., 2008. Phosphatase SHP-1 promotes TLR- and RIG-I-activated production of type I interferon by inhibiting the kinase IRAK1. *Nature Immunology*, 9(5), pp.542–550. https://doi.org/10.1038/ni.1604.

Anderson, D.E., Pfeffermann, K., Kim, S.Y., Sawatsky, B., Pearson, J., Kovtun, M., Corcoran, D.L., Krebs, Y., Sigmundsson, K., Jamison, S.F., Yeo, Z.Z.J., Rennick, L.J., Wang, L.-F., Talbot, P.J., Duprex, W.P., Garcia-Blanco, M.A. and von Messling, V., 2019a. Comparative Loss-of-Function Screens Reveal ABCE1 as an Essential Cellular Host Factor for Efficient Translation of Paramyxoviridae and Pneumoviridae. *mBio*, 10(3). https://doi.org/10.1128/mBio.00826-19.

Anderson, D.E. and Wang, L.F., 2016. Zoonotic Paramyxoviruses. *Clinical Virology*, pp.949–966. https://doi.org/10.1128/9781555819439.CH40.

Anderson, S.M., Cheesman, H.K., Peterson, N.D., Salisbury, J.E., Soukas, A.A. and Pukkila-Worley, R., 2019b. The fatty acid oleate is required for innate immune activation and pathogen defense in caenorhabditis elegans. *PLoS Pathogens*, 15(6). https://doi.org/10.1371/journal.ppat.1007893.

Andrejeva, J., Childs, K.S., Young, D.F., Carlos, T.S., Stock, N., Goodbourn, S. and Randall, R.E., 2004. The V proteins of paramyxoviruses bind the IFN-inducible RNA helicase, mda-5, and inhibit its activation of the IFN-β promoter. *Proceedings of the National Academy of Sciences of the United States of America*, 101(49), p.17264. https://doi.org/10.1073/PNAS.0407639101.

Andrejeva, J., Norsted, H., Habjan, M., Thiel, V., Goodbourn, S. and Randall, R.E., 2013. ISG56/IFIT1 is primarily responsible for interferoninduced changes to patterns of parainfluenza virus type 5 transcription and protein synthesis. *Journal of General Virology*, 94(PART11), pp.59–60. https://doi.org/10.1099/vir.0.046797-0.

Ashley, C.L., Abendroth, A., McSharry, B.P. and Slobedman, B., 2019. Interferon-Independent Innate Responses to Cytomegalovirus. *Frontiers in immunology*, 10. https://doi.org/10.3389/FIMMU.2019.02751.

Badia, R., Garcia-Vidal, E. and Ballana, E., 2022. Viral-Host Dependency Factors as Therapeutic Targets to Overcome Antiviral Drug-Resistance: A Focus on Innate Immune Modulation. *Frontiers in Virology*, 2, p.935933. https://doi.org/10.3389/FVIRO.2022.935933.

Bailly, J.E., McAuliffe, J.M., Skiadopoulos, M.H., Collins, P.L. and Murphy, B.R., 2000. Sequence determination and molecular analysis of two strains of bovine parainfluenza virus type 3 that are attenuated for primates. *Virus Genes*, 20(2), pp.173–182. https://doi.org/10.1023/A:1008130917204/METRICS.

Balachandran, S., Roberts, P.C., Brown, L.E., Truong, H., Pattnaik, A.K., Archer, D.R. and Barber, G.N., 2000. Essential role for the dsRNA-dependent protein kinase PKR in innate immunity to viral infection. *Immunity*, 13(1), pp.129–141. https://doi.org/10.1016/S1074-7613(00)00014-5.

Barrows, N.J., Le Sommer, C., Garcia-Blanco, M.A. and Pearson, J.L., 2010. Factors affecting reproducibility between genome-scale siRNA-based screens. *Journal of Biomolecular Screening*, 15(7), pp.735–747. https://doi.org/10.1177/1087057110374994.

Battisti, A.J., Meng, G., Winkler, D.C., McGinnes, L.W., Plevka, P., Steven, A.C., Morrison, T.G. and Rossmann, M.G., 2012. Structure and assembly of a paramyxovirus matrix protein. *Proceedings of the National Academy of Sciences of the United States of America*, 109(35), pp.13996–14000. https://doi.org/10.1073/pnas.1210275109.

Baum, A. and García-Sastre, A., 2010. *Induction of type i interferon by RNA viruses: Cellular receptors and their substrates*. *Amino Acids*, https://doi.org/10.1007/s00726-009-0374-0.

Beard, P.M., Griffiths, S.J., Gonzalez, O., Haga, I.R., Jowers, T.P., Reynolds, D.K., Wildenhain, J., Tekotte, H., Auer, M., Tyers, M., Ghazal, P., Zimmer, R. and Haas, J., 2014. A loss of function analysis of host factors influencing Vaccinia virus replication by RNA interference. *PLoS ONE*, 9(6), p.e98431. https://doi.org/10.1371/journal.pone.0098431.

Bender, A.T., Tzvetkov, E., Pereira, A., Wu, Y., Kasar, S., Przetak, M.M., Vlach, J., Niewold, T.B., Jensen, M.A. and Okitsu, S.L., 2020. TLR7 and TLR8 Differentially Activate the IRF and NF-κB Pathways in Specific Cell Types to Promote Inflammation. *ImmunoHorizons*, 4(2), pp.93–107. https://doi.org/10.4049/immunohorizons.2000002.

Bick, M.J., Carroll, J.-W.N., Gao, G., Goff, S.P., Rice, C.M. and MacDonald, M.R., 2003. Expression of the Zinc-Finger Antiviral Protein Inhibits Alphavirus Replication. *Journal of Virology*, 77(21), pp.11555–11562. https://doi.org/10.1128/JVI.77.21.11555-11562.2003/ASSET/432200B6-8C07-417E-BBFD-38605F2B344C/ASSETS/GRAPHIC/JV2131156008.JPEG.

Birmingham, A., Anderson, E.M., Reynolds, A., Ilsley-Tyree, D., Leake, D., Fedorov, Y., Baskerville, S., Maksimova, E., Robinson, K., Karpilow, J., Marshall, W.S. and Khvorova, A., 2006. 3' UTR seed matches, but not overall identity, are associated with RNAi off-targets. *Nature methods*, 3(3), pp.199–204. https://doi.org/10.1038/nmeth854.

Blomen, V.A., Májek, P., Jae, L.T., Bigenzahn, J.W., Nieuwenhuis, J., Staring, J., Sacco, R., Van Diemen, F.R., Olk, N., Stukalov, A., Marceau, C., Janssen, H., Carette, J.E., Bennett, K.L., Colinge, J., Superti-Furga, G. and Brummelkamp, T.R., 2015. Gene essentiality and synthetic lethality in haploid human cells. *Science*, 350(6264), pp.1092–1096. https://doi.org/10.1126/SCIENCE.AAC7557/SUPPL_FILE/BLOMEN-SM.PDF.

Bloyet, L.M., 2021. The Nucleocapsid of Paramyxoviruses: Structure and Function of an Encapsidated Template. *Viruses*, 13(12). https://doi.org/10.3390/V13122465.

Boldogh, I., Albrecht, T. and Porter, D.D., 1996. Persistent Viral Infections. *Medical Microbiology*.

Bonaventure, B., Rebendenne, A., Chaves Valadão, A.L., Arnaud-Arnould, M., Gracias, S., Garcia de Gracia, F., McKellar, J., Labaronne, E., Tauziet, M., Vivet-Boudou, V., Bernard, E., Briant, L., Gros, N., Djilli, W., Courgnaud, V., Parrinello, H., Rialle, S., Blaise, M., Lacroix, L., Lavigne, M., Paillart, J., Ricci, E.P., Schulz, R., Jouvenet, N., Moncorgé, O. and Goujon, C., 2022. The DEAD box RNA helicase DDX42 is an intrinsic inhibitor of positive-strand RNA viruses. *EMBO reports*, 23(11). https://doi.org/10.15252/embr.202154061.

Bose, S. and Banerjee, A.K., 2002. Role of heparan sulfate in human parainfluenza virus type 3 infection. *Virology*, 298(1), pp.73–83. https://doi.org/10.1006/viro.2002.1484.

Bossart, K.N., Fusco, D.L. and Broder, C.C., 2013. Paramyxovirus entry. *Advances in Experimental Medicine and Biology*, 790, pp.95–127. https://doi.org/10.1007/978-1-4614-7651-1_6/COVER.

Brass, A.L., Huang, I.C., Benita, Y., John, S.P., Krishnan, M.N., Feeley, E.M., Ryan, B.J., Weyer, J.L., van der Weyden, L., Fikrig, E., Adams, D.J., Xavier, R.J., Farzan, M. and Elledge, S.J., 2009. The IFITM Proteins Mediate Cellular Resistance to Influenza A H1N1 Virus, West Nile Virus, and Dengue Virus. *Cell*, 139(7), pp.1243–1254. https://doi.org/10.1016/j.cell.2009.12.017.

Bruni, D., Sebastia, J., Dunne, S., Schröder, M. and Butler, M.P., 2013. A Novel IRAK1–IKKε Signaling Axis Limits the Activation of TAK1–IKKβ Downstream of TLR3. *The Journal of Immunology*, 190(6), pp.2844–2856. https://doi.org/10.4049/JIMMUNOL.1202042.

Cakir, M., Obernier, K., Forget, A. and Krogan, N.J., 2021. Target Discovery for Host-Directed Antiviral Therapies: Application of Proteomics Approaches. *mSystems*, 6(5). https://doi.org/10.1128/MSYSTEMS.00388-21.

Carlos, T.S., Young, D., Stertz, S., Kochs, G. and Randall, R.E., 2007. Interferon-induced inhibition of parainfluenza virus type 5; the roles of MxA, PKR and oligo A synthetase/RNase L. *Virology*, 363(1), pp.166–173. https://doi.org/10.1016/j.virol.2007.01.014.

CDC, 2015. *Human Parainfluenza Viruses | Clinical Overview of HPIVs | CDC*. [online] cdc. Available at: <https://www.cdc.gov/parainfluenza/hcp/clinical.html> [Accessed 9 June 2023].

Cella, M., Jarrossay, D., Facchetti, F., Alebardi, O., Nakajima, H., Lanzavecchia, A. and Colonna, M., 1999. Plasmacytoid monocytes migrate to inflamed lymph nodes and produce large amounts of type I interferon. *Nature Medicine*, 5(8), pp.919–923. https://doi.org/10.1038/11360.

Chang, A. and Dutch, R.E., 2012. Paramyxovirus Fusion and Entry: Multiple Paths to a Common End. *Viruses*, 4(4), p.613. https://doi.org/10.3390/V4040613.

Chang, A., Masante, C., Buchholz, U.J. and Dutch, R.E., 2012. Human metapneumovirus (HMPV) binding and infection are mediated by interactions between the HMPV fusion protein and heparan sulfate. *Journal of virology*, 86(6), pp.3230–3243. https://doi.org/10.1128/JVI.06706-11.

Chemudupati, M., Kenney, A.D., Bonifati, S., Zani, A., McMichael, T.M., Wu, L. and Yount, J.S., 2019. *From APOBEC to ZAP: Diverse mechanisms used by cellular restriction factors to inhibit virus infections*. *Biochimica et Biophysica Acta - Molecular Cell Research*, https://doi.org/10.1016/j.bbamcr.2018.09.012.

Chen, C.H., Xiao, T., Xu, H., Jiang, P., Meyer, C.A., Li, W., Brown, M. and Liu, X.S., 2018. Improved design and analysis of CRISPR knockout screens. *Bioinformatics*, 34(23), pp.4095–4101. https://doi.org/10.1093/bioinformatics/bty450.

Chen, Z., Rijnbrand, R., Jangra, R.K., Devaraj, S.G., Qu, L., Ma, Y., Lemon, S.M. and Li, K., 2007. Ubiquitination and Proteasomal Degradation of Interferon Regulatory Factor-3 induced by Npro from a Cytopathic Bovine Viral Diarrhea Virus. *Virology*, 366(2), p.277. https://doi.org/10.1016/J.VIROL.2007.04.023.

Chew, S.K., Rad, R., Futreal, P.A., Bradley, A. and Liu, P., 2011. Genetic screens using the piggyBac transposon. *Methods*, 53(4), pp.366–371. https://doi.org/10.1016/j.ymeth.2010.12.022.

Childs, K., Stock, N., Ross, C., Andrejeva, J., Hilton, L., Skinner, M., Randall, R. and Goodbourn, S., 2007. mda-5, but not RIG-I, is a common target for paramyxovirus V proteins. *Virology*, 359(1), pp.190–200. https://doi.org/10.1016/J.VIROL.2006.09.023.

Chiu, H.P., Chiu, H., Yang, C.F., Lee, Y.L., Chiu, F.L., Kuo, H.C., Lin, R.J. and Lin, Y.L., 2018. Inhibition of Japanese encephalitis virus infection by the host zinc-finger antiviral protein. *PLOS Pathogens*, 14(7), p.e1007166. https://doi.org/10.1371/JOURNAL.PPAT.1007166.

Choppin, P.W., 1964. Multiplication of a myxovirus (SV5) with minimal cytopathic effects and without interference. *Virology*, 23(2), pp.224–233. https://doi.org/10.1016/0042-6822(64)90286-7.

Chow, R.D., Guzman, C.D., Wang, G., Schmidt, F., Youngblood, M.W., Ye, L., Errami, Y., Dong, M.B., Martinez, M.A., Zhang, S., Renauer, P., Bilguvar, K., Gunel, M., Sharp, P.A., Zhang, F., Platt, R.J. and Chen, S., 2017. AAV-mediated direct in vivo CRISPR screen identifies functional suppressors in glioblastoma. *Nature Neuroscience*, 20(10), pp.1329–1341. https://doi.org/10.1038/nn.4620.

Cisneros, W.J., Cornish, D. and Hultquist, J.F., 2022. Application of CRISPR-Cas9 Gene Editing for HIV Host Factor Discovery and Validation. *Pathogens*, 11(8). https://doi.org/10.3390/PATHOGENS11080891.

Cong, L., Ran, F.A., Cox, D., Lin, S., Barretto, R., Habib, N., Hsu, P.D., Wu, X., Jiang, W., Marraffini,

L.A. and Zhang, F., 2013. Multiplex genome engineering using CRISPR/Cas systems. *Science*, 339(6121), pp.819–823. https://doi.org/10.1126/science.1231143.

Conrad, C. and Gerlich, D.W., 2010. Automated microscopy for high-content RNAi screening. *The Journal of Cell Biology*, 188(4), pp.453–461. https://doi.org/10.1083/jcb.200910105.

Cox, R.M. and Plemper, R.K., 2017. Structure and organization of paramyxovirus particles. *Current Opinion in Virology*, 24, pp.105–114. https://doi.org/10.1016/J.COVIRO.2017.05.004.

Daffis, S., Szretter, K.J., Schriewer, J., Li, J., Youn, S., Errett, J., Lin, T.Y., Schneller, S., Zust, R., Dong, H., Thiel, V., Sen, G.C., Fensterl, V., Klimstra, W.B., Pierson, T.C., Buller, R.M., Gale Jr, M., Shi, P.Y. and Diamond, M.S., 2010. 2′-O methylation of the viral mRNA cap evades host restriction by IFIT family members. *Nature*, 468(7322), pp.452–456. https://doi.org/10.1038/nature09489.

Daniloski, Z., Jordan, T.X., Wessels, H.-H., Hoagland, D.A., Kasela, S., Legut, M., Maniatis, S., Mimitou, E.P., Lu, L., Geller, E., Danziger, O., Rosenberg, B.R., Phatnani, H., Smibert, P., Lappalainen, T., TenOever, B.R. and Sanjana, N.E., 2021. Identification of Required Host Factors for SARS-CoV-2 Infection in Human Cells. *Cell*, 184(1), pp.92-105.e16. https://doi.org/10.1016/j.cell.2020.10.030.

Diamond, M.S. and Farzan, M., 2012. The broad-spectrum antiviral functions of IFIT and IFITM proteins. *Nature Reviews Immunology 2012 13:1*, 13(1), pp.46–57. https://doi.org/10.1038/nri3344.

Didcock, L., Young, D.F., Randall, R.E. and Goodbourn, S., 1999. The V protein of simian virus 5 inhibits interferon signalling by targeting STAT1 for proteasome-mediated degradation. *Journal of Virology*, 73(12), pp.9928–9933.

Doench, J.G., Fusi, N., Sullender, M., Hegde, M., Vaimberg, E.W., Donovan, K.F., Smith, I., Tothova, Z., Wilen, C., Orchard, R., Virgin, H.W., Listgarten, J. and Root, D.E., 2016. Optimized sgRNA design to maximize activity and minimize off-target effects of CRISPR-Cas9. *Nature Biotechnology*, 34(2), pp.184–191. https://doi.org/10.1038/nbt.3437.

Doench, J.G., Petersen, C.P. and Sharp, P.A., 2003. siRNAs can function as miRNAs. *Genes and Development*, 17(4), pp.438–442. https://doi.org/10.1101/gad.1064703.

Doudna, J.A. and Charpentier, E., 2014. The new frontier of genome engineering with CRISPR-Cas9. *Science*, 346(6213), p.1258096. https://doi.org/10.1126/science.1258096.

Duncan, J.K.S., Xu, D., Licursi, M., Joyce, M.A., Saffran, H.A., Liu, K., Gohda, J., Tyrrell, D.L., Kawaguchi, Y. and Hirasawa, K., 2023. Interferon regulatory factor 3 mediates effective antiviral responses to human coronavirus 229E and OC43 infection. *Frontiers in immunology*, 14, p.930086. https://doi.org/10.3389/FIMMU.2023.930086/BIBTEX.

Echeverri, C.J. and Perrimon, N., 2006. High-throughput RNAi screening in cultured cells: a user's guide. *Nature Reviews Genetics*, 7(5), pp.373–384. https://doi.org/10.1038/nrg1836.

Fang, C., Li, J., Qi, S., Lei, Y., Zeng, Y., Yu, P., Hu, Z., Zhou, Y., Wang, Y., Dai, R., Li, J., Huang, S., Xu, P., Chen, K., Ding, C. and Yu, F., 2019. An alternatively transcribed TAZ variant negatively regulates JAK - STAT signaling. *EMBO reports*, 20(6). https://doi.org/10.15252/embr.201847227.

Fearns, R., Young, D.F. and Randall, R.E., 1994. Evidence that the paramyxovirus simian virus 5 can establish quiescent infections by remaining inactive in cytoplasmic inclusion bodies. *Journal of General Virology*, 75(12), pp.3525–3539.

Feng, J., Wickenhagen, A., Turnbull, M.L., Rezelj, V. V., Kreher, F., Tilston-Lunel, N.L., Slack, G.S., Brennan, B., Koudriakova, E., Shaw, A.E., Rihn, S.J., Rice, C.M., Bieniasz, P.D., Elliott, R.M., Shi, X. and Wilson, S.J., 2018. Interferon-Stimulated Gene (ISG)-Expression Screening Reveals the Specific Antibunyaviral Activity of ISG20. *Journal of Virology*, 92(13), pp.e02140-17. https://doi.org/10.1128/JVI.02140-17.

Fensterl, V., Chattopadhyay, S. and Sen, G.C., 2015. No Love Lost Between Viruses and Interferons. *Annual Review of Virology*, 2(1), pp.549–572. https://doi.org/10.1146/annurev-virology-100114-055249.

Ficarelli, M., Neil, S.J.D. and Swanson, C.M., 2021. *Targeted Restriction of Viral Gene Expression*

and Replication by the ZAP Antiviral System. *Annual Review of Virology*, https://doi.org/10.1146/annurev-virology-091919-104213.

Ficarelli, M., Wilson, H., Galão, R.P., Mazzon, M., Antzin-Anduetza, I., Marsh, M., Neil, S.J.D. and Swanson, C.M., 2019. KHNYN is essential for the zinc finger antiviral protein (ZAP) to restrict HIV-1 containing clustered CpG dinucleotides. *eLife*, 8. https://doi.org/10.7554/ELIFE.46767.

Fire, A., Xu, S., Montgomery, M.K., Kostas, S.A., Driver, S.E. and Mello, C.C., 1998. Potent and specific genetic interference by double-stranded RNA in Caenorhabditis elegans. *Nature*, 391(6669), pp.806–811. https://doi.org/10.1038/35888.

Fitzgerald, K.A., McWhirter, S.M., Faia, K.L., Rowe, D.C., Latz, E., Golenbock, D.T., Coyle, A.J., Liao, S.-M. and Maniatis, T., 2003. IKKε and TBK1 are essential components of the IRF3 signaling pathway. *Nature Immunology*, 4(5), pp.491–496. https://doi.org/10.1038/ni921.

Flint, M., Chatterjee, P., Lin, D.L., McMullan, L.K., Shrivastava-Ranjan, P., Bergeron, É., Lo, M.K., Welch, S.R., Nichol, S.T., Tai, A.W. and Spiropoulou, C.F., 2019. A genome-wide CRISPR screen identifies N-acetylglucosamine-1-phosphate transferase as a potential antiviral target for Ebola virus. *Nature Communications*, 10(1), p.285. https://doi.org/10.1038/s41467-018-08135-4.

Fusco, D.N., Brisac, C., John, S.P., Huang, Y., Chin, C.R., Xie, T., Zhao, H., Jilg, N., Zhang, L., Chevaliez, S., Wambua, D., Lin, W., Peng, L., Chung, R.T. and Brass, A.L., 2013. A Genetic Screen Identifies Interferon-α Effector Genes Required to Suppress Hepatitis C Virus Replication. *Gastroenterology*, 144(7), pp.1438-1449.e9. https://doi.org/10.1053/j.gastro.2013.02.026.

Ganar, K., Das, M., Sinha, S. and Kumar, S., 2014. Newcastle disease virus: Current status and our understanding. *Virus Research*, 184, p.71. https://doi.org/10.1016/J.VIRUSRES.2014.02.016.

Gaunt, E., Wise, H.M., Zhang, H., Lee, L.N., Atkinson, N.J., Nicol, M.Q., Highton, A.J., Klenerman, P., Beard, P.M., Dutia, B.M., Digard, P. and Simmonds, P., 2016. Elevation of CpG frequencies in influenza a genome attenuates pathogenicity but enhances host response to infection. *eLife*, 5(FEBRUARY2016). https://doi.org/10.7554/eLife.12735.

Gaunt, E.R. and Digard, P., 2022. Compositional biases in RNA viruses: Causes, consequences and applications. *Wiley Interdisciplinary Reviews: RNA*, 13(2), p.e1679. https://doi.org/10.1002/WRNA.1679.

Genoyer, E. and López, C.B., 2019. The Impact of Defective Viruses on Infection and Immunity. https://doi.org/10.1146/annurev-virology-092818.

Gonçalves-Carneiro, D., Takata, M.A., Ong, H., Shilton, A. and Bieniasz, P.D., 2021. Origin and evolution of the zinc finger antiviral protein. *PLOS Pathogens*, 17(4), p.e1009545. https://doi.org/10.1371/JOURNAL.PPAT.1009545.

Gonzalez-Perez, A.C., Stempel, M., Wyler, E., Urban, C., Piras, A., Hennig, T., Ganskih, S., Wei, Y., Heim, A., Landthaler, M., Pichlmair, A., Dölken, L., Munschauer, M., Erhard, F. and Brinkmann, M.M., 2021. The zinc finger antiviral protein zap restricts human cytomegalovirus and selectively binds and destabilizes viral ul4/ul5 transcripts. *mBio*, 12(3). https://doi.org/10.1128/mBio.02683-20.

Goodbourn, S. and Randall, R.E., 2009. *The regulation of type i interferon production by paramyxoviruses*. *Journal of Interferon and Cytokine Research*, https://doi.org/10.1089/jir.2009.0071.

Gorden, K.B., Gorski, K.S., Gibson, S.J., Kedl, R.M., Kieper, W.C., Qiu, X., Tomai, M.A., Alkan, S.S. and Vasilakos, J.P., 2005. Synthetic TLR Agonists Reveal Functional Differences between Human TLR7 and TLR8. *The Journal of Immunology*, 174(3), pp.1259–1268. https://doi.org/10.4049/jimmunol.174.3.1259.

Grégoire, I.P., Richetta, C., Meyniel-Schicklin, L., Borel, S. and Pradezynski, F., 2011. IRGM Is a Common Target of RNA Viruses that Subvert the Autophagy Network. *PLoS Pathog*, 7(12), p.1002422. https://doi.org/10.1371/journal.ppat.1002422.

Gupta, S., Schoer, R.A., Egan, J.E., Hannon, G.J. and Mittal, V., 2004. Inducible, reversible, and stable RNA interference in mammalian cells. *Proceedings of the National Academy of Sciences of the United States of America*, 101(7), pp.1927–1932. https://doi.org/10.1073/pnas.0306111101.

Habjan, M., Hubel, P., Lacerda, L., Benda, C., Holze, C., Eberl, C.H., Mann, A., Kindler, E., Gil-Cruz, C., Ziebuhr, J., Thiel, V. and Pichlmair, A., 2013. Sequestration by IFIT1 Impairs Translation of 2′O-unmethylated Capped RNA. *PLoS Pathogens*, 9(10), p.e1003663. https://doi.org/10.1371/journal.ppat.1003663.

Hadley, B., Litfin, T., Day, C.J., Haselhorst, T., Zhou, Y. and Tiralongo, J., 2019. Nucleotide Sugar Transporter SLC35 Family Structure and Function. *Computational and Structural Biotechnology Journal*, 17, p.1123. https://doi.org/10.1016/J.CSBJ.2019.08.002.

Hall, C.B., Weinberg, G.A., Iwane, M.K., Blumkin, A.K., Edwards, K.M., Staat, M.A., Auinger, P., Griffin, M.R., Poehling, K.A., Erdman, D., Grijalva, C.G., Zhu, Y. and Szilagyi, P., 2009. The Burden of respiratory syncytial virus infection in young children. *New England Journal of Medicine*, 360(6), pp.588–598. https://doi.org/10.1056/NEJMoa0804877.

Hambleton, S., Goodbourn, S., Young, D.F., Dickinson, P., Mohamad, S.M.B., Valappil, M., McGovern, N., Cant, A.J., Hackett, S.J., Ghazal, P., Morgan, N. V. and Randall, R.E., 2013. STAT2 deficiency and susceptibility to viral illness in humans. *Proceedings of the National Academy of Sciences of the United States of America*, 110(8), pp.3053–3058. https://doi.org/10.1073/PNAS.1220098110/-/DCSUPPLEMENTAL.

Han, J., Perez, J.T., Chen, C., Li, Y., Benitez, A., Kandasamy, M., Lee, Y., Andrade, J., TenOever, B. and Manicassamy, B., 2018. Genome-wide CRISPR/Cas9 Screen Identifies Host Factors Essential for Influenza Virus Replication. *Cell Reports*, 23(2), pp.596–607. https://doi.org/10.1016/j.celrep.2018.03.045.

Hao, L., Sakurai, A., Watanabe, T., Sorensen, E., Nidom, C.A., Newton, M.A., Ahlquist, P. and Kawaoka, Y., 2008. Drosophila RNAi screen identifies host genes important for influenza virus replication. *Nature*, 454(7206), p.890. https://doi.org/10.1038/NATURE07151.

Harada, Y., Ohkawa, Y., Kizuka, Y. and Taniguchi, N., 2019. Oligosaccharyltransferase: A Gatekeeper of Health and Tumor Progression. *International Journal of Molecular Sciences*, 20(23). https://doi.org/10.3390/IJMS20236074.

Hart, T., Chandrashekhar, M., Aregger, M., Steinhart, Z., Brown, K.R., MacLeod, G., Mis, M., Zimmermann, M., Fradet-Turcotte, A., Sun, S., Mero, P., Dirks, P., Sidhu, S., Roth, F.P., Rissland, O.S., Durocher, D., Angers, S. and Moffat, J., 2015. High-Resolution CRISPR Screens Reveal Fitness Genes and Genotype-Specific Cancer Liabilities. *Cell*, 163(6), pp.1515–1526. https://doi.org/10.1016/J.CELL.2015.11.015.

Hayakawa, S., Shiratori, S., Yamato, H., Kameyama, T., Kitatsuji, C., Kashigi, F., Goto, S., Kameoka, S., Fujikura, D., Yamada, T., Mizutani, T., Kazumata, M., Sato, M., Tanaka, J., Asaka, M., Ohba, Y., Miyazaki, T., Imamura, M. and Takaoka, A., 2011. ZAPS is a potent stimulator of signaling mediated by the RNA helicase RIG-I during antiviral responses. *Nature Immunology*, 12(1), pp.37–44. https://doi.org/10.1038/ni.1963.

Heikelä, H., Ruohonen, S.T., Adam, M., Viitanen, R., Liljenbäck, H., Eskola, O., Gabriel, M., Mairinoja, L., Pessia, A., Velagapudi, V., Roivainen, A., Zhang, F.P., Strauss, L. and Poutanen, M., 2020. Hydroxysteroid (17β) dehydrogenase 12 is essential for metabolic homeostasis in adult mice. *American Journal of Physiology - Endocrinology and Metabolism*, 319(3), pp.E494–E508. https://doi.org/10.1152/AJPENDO.00042.2020/ASSET/IMAGES/LARGE/ZH10082084300005.JPEG.

Hilton, L., Moganeradj, K., Zhang, G., Chen, Y.-H., Randall, R.E., McCauley, J.W. and Goodbourn, S., 2006. The NPro product of bovine viral diarrhea virus inhibits DNA binding by interferon regulatory factor 3 and targets it for proteasomal degradation. *Journal of virology*, 80(23), pp.11723–11732. https://doi.org/10.1128/JVI.01145-06.

Hoffmann, H.-H., Sánchez-Rivera, F.J., Schneider, W.M., Luna, J.M., Soto-Feliciano, Y.M., Ashbrook, A.W., Le Pen, J., Leal, A.A., Ricardo-Lax, I., Michailidis, E., Hao, Y., Stenzel, A.F., Peace, A., Zuber, J., Allis, C.D., Lowe, S.W., MacDonald, M.R., Poirier, J.T. and Rice, C.M., 2020. Functional interrogation of a SARS-CoV-2 host protein interactome identifies unique and shared coronavirus host factors. *Cell Host & Microbe*, 0(0), p.2020.09.11.291716. https://doi.org/10.1016/j.chom.2020.12.009.

Holen, H.L., Zernichow, L., Fjelland, K.E., Evenroed, I.M., Prydz, K., Tveit, H. and Aasheim, H.C., 2011. Ephrin-B3 binds to a sulfated cell-surface receptor. *The Biochemical journal*, 433(1), pp.215–

223. https://doi.org/10.1042/BJ20100865.

Holthaus, D., Vasou, A., Bamford, C.G.G., Andrejeva, J., Paulus, C., Randall, R.E., McLauchlan, J. and Hughes, D.J., 2020. Direct Antiviral Activity of IFN-Stimulated Genes Is Responsible for Resistance to Paramyxoviruses in ISG15-Deficient Cells. *The Journal of Immunology*, 205(1), pp.261–271. https://doi.org/10.4049/jimmunol.1901472.

Horikami, S.M., Curran, J., Kolakofsky, D. and Moyer, S.A., 1992. Complexes of Sendai virus NP-P and P-L proteins are required for defective interfering particle genome replication in vitro. *Journal of virology*, 66(8), pp.4901–4908. https://doi.org/10.1128/JVI.66.8.4901-4908.1992.

Hu, X., li, J., Fu, M., Zhao, X. and Wang, W., 2021. The JAK/STAT signaling pathway: from bench to clinic. *Signal Transduction and Targeted Therapy 2021 6:1*, 6(1), pp.1–33. https://doi.org/10.1038/s41392-021-00791-1.

Hu, Z., He, X., Deng, J., Hu, J. and Liu, X., 2022. Current situation and future direction of Newcastle disease vaccines. *Veterinary Research 2022 53:1*, 53(1), pp.1–13. https://doi.org/10.1186/S13567-022-01118-W.

Huang, H.C., Lai, Y.J., Liao, C.C., Yang, W.F., Huang, K. Bin, Lee, I.J., Chou, W.C., Wang, S.H., Wang, L.H., Hsu, J.M., Sun, C.P., Kuo, C.T., Wang, J., Hsiao, T.C., Yang, P.J., Lee, T.A., Huang, W., Li, F.A., Shen, C.Y., Lin, Y.L., Tao, M.H. and Li, C.W., 2021. Targeting conserved N-glycosylation blocks SARS-CoV-2 variant infection in vitro. *EBioMedicine*, 74. https://doi.org/10.1016/J.EBIOM.2021.103712.

Hubel, P., Urban, C., Bergant, V., Schneider, W.M., Knauer, B., Stukalov, A., Scaturro, P., Mann, A., Brunotte, L., Hoffmann, H.H., Schoggins, J.W., Schwemmle, M., Mann, M., Rice, C.M. and Pichlmair, A., 2019. A protein-interaction network of interferon-stimulated genes extends the innate immune system landscape. *Nature Immunology 2019 20:4*, 20(4), pp.493–502. https://doi.org/10.1038/s41590-019-0323-3.

Hull, R.N., Minner, J.R. and Smith, J.W., 1956. New viral agents recovered from tissue cultures of monkey kidney cells: I. Origin and properties of cytopathogenic agents s.v.1s.v.2, s.v.4, s.v.5, s.v.6, s.v.11, s.v.12and s.v.15. *American Journal of Epidemiology*, 63(2), pp.204–215. https://doi.org/10.1093/oxfordjournals.aje.a119804.

Illumina, 2020. What is nucleotide diversity and why is it important?

Isaacs, A. and Lindenmann, J., 1987. Virus interference. I. The interferon. *Journal of Interferon Research*, 7(5), pp.429–438. https://doi.org/10.1089/jir.1987.7.429.

Ivashkiv, L.B., 2018. *IFNγ: signalling, epigenetics and roles in immunity, metabolism, disease and cancer immunotherapy*. *Nature Reviews Immunology*, https://doi.org/10.1038/s41577-018-0029-z.

Jackson, A.L., Bartz, S.R., Schelter, J., Kobayashi, S. V, Burchard, J., Mao, M., Li, B., Cavet, G. and Linsley, P.S., 2003. Expression profiling reveals off-target gene regulation by RNAi. *Nature Biotechnology*, 21(6), pp.635–637. https://doi.org/10.1038/nbt831.

Jackson, A.L., Burchard, J., Schelter, J., Chau, B.N., Cleary, M., Lim, L. and Linsley, P.S., 2006. Widespread siRNA 'off-target' transcript silencing mediated by seed region sequence complementarity. *RNA*, 12(7), pp.1179–1187. https://doi.org/10.1261/rna.25706.

Jae, L.T., Raaben, M., Riemersma, M., Van Beusekom, E., Blomen, V.A., Velds, A., Kerkhoven, R.M., Carette, J.E., Topaloglu, H., Meinecke, P., Wessels, M.W., Lefeber, D.J., Whelan, S.P., Van Bokhoven, H. and Brummelkamp, T.R., 2013. Deciphering the glycosylome of dystroglycanopathies using haploid screens for Lassa virus entry. *Science*, 340(6131), pp.479–483. https://doi.org/10.1126/SCIENCE.1233675/SUPPL_FILE/JAE.SM.PDF.

Jardetzky, T.S. and Lamb, R.A., 2014. Activation of paramyxovirus membrane fusion and virus entry. *Current Opinion in Virology*, 5(1), pp.24–33. https://doi.org/10.1016/J.COVIRO.2014.01.005.

Jeong, H.H., Kim, S.Y., Rousseaux, M.W.C., Zoghbi, H.Y. and Liu, Z., 2019. Beta-binomial modeling of CRISPR pooled screen data identifies target genes with greater sensitivity and fewer false negatives. *Genome Research*, 29(6), pp.999–1008. https://doi.org/10.1101/gr.245571.118.

Jiang, F. and Doudna, J.A., 2017. CRISPR–Cas9 Structures and Mechanisms. *Annual Review of Biophysics*, 46(1), pp.505–529. https://doi.org/10.1146/annurev-biophys-062215-010822.

Jinek, M., East, A., Cheng, A., Lin, S., Ma, E. and Doudna, J., 2013. RNA-programmed genome editing in human cells. *eLife*, 2(2). https://doi.org/10.7554/eLife.00471.

Jones, C.E., Tan, W.S., Grey, F. and Hughes, D.J., 2021. *Discovering antiviral restriction factors and pathways using genetic screens*. *Journal of General Virology*, https://doi.org/10.1099/JGV.0.001603.

Joung, J., Konermann, S., Gootenberg, J.S., Abudayyeh, O.O., Platt, R.J., Brigham, M.D., Sanjana, N.E. and Zhang, F., 2017. Genome-scale CRISPR-Cas9 knockout and transcriptional activation screening. *Nature Protocols*, 12(4), pp.828–863. https://doi.org/10.1038/nprot.2017.016.

Mac Kain, A., Maarifi, G., Aicher, S.M., Arhel, N., Baidaliuk, A., Munier, S., Donati, F., Vallet, T., Tran, Q.D., Hardy, A., Chazal, M., Porrot, F., OhAinle, M., Carlson-Stevermer, J., Oki, J., Holden, K., Zimmer, G., Simon-Lorière, E., Bruel, T., Schwartz, O., van der Werf, S., Jouvenet, N., Nisole, S., Vignuzzi, M. and Roesch, F., 2022. Identification of DAXX as a restriction factor of SARS-CoV-2 through a CRISPR/Cas9 screen. *Nature Communications*, 13(1), pp.1–13. https://doi.org/10.1038/s41467-022-30134-9.

Kane, M., Zang, T.M., Rihn, S.J., Zhang, F., Kueck, T., Alim, M., Schoggins, J., Rice, C.M., Wilson, S.J. and Bieniasz, P.D., 2016. Identification of Interferon-Stimulated Genes with Antiretroviral Activity. *Cell Host and Microbe*, 20(3), pp.392–405. https://doi.org/10.1016/j.chom.2016.08.005.

Kang, J.A., Kim, Y.J. and Jeon, Y.J., 2022. The diverse repertoire of ISG15: more intricate than initially thought. *Experimental & Molecular Medicine 2022 54:11*, 54(11), pp.1779–1792. https://doi.org/10.1038/s12276-022-00872-3.

Karikó, K., Buckstein, M., Ni, H. and Weissman, D., 2005. Suppression of RNA recognition by Toll-like receptors: The impact of nucleoside modification and the evolutionary origin of RNA. *Immunity*, 23(2), pp.165–175. https://doi.org/10.1016/j.immuni.2005.06.008.

Kawai, T., Takahashi, K., Sato, S., Coban, C., Kumar, H., Kato, H., Ishii, K.J., Takeuchi, O. and Akira, S., 2005. IPS-1, an adaptor triggering RIG-I- and Mda5-mediated type I interferon induction. *Nature Immunology*, 6(10), pp.981–988. https://doi.org/10.1038/ni1243.

Kemiläinen, H., Adam, M., Mäki-Jouppila, J., Damdimopoulou, P., Damdimopoulos, A.E., Kere, J., Hovatta, O., Laajala, T.D., Aittokallio, T., Adamski, J., Ryberg, H., Ohlsson, C., Strauss, L. and Poutanen, M., 2016. The Hydroxysteroid (17β) Dehydrogenase Family Gene HSD17B12 Is Involved in the Prostaglandin Synthesis Pathway, the Ovarian Function, and Regulation of Fertility. *Endocrinology*, 157(10), pp.3719–3730. https://doi.org/10.1210/EN.2016-1252.

Khan, S., Mahmood, M.S., Rahman, S.U., Zafar, H., Habibullah, S., Khan, Z. and Ahmad, A., 2018. CRISPR/Cas9: The Jedi against the dark empire of diseases. *Journal of Biomedical Science*, 25(1), pp.1–18. https://doi.org/10.1186/s12929-018-0425-5.

Kim, D.H. and Rossi, J.J., 2008. *RNAi mechanisms and applications*. *BioTechniques*, https://doi.org/10.2144/000112792.

Kim, H.S., Lee, K., Kim, S.J., Cho, S., Shin, H.J., Kim, C. and Kim, J.S., 2018. Arrayed CRISPR screen with image-based assay reliably uncovers host genes required for coxsackievirus infection. *Genome Research*, 28(6), pp.859–868. https://doi.org/10.1101/gr.230250.117.

Klippmark, E., Rydbeck, R., Shibuta, H. and Norrby, E., 1990. Antigenic variation of human and bovine parainfluenza virus type 3 strains. *Journal of General Virology*, 71(7), pp.1577–1580. https://doi.org/10.1099/0022-1317-71-7-1577/CITE/REFWORKS.

Kumar, N., Sharma, S., Kumar, R., Tripathi, B.N., Barua, S., Ly, H. and Rouse, B.T., 2020. Host-Directed Antiviral Therapy. *Clinical Microbiology Reviews*, 33(3). https://doi.org/10.1128/CMR.00168-19.

Kumar, P., Sweeney, T.R., Skabkin, M.A., Skabkina, O. V., Hellen, C.U.T. and Pestova, T. V., 2014. Inhibition of translation by IFIT family members is determined by their ability to interact selectively with the 5′-terminal regions of cap0-, cap1- and 5′ppp- mRNAs. *Nucleic Acids Research*, 42(5), pp.3228–3245. https://doi.org/10.1093/nar/gkt1321.

Kuroda, M., Halfmann, P.J., Hill-Batorski, L., Ozawa, M., Lopes, T.J.S., Neumann, G., Schoggins, J.W., Rice, C.M. and Kawaoka, Y., 2020. Identification of interferon-stimulated genes that attenuate Ebola virus infection. *Nature Communications*, 11(1), p.2953. https://doi.org/10.1038/s41467-020-16768-7.

Kvellestad, A., Falk, K., Nygaard, S.M.R., Flesjå, K. and Holm, J.A., 2005. Atlantic salmon paramyxovirus (ASPV) infection contributes to proliferative gill inflammation (PGI) in seawater-reared Salmo salar. *Diseases of aquatic organisms*, 67(1–2), pp.47–54. https://doi.org/10.3354/DAO067047.

Lahaye, X., Vidy, A., Pomier, C., Obiang, L., Harper, F., Gaudin, Y. and Blondel, D., 2009. Functional Characterization of Negri Bodies (NBs) in Rabies Virus-Infected Cells: Evidence that NBs Are Sites of Viral Transcription and Replication. *Journal of Virology*, 83(16), pp.7948–7958. https://doi.org/10.1128/JVI.00554-09/ASSET/9E76626E-DEAE-403A-B76F-ABDC9AE82AD8/ASSETS/GRAPHIC/ZJV0160921940009.JPEG.

Lallemand, D., Curto, M., Saotome, I., Giovannini, M. and McClatchey, A.I., 2003. NF2 deficiency promotes tumorigenesis and metastasis by destabilizing adherens junctions. *Genes & Development*, 17(9), pp.1090–1100. https://doi.org/10.1101/GAD.1054603.

Laudenbach, B.T., Krey, K., Emslander, Q., Andersen, L.L., Reim, A., Scaturro, P., Mundigl, S., Dächert, C., Manske, K., Moser, M., Ludwig, J., Wohlleber, D., Kröger, A., Binder, M. and Pichlmair, A., 2021. NUDT2 initiates viral RNA degradation by removal of 5′-phosphates. *Nature Communications*, 12(1). https://doi.org/10.1038/S41467-021-27239-Y.

Lee, A.J. and Ashkar, A.A., 2018. *The dual nature of type I and type II interferons*. *Frontiers in Immunology*, https://doi.org/10.3389/fimmu.2018.02061.

Lee, S., Lee, Y. suk, Choi, Y., Son, A., Park, Y., Lee, K.M., Kim, J., Kim, J.S. and Kim, V.N., 2021a. The SARS-CoV-2 RNA interactome. *Molecular Cell*, 81(13), pp.2838-2850.e6. https://doi.org/10.1016/j.molcel.2021.04.022.

Lee, S.H., Kim, K., Kim, J., No, J.S., Park, K., Budhathoki, S., Lee, S.H., Lee, J., Cho, S.H., Cho, S., Lee, G.Y., Hwang, J., Kim, H.C., Klein, T.A., Uhm, C.S., Kim, W.K. and Song, J.W., 2021b. Discovery and Genetic Characterization of Novel Paramyxoviruses Related to the Genus Henipavirus in Crocidura Species in the Republic of Korea. *Viruses*, 13(10). https://doi.org/10.3390/V13102020.

Levy, D.E., Marié, I.J. and Durbin, J.E., 2011. Induction and function of type I and III interferon in response to viral infection. *Current opinion in virology*, 1(6), pp.476–86. https://doi.org/10.1016/j.coviro.2011.11.001.

Li, B., Clohisey, S.M., Chia, B.S., Wang, B., Cui, A., Eisenhaure, T., Schweitzer, L.D., Hoover, P., Parkinson, N.J., Nachshon, A., Smith, N., Regan, T., Farr, D., Gutmann, M.U., Bukhari, S.I., Law, A., Sangesland, M., Gat-Viks, I., Digard, P., Vasudevan, S., Lingwood, D., Dockrell, D.H., Doench, J.G., Baillie, J.K. and Hacohen, N., 2020. Genome-wide CRISPR screen identifies host dependency factors for influenza A virus infection. *Nature Communications*, 11(1), p.164. https://doi.org/10.1038/s41467-019-13965-x.

Li, J., Ding, S.C., Cho, H., Chung, B.C., Gale, M., Chanda, S.K., Diamond, M.S., Michael, G., Chanda, S.K. and Diamond, M.S., 2013. A short hairpin RNA screen of interferon-stimulated genes identifies a novel negative regulator of the cellular antiviral response. *mBio*, 4(3), pp.e00385-13. https://doi.org/10.1128/mBio.00385-13.

Li, M.M.H., Aguilar, E.G., Michailidis, E., Pabon, J., Park, P., Wu, X., de Jong, Y.P., Schneider, W.M., Molina, H., Rice, C.M. and MacDonald, M.R., 2019a. Characterization of Novel Splice Variants of Zinc Finger Antiviral Protein (ZAP). *Journal of Virology*, 93(18), pp.715–734. https://doi.org/10.1128/JVI.00715-19/FORMAT/EPUB.

Li, M.M.H., Lau, Z., Cheung, P., Aguilar, E.G., Schneider, W.M., Bozzacco, L., Molina, H., Buehler, E., Takaoka, A., Rice, C.M., Felsenfeld, D.P. and MacDonald, M.R., 2017. TRIM25 Enhances the Antiviral Action of Zinc-Finger Antiviral Protein (ZAP). *PLOS Pathogens*, 13(1), p.e1006145. https://doi.org/10.1371/JOURNAL.PPAT.1006145.

Li, Q., Brass, A.L., Ng, A., Hu, Z., Xavier, R.J., Liang, T.J. and Elledge, S.J., 2009. A genome-wide genetic screen for host factors required for hepatitis C virus propagation. *Proceedings of the National*

Academy of Sciences of the United States of America, 106(38), pp.16410–16415. https://doi.org/10.1073/pnas.0907439106.

Li, W., Xiao, J., Zhou, X., Xu, M., Hu, C., Xu, X., Lu, Y., Liu, C., Xue, S., Nie, L., Zhang, H., Li, Z., Zhang, Y., Ji, F., Hui, L., Tao, W., Wei, B. and Wang, H., 2015. STK4 regulates TLR pathways and protects against chronic inflammation–related hepatocellular carcinoma. *Journal of Clinical Investigation*, 125(11), pp.4239–4254. https://doi.org/10.1172/JCI81203.

Li, W., Xu, H., Xiao, T., Cong, L., Love, M.I., Zhang, F., Irizarry, R.A., Liu, J.S., Brown, M. and Liu, X.S., 2014. MAGeCK enables robust identification of essential genes from genome-scale CRISPR/Cas9 knockout screens. *Genome biology*, 15(12), p.554. https://doi.org/10.1186/s13059-014-0554-4.

Li, Y., Muffat, J., Omer Javed, A., Keys, H.R., Lungjangwa, T., Bosch, I., Khan, M., Virgilio, M.C., Gehrke, L., Sabatini, D.M. and Jaenisch, R., 2019b. Genome-wide CRISPR screen for Zika virus resistance in human neural cells. *Proceedings of the National Academy of Sciences*, 116(19), pp.9527–9532. https://doi.org/10.1073/pnas.1900867116.

Lin, R., Heylbroeck, C., Pitha, P.M. and Hiscott, J., 1998. Virus-dependent phosphorylation of the IRF-3 transcription factor regulates nuclear translocation, transactivation potential, and proteasome-mediated degradation. *Molecular and cellular biology*, 18(5), pp.2986–96. https://doi.org/10.1128/mcb.18.5.2986.

Lin, Y.-T., Chiweshe, S., McCormick, D., Raper, A., Wickenhagen, A., DeFillipis, V., Gaunt, E., Simmonds, P., Wilson, S.J. and Grey, F., 2020. Human cytomegalovirus evades ZAP detection by suppressing CpG dinucleotides in the major immediate early 1 gene. *PLOS Pathogens*, 16(9), p.e1008844. https://doi.org/10.1371/journal.ppat.1008844.

Lipovsky, A., Popa, A., Pimienta, G., Wyler, M., Bhan, A., Kuruvilla, L., Guie, M.A., Poffenberger, A.C., Nelson, C.D.S., Atwood, W.J. and DiMaio, D., 2013. Genome-wide siRNA screen identifies the retromer as a cellular entry factor for human papillomavirus. *Proceedings of the National Academy of Sciences of the United States of America*, 110(18), pp.7452–7457. https://doi.org/10.1073/pnas.1302164110.

Liu, T., Zhang, L., Joo, D. and Sun, S.C., 2017. *NF-κB signaling in inflammation*. *Signal Transduction and Targeted Therapy*, https://doi.org/10.1038/sigtrans.2017.23.

Lo, M.S., Brazas, R.M. and Holtzman, M.J., 2005. Respiratory syncytial virus nonstructural proteins NS1 and NS2 mediate inhibition of Stat2 expression and alpha/beta interferon responsiveness. *Journal of virology*, 79(14), pp.9315–9. https://doi.org/10.1128/JVI.79.14.9315-9319.2005.

Lozano, R., Naghavi, M., Foreman, K., Lim, S., Shibuya, K., Aboyans, V., Abraham, J., Adair, T., Aggarwal, R., Ahn, S.Y., AlMazroa, M.A., Alvarado, M., Anderson, H.R., Anderson, L.M., Andrews, K.G., Atkinson, C., Baddour, L.M., Barker-Collo, S., Bartels, D.H., Bell, M.L., Benjamin, E.J., Bennett, D., Bhalla, K., Bikbov, B., Bin Abdulhak, A., Birbeck, G., Blyth, F., Bolliger, I., Boufous, S., Bucello, C., Burch, M., Burney, P., Carapetis, J., Chen, H., Chou, D., Chugh, S.S., Coffeng, L.E., Colan, S.D., Colquhoun, S., Colson, K.E., Condon, J., Connor, M.D., Cooper, L.T., Corriere, M., Cortinovis, M., Courville De Vaccaro, K., Couser, W., Cowie, B.C., Criqui, M.H., Cross, M., Dabhadkar, K.C., Dahodwala, N., De Leo, D., Degenhardt, L., Delossantos, A., Denenberg, J., Des Jarlais, D.C., Dharmaratne, S.D., Dorsey, E.R., Driscoll, T., Duber, H., Ebel, B., Erwin, P.J., Espindola, P., Ezzati, M., Feigin, V., Flaxman, A.D., Forouzanfar, M.H., Fowkes, F.G.R., Franklin, R., Fransen, M., Freeman, M.K., Gabriel, S.E., Gakidou, E., Gaspari, F., Gillum, R.F., Gonzalez-Medina, D., Halasa, Y.A., Haring, D., Harrison, J.E., Havmoeller, R., Hay, R.J., Hoen, B., Hotez, P.J., Hoy, D., Jacobsen, K.H., James, S.L., Jasrasaria, R., Jayaraman, S., Johns, N., Karthikeyan, G., Kassebaum, N., Keren, A., Khoo, J.P., Knowlton, L.M., Kobusingye, O., Koranteng, A., Krishnamurthi, R., Lipnick, M., Lipshultz, S.E., Lockett Ohno, S., Mabweijano, J., MacIntyre, M.F., Mallinger, L., March, L., Marks, G.B., Marks, R., Matsumori, A., Matzopoulos, R., Mayosi, B.M., McAnulty, J.H., McDermott, M.M., McGrath, J., Memish, Z.A., Mensah, G.A., Merriman, T.R., Michaud, C., Miller, M., Miller, T.R., Mock, C., Mocumbi, A.O., Mokdad, A.A., Moran, A., Mulholland, K., Nair, M.N., Naldi, L., Narayan, K.M.V., Nasseri, K., Norman, P., O'Donnell, M., Omer, S.B., Ortblad, K., Osborne, R., Ozgediz, D., Pahari, B., Pandian, J.D., Panozo Rivero, A., Perez Padilla, R., Perez-Ruiz, F., Perico, N., Phillips, D., Pierce, K., Pope, C.A., Porrini, E., Pourmalek, F., Raju, M., Ranganathan, D., Rehm, J.T., Rein, D.B., Remuzzi, G., Rivara, F.P., Roberts, T., Rodriguez De León, F., Rosenfeld, L.C., Rushton, L., Sacco, R.L.,

Salomon, J.A., Sampson, U., Sanman, E., Schwebel, D.C., Segui-Gomez, M., Shepard, D.S., Singh, D., Singleton, J., Sliwa, K., Smith, E., Steer, A., Taylor, J.A., Thomas, B., Tleyjeh, I.M., Towbin, J.A., Truelsen, T., Undurraga, E.A., Venketasubramanian, N., Vijayakumar, L., Vos, T., Wagner, G.R., Wang, M., Wang, W., Watt, K., Weinstock, M.A., Weintraub, R., Wilkinson, J.D., Woolf, A.D., Wulf, S., Yeh, P.H., Yip, P., Zabetian, A., Zheng, Z.J., Lopez, A.D. and Murray, C.J., 2012. Global and regional mortality from 235 causes of death for 20 age groups in 1990 and 2010: A systematic analysis for the Global Burden of Disease Study 2010. *The Lancet*, 380(9859), pp.2095–2128. https://doi.org/10.1016/S0140-6736(12)61728-0.

Lu, H., Cherepanova, N.A., Gilmore, R., Contessa, J.N. and Lehrman, M.A., 2019. Targeting STT3A-oligosaccharyltransferase with NGI-1 causes herpes simplex virus 1 dysfunction. *The FASEB Journal*, 33(6), pp.6801–6812. https://doi.org/10.1096/fj.201802044RR.

Lu, H., Fermaintt, C.S., Cherepanova, N.A., Reid, G., Yan, N. and Lehrman, M.A., 2018. Mammalian STT3A/B oligosaccharyltransferases segregate N-glycosylation at the translocon from lipid-linked oligosaccharide hydrolysis. *Proceedings of the National Academy of Sciences of the United States of America*, 115(38), pp.9557–9562. https://doi.org/10.1073/PNAS.1806034115/-/DCSUPPLEMENTAL.

Luczak, M., Gumulka, W., Szmigielski, S. and Korbecki, M., 1975. Inhibition of multiplication of parainfluenza 3 virus in prostaglandin-treated WISH cells. *Archives of Virology*, 49(4), pp.377–380. https://doi.org/10.1007/BF01318248.

Ludwig, J., Schuberth, C., Goldeck, M., Schlee, M., Li, H., Juranek, S., Sheng, G., Micura, R., Tuschl, T., Hartmann, G. and Patel, D.J., 2010. Structural and functional insights into 5′-ppp RNA pattern recognition by the innate immune receptor RIG-I. *Nature Structural and Molecular Biology*, 17(7), pp.781–787. https://doi.org/10.1038/nsmb.1863.

Luthra, P., Sun, D., Silverman, R.H. and He, B., 2011. Activation of IFN-β expression by a viral mRNA through RNase L and MDA5. *Proceedings of the National Academy of Sciences of the United States of America*, 108(5), pp.2118–2123. https://doi.org/10.1073/PNAS.1012409108/SUPPL_FILE/PNAS.201012409SI.PDF.

Ma, H., Dang, Y., Wu, Y., Jia, G., Anaya, E., Zhang, J., Abraham, S., Choi, J.G., Shi, G., Qi, L., Manjunath, N. and Wu, H., 2015. A CRISPR-based screen identifies genes essential for west-nile-virus-induced cell death. *Cell Reports*, 12(4), pp.673–683. https://doi.org/10.1016/j.celrep.2015.06.049.

Major, J., Crotta, S., Llorian, M., McCabe, T.M., Gad, H.H., Priestnall, S.L., Hartmann, R. and Wack, A., 2020. Type I and III interferons disrupt lung epithelial repair during recovery from viral infection. *Science*, 369(6504), pp.712–717. https://doi.org/10.1126/SCIENCE.ABC2061/SUPPL_FILE/ABC2061_MDAR-CHECKLIST.PDF.

Mali, P., Yang, L., Esvelt, K.M., Aach, J., Guell, M., DiCarlo, J.E., Norville, J.E. and Church, G.M., 2013. RNA-Guided Human Genome Engineering via Cas9. *Science*, 339(6121), pp.823–826. https://doi.org/10.1126/science.1232033.

Malur, A.G., Chattopadhyay, S., Maitra, R.K. and Banerjee, A.K., 2005. Inhibition of STAT 1 phosphorylation by human parainfluenza virus type 3 C protein. *Journal of virology*, 79(12), pp.7877–82. https://doi.org/10.1128/JVI.79.12.7877-7882.2005.

Mao, R., Nie, H., Cai, D., Zhang, J., Liu, H., Yan, R., Cuconati, A., Block, T.M., Guo, J.T. and Guo, H., 2013. Inhibition of Hepatitis B Virus Replication by the Host Zinc Finger Antiviral Protein. *PLOS Pathogens*, 9(7), p.e1003494. https://doi.org/10.1371/JOURNAL.PPAT.1003494.

Marceau, C.D., Puschnik, A.S., Majzoub, K., Ooi, Y.S., Brewer, S.M., Fuchs, G., Swaminathan, K., Mata, M.A., Elias, J.E., Sarnow, P. and Carette, J.E., 2016. Genetic dissection of Flaviviridae host factors through genome-scale CRISPR screens. *Nature*, 535(7610), pp.159–163. https://doi.org/10.1038/nature18631.

Marques, J.T. and Williams, B.R.G., 2005. *Activation of the mammalian immune system by siRNAs*. *Nature Biotechnology*, https://doi.org/10.1038/nbt1161.

Marsh, G.A., de Jong, C., Barr, J.A., Tachedjian, M., Smith, C., Middleton, D., Yu, M., Todd, S., Foord, A.J., Haring, V., Payne, J., Robinson, R., Broz, I., Crameri, G., Field, H.E. and Wang, L.F.,

2012. Cedar Virus: A Novel Henipavirus Isolated from Australian Bats. *PLOS Pathogens*, 8(8), p.e1002836. https://doi.org/10.1371/JOURNAL.PPAT.1002836.

Mathieu, C., Dhondt, K.P., Châlons, M., Mély, S., Raoul, H., Negre, D., Cosset, F.L., Gerlier, D., Vivès, R.R. and Horvat, B., 2015. Heparan sulfate-dependent enhancement of henipavirus infection. *mBio*, 6(2). https://doi.org/10.1128/MBIO.02427-14.

Mayers, J., Mansfield, K.L. and Brown, I.H., 2017. The role of vaccination in risk mitigation and control of Newcastle disease in poultry. *Vaccine*, 35(44), pp.5974–5980. https://doi.org/10.1016/J.VACCINE.2017.09.008.

McCusker, C. and Warrington, R., 2011. Primary immunodeficiency. *Allergy, Asthma & Clinical Immunology 2011 7:1*, 7(1), pp.1–8. https://doi.org/10.1186/1710-1492-7-S1-S11.

McNab, F., Mayer-Barber, K., Sher, A., Wack, A. and O'Garra, A., 2015. *Type I interferons in infectious disease*. *Nature Reviews Immunology*, https://doi.org/10.1038/nri3787.

Mears, H. V. and Sweeney, T.R., 2018. Better together: The role of IFIT protein-protein interactions in the antiviral response. *Journal of General Virology*, 99(11), pp.1463–1477. https://doi.org/10.1099/jgv.0.001149.

Meng, F., Yu, Z., Zhang, D., Chen, S., Guan, H., Zhou, R., Wu, Q., Zhang, Q., Liu, S., Venkat Ramani, M.K., Yang, B., Ba, X.Q., Zhang, J., Huang, J., Bai, X., Qin, J., Feng, X.H., Ouyang, S., Zhang, Y.J., Liang, T. and Xu, P., 2021. Induced phase separation of mutant NF2 imprisons the cGAS-STING machinery to abrogate antitumor immunity. *Molecular Cell*, 81(20), pp.4147-4164.e7. https://doi.org/10.1016/j.molcel.2021.07.040.

Meng, F., Zhou, R., Wu, S., Zhang, Q., Jin, Q., Zhou, Y., Plouffe, S.W., Liu, S., Song, H., Xia, Z., Zhao, B., Ye, S., Feng, X.H., Guan, K.L., Zou, J. and Xu, P., 2016. Mst1 shuts off cytosolic antiviral defense through IRF3 phosphorylation. *Genes & Development*, 30(9), pp.1086–1100. https://doi.org/10.1101/GAD.277533.116.

Mercer, J., Snijder, B., Sacher, R., Burkard, C., Bleck, C.K.E., Stahlberg, H., Pelkmans, L. and Helenius, A., 2012. RNAi Screening Reveals Proteasome- and Cullin3-Dependent Stages in Vaccinia Virus Infection. *Cell Reports*, 2(4), pp.1036–1047. https://doi.org/10.1016/J.CELREP.2012.09.003.

Micklem, D.R., Blø, M., Bergström, P., Hodneland, E., Tiron, C., Høiby, T., Gjerdrum, C., Hammarsten, O. and Lorens, J.B., 2014. Flow cytometry-based functional selection of RNA interference triggers for efficient epi-allelic analysis of therapeutic targets. *BMC Biotechnology*, 14(1), p.57. https://doi.org/10.1186/1472-6750-14-57.

Miles, L.A., Garippa, R.J. and Poirier, J.T., 2016. *Design, execution, and analysis of pooled in vitro CRISPR/Cas9 screens*. *FEBS Journal*, https://doi.org/10.1111/febs.13770.

Misra, A. and Green, M.R., 2017. Fluorescence reporter-based genome-wide RNA interference screening to identify alternative splicing regulators. In: *Methods in Molecular Biology*. pp.1–12. https://doi.org/10.1007/978-1-4939-6518-2_1.

Mohamed, B., Mazeaud, C., Baril, M., Poirier, D., Sow, A.A., Chatel-Chaix, L., Titorenko, V. and Lamarre, D., 2020. Very-long-chain fatty acid metabolic capacity of 17-beta-hydroxysteroid dehydrogenase type 12 (HSD17B12) promotes replication of hepatitis C virus and related flaviviruses. *Scientific Reports*, 10(1), pp.1–15. https://doi.org/10.1038/s41598-020-61051-w.

Monson, E., Crosse, K., Duan, M., Chen, W., O'Shea, R., Wakim, L., Carr, J., Whelan, D. and Helbig, K., 2021a. Intracellular lipid droplet accumulation occurs early following viral infection and is required for an efficient interferon response. *Nature Communications*, 12(1), p.4303. https://doi.org/10.1038/s41467-021-24632-5.

Monson, E., Laws, J., Telikani, Z., Milligan, A., Rozario, A., Amarasinghe, I., Smith, M., Tran, V., Dinh, Q., Williamson, N., Mechler, A., Johnson, C., Hofer, M., Nie, S., Whelan, D. and Helbig, K., 2023. Virally induced lipid droplets are a platform for innate immune signalling complexes. *bioRxiv*, p.2023.04.20.537741. https://doi.org/10.1101/2023.04.20.537741.

Monson, E., Trenerry, A., Laws, J., Mackenzie, J. and Helbig, K., 2021b. Lipid droplets and lipid mediators in viral infection and immunity. *FEMS Microbiology Reviews*, 45(4), pp.1–20.

https://doi.org/10.1093/femsre/fuaa066.

Moresco, E.M.Y., Li, X. and Beutler, B., 2013. Going forward with genetics: Recent technological advances and forward genetics in mice. *American Journal of Pathology*, 182(5), pp.1462–1473. https://doi.org/10.1016/j.ajpath.2013.02.002.

Morgens, D.W., Deans, R.M., Li, A. and Bassik, M.C., 2016. Systematic comparison of CRISPR/Cas9 and RNAi screens for essential genes. *Nature Biotechnology*, 34(6), pp.634–636. https://doi.org/10.1038/nbt.3567.

Moskovskich, A., Goldmann, U., Kartnig, F., Lindinger, S., Konecka, J., Fiume, G., Girardi, E. and Superti-Furga, G., 2019. The transporters SLC35A1 and SLC30A1 play opposite roles in cell survival upon VSV virus infection. *Scientific Reports*, 9(1), p.10471. https://doi.org/10.1038/s41598-019-46952-9.

Murphy, E. and Shenk, T.E., 2008. Human cytomegalovirus genome. *Current Topics in Microbiology and Immunology*, 325, pp.1–19. https://doi.org/10.1007/978-3-540-77349-8_1/COVER.

Nagasaki, S., Suzuki, T., Miki, Y., Akahira, J.I., Kitada, K., Ishida, T., Handa, H., Ohuchi, N. and Sasano, H., 2009. 17Beta-hydroxysteroid dehydrogenase type 12 in human breast carcinoma: a prognostic factor via potential regulation of fatty acid synthesis. *Cancer research*, 69(4), pp.1392–1399. https://doi.org/10.1158/0008-5472.CAN-08-0821.

El Najjar, F., Schmitt, A.P. and Dutch, R.E., 2014. Paramyxovirus Glycoprotein Incorporation, Assembly and Budding: A Three Way Dance for Infectious Particle Production. *Viruses 2014, Vol. 6, Pages 3019-3054*, 6(8), pp.3019–3054. https://doi.org/10.3390/V6083019.

Nan, Y., Nan, G. and Zhang, Y.J., 2014. Interferon Induction by RNA Viruses and Antagonism by Viral Pathogens. *Viruses 2014, Vol. 6, Pages 4999-5027*, 6(12), pp.4999–5027. https://doi.org/10.3390/V6124999.

Ng, T.I., Mo, H., Pilot-Matias, T., He, Y., Koev, G., Krishnan, P., Mondal, R., Pithawalla, R., He, W., Dekhtyar, T., Packer, J., Schurdak, M. and Molla, A., 2007. Identification of host genes involved in hepatitis C virus replication by small interfering RNA technology. *Hepatology*, 45(6), pp.1413–1421. https://doi.org/10.1002/hep.21608.

Nguyen, L.A.P., Aldana, K.S., Yang, E., Yao, Z. and Li, M.M.H., 2023. Alphavirus Evasion of Zinc Finger Antiviral Protein (ZAP) Correlates with CpG Suppression in a Specific Viral nsP2 Gene Sequence. *Viruses*, 15(4). https://doi.org/10.3390/V15040830.

Nilsson-Payant, B.E., Blanco-Melo, D., Uhl, S., Escudero-Pérez, B., Olschewski, S., Thibault, P., Panis, M., Rosenthal, M., Muñoz-Fontela, C., Lee, B. and tenOever, B.R., 2021. Reduced Nucleoprotein Availability Impairs Negative-Sense RNA Virus Replication and Promotes Host Recognition. *Journal of Virology*, 95(9). https://doi.org/10.1128/JVI.02274-20/SUPPL_FILE/JVI.02274-20-S0001.XLSX.

Nishiya, T., Kajita, E., Miwa, S. and DeFranco, A.L., 2005. TLR3 and TLR7 are targeted to the same intracellular compartments by distinct regulatory elements. *Journal of Biological Chemistry*, 280(44), pp.37107–37117. https://doi.org/10.1074/jbc.M504951200.

Noton, S.L. and Fearns, R., 2015. Initiation and regulation of paramyxovirus transcription and replication. *Virology*, 479–480, pp.545–554. https://doi.org/10.1016/j.virol.2015.01.014.

O'Brien, K.L., Baggett, H.C., Brooks, W.A., Feikin, D.R., Hammitt, L.L., Higdon, M.M., Howie, S.R.C., Deloria Knoll, M., Kotloff, K.L., Levine, O.S., Madhi, S.A., Murdoch, D.R., Prosperi, C., Scott, J.A.G., Shi, Q., Thea, D.M., Wu, Z., Zeger, S.L., Adrian, P. V., Akarasewi, P., Anderson, T.P., Antonio, M., Awori, J.O., Baillie, V.L., Bunthi, C., Chipeta, J., Chisti, M.J., Crawley, J., DeLuca, A.N., Driscoll, A.J., Ebruke, B.E., Endtz, H.P., Fancourt, N., Fu, W., Goswami, D., Groome, M.J., Haddix, M., Hossain, L., Jahan, Y., Kagucia, E.W., Kamau, A., Karron, R.A., Kazungu, S., Kourouma, N., Kuwanda, L., Kwenda, G., Li, M., Machuka, E.M., Mackenzie, G., Mahomed, N., Maloney, S.A., McLellan, J.L., Mitchell, J.L., Moore, D.P., Morpeth, S.C., Mudau, A., Mwananyanda, L., Mwansa, J., Silaba Ominde, M., Onwuchekwa, U., Park, D.E., Rhodes, J., Sawatwong, P., Seidenberg, P., Shamsul, A., Simões, E.A.F., Sissoko, S., Wa Somwe, S., Sow, S.O., Sylla, M., Tamboura, B., Tapia, M.D., Thamthitiwat, S., Toure, A., Watson, N.L., Zaman, K. and Zaman, S.M.A., 2019. Causes of severe pneumonia

requiring hospital admission in children without HIV infection from Africa and Asia: the PERCH multi-country case-control study. *The Lancet*, 394(10200), pp.757–779. https://doi.org/10.1016/S0140-6736(19)30721-4.

Odon, V., Fros, J.J., Goonawardane, N., Dietrich, I., Ibrahim, A., Alshaikhahmed, K., Nguyen, D. and Simmonds, P., 2019. The role of ZAP and OAS3/RNAseL pathways in the attenuation of an RNA virus with elevated frequencies of CpG and UpA dinucleotides. *Nucleic Acids Research*, 47(15), pp.8061–8083. https://doi.org/10.1093/nar/gkz581.

Oganesyan, G., Saha, S.K., Guo, B., He, J.Q., Shahangian, A., Zarnegar, B., Perry, A. and Cheng, G., 2005. Critical role of TRAF3 in the Toll-like receptor-dependent and -independent antiviral response. *Nature 2005 439:7073*, 439(7073), pp.208–211. https://doi.org/10.1038/nature04374.

OhAinle, M., Helms, L., Vermeire, J., Roesch, F., Humes, D., Basom, R., Delrow, J.J., Overbaugh, J. and Emerman, M., 2018. A virus-packageable CRISPR screen identifies host factors mediating interferon inhibition of HIV. *eLife*, 7. https://doi.org/10.7554/eLife.39823.

Oliveira, V.H.S., Dean, K.R., Qviller, L., Kirkeby, C. and Bang Jensen, B., 2021. Factors associated with baseline mortality in Norwegian Atlantic salmon farming. *Scientific Reports 2021 11:1*, 11(1), pp.1–14. https://doi.org/10.1038/s41598-021-93874-6.

Panda, D. and Cherry, S., 2015. A genome-wide RNAi screening method to discover novel genes involved in virus infection. *Methods*, 91, pp.75–81. https://doi.org/10.1016/J.YMETH.2015.07.002.

Parisien, J.-P., Lau, J.F., Rodriguez, J.J., Ulane, C.M. and Horvath, C.M., 2002. Selective STAT Protein Degradation Induced by Paramyxoviruses Requires both STAT1 and STAT2 but Is Independent of Alpha/Beta Interferon Signal Transduction. *Journal of Virology*, 76(9), pp.4190–4198. https://doi.org/10.1128/jvi.76.9.4190-4198.2002.

Parisien, J.P., Lau, J.F., Rodriguez, J.J., Sullivan, B.M., Moscona, A., Parks, G.D., Lamb, R.A. and Horvath, C.M., 2001. The V protein of human parainfluenza virus 2 antagonizes type I interferon responses by destabilizing signal transducer and activator of transcription 2. *Virology*, 283(2), pp.230–239. https://doi.org/10.1006/viro.2001.0856.

Park, R.J., Wang, T., Koundakjian, D., Hultquist, J.F., Lamothe-Molina, P., Monel, B., Schumann, K., Yu, H., Krupzcak, K.M., Garcia-Beltran, W., Piechocka-Trocha, A., Krogan, N.J., Marson, A., Sabatini, D.M., Lander, E.S., Hacohen, N. and Walker, B.D., 2017. A genome-wide CRISPR screen identifies a restricted set of HIV host dependency factors. *Nature Genetics*, 49(2), pp.193–203. https://doi.org/10.1038/ng.3741.

De Pasquale, V., Quiccione, M.S., Tafuri, S., Avallone, L. and Pavone, L.M., 2021. Heparan Sulfate Proteoglycans in Viral Infection and Treatment: A Special Focus on SARS-CoV-2. *International Journal of Molecular Sciences*, 22(12). https://doi.org/10.3390/IJMS22126574.

Payne, S., 2017. Families Paramyxoviridae and Pneumoviridae. In: *Viruses*. Elsevier. pp.173–181. https://doi.org/10.1016/B978-0-12-803109-4.00020-9.

Peppel, K. and Baglioni, C., 1991. Deadenylation and turnover of interferon-β mRNA. *Journal of Biological Chemistry*, 266(11), pp.6663–6666. https://doi.org/10.1016/s0021-9258(20)89546-5.

Perry, R.T. and Halsey, N.A., 2004. The Clinical Significance of Measles: A Review. *The Journal of Infectious Diseases*, 189(Supplement_1), pp.S4–S16. https://doi.org/10.1086/377712.

Pettipher, E.R., 1998. Prostaglandins. *Encyclopedia of Immunology*, pp.2024–2027. https://doi.org/10.1006/RWEI.1999.0512.

Pfeffer, L.M., 2011. The Role of Nuclear Factor κB in the Interferon Response. *Journal of Interferon & Cytokine Research*, 31(7), p.553. https://doi.org/10.1089/JIR.2011.0028.

Pichlmair, A., Lassnig, C., Eberle, C.A., Górna, M.W., Baumann, C.L., Burkard, T.R., Búrckstúmmer, T., Stefanovic, A., Krieger, S., Bennett, K.L., Rúlicke, T., Weber, F., Colinge, J., Múller, M. and Superti-Furga, G., 2011. IFIT1 is an antiviral protein that recognizes 5′-triphosphate RNA. *Nature Immunology*, 12(7), pp.624–630. https://doi.org/10.1038/ni.2048.

Pichlmair, A., Schulz, O., Tan, C.P., Näslund, T.I., Liljeström, P., Weber, F. and Reis e Sousa, C.,

2006. RIG-I-mediated antiviral responses to single-stranded RNA bearing 5’-phosphates. *Science (New York, N.Y.)*, 314(5801), pp.997–1001. https://doi.org/10.1126/science.1132998.

Platanias, L.C., 2005. *Mechanisms of type-I- and type-II-interferon-mediated signalling*. *Nature Reviews Immunology*, https://doi.org/10.1038/nri1604.

Platanitis, E., Demiroz, D., Schneller, A., Fischer, K., Capelle, C., Hartl, M., Gossenreiter, T., Müller, M., Novatchkova, M. and Decker, T., 2019. A molecular switch from STAT2-IRF9 to ISGF3 underlies interferon-induced gene transcription. *Nature Communications 2019 10:1*, 10(1), pp.1–17. https://doi.org/10.1038/s41467-019-10970-y.

Poltorak, A., He, X., Smirnova, I., Liu, M.Y., Van Huffel, C., Du, X., Birdwell, D., Alejos, E., Silva, M., Galanos, C., Freudenberg, M., Ricciardi-Castagnoli, P., Layton, B. and Beutler, B., 1998. Defective LPS signaling in C3H/HeJ and C57BL/10ScCr mice: Mutations in Tlr4 gene. *Science*, 282(5396), pp.2085–2088. https://doi.org/10.1126/SCIENCE.282.5396.2085/SUPPL_FILE/985613.XHTML.

Puschnik, A.S., Majzoub, K., Ooi, Y.S. and Carette, J.E., 2017. *A CRISPR toolbox to study virus-host interactions*. *Nature Reviews Microbiology*, https://doi.org/10.1038/nrmicro.2017.29.

Rabbani, M.A.G., Ribaudo, M., Guo, J.-T. and Barik, S., 2016. Identification of Interferon-Stimulated Gene Proteins That Inhibit Human Parainfluenza Virus Type 3. *Journal of Virology*, 90(24), pp.11145–11156. https://doi.org/10.1128/jvi.01551-16.

Ramachandran, A. and Horvath, C.M., 2009. Paramyxovirus disruption of interferon signal transduction: STATus report. *Journal of interferon & cytokine research : the official journal of the International Society for Interferon and Cytokine Research*, 29(9), pp.531–7. https://doi.org/10.1089/jir.2009.0070.

Ramadan, N., Flockhart, I., Booker, M., Perrimon, N. and Mathey-Prevot, B., 2007. Design and implementation of high-throughput RNAi screens in cultured Drosophila cells. *Nature Protocols*, 2(9), pp.2245–2264. https://doi.org/10.1038/nprot.2007.250.

Randall, R.E., Young, D.F., Goswami, K.K. and Russell, W.C., 1987. Isolation and characterization of monoclonal antibodies to simian virus 5 and their use in revealing antigenic differences between human, canine and simian isolates. *The Journal of general virology*, 68 (Pt 11, pp.2769–2780. https://doi.org/10.1099/0022-1317-68-11-2769.

Rathore, A., Iketani, S., Wang, P., Jia, M., Sahi, V. and Ho, D.D., 2020. CRISPR-based gene knockout screens reveal deubiquitinases involved in HIV-1 latency in two Jurkat cell models. *Scientific Reports*, 10(1), p.5350. https://doi.org/10.1038/s41598-020-62375-3.

Reeves, R.M., Hardelid, P., Gilbert, R., Warburton, F., Ellis, J. and Pebody, R.G., 2017. Estimating the burden of respiratory syncytial virus (RSV) on respiratory hospital admissions in children less than five years of age in England, 2007-2012. *Influenza and other Respiratory Viruses*, 11(2), pp.122–129. https://doi.org/10.1111/irv.12443.

Regulation of type i interferon responses. 14. Nature Reviews Immunology. https://doi.org/10.1038/nri3581.

Rehwinkel, J. and Gack, M.U., 2020. RIG-I-like receptors: their regulation and roles in RNA sensing. *Nature Reviews Immunology 2020 20:9*, 20(9), pp.537–551. https://doi.org/10.1038/s41577-020-0288-3.

Ribaudo, M. and Barik, S., 2017. The nonstructural proteins of Pneumoviruses are remarkably distinct in substrate diversity and specificity. *Virology Journal*, 14(1), p.215. https://doi.org/10.1186/s12985-017-0881-7.

Riblett, A.M., Blomen, V.A., Jae, L.T., Altamura, L.A., Doms, R.W., Brummelkamp, T.R. and Wojcechowskyj, J.A., 2016. A Haploid Genetic Screen Identifies Heparan Sulfate Proteoglycans Supporting Rift Valley Fever Virus Infection. *Journal of Virology*, 90(3), pp.1414–1423. https://doi.org/10.1128/JVI.02055-15/ASSET/721CDB50-E759-4F2F-927A-113907CA98B9/ASSETS/GRAPHIC/ZJV9990912230007.JPEG.

Richardson, R.B., Ohlson, M.B., Eitson, J.L., Kumar, A., McDougal, M.B., Boys, I.N., Mar, K.B., De La Cruz-Rivera, P.C., Douglas, C., Konopka, G., Xing, C. and Schoggins, J.W., 2018. A CRISPR screen

identifies IFI6 as an ER-resident interferon effector that blocks flavivirus replication. *Nature Microbiology*, 3(11), pp.1214–1223. https://doi.org/10.1038/s41564-018-0244-1.

Rihn, S.J., Aziz, M.A., Stewart, D.G., Hughes, J., Turnbull, M.L., Varela, M., Sugrue, E., Herd, C.S., Stanifer, M., Sinkins, S.P., Palmarini, M. and Wilson, S.J., 2019. TRIM69 Inhibits Vesicular Stomatitis Indiana Virus. *Journal of Virology*, 93(20). https://doi.org/10.1128/JVI.00951-19.

Rima, B., Balkema-Buschmann, A., Dundon, W.G., Duprex, P., Easton, A., Fouchier, R., Kurath, G., Lamb, R., Lee, B., Rota, P., Wang, L. and Ictv Report Consortium, 2019. ICTV Virus Taxonomy Profile: Paramyxoviridae. *The Journal of general virology*, 100(12), pp.1593–1594. https://doi.org/10.1099/JGV.0.001328/CITE/REFWORKS.

Rima, B., Collins, P., Easton, A., Fouchier, R., Kurath, G., Lamb, R.A., Lee, B., Maisner, A., Rota, P., Wang, L. and Ictv Report Consortium, I.R., 2017. ICTV Virus Taxonomy Profile: Pneumoviridae. *The Journal of general virology*, 98(12), pp.2912–2913. https://doi.org/10.1099/jgv.0.000959.

Risso-Ballester, J., Galloux, M., Cao, J., Le Goffic, R., Hontonnou, F., Jobart-Malfait, A., Desquesnes, A., Sake, S.M., Haid, S., Du, M., Zhang, X., Zhang, H., Wang, Z., Rincheval, V., Zhang, Y., Pietschmann, T., Eléouët, J.-F., Rameix-Welti, M.-A. and Altmeyer, R., 2021. A condensate-hardening drug blocks RSV replication in vivo. *Nature*, 595(7868), pp.596–599. https://doi.org/10.1038/s41586-021-03703-z.

Robinson, M., Schor, S., Barouch-Bentov, R. and Einav, S., 2018. *Viral journeys on the intracellular highways*. *Cellular and Molecular Life Sciences*, https://doi.org/10.1007/s00018-018-2882-0.

Rohwedder, A., Zhang, Q., Rudge, S.A. and Wakelam, M.J.O., 2014. Lipid droplet formation in response to oleic acid in Huh-7 cells is mediated by the fatty acid receptor FFAR4. *Journal of Cell Science*, 127(14), pp.3104–3115. https://doi.org/10.1242/jcs.145854.

Rubin, S., Eckhaus, M., Rennick, L.J., Bamford, C.G.G. and Duprex, W.P., 2015. Molecular biology, pathogenesis and pathology of mumps virus. *The Journal of pathology*, 235(2), p.242. https://doi.org/10.1002/PATH.4445.

Ruiz-Canada, C., Kelleher, D.J. and Gilmore, R., 2009. Cotranslational and Posttranslational N-Glycosylation of Polypeptides by Distinct Mammalian OST Isoforms. *Cell*, 136(2), pp.272–283. https://doi.org/10.1016/J.CELL.2008.11.047.

Rusinova, I., Forster, S., Yu, S., Kannan, A., Masse, M., Cumming, H., Chapman, R. and Hertzog, P.J., 2013. INTERFEROME v2.0: an updated database of annotated interferon-regulated genes. *Nucleic Acids Research*, 41(D1), pp.D1040–D1046. https://doi.org/10.1093/NAR/GKS1215.

Saito, T. and Gale, M., 2008. *Differential recognition of double-stranded RNA by RIG-I-like receptors in antiviral immunity*. *Journal of Experimental Medicine*, https://doi.org/10.1084/jem.20081210.

Sander, W.J., O'Neill, H.G. and Pohl, C.H., 2017. Prostaglandin E2 as a modulator of viral infections. *Frontiers in Physiology*, 8(FEB), p.240454. https://doi.org/10.3389/FPHYS.2017.00089/BIBTEX.

Sanjana, N.E., Shalem, O. and Zhang, F., 2014. *Improved vectors and genome-wide libraries for CRISPR screening*. *Nature Methods*, https://doi.org/10.1038/nmeth.3047.

dos Santos, P.F. and Mansur, D.S., 2017. Beyond ISGlylation: Functions of Free Intracellular and Extracellular ISG15. *Journal of Interferon & Cytokine Research*, 37(6), pp.246–253. https://doi.org/10.1089/jir.2016.0103.

Schneeberger, K., 2014. *Using next-generation sequencing to isolate mutant genes from forward genetic screens*. *Nature Reviews Genetics*, https://doi.org/10.1038/nrg3745.

Schneider, W.M., Chevillotte, M.D. and Rice, C.M., 2014. Interferon-Stimulated Genes: A Complex Web of Host Defenses. *Annual Review of Immunology*, 32(1), pp.513–545. https://doi.org/10.1146/annurev-immunol-032713-120231.

Schoggins, J.W., MacDuff, D.A., Imanaka, N., Gainey, M.D., Shrestha, B., Eitson, J.L., Mar, K.B., Richardson, R.B., Ratushny, A. V., Litvak, V., Dabelic, R., Manicassamy, B., Aitchison, J.D., Aderem, A., Elliott, R.M., García-Sastre, A., Racaniello, V., Snijder, E.J., Yokoyama, W.M., Diamond, M.S., Virgin, H.W. and Rice, C.M., 2014. Pan-viral specificity of IFN-induced genes reveals new roles for

cGAS in innate immunity. *Nature*, 505(7485), pp.691–695. https://doi.org/10.1038/nature12862.

Schoggins, J.W. and Rice, C.M., 2011. *Interferon-stimulated genes and their antiviral effector functions*. *Current Opinion in Virology*, https://doi.org/10.1016/j.coviro.2011.10.008.

Schoggins, J.W., Wilson, S.J., Panis, M., Murphy, M.Y., Jones, C.T., Bieniasz, P. and Rice, C.M., 2011. A diverse range of gene products are effectors of the type i interferon antiviral response. *Nature*, 472(7344), pp.481–485. https://doi.org/10.1038/nature09907.

Schomacker, H., Hebner, R.M., Boonyaratanakornkit, J., Surman, S., Amaro-Carambot, E., Collins, P.L. and Schmidt, A.C., 2012. The C proteins of human parainfluenza virus type 1 block IFN signaling by binding and retaining Stat1 in perinuclear aggregates at the late endosome. *PloS one*, 7(2), p.e28382. https://doi.org/10.1371/journal.pone.0028382.

Schuster, A., Erasimus, H., Fritah, S., Nazarov, P. V., van Dyck, E., Niclou, S.P. and Golebiewska, A., 2019. *RNAi/CRISPR Screens: from a Pool to a Valid Hit*. *Trends in Biotechnology*, https://doi.org/10.1016/j.tibtech.2018.08.002.

Schwerk, J., Soveg, F.W., Ryan, A.P., Thomas, K.R., Hatfield, L.D., Ozarkar, S., Forero, A., Kell, A.M., Roby, J.A., So, L., Hyde, J.L., Gale, M., Daugherty, M.D. and Savan, R., 2019. RNA-binding protein isoforms ZAP-S and ZAP-L have distinct antiviral and immune resolution functions. *Nature Immunology*, 20(12), pp.1610–1620. https://doi.org/10.1038/s41590-019-0527-6.

Shahar, E., Haddas, R., Goldenberg, D., Lublin, A., Bloch, I., Bachner Hinenzon, N. and Pitcovski, J., 2018. Newcastle disease virus: is an updated attenuated vaccine needed? *Avian pathology : journal of the W.V.P.A*, 47(5), pp.467–478. https://doi.org/10.1080/03079457.2018.1488240.

Shalem, O., Sanjana, N.E., Hartenian, E., Shi, X., Scott, D.A., Mikkelsen, T.S., Heckl, D., Ebert, B.L., Root, D.E., Doench, J.G. and Zhang, F., 2014. Genome-Scale CRISPR-Cas9 Knockout Screening in Human Cells. *Science*, 343(6166), pp.84–87. https://doi.org/10.1126/science.1247005.

Shalem, O., Sanjana, N.E. and Zhang, F., 2015. *High-throughput functional genomics using CRISPR-Cas9*. *Nature Reviews Genetics*, https://doi.org/10.1038/nrg3899.

Sharma, S. and Petsalaki, E., 2018. Application of CRISPR-Cas9 Based Genome-Wide Screening Approaches to Study Cellular Signalling Mechanisms. *International Journal of Molecular Sciences*, 19(4), p.933. https://doi.org/10.3390/ijms19040933.

Sharon, D.M., Nesdoly, S., Yang, H.J., Gélinas, J.F., Xia, Y., Ansorge, S. and Kamen, A.A., 2020. A pooled genome-wide screening strategy to identify and rank influenza host restriction factors in cell-based vaccine production platforms. *Scientific Reports 2020 10:1*, 10(1), pp.1–15. https://doi.org/10.1038/s41598-020-68934-y.

Silva-Ayala, D., López, T., Gutiérrez, M., Perrimon, N., López, S., Arias, C.F. and Estes, M.K., 2013. Genome-wide RNAi screen reveals a role for the ESCRT complex in rotavirus cell entry. *Proceedings of the National Academy of Sciences of the United States of America*, 110(25), pp.10270–10275. https://doi.org/10.1073/pnas.1304932110.

Silverman, R.H., 2007. Viral encounters with 2',5'-oligoadenylate synthetase and RNase L during the interferon antiviral response. *Journal of virology*, 81(23), pp.12720–9. https://doi.org/10.1128/JVI.01471-07.

Sivan, G., Martin, S.E., Myers, T.G., Buehler, E., Szymczyk, K.H., Ormanoglu, P. and Moss, B., 2013. Human genome-wide RNAi screen reveals a role for nuclear pore proteins in poxvirus morphogenesis. *Proceedings of the National Academy of Sciences*, 110(9), pp.3519–3524. https://doi.org/10.1073/pnas.1300708110.

Smith, S.E., Busse, D.C., Binter, S., Weston, S., Diaz Soria, C., Laksono, B.M., Clare, S., Van Nieuwkoop, S., Van den Hoogen, B.G., Clement, M., Marsden, M., Humphreys, I.R., Marsh, M., de Swart, R.L., Wash, R.S., Tregoning, J.S. and Kellam, P., 2018. Interferon-Induced Transmembrane Protein 1 Restricts Replication of Viruses That Enter Cells via the Plasma Membrane. *Journal of Virology*, 93(6), pp.e02003-18. https://doi.org/10.1128/jvi.02003-18.

So, R.W.L., Chung, S.W., Lau, H.H.C., Watts, J.J., Gaudette, E., Al-Azzawi, Z.A.M., Bishay, J., Lin, L.T.W., Joung, J., Wang, X. and Schmitt-Ulms, G., 2019. *Application of CRISPR genetic screens to*

investigate neurological diseases. *Molecular Neurodegeneration*, https://doi.org/10.1186/s13024-019-0343-3.

Speer, S.D., Li, Z., Buta, S., Payelle-Brogard, B., Qian, L., Vigant, F., Rubino, E., Gardner, T.J., Wedeking, T., Hermann, M., Duehr, J., Sanal, O., Tezcan, I., Mansouri, N., Tabarsi, P., Mansouri, D., Francois-Newton, V., Daussy, C.F., Rodriguez, M.R., Lenschow, D.J., Freiberg, A.N., Tortorella, D., Piehler, J., Lee, B., García-Sastre, A., Pellegrini, S. and Bogunovic, D., 2016a. ISG15 deficiency and increased viral resistance in humans but not mice. *Nature Communications*, 7(1), p.11496. https://doi.org/10.1038/ncomms11496.

Speer, S.D., Li, Z., Buta, S., Payelle-Brogard, B., Qian, L., Vigant, F., Rubino, E., Gardner, T.J., Wedeking, T., Hermann, M., Duehr, J., Sanal, O., Tezcan, I., Mansouri, N., Tabarsi, P., Mansouri, D., Francois-Newton, V., Daussy, C.F., Rodriguez, M.R., Lenschow, D.J., Freiberg, A.N., Tortorella, D., Piehler, J., Lee, B., García-Sastre, A., Pellegrini, S. and Bogunovic, D., 2016b. ISG15 deficiency and increased viral resistance in humans but not mice. *Nature Communications*, 7. https://doi.org/10.1038/ncomms11496.

Stokes, A., Tierney, E.L., Murphy, B.R. and Hall, S.L., 1992. The complete nucleotide sequence of the JS strain of human parainfluenza virus type 3: comparison with the Wash/47885/57 prototype strain. *Virus Research*, 25(1–2), pp.91–103. https://doi.org/10.1016/0168-1702(92)90102-F.

Su, J., Wilson, M., Samuel, C. and Ma, D., 2021. Formation and Function of Liquid-Like Viral Factories in Negative-Sense Single-Stranded RNA Virus Infections. *Viruses*, 13(1), p.126. https://doi.org/10.3390/v13010126.

Subramanian, G., Kuzmanovic, T., Zhang, Y., Peter, C.B., Veleeparambil, M., Chakravarti, R., Sen, G.C. and Chattopadhyay, S., 2018. A new mechanism of interferon's antiviral action: Induction of autophagy, essential for paramyxovirus replication, is inhibited by the interferon stimulated gene, TDRD7. *PLOS Pathogens*, 14(1), p.e1006877. https://doi.org/10.1371/journal.ppat.1006877.

Subramanian, G., Popli, S., Chakravarty, S., Taylor, R.T., Chakravarti, R. and Chattopadhyay, S., 2020. The interferon-inducible protein TDRD7 inhibits AMP-activated protein kinase and thereby restricts autophagy-independent virus replication. *The Journal of biological chemistry*, p.jbc.RA120.013533. https://doi.org/10.1074/jbc.RA120.013533.

Sudbery, I., Enright, A.J., Fraser, A.G. and Dunham, I., 2010. Systematic analysis of off-target effects in an RNAi screen reveals microRNAs affecting sensitivity to TRAIL-induced apoptosis. *BMC Genomics*, 11(1), p.175. https://doi.org/10.1186/1471-2164-11-175.

Suzuki, T., Portner, A., Scroggs, R.A., Uchikawa, M., Koyama, N., Matsuo, K., Suzuki, Y. and Takimoto, T., 2001. Receptor Specificities of Human Respiroviruses. *Journal of Virology*, 75(10), pp.4604–4613. https://doi.org/10.1128/JVI.75.10.4604-4613.2001/ASSET/E064AB02-CB52-4C11-AFFE-40A232A3ABD9/ASSETS/GRAPHIC/JV1012084008.JPEG.

Suzuki, T., Sato, Y., Okuno, Y., Goshima, F., Mikami, T., Umeda, M., Murata, T., Watanabe, T., Watashi, K., Wakita, T., Kitagawa, H. and Kimura, H., 2022. Genome-wide CRISPR screen for HSV-1 host factors reveals PAPSS1 contributes to heparan sulfate synthesis. *Communications Biology 2022 5:1*, 5(1), pp.1–11. https://doi.org/10.1038/s42003-022-03581-9.

Swiecki, M. and Colonna, M., 2011. *Type i interferons: Diversity of sources, production pathways and effects on immune responses*. *Current Opinion in Virology*, https://doi.org/10.1016/j.coviro.2011.10.026.

Taft, J. and Bogunovic, D., 2018. The Goldilocks Zone of Type I IFNs: Lessons from Human Genetics. *The Journal of Immunology*, 201(12), pp.3479–3485. https://doi.org/10.4049/JIMMUNOL.1800764.

Tai, A.W., Benita, Y., Peng, L.F., Kim, S.S., Sakamoto, N., Xavier, R.J. and Chung, R.T., 2009. A Functional Genomic Screen Identifies Cellular Cofactors of Hepatitis C Virus Replication. *Cell Host and Microbe*, 5(3), pp.298–307. https://doi.org/10.1016/j.chom.2009.02.001.

Tan, W.S., Rong, E., Dry, I., Lillico, S.G., Law, A., Whitelaw, C.B.A. and Dalziel, R.G., 2020. Genome-wide CRISPR knockout screen reveals membrane tethering complexes EARP and GARP important for Bovine Herpes Virus Type 1 replication. *bioRxiv*, p.2020.06.17.155788.

https://doi.org/10.1101/2020.06.17.155788.

Tian, X., Zhou, Y., Wang, S., Gao, M., Xia, Y., Li, Y., Zhong, Y., Xu, W., Bai, L., Fu, B., Zhou, Y., Lee, H.R., Deng, H., Lan, K., Feng, P. and Zhang, J., 2023. Genome-Wide CRISPR-Cas9 Screen Identifies SMCHD1 as a Restriction Factor for Herpesviruses. *mBio*, 14(2), p.e0054923. https://doi.org/10.1128/mbio.00549-23.

Tokarz, S., Berset, C., La Rue, J., Friedman, K., Nakayama, K.I., Nakayama, K., Zhang, D.E. and Lanker, S., 2004. The ISG15 isopeptidase UBP43 is regulated by proteolysis via the SCF Skp2 ubiquitin ligase. *Journal of Biological Chemistry*, 279(45), pp.46424–46430. https://doi.org/10.1074/jbc.M403189200.

Tzelepis, K., Koike-Yusa, H., De Braekeleer, E., Li, Y., Metzakopian, E., Dovey, O.M., Mupo, A., Grinkevich, V., Li, M., Mazan, M., Gozdecka, M., Ohnishi, S., Cooper, J., Patel, M., McKerrell, T., Chen, B., Domingues, A.F., Gallipoli, P., Teichmann, S., Ponstingl, H., McDermott, U., Saez-Rodriguez, J., Huntly, B.J.P., Iorio, F., Pina, C., Vassiliou, G.S. and Yusa, K., 2016. A CRISPR Dropout Screen Identifies Genetic Vulnerabilities and Therapeutic Targets in Acute Myeloid Leukemia. *Cell Reports*, 17(4), pp.1193–1205. https://doi.org/10.1016/j.celrep.2016.09.079.

Vasou, A., Nightingale, K., Cetkovská, V., Bamford, C.G.G., Andrejeva, J., Randall, R.E., McLauchlan, J., Weekes, M.P. and Hughes, D.J., 2021. A co-opted ISG15-USP18 binding mechanism normally reserved for deISGylation controls type I IFN signalling. *bioRxiv*, p.2021.06.01.446527. https://doi.org/10.1101/2021.06.01.446527.

Virgo, P.F. and Gibbs, G.J., 2012. Flow cytometry in clinical pathology. *Annals of clinical biochemistry*, 49(Pt 1), pp.17–28. https://doi.org/10.1258/ACB.2011.011128.

Vuillier, F., Li, Z., Commere, P.H., Dynesen, L.T. and Pellegrini, S., 2019. USP18 and ISG15 coordinately impact on SKP2 and cell cycle progression. *Scientific Reports 2019 9:1*, 9(1), pp.1–11. https://doi.org/10.1038/s41598-019-39343-7.

Walter, M.R., 2020. *The Role of Structure in the Biology of Interferon Signaling*. *Frontiers in Immunology*, https://doi.org/10.3389/fimmu.2020.606489.

Wang, N., Dong, Q., Li, J., Jangra, R.K., Fan, M., Brasier, A.R., Lemon, S.M., Pfeffer, L.M. and Li, K., 2010. Viral induction of the zinc finger antiviral protein is IRF3-dependent but NF-κB-independent. *Journal of Biological Chemistry*, 285(9), pp.6080–6090. https://doi.org/10.1074/jbc.M109.054486.

Wang, S., Xie, F., Chu, F., Zhang, Z., Yang, B., Dai, T., Gao, L., Wang, L., Ling, L., Jia, J., van Dam, H., Jin, J., Zhang, L. and Zhou, F., 2017. YAP antagonizes innate antiviral immunity and is targeted for lysosomal degradation through IKKε-mediated phosphorylation. *Nature Immunology*, 18(7), pp.733–743. https://doi.org/10.1038/ni.3744.

Wang, S., Zhou, L., Ling, L., Meng, X., Chu, F., Zhang, S. and Zhou, F., 2020. *The Crosstalk Between Hippo-YAP Pathway and Innate Immunity*. *Frontiers in Immunology*, https://doi.org/10.3389/fimmu.2020.00323.

Wang, T., Birsoy, K., Hughes, N.W., Krupczak, K.M., Post, Y., Wei, J.J., Lander, E.S. and Sabatini, D.M., 2015. Identification and characterization of essential genes in the human genome. *Science*, 350(6264), pp.1096–1101. https://doi.org/10.1126/science.aac7041.

Wei, J., Alfajaro, M., Hanna, R., DeWeirdt, P., Strine, M., Lu-Culligan, W., Zhang, S.-M., Graziano, V., Schmitz, C., Chen, J., Mankowski, M., Filler, R., Gasque, V., Miguel, F. de, Chen, H., Oguntuyo, K.Y., Abriola, L., Surovtseva, Y., Orchard, R., Lee, B., Lindenbach, B., Politi, K., Dijk, D. van, Simon, M., Yan, Q., Doench, J.G. and Wilen, C.B., 2020. Genome-wide CRISPR screen reveals host genes that regulate SARS-CoV-2 infection. *bioRxiv*, p.2020.06.16.155101. https://doi.org/10.1101/2020.06.16.155101.

Whittemore, L.A. and Maniatis, T., 1990. Postinduction turnoff of beta-interferon gene expression. *Molecular and cellular biology*, 10(4), pp.1329–1337. https://doi.org/10.1128/MCB.10.4.1329-1337.1990.

Wignall-Fleming, E., Young, D.F., Goodbourn, S., Davison, A.J. and Randall, R.E., 2016. Genome Sequence of the Parainfluenza Virus 5 Strain That Persistently Infects AGS Cells. *Genome*

Announcements, 4(4), pp.653–669. https://doi.org/10.1128/GENOMEA.00653-16.

Wignall-Fleming, E.B., Hughes, D.J., Vattipally, S., Modha, S., Goodbourn, S., Davison, A.J. and Randall, R.E., 2019. Analysis of Paramyxovirus Transcription and Replication by High-Throughput Sequencing. *Journal of virology*, 93(17), pp.e00571-19. https://doi.org/10.1128/JVI.00571-19.

Wilson, R.L., Fuentes, S.M., Wang, P., Taddeo, E.C., Klatt, A., Henderson, A.J. and He, B., 2006. Function of Small Hydrophobic Proteins of Paramyxovirus. *Journal of Virology*, 80(4), p.1700. https://doi.org/10.1128/JVI.80.4.1700-1709.2006.

Xu, K., Broder, C.C. and Nikolov, D.B., 2012. Ephrin-B2 and ephrin-B3 as functional henipavirus receptors. *Seminars in Cell & Developmental Biology*, 23(1), pp.116–123. https://doi.org/10.1016/J.SEMCDB.2011.12.005.

Yang, Y., Zengel, J., Sun, M., Sleeman, K., Timani, K.A., Aligo, J., Rota, P., Wu, J. and He, B., 2015. Regulation of Viral RNA Synthesis by the V Protein of Parainfluenza Virus 5. *Journal of Virology*, 89(23), pp.11845–11857. https://doi.org/10.1128/JVI.01832-15/ASSET/DCE2BE21-F62E-4FA8-AE1F-C4FE1A0E9FA8/ASSETS/GRAPHIC/ZJV9990909890009.JPEG.

Yau, E.H. and Rana, T.M., 2018. Next-generation sequencing of genome-wide CRISPR screens. In: *Methods in Molecular Biology*. NIH Public Access. pp.203–216. https://doi.org/10.1007/978-1-4939-7514-3_13.

Ye, L., Schnepf, D. and Staeheli, P., 2019. *Interferon-λ orchestrates innate and adaptive mucosal immune responses*. *Nature Reviews Immunology*, https://doi.org/10.1038/s41577-019-0182-z.

Yi, C., Cai, C., Cheng, Z., Zhao, Y., Yang, X., Wu, Y., Wang, X., Jin, Z., Xiang, Y., Jin, M., Han, L. and Zhang, A., 2022. Genome-wide CRISPR-Cas9 screening identifies the CYTH2 host gene as a potential therapeutic target of influenza viral infection. *Cell Reports*, 38(13), p.110559. https://doi.org/10.1016/J.CELREP.2022.110559/ATTACHMENT/2DFC7D14-EDA4-4146-B69B-5637235D709D/MMC1.PDF.

Yin, F., Yu, J., Zheng, Y., Chen, Q., Zhang, N. and Pan, D., 2013. Spatial organization of hippo signaling at the plasma membrane mediated by the tumor suppressor merlin/NF2. *Cell*, 154(6), p.1342. https://doi.org/10.1016/j.cell.2013.08.025.

Yoneyama, M., Kikuchi, M., Natsukawa, T., Shinobu, N., Imaizumi, T., Miyagishi, M., Taira, K., Akira, S. and Fujita, T., 2004. The RNA helicase RIG-I has an essential function in double-stranded RNA-induced innate antiviral responses. *Nature Immunology*, 5(7), pp.730–737. https://doi.org/10.1038/ni1087.

Young, D.F., Andrejeva, J., Li, X., Inesta-Vaquera, F., Dong, C., Cowling, V.H., Goodbourn, S. and Randall, R.E., 2016. Human IFIT1 Inhibits mRNA Translation of Rubulaviruses but Not Other Members of the Paramyxoviridae Family. *Journal of Virology*, 90(20), pp.9446–9456. https://doi.org/10.1128/jvi.01056-16.

Young, D.F., Wignall-Fleming, E.B., Busse, D.C., Pickin, M.J., Hankinson, J., Randall, E.M., Tavendale, A., Davison, A.J., Lamont, D., Tregoning, J.S., Goodbourn, S. and Randall, R.E., 2019. The switch between acute and persistent paramyxovirus infection caused by single amino acid substitutions in the RNA polymerase P subunit. *PLoS Pathogens*, 15(2), p.e1007561. https://doi.org/10.1371/journal.ppat.1007561.

Yu, H., Lin, L., Zhang, Z., Zhang, H. and Hu, H., 2020. Targeting NF-κB pathway for the therapy of diseases: mechanism and clinical study. *Signal Transduction and Targeted Therapy 2020 5:1*, 5(1), pp.1–23. https://doi.org/10.1038/s41392-020-00312-6.

Yuan, L., Mao, Y., Luo, W., Wu, W., Xu, H., Wang, X.L. and Shen, Y.H., 2017. Palmitic acid dysregulates the Hippo-YAP pathway and inhibits angiogenesis by inducing mitochondrial damage and activating the cytosolic DNA sensor cGAS-STING-IRF3 signaling mechanism. *Journal of Biological Chemistry*, 292(36), pp.15002–15015. https://doi.org/10.1074/jbc.M117.804005.

Zadoorian, A., Du, X. and Yang, H., 2023. Lipid droplet biogenesis and functions in health and disease. *Nature Reviews Endocrinology*, 19(8), pp.443–459. https://doi.org/10.1038/s41574-023-00845-0.

Zhang, B., Goraya, M.U., Chen, N., Xu, L., Hong, Y., Zhu, M. and Chen, J.L., 2020. Zinc Finger CCCH-Type Antiviral Protein 1 Restricts the Viral Replication by Positively Regulating Type I Interferon Response. *Frontiers in Microbiology*, 11, p.527489. https://doi.org/10.3389/fmicb.2020.01912.

Zhang, L., Bukreyev, A., Thompson, C.I., Watson, B., Peeples, M.E., Collins, P.L. and Pickles, R.J., 2005. Infection of ciliated cells by human parainfluenza virus type 3 in an in vitro model of human airway epithelium. *Journal of virology*, 79(2), pp.1113–1124. https://doi.org/10.1128/JVI.79.2.1113-1124.2005.

Zhang, M., Tian, Y., Wang, R.-P., Gao, D., Zhang, Y., Diao, F.-C., Chen, D.-Y., Zhai, Z.-H. and Shu, H.-B., 2008. Negative feedback regulation of cellular antiviral signaling by RBCK1-mediated degradation of IRF3. *Cell Research*, 18(11), pp.1096–1104. https://doi.org/10.1038/cr.2008.277.

Zhang, Q., Meng, F., Chen, S., Plouffe, S.W., Wu, S., Liu, S., Li, X., Zhou, R., Wang, J., Zhao, B., Liu, J., Qin, J., Zou, J., Feng, X.-H., Guan, K.-L. and Xu, P., 2017. Hippo signalling governs cytosolic nucleic acid sensing through YAP/TAZ-mediated TBK1 blockade. *Nature Cell Biology*, 19(4), pp.362–374. https://doi.org/10.1038/ncb3496.

Zhang, R., Miner, J.J., Gorman, M.J., Rausch, K., Ramage, H., White, J.P., Zuiani, A., Zhang, P., Fernandez, E., Zhang, Q., Dowd, K.A., Pierson, T.C., Cherry, S. and Diamond, M.S., 2016. A CRISPR screen defines a signal peptide processing pathway required by flaviviruses. *Nature*, 535(7610), pp.164–168. https://doi.org/10.1038/nature18625.

Zhang, W., Zhang, L., Zan, Y., Du, N., Yang, Y. and Tien, P., 2015a. Human respiratory syncytial virus infection is inhibited by IFN-induced transmembrane proteins. *Journal of General Virology*, 96(1), pp.170–182. https://doi.org/10.1099/vir.0.066555-0.

Zhang, X., Bogunovic, D., Payelle-Brogard, B., Francois-Newton, V., Speer, S.D., Yuan, C., Volpi, S., Li, Z., Sanal, O., Mansouri, D., Tezcan, I., Rice, G.I., Chen, C., Mansouri, N., Mahdaviani, S.A., Itan, Y., Boisson, B., Okada, S., Zeng, L., Wang, X., Jiang, H., Liu, W., Han, T., Liu, D., Ma, T., Wang, B., Liu, M., Liu, J.Y., Wang, Q.K., Yalnizoglu, D., Radoshevich, L., Uzé, G., Gros, P., Rozenberg, F., Zhang, S.Y., Jouanguy, E., Bustamante, J., García-Sastre, A., Abel, L., Lebon, P., Notarangelo, L.D., Crow, Y.J., Boisson-Dupuis, S., Casanova, J.L. and Pellegrini, S., 2015b. Human intracellular ISG15 prevents interferon-α/β over-amplification and auto-inflammation. *Nature*, 517(7532), pp.89–93. https://doi.org/10.1038/nature13801.

Zhao, C., Liu, H., Xiao, T., Wang, Z., Nie, X., Li, X., Qian, P., Qin, L., Han, X., Zhang, J., Ruan, J., Zhu, M., Miao, Y.L., Zuo, B., Yang, K., Xie, S. and Zhao, S., 2020. CRISPR screening of porcine sgRNA library identifies host factors associated with Japanese encephalitis virus replication. *Nature Communications 2020 11:1*, 11(1), pp.1–15. https://doi.org/10.1038/s41467-020-18936-1.

Zhou, A., Paranjape, J.M., Der, S.D., Williams, B.R.G. and Silverman, R.H., 1999. Interferon Action in Triply Deficient Mice Reveals the Existence of Alternative Antiviral Pathways. *Virology*, 258(2), pp.435–440. https://doi.org/10.1006/VIRO.1999.9738.

Zhou, H., Yu, M., Fukuda, K., Im, J., Yao, P., Cui, W., Bulek, K., Zepp, J., Wan, Y., Whan Kim, T., Yin, W., Ma, V., Thomas, J., Gu, J., Wang, J.A., Dicorleto, P.E., Fox, P.L., Qin, J. and Li, X., 2013. IRAK-M mediates Toll-like receptor/IL-1R-induced NFκB activation and cytokine production. *EMBO Journal*, 32(4), pp.583–596. https://doi.org/10.1038/emboj.2013.2.

Appendix

Appendix 1: Code for the analysis of NGS screening data and generation of volcano plots

Note: Code within [ ] is representative of file or folder names to be inserted with own data

```
### Package Install

conda create -n CRISPR_analysis python=2.7

conda install --name CRISPR_analysis -c bioconda fastqc=0.11.4 cutadapt=1.16
mageck=0.5.8

y

source activate CRISPR_analysis

#Check that all of the packages are installed correctly

cutadapt -v

mageck -v

fastqc -v

### Sort Data

cd ~/[screen folder]

mkdir [CRISPRko_analysis]

data_dir=~/[screen folder]/[CRISPRko_analysis]

cd $data_dir

# At this point the de multiplexed files are all in individual folders as
.fastq.qz files

# To use Spring coding (sequence_processing) need to zip into .tar.gz file

# Copy and paste the individual files into [CRISPRko_analysis]

# Use following code to zip all .fastq.gz files into tar.gz file

# [screen data].tar.gz names the zip file all files are going into

# * indicates all files of that type should be zipped

tar -czf [screen data].tar.gz *.fastq.gz

### Sequencing Processing

source activate CRISPR_analysis

# Upack the data from the previously made tar.gz file
```

```
# Make sure in [CRISPRko_analysis] directory to use the following code

tar xvzf [screen data].tar.gz

# Manually move the unzipped files into a new folder [new folder]

# Give all permissions to new folder containing unzipped files

chmod 777 [new folder]

ls -l

[data]=~/[screen folder]/[CRISPRko_analysis]/[new folder]

# Process the data by creating trimmed reads

# gunzip command concatenates all reads for each sample

# cutadapt trims 5' and 3' of each read and saves the trimmed reads in files named xx_trimmed.fastq, leaving only the 19bp CRISPR sequences for read counting using MaGeCK.

# fastqc looks at sequencing quality which is recorded in the html file

cd $[data]

## This is code does not include a loop so each file needs doing separately

## Manually input each line after the last has finished running

## Will remove [fraction file] after processing whilst keeping [fraction file trimmed] file

zcat [fraction file].fastq.gz > [fraction file].fastq

cutadapt -a GTTTAAGAGC --discard-untrimmed [fraction file].fastq | cutadapt -g CGAAACACCG --discard-untrimmed -o [fraction file trimmed].fastq --minimum-length 18 --maximum-length 20 -

rm [fraction file].fastq

fastqc [fraction file trimmed].fastq

### Time to analyse the trimmed files, make a new folder in the same folder as the data

cd $[data]

mkdir [counts_files]

## The following code counts reads for each sample using MaGeCK
```

```
## awk command keeps header at top while sorting line 2 to the end alphabetically

## As above, each file and line needs running independently

## Substitute in sample/ fraction name after library file, substitute in
individual trimmed file fastq at end of first line

## Substitute in name of file in bottom line

## Need to put in name of sample after sample-label to name column headings in all
counts file

mageck count -l Yusa_gDNAlist.csv -n [fraction name] --sample-label [fraction
name] --fastq [fraction file trimmed].fastq

mv -v *log *count.txt *countsummary.txt *normalized.txt *.R *.Rnw [counts_files]

awk 'NR==1; NR>1 {print $0 | "sort -k1"}' [counts_files]/[fraction name].count.txt
> [counts_files]/[fraction name].count.sorted.txt

## SPRING: Combine counts for each sample, and counts for the plasmid library into
one big file called 'all_counts'

paste [counts_files]/*count.sorted.txt $lib_info/PLASMID_g5.count.sorted.txt \

| cut -f1,2,3,6,9,12,15,18,21,24,27,30,33,36,39,42,45,48,51,54 > [all_counts].txt

cat *.countsummary.txt | sed -n 'n;p' > counts_summary.txt

cd [counts_files]

## Keep plasmid counts within [counts_files] folder so don't need to retrieve from
other location

paste *count.sorted.txt \

| cut -f1,2,3,6,9,12,15,18,21,24,27,30,33,36,39,42,45,48,51,54,57,60,63,66 >
all_counts_3.txt

cat *.countsummary.txt | sed -n 'n;p' > [counts_summary].txt

## May come across some error messages so here are some bits of code that might
come in useful

## '> [all_counts_new].txt' saves the formatted table as new file

column -t [all_counts].txt > [all_counts_new].txt ## To align table headings with
rest of columns use the following command
```

```
head -n 1 [all_counts_new].txt | awk ' {print NF}' ## Tells you how many columns there are in the file

wc -l [all_counts_new].txt ## Tells you how many rows there are in the file

cat [all_counts_new].txt | awk '{print NF}' ## Prints the number of columns for every row individually

## Library performance check by comparing non-infected samples [control_1,control_2] to plasmid library [plasmid]

mageck test -k [all_counts].txt -t [control_1,control_1[ -c [plasmid] -n [control_vs_plasmid]

sort -k 11,11n [control_vs_plasmid].gene_summary.txt > [control_vs_plasmid].gene_summary.sorted.txt

## Compare samples in fraction A (fraction_a1,fraction_a2,fraction_a3) with fraction B (fraction_b1,fraction_b2,fraction_b3) of interest

## To include multiple repeats in analysis separate fraction names with a comma

## NOTE: no spaces between the samples when listing

mageck test -k [all_counts].txt -t [fraction_a1,fraction_a2,fraction_a3] -c [fraction_b1,fraction_b2,fraction_b3] -n [fraction_a_vs_fraction_b]

sort -k 11,11n [fraction_a_vs_fraction_b].gene_summary.txt > [fraction_a_vs_fraction_b].gene_summary.sorted.txt

## Repeat above code for all fraction comparisons required
```

Appendix 2: Additional data from biological repeats of PIV3 NP time course in NF2, HSD17B12 and ZAP deficient cells.

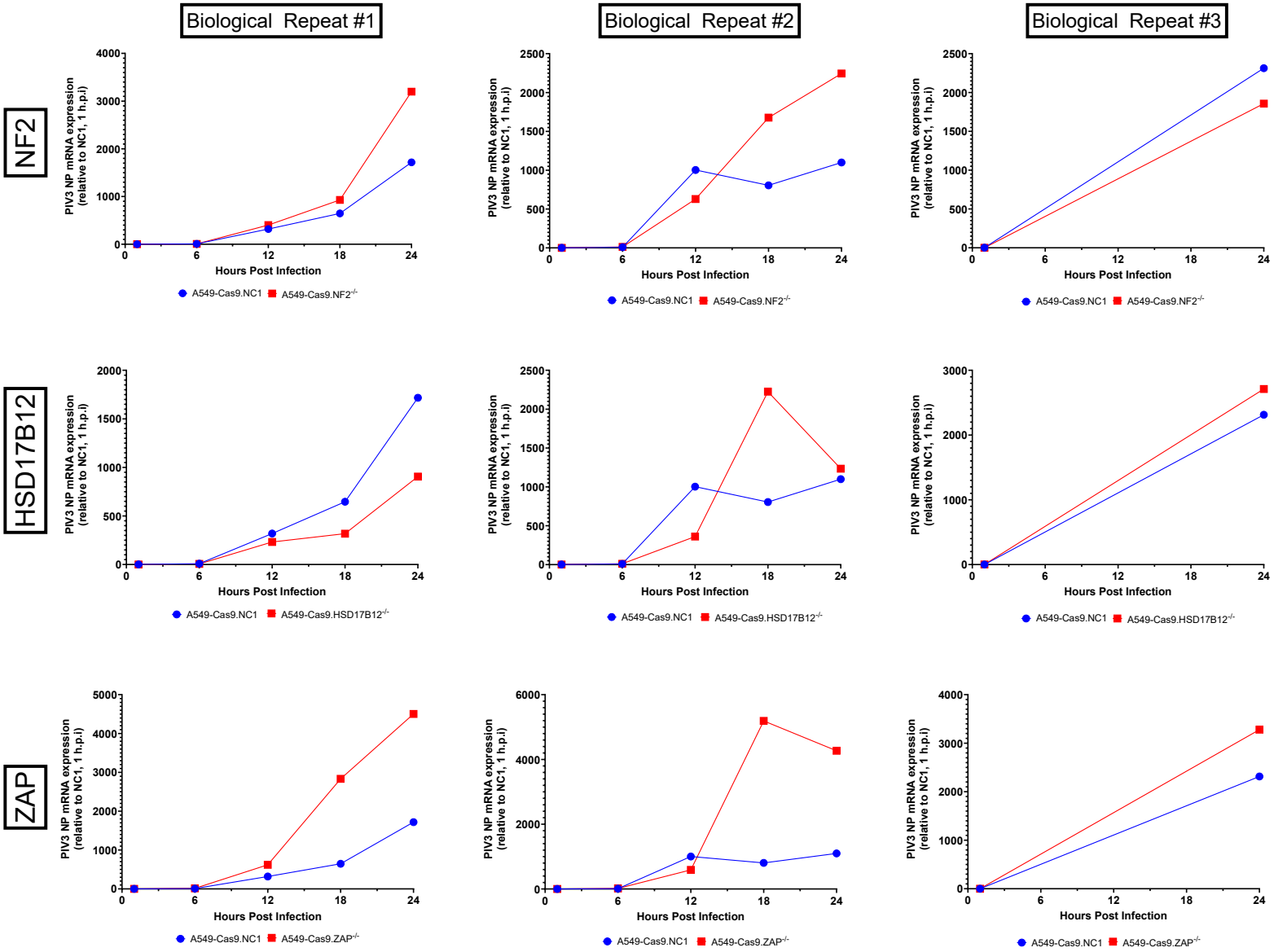

Appendix 3: Additional data from biological repeats investigating IFN-β mRNA expression following DI treatment using RT-qPCR.

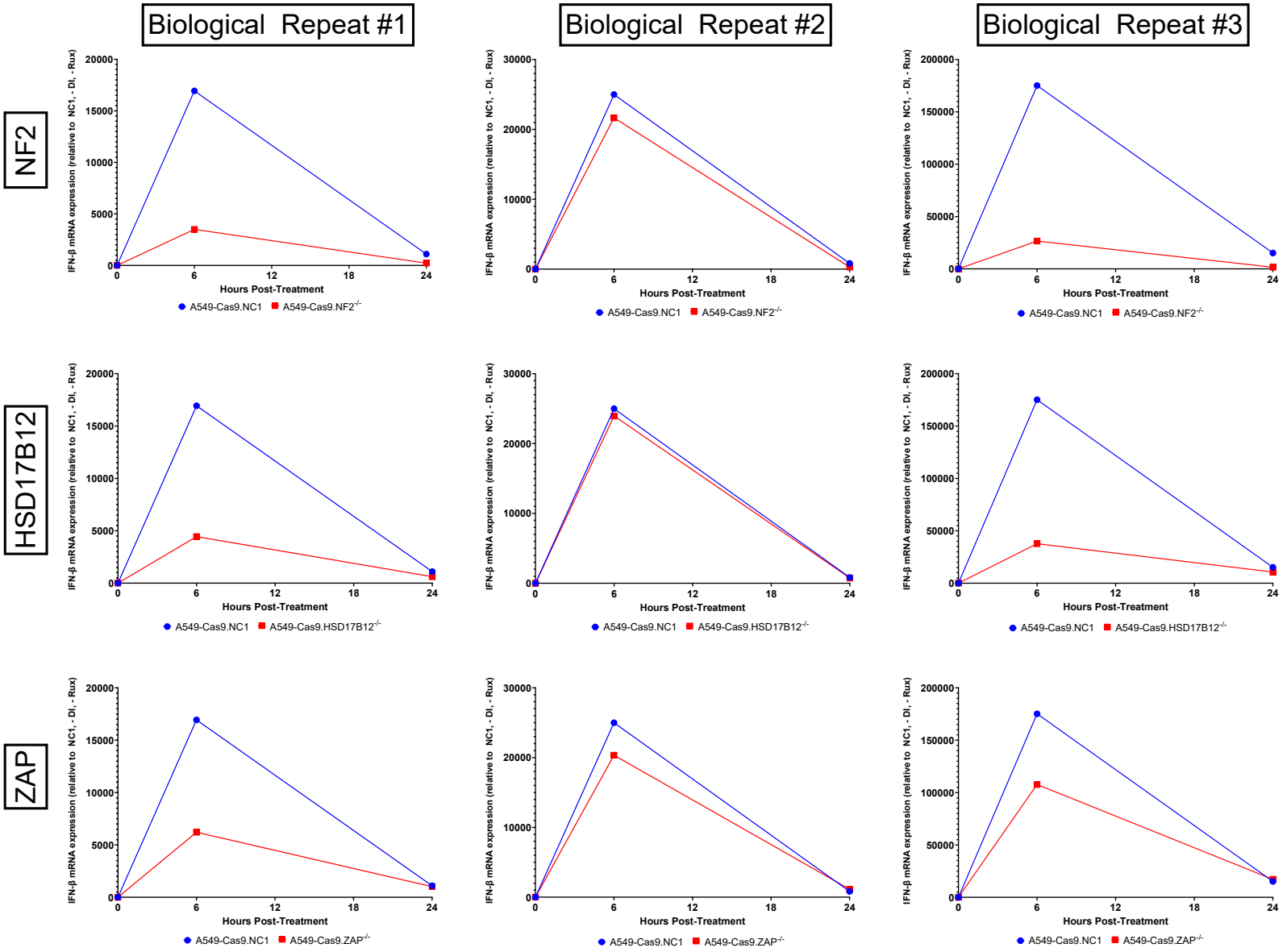

Appendix 4: Additional data from biological repeats investigating ISG15 mRNA expression following DI treatment using RT-qPCR.

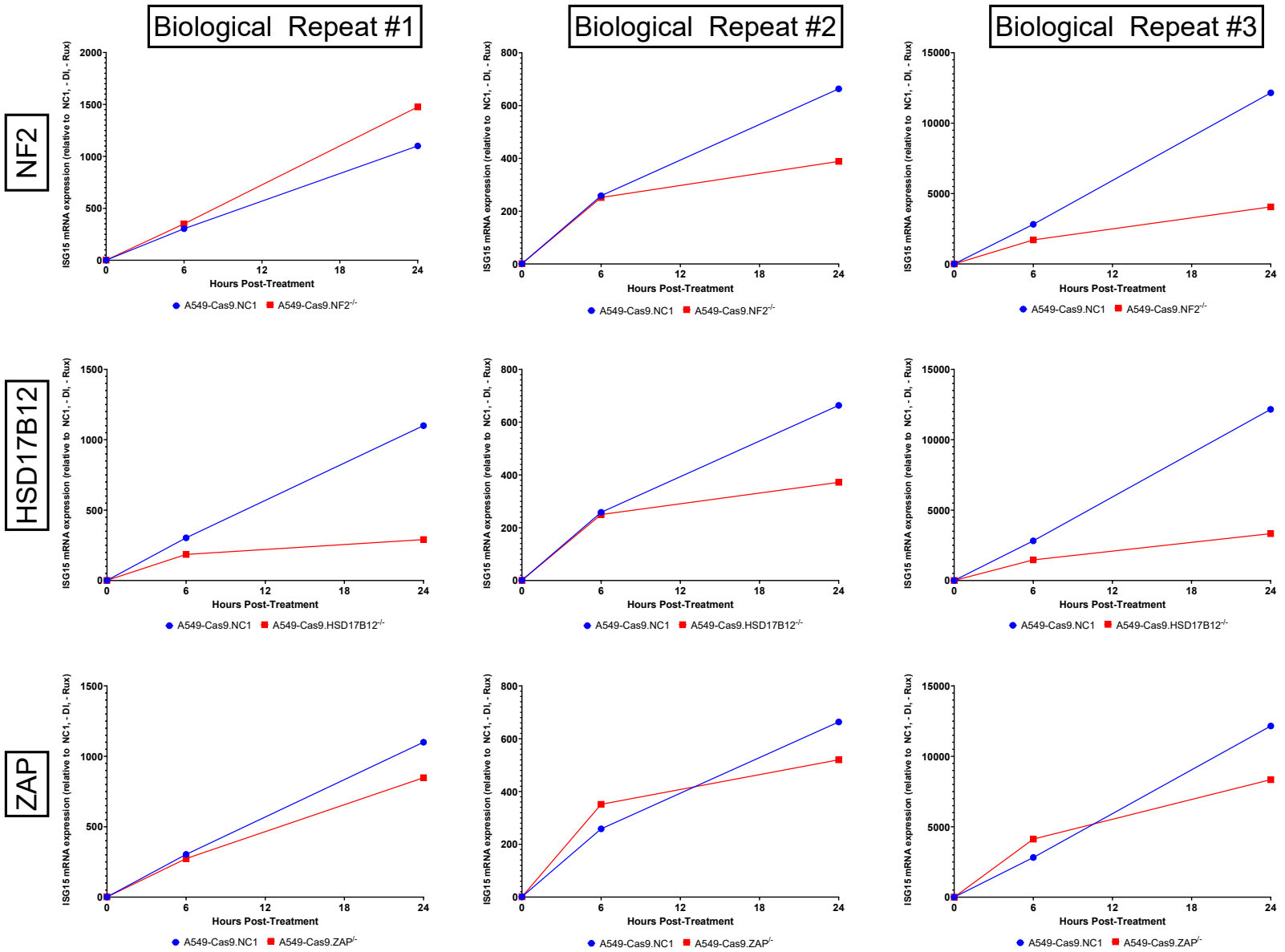

Appendix 5: Additional data from biological repeats investigating MxA mRNA expression following IFN treatment using RT-qPCR.

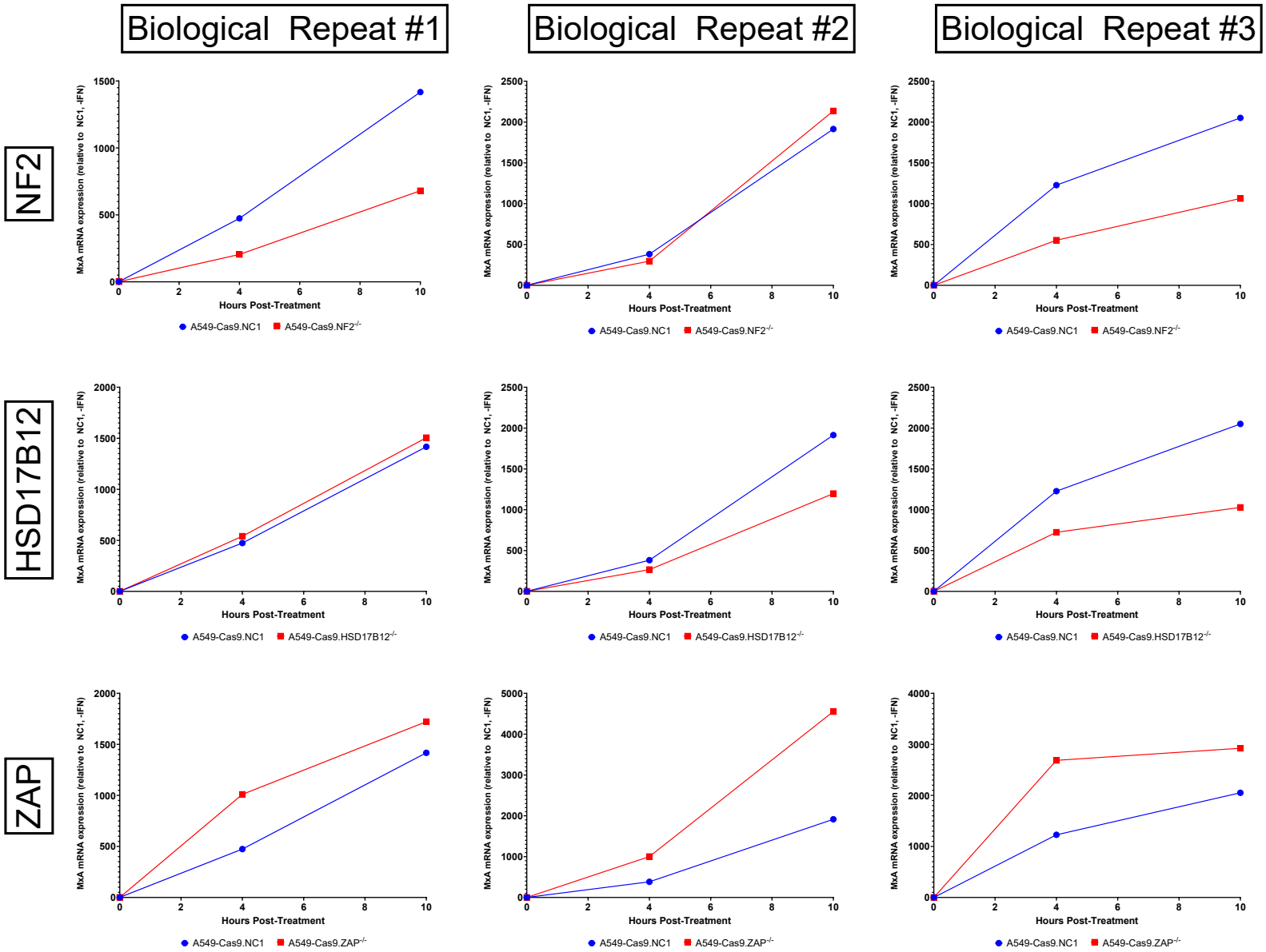

Appendix 6: Additional data from biological repeats investigating ISG15 mRNA expression following IFN treatment using RT-qPCR.

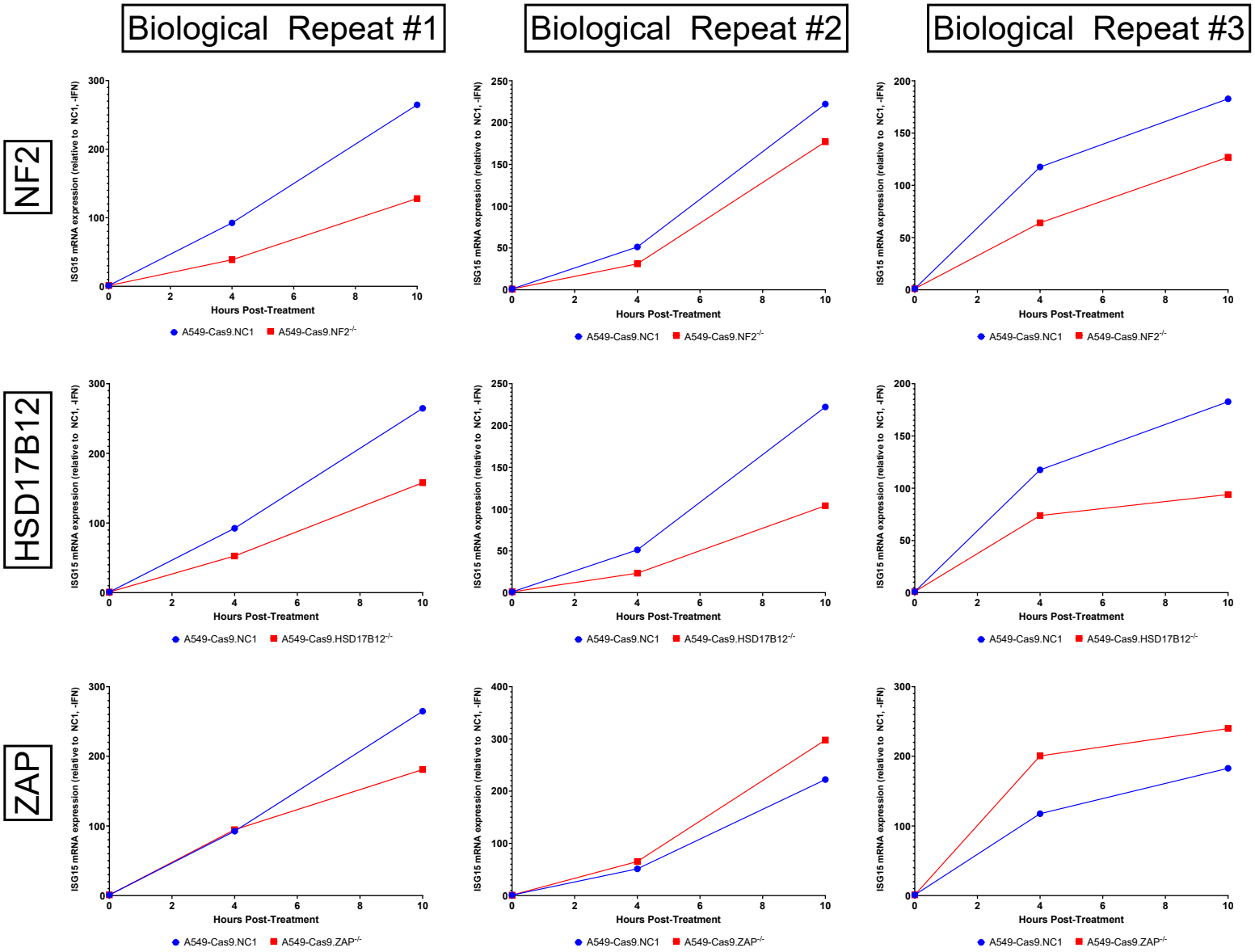

Appendix 7: Additional data from biological repeats investigating HERC5 mRNA expression following IFN treatment using RT-qPCR.